EXPLORING AND ANALYSING THE STRUCTURAL DIVERSITY OF ORGANIC CO-CRYSTALS

A thesis submitted for the degree of Doctor of Philosophy by

YUNCHENG YAN

Supervisor: K. D. M. Harris

School of Chemistry

Cardiff University

June 2014

DECLARATION

This work has not been submitted in substance for any other degree or award at this or any other university or place of learning, nor is being submitted concurrently in candidature for any degree or other award.

Signed……(candidate) Date ……

STATEMENT 1

This thesis is being submitted in partial fulfilment of the requirements for the degree of ……(insert MCh, MD, MPhil, PhD etc, as appropriate)

Signed……(candidate) Date ……

STATEMENT 2

This thesis is the result of my own independent work/investigation, except where otherwise stated.
Other sources are acknowledged by explicit references. The views expressed are my own.

Signed……(candidate) Date ……

STATEMENT 3

I hereby give consent for my thesis, if accepted, to be available for photocopying and for inter-library loan, and for the title and summary to be made available to outside organisations.

Signed……(candidate) Date ……

Abstract

Organic co-crystals are a class of promising materials in industries such as pharmaceuticals and energy industry. The work described in this thesis is the result of studying a series of organic co-crystals, which are synthesized by several different crystallization methods, and includes structures determined by single-crystal X-ray diffraction and powder X-ray diffraction.

Chapter 1 is a general introduction to organic co-crystals and the phenomenon of polymorphism in organic crystalline materials. The importance of intermolecular interactions such as hydrogen bonding and π-π stacking interactions for the design of organic co-crystals are also highlighted.

Chapter 2 describes the experimental techniques which have been used for studying organic co-crystals. These include co-crystallization methods and characterization methods such as single-crystal X-ray diffraction, powder X-ray diffraction, thermal analysis techniques and solid-state nuclear magnetic resonance.

Chapter 3 reports two novel polymorphic co-crystal systems of trimesic acid (TMA) and *tert*-butylamine (TBA) with different stoichiometric ratios and analyses the crystal structures of the two polymorphic systems.

Apart from the phenomenon of polymorphism of co-crystals of TMA and TBA, the structural diversity of other co-crystals of TMA and TBA are discussed in Chapter 4. In this chapter, all co-crystals of TMA and TBA are classified into four families based on the stoichiometric ratio between TMA and TBA, and the structural features of each family are investigated from the view point of hydrogen bonding with graph set notation.

Chapters 5 and 6 demonstrate the processes of structure determination of co-crystals of TMA and L-arginine (Chapter 5) and the co-crystal of pillar[5]quinone and 1,1,2,2-tetrachloroethane (Chapter 6) from powder X-ray diffraction data.

Acknowledgements

There are many people I would like to acknowledge for their great help during the study of my PhD.

First of all I would like to thank my supervisor Prof. Kenneth D. M. Harris for offering me the opportunity to study in this group and I am very grateful to his for all his supervision, guidance and support.

I am extremely grateful to Dr Colan E. Hughes for all his unconditional help and very useful advice in the course of my research. With his great help in every aspect over the past four years, the journey of my PhD has become much more enjoyable and easier.

I would like to thank Dr Benson Kariuki for recording and solving all single crystal structures presented in this thesis and discussions about these single crystal structures.

I would like to express my gratitude to all members in this research group, both past and present: Dr Gin Keat Lim, Dr Benjamin A. Palmer, Dr Vasileios Charalampopoulos, Philip Andrew Williams, Gregory Edwards-Gau and Victoria Keast. It was a great fun working with you.

I also would like to thank the members of staff of the School of Chemistry for their serious work and assistance for my research work.

Finally, I would like to thank my parents and sisters for their love, support and encouragement throughout these years. A special thanks to my lovely girlfriend Joyce and all my friends in Cardiff, you guys made my life in Cardiff more joyful and unforgettable.

Table of Contents

Chapter 1 Introduction

1.1 Organic Co-Crystals

The subject of organic co-crystals is not a new research direction, having been studied for over one hundred years. Originally, due to the lack of relevant knowledge of the intermolecular interactions and their effects on crystal formation, organic co-crystals were discovered primarily by chance. With passing time, more and more organic co-crystals were synthesized and scientists gradually noticed that intermolecular interactions, especially hydrogen bonding, play a key role in the formation of organic co-crystals. In recent decades, due to its potential applications in the pharmaceutical industry, a great deal of attention has been attracted towards organic co-crystals research and, thus, the number of reported organic co-crystals has increased dramatically.

1.1.1 The Definition of a Co-Crystal

Although the area of co-crystals is flourishing, the issue of nomenclature for co-crystals is not settled. Up to now, many papers and patents concerning co-crystals have been published and reported, and the number is still rising very quickly every year. However, the precise definition of co-crystals has been a controversial issue in the scientific community. Nevertheless, in general, the term co-crystal (also written as cocrystal) has, by common consent, been used to describe multi-component crystals.

Currently, it is very difficult to know exactly when the term co-crystals came into use. However, in 2003, Desiraju[1] wrote an article insisting that the term co-crystals is ambiguous and suggesting that the term should be discarded; on the other hand, at the same time, Dunitz[2] argued that, although the term co-crystals is not well-defined, the term should be retained in consideration of its popularity and difficulty to displace. Then, in 2005, Aakeröy and Salmon,[3] while not providing a new definition of co-crystals, listed some rules for co-crystals, such as that co-crystals can only be composed of neutral molecular species, only those compounds formed from reactants that are solids under ambient conditions can be considered as co-crystals, and that the amounts of components of co-crystals should be definite. Obviously, these rules greatly narrow down the definition of co-crystals and a large number of multi-component crystals are excluded, such as all crystals containing ions, all hydrates and solvates and many

inclusion compounds. Although some researchers [4-7] accepted one or all these rules and used them as the definition of co-crystals, not all researchers agree with these rules. For example, Bond[8] states that the requirement that all components are solids under ambient conditions is "contrived and inappropriate" and presents some compelling examples, such as the *n*-alkyl carboxylic acids (from formic acid up to tridecanoic acid) which form a series of two-component crystals with pyrazine. This series is obviously continuous. However, the members of the series from formic acid up to nonanoic acid are all liquids under ambient conditions, while those from decanoic acid and above are solids. Therefore, it is not appropriate to call the early members of this series solvates, while calling decanoic acid/pyrazine (and those with longer acids) a co-crystal. In addition, Bond also insisted that, due to the popularity of the term co-crystal and in order to avoid the scientific offence, researchers should use co-crystal only as "a synonym for multi-component molecular crystal".

Now, let us turn our attention to industry. Medications need to receive regulatory approval by governments. The European Medicines Agency (EMA) is the agency responsible for the scientific evaluation of medicines used in the European Union. So far, there is no guidance or definitions for co-crystals to be found on EMA's website and only one pharmaceutical co-crystal drug, tramadol (hydrochloride)/celecoxib (EMEA-001279-PIP01-12), was approved by EMA in 2012. The UK equivalent to the EMA is the Medicines and Healthcare Products Regulatory Agency (MHRA). No information about co-crystals is to be found on their websites.

With the rapid development of pharmaceutical co-crystals and in response to the need for regulatory guidance, the United States Food and Drug Administration (FDA) in December 2011 released draft guidance concerning the classification of pharmaceutical co-crystals of active pharmaceutical ingredients (APIs) and one of the main subjects of the draft guidance was the definition of co-crystals.[9] Subsequently, in February 2012, the Indo-U.S. Bilateral Meeting was held in India. Over 70 industrial and academic researchers from the US and India discussed the FDA guidance draft and the results of this discussion were summarised and published in April 2012.[10] According to this perspective, after discussing the FDA guidance draft, the participants in the meeting all strongly agreed that the term co-crystal needed to be defined more broadly. They proposed the following definition: "co-crystals are solids that are crystalline single phase materials composed of two or more different molecular and/or ionic compounds

generally in a stoichiometric ratio". This definition includes solvates and hydrates but excludes many inclusion compounds. A year later, in April 2013, the FDA released the formal Guidance for Industry[11]: Regulatory Classification of Pharmaceutical Co-Crystals. In that formal guidance, the FDA proposed the definition of co-crystals as "crystalline materials composed of two or more molecules within the same crystal lattice". From that definition, we can see that the definition of co-crystal is also broadly defined to some extent. The components can be solid or liquid at room temperature. According to this view, it covers many types of compounds, including hydrates, solvates and inclusion compounds.

However, this definition requires that the components in co-crystals should exist in their neutral states and interact via non-ionic interactions. In general, all definitions agree that both salts and co-crystals are multi-component crystals, but this does not mean a salt is a co-crystal.

Conventionally, the way to determine if a multi-component crystal containing an organic acid and organic base is a salt or co-crystal depends on the position of the proton, i.e., it depends on whether proton transfer has occurred from the acid to the base or not. If the proton is attached to the base, proton transfer has occurred and the crystal is a salt. If the proton remains on the acid, no proton transfer has occurred and the material is a co-crystal. In general, the acid ionization constant, pK_a, is employed for predicting solid-form molecular ionization states.[12-17] For larger values of ΔpK_a (greater than 3) (where $\Delta pK_a = pK_a$ (base) – pK_a (acid)) the acid and base will form a salt whereas for smaller values of ΔpK_a (less than 0), they will form a co-crystal. However, in the range $0 < \Delta pK_a < 3$, the acid and the base may form a salt, a co-crystal or a disordered crystal with partial proton transfer, depending on the specific packing environment. In the third case, in which the position of the acidic proton is not located on a specific molecule, how can we assign the multi-component crystal as a salt or a co-crystal?

In addition, in some cases, multi-component crystals can neither be classified as a salt or a co-crystal under the new definition of FDA. For example, in the course of studying fluconazole co-crystals with di-carboxylic acids, Kastelic and co-workers[18] synthesized three multi-component crystals, one containing a neutral maleic acid

molecule, an ionized maleic acid molecule and an ionized fluconazole molecule in the asymmetric unit. Is this a salt or a co-crystal?

Although the final definition of co-crystal is still not settled, it is clear that the term co-crystal should be defined more broadly. Personally, in my thesis, the term of co-crystal refers to solids that are crystalline materials composed of two or more components in the same crystal structure, where the components may be neutral, ionic, atomic or molecular.

1.1.2 The Developments of Organic Co-Crystals

There are tens of thousands of papers relating to co-crystals and the number is still increasing rapidly. To the best of our knowledge, in 1844, German chemist Friedrich Wöhler published a paper concerning quinhydrone, which may be the earliest reported organic co-crystal.[19] The components of quinhydrone are 1,4-benzoquinone and hydroquinone in a 1:1 molar ratio. However, at that time, single-crystal X-ray diffraction had not been invented and chemists were not sure what types of intermolecular interactions existed. Even so, from then on, chemists began to synthesize all types of organic co-crystals by all kinds of methods.

In the 20th century, a large number of organic co-crystals were synthesized and published. Originally, these co-crystals were often reported by chance, and almost all of these organic co-crystals contained aromatic compounds. Initially, chemists considered that π-π stacking interactions may be the necessary driving force between components in the formation of co-crystals but, with passing time, more and more co-crystals without aromatic components were synthesized and knowledge of the formation mechanisms of co-crystals accumulated gradually. Researchers realized that π-π stacking interactions are not necessary for the formation of many types of co-crystals. Other intermolecular interactions, especially hydrogen bonding, play a more important role in the formation of co-crystals and chemists now consider that intermolecular interactions can be viewed as a useful tool for the design of co-crystals.[20,21]

After entering the 21st century, the field of co-crystals research has become more and more important. Due to its potential applications in improving the physicochemical properties of drug products, there has been enormous interest in pharmaceutical co-crystals as a research area, with hundreds of publications relating to pharmaceutical co-

crystals reported annually.[7,22] I will give more details about pharmaceutical co-crystals in the next section.

Although pharmaceutical co-crystals have attracted extensive attention in the last ten years, we should realize that the subject of co-crystals research is not new and has already been the subject of research for more than 100 years. Apart from the pharmaceutical industry, other industries such as dyes and pigments,[23,24] organic nonlinear optical materials,[25-30] and biological research[31-34] have also studied co-crystals for a long time and used co-crystals for commercial purposes. It is not hard to imagine that, in the future, an increasing number of co-crystal products will appear on the market.

1.1.3 Applications of Organic Co-Crystals in Pharmaceuticals

In the pharmaceuticals industry, every year many active pharmaceutical compounds are eliminated from further development due to poor solubility, poor dissolution rate or poor stability, rather than toxicity or lack of efficacy. In order to improve or overcome these weaknesses of drug candidates, a series of techniques have been used by pharmaceutical scientists. In general, the conventional approaches to enhancing the physical or chemical properties of active pharmaceutical ingredients (APIs) include the use of salt forms, hydrates, solvates and polymorphs. These methods have been shown to be successful to some extent, but scientists still attempt to investigate new and better ways for improving drug quality. Over the last decades, pharmaceutical co-crystals have become a promising and interesting approach for enhancing the quality of drugs during drug development.

Pharmaceutical co-crystals are composed of an API (the main component) and other component(s), called coformers or excipients. Pharmaceutical co-crystals can offer great opportunities to improve the bioavailability of the API. In principle, by using coformers co-crystallized with APIs, the aim is to change the structure and composition of the drug and, thus, to greatly influence the biopharmaceutical properties of the drug rather than the efficacy of the drug. As mentioned before, the main idea of pharmaceutical co-crystals is to adjust the physiochemical properties of the solid form in which the API is administered, including melting point, solubility, dissolution rate and stability. All these properties have been studied extensively by chemists. For example, Stanton and Bak synthesized ten co-crystals of API AMG517 (an insoluble

small molecule VR 1 antagonist) with a series of coformers, and then compared their melting points with the API and their corresponding coformers. The result showed that all the melting points of these co-crystals fell between the melting point of API AMG517 and their corresponding coformers.[15,35]

Among the physiochemical properties, solubility is a key parameter. Many drug candidates are discarded due to their low solubility. Shiraki and co-workers synthesized two novel co-crystals, exemestane (the API) with maleic acid and megestrol (the API) with saccharin. The results showed that co-crystallization improved initial dissolution rates compared to the respective pure crystals.[36] Bruni and co-workers prepared two new co-crystals of acyclovir/glutaric acid and acyclovir/fumaric acid to improve the solubility of acyclovir and its dissolution properties. The experiments showed that, compared to pure acyclovir, the water solubility of the acyclovir/glutaric acid was not improved, while for acyclovir/fumaric acid it was slightly increased. In the case of dissolution rates, both of these co-crystals dissolved much faster compared with pure acyclovir.[37]

Stability of drugs is also an important issue for the pharmaceutical industry. In general, four aspects of stability need to be considered: relative humidity stress, thermal stress, chemical stability and solution stability.[38] Different aspects of stability need to be tested depending on the specific substance. In the case of co-crystals, researchers usually focus on solution stability, since dissociation of the co-crystals may result in precipitation of the single component crystal or a hydrate. For example, a 2:1 co-crystal of caffeine/oxalic acid was found to be stable at all relative humidities up to 98% RH for seven weeks and the co-crystal maintains its physical form for two days when it is slurried in water at room temperature.[39] In another example, Jung and co-workers reported two co-crystals of adefovir dipivoxil with suberic acid and succinic acid; both co-crystals displayed superior thermal stability compared to pure adefovir dipivoxil.[40]

Due to the rapidly increasing number of pharmaceutical co-crystals, a series of reviews in this subject have been published giving more detailed examples about their physicochemical properties compared with the corresponding pure crystals.[7,22,38,41] Through a large amount of research, it has been found that pharmaceutical co-crystals are not only able to offer potential enhancements in solubility, dissolution rate and physical stability, but may also enhance other properties of drugs, including flowability

or compressibility.[42] According to the scientific literature, the development of this area has grown explosively, and a large number of literature reviews concentrated on pharmaceutical co-crystals from different perspectives and aspects have been published.[5,38,41,43-50] Owing to its popularity, there is no doubt that the number will continue to grow. These articles provide detailed and systematic overviews of pharmaceutical co-crystals, and also present and discuss almost all crucial issues of pharmaceutical co-crystals.

From these articles, we can understand and learn about the development of co-crystals, the importance of pharmaceutical co-crystals, and some very useful strategies for design and synthesis of pharmaceutical co-crystals. For example, we may take advantage of intermolecular interactions including hydrogen bonding and π-π stacking for the design of pharmaceutical co-crystals, and we also should realize that there is no general strategy for improving the physicochemical properties of all APIs. Thus each API must be investigated case by case. The basic preparation methods of pharmaceutical co-crystals, [41,45] including solution methods and solid-state grinding methods are summarized. The improved physicochemical properties of pharmaceutical co-crystals, including melting point, solubility, dissolution rate, stability, bioavailability, etc., are described in detail. The characterization techniques for pharmaceutical co-crystals such as X-ray diffraction methods (single-crystal and powder XRD methods), spectroscopy techniques (infrared and nuclear magnetic resonance spectroscopy), thermal analysis (DSC and TGA), etc., are also mentioned, and plenty of pharmaceutical co-crystal examples are presented in these articles. In addition, the potential influence and growing trend of pharmaceutical co-crystals are also discussed.

1.1.4 Design of Co-Crystals

In general, there are many strategies for co-crystal design in the literature. However, these strategies are almost all based on empirical observations and the mechanism of co-crystal formation is not fully understood. Therefore, the design strategies for co-crystals are still being explored. As we all know, intermolecular interactions between components control the formation of co-crystals and, thus, the resulting co-crystal may have certain new physical properties that differ from the properties of the pure crystals of each component. In order to design and prepare co-crystals to our requirement and benefit, comprehensive understanding of the intermolecular interactions in the co-crystals is essential. In general, in the process of

formation of organic co-crystals, intermolecular interactions are the driving force and the final co-crystals structure is controlled by these intermolecular interactions. Among these intermolecular interactions, hydrogen bonding and π-π stacking are among the most common influential intermolecular interactions in the process of formation of organic co-crystals.

1.1.5 Hydrogen-Bonding Interactions

Hydrogen bonding is the predominant interaction in the design of organic co-crystals and, thus, having good understanding of hydrogen bonding is vital in crystal engineering. According to the latest definition of hydrogen bonding recommended by IUPAC in 2011,[51] a hydrogen bond is "an attractive interaction between a hydrogen atom from a molecule or molecular fragment X–H in which X is more electronegative than H, and an atom or a group of atoms in the same or a different molecule, in which there is evidence of bond formation." The hydrogen-bonding interaction between water molecules is the prototype of all hydrogen bonds. Owing to the big difference in electro-negativity between the O and the H atoms, the O–H bonds of each water molecule are polar. Thus, the distance between two neighbouring water molecules (referring to the distance of the O–H···O hydrogen bond) is shorter than the sum of the van der Waals radii for the O and H atoms. Therefore, a hydrogen bond forms. Today, a typical hydrogen bond is described as X–H···Y–Z, where the three dots denote the hydrogen bonding, X–H represents the hydrogen bond donor and Y represents the hydrogen bond acceptor. Y may be an atom, or part of an anion or a molecule.

The hydrogen bond was discovered almost 100 years ago and has been a subject for research ever since.[52] However, because of its importance for chemistry, it is a vital subject which deserves further research. Due to the short contact distances and specific directionalities associated with hydrogen bonding, it can easily be recognized in crystal structures. Moreover, hydrogen bonding is a vital tool in crystal engineering. Strong hydrogen bonding, such as O–H···O, N–H···O or O–H···N, is very common and important in organic solids but, in addition, weak hydrogen bonding, including C–H···O,[53] C–H···N, and N–H···π,[54] is also significant in organic crystal structures. In order to describe hydrogen-bonding interactions more easily, a straightforward method is required. Etter and co-workers [55,56] created a graph-set system for describing hydrogen-bonding patterns.

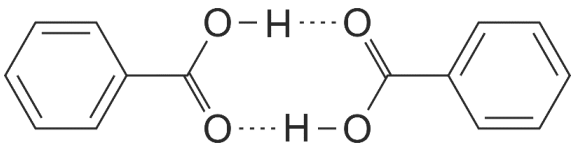

Figure 1.1. *Hydrogen-bonding ring of the benzoic acid dimer.*

Generally, in order to make the graph-set method applicable to many different kinds of systems, a straightforward approach has been developed using four main types of motif: chains (C), dimers or other finite set (D), rings (R), and intramolecular hydrogen bonds (S). In each motif, the numbers of donors and acceptors are assigned as subscripts and superscripts, respectively, and the number of atoms in the pattern is indicated in parentheses. For example, the hydrogen-bonding interaction between a benzoic acid dimer can be described by graph set $R_2^2(8)$ (see Figure 1.1). Due to its simplicity, the graph-set approach has been widely accepted and used by researchers to describe hydrogen bond patterns.

At the same time, some empirical but very useful guidelines have also been proposed for the design of hydrogen-bonded crystals. [56] There are three general rules:

1. All good proton donors and acceptors are used in hydrogen bonding;
2. Six-membered ring intramolecular hydrogen bonds form in preference to intermolecular hydrogen bonds;
3. The strongest hydrogen-bond donors and acceptors that remain after the formation of intramolecular hydrogen bonds form intermolecular hydrogen bonds to one another.

Apart from these three general rules, some specific hydrogen bonding rules are also summarized by Etter.[56] By using these guidelines, it might be possible to design co-crystals with a certain degree of accuracy. Even so, it is still essential not only to understand the structure of individual molecules, but also to be able to exploit the hydrogen bonding rules skilfully.

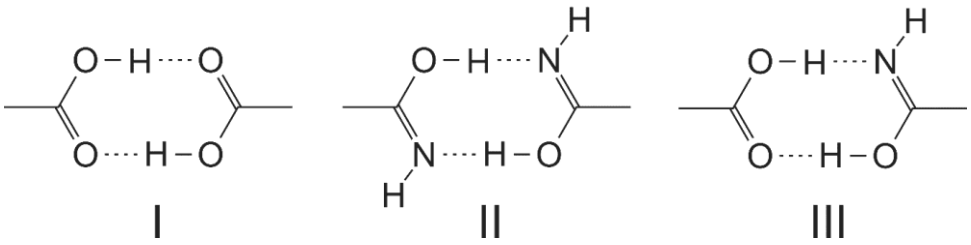

Figure 1.2. *Homomeric (I and II) and heteromeric (III) hydrogen-bonding dimers.*

For example, since carboxylic acids and suitable N-containing compounds such as amides have self-complementary hydrogen-bond donor and acceptor groups, they can form homomeric hydrogen-bonding dimers (Figures 1.2 I and 1.2 II, homomeric hydrogen-bonding dimers) in their pure crystal structures through C=O···H–O and C=N···H–O hydrogen bonds, respectively. If we use suitable combinations of carboxylic acids and N-containing compounds as components for assembly of co-crystals, they can instead interact to form heteromeric systems (Figure 1.2 III, heteromeric system) rather than homomeric systems. In fact, studies of a series of this type of co-crystals (acid-base type) have proven to be extremely successful.[57-61] In all these cases, the two components form heteromeric systems as expected and the resulting hydrogen-bonding pattern is very common and clear. The preference to form heteromeric systems is partly because the forces between the two acid-base components are stronger than those in each homomeric system.[62]

It is worth noting that, although the use of empirical hydrogen bonding rules can be very helpful in the design of co-crystals, prediction of the structure of co-crystals is still difficult. In the last couple of decades, with the development of computational chemistry, researchers developed several new algorithms and mathematical models [63-70] to predict crystal structure. Combined with the statistical analysis of hydrogen bonding in the Cambridge Structural Database (CSD), researchers use computer programs to predict hydrogen bonding in crystal structures leading to prediction of single component crystal and co-crystal structures. Although, progress in this field has led to more and more successful predictions, the challenge of crystal structure prediction is far from solved and needs further substantial investigation.

1.1.6 π-π Stacking Interactions

As mentioned above, hydrogen bonding is not the only important type of intermolecular interaction in organic co-crystals, and the π-π stacking interaction is also

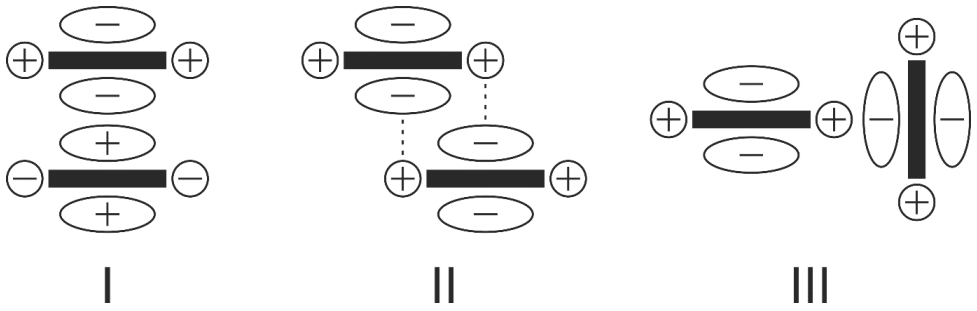

Figure 1.3. *Three types of π-π stacking interactions.*

significant. The reason why π-π stacking interactions are important in organic co-crystals is that many organic co-crystals contain phenyl rings. Therefore, π-π interactions may have influences on molecular arrangement of these crystal structures.[71] In addition, π-π stacking interactions are widespread in the natural world, such as the structures of DNA, RNA, peptides and proteins.

The π-π stacking interactions (also called aromatic interactions) refer to the intermolecular interactions between molecules containing aromatic fragments.[72,73] In general, π-π stacking interactions are composed of van der Waals interactions and electrostatic forces, but the relative contribution of these components are complicated, depending on the nature of the aromatic rings involved and their geometries.[74] It is not easy to propose straightforward rules as for hydrogen bonding. Even so, several basic geometries of π-π stacking interactions are attractive, and are commonly observed. In consideration of the electron distribution and their shapes, these π-π stacking interactions can be summarized into three types: (I) parallel type, (II) parallel offset type and (III) T-shaped (edge-to-face) type (Figure 1.3).[75,76]

As an example of the parallel (also called face-to-face) type, the 1:1 co-crystal of benzene/hexafluorobenzene is an ideal example.[77] The structure of this co-crystal contains stacks of alternating benzene and hexafluorobenzene molecules and this parallel stacking arrangement of benzene and hexafluorobenzene maximises the electrostatic interaction energy.[78,79] Offset type π-π stacking interaction is widespread in proteins and DNA; this arrangement can minimise electron repulsion and maximise the attraction between adjacent aromatic rings. Edge-to-face type π-π stacking interactions describe the T-shaped, perpendicular arrangement of adjacent aromatic molecules, often involving CH⋯ π interactions, which is found in the crystal structure of benzene.

In addition, π-π stacking interactions in organic co-crystals can be affected by different substituents. An electron donating substituent (e.g., $–NH_2$, $–NR_2$, –OH) will increase the electron density on the aromatic ring, consequently increasing the electron repulsion. An electron withdrawing substituent (e.g., $–NO_2$, $–CF_3$, –CN) has the opposite effect. Therefore, when two aromatic molecules are polarized, like polarizations repel but unlike polarizations attract.

1.1.7 Other Intermolecular Interactions

Apart from hydrogen bonding and π-π stacking interactions, other intermolecular interactions such as halogen bonding interactions [80,81] have also been used in the design of co-crystals. In addition, many co-crystal structures are controlled by not just one type of intermolecular interaction (for example, hydrogen bonding) but secondary interactions such as π-π stacking or halogen bonding also play an important role in assembling their structures.[82] On the whole, the strategies for design and preparation of co-crystals are still being investigated and crystal structural prediction remains a far-away goal.

1.2 Polymorphism of Organic Crystals

Polymorphism is a very interesting solid-state phenomenon. The phenomenon of polymorphism in organic crystals was discovered in 1832, when Wöhler and Liebig reported two polymorphs of benzamide[83]. As single-crystal X-ray diffraction was not available at that time, scientists had no idea about these two polymorphic structures. In 1936, Robertson determined the crystal structure of α-resorcinol using single-crystal X-ray diffraction. Then, in 1938, Robertson and Ubbelohde [84] discovered a new form of resorcinol (β) and determined the structure, representing the first time that detailed structural information about polymorphism had been established. Subsequently, many more new polymorphs of organic compounds were published. About half a century ago, driven in part by regulatory issues in the pharmaceutical industry, scientists gradually recognized the importance of polymorphism. In the pharmaceutical industry, the differences in the structures of polymorphs of a given API result in different physical properties, such as solubility, melting point, stability, etc. As a consequence, the polymorphic form affects the quality of the drug. Therefore, all polymorphic forms of a given drug must be identified. In most cases, pharmaceutical companies would chose

the most stable form of the API as the designed product, because the most stable form would be reliable and robust during the course of drug manufacture.

With the passing of time, many APIs and drugs turn out to have more than one form.[85-91] For aspirin, also known as acetylsalicylic acid, the first form was reported in 1964,[92] while a new form was reported in 2005.[93] Nowadays, apart from the pharmaceutical industry, polymorphism has been studied extensively and has found wide potential applications in many research areas, such as crystal engineering, which attempts to understand the intermolecular interactions of organic crystals [94,95] and other industries, such as dyes and pigments.[96] From the literature, we can see that the number of papers concerning polymorphism is numerous and increases dramatically every year.

1.2.1 The Definition of Polymorphism

Similar to the definition of co-crystals, the precise definition of polymorphism is also disputable. From the literature, we can find several different definitions of polymorph. An early and well-known definition given by McCrone in his book "Physics and Chemistry of the Organic Solid State" in 1965 is: "A polymorph is a solid crystalline phase of a given compound resulting from the possibility of at least two different arrangements of the molecules of that compound in the solid state". Subsequently, different definitions have arisen in the literature [97,98]. In 1987, Sharma suggested[97] that polymorphism means "different crystal forms, belonging to the same or different crystal systems, in which identical units of the same element or identical units of the same compound, or identical ionic formulas or identical repeating units are packed differently". In 2007, Gavezzotti proposed a definition of polymorphism with three key points: "polymorphs are a set of crystals (a) with identical chemical composition, (b) made of molecules with the same molecular connectivity but allowing for different conformations by rotation about single bonds, and (c) with distinctly different three-dimensional translational periodic symmetry operations".

According to the latest definition of polymorphism from the guidance of the U.S. FDA in 2013, polymorphism means "the different crystal forms of the same chemical compounds or substance; this may include solvation or hydration products (also known as pseudo-polymorphs or solvatomorphs) and amorphous forms." This definition is quite similar to the definition proposed by European Medicines Agency (EMA) in

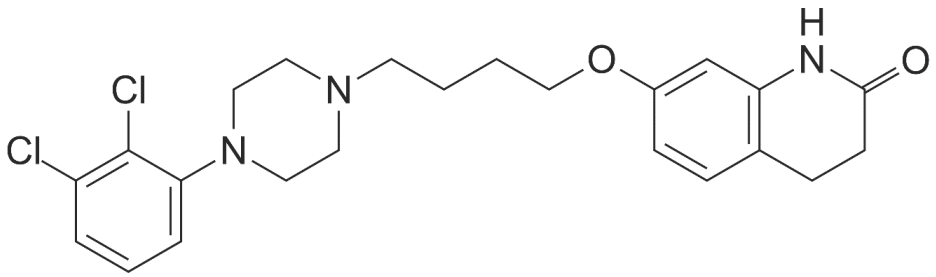

Figure 1.4. *The structure of aripiprazole.*

2005.[99] EMA defined polymorphism as "the occurrence of different crystalline forms of the same drug substance; this may include solvation or hydration products (also known as pseudopolymorphs) and amorphous forms." Obviously, both the FDA and the EMA define the term polymorphism in a broad sense. However, the term pseudo-polymorph may confuse. Thus, it is better not to use the term pseudo-polymorph but instead to use terms such as solvate or hydrate. Excluding solvates, hydrates and amorphous solids allowed by the FDA and the EMA definitions of polymorphism, generally polymorphism is defined in a more rigorous manner to include only a set of materials with identical chemical composition (as in the definition of Gavezzotti discussed above).

When different conformers of the same molecule pack in different crystal forms, it is called conformational polymorphism. In general, organic molecules with multiple flexible torsional angles (single bond torsions) can exhibit several possible conformations, and therefore have a greater chance of exhibiting conformational polymorphism.[85,100-102] For example, aripiprazole (Figure 1.4), used as an antipsychotic drug, was approved by the U.S. FDA for schizophrenia in 2002 and the EMA in 2004. Up to now, six polymorphs of aripiprazole have been reported.[85] The molecular structure of aripiprazole has seven freely rotatable bonds, which can explain why aripiprazole is such a rich conformational polymorphic system. Another reason may be that there are many different functional groups in aripiprazole molecule. Therefore, various hydrogen-bond donor and acceptor groups are able to be utilized in different crystal forms; thus, the variety of possible molecular conformations and hydrogen bonding schemes lead to a wide variety of plausible crystal packing arrangements.[103]

Apart from conformational polymorphism, in other cases, all components have the same or almost the same conformation but, owing to different spatial arrangements of these components (resulting from different intermolecular interactions), different crystal

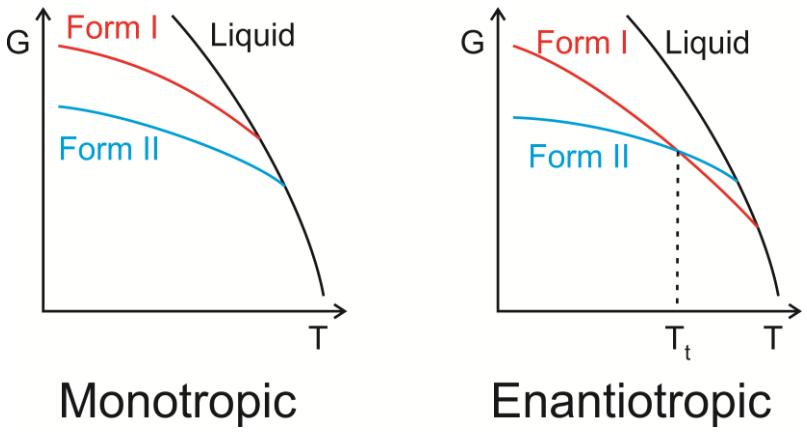

Figure 1.5. *Types of polymorphism (monotropic and enantiotropic relationships).*

forms arise. The nomenclature of polymorphs does not follow a specific rule, and labels such as I, II, III… or α, β, γ… are often used to assign the different polymorphs.

1.2.2 The Different Properties of Polymorphs

Since different polymorphs have different physicochemical properties, scientists attempt to understand the structure-property relationships in polymorphs of the same substance. As time goes on, more and more knowledge in this regard is accumulated but the mechanism of polymorphism is still not fully understood and still remain mysterious in certain aspects.[104] In terms of thermodynamics, the relationship between two polymorphs can be enantiotropic or monotropic, depending on their relative stability as a function of temperature and pressure.

For a monotropic relationship between two polymorphs (Figure 1.5, left), the stable and the metastable polymorphs can coexist only as a result of kinetic stability, and the transformation from the metastable polymorph to the stable polymorph is irreversible. On the other hand, for an enantiotropic relationship between two polymorphs (Figure 1.5, right), the transformation between the two polymorphs is reversible below their melting points by means of heating and cooling. Thus, over a certain temperature range, just one polymorph is stable, the other polymorph being unstable and will transform to the stable form.

It is not hard to image that the polymorphic form with the lower free energy is more stable than the form with higher free energy. In both systems (monotropic system and enantiotropic system), the metastable polymorph is unstable and should transform to the stable form. The life-time of the metastable polymorph depends on the rate of transformation into the stable form. In practice, the rates of transformation may range

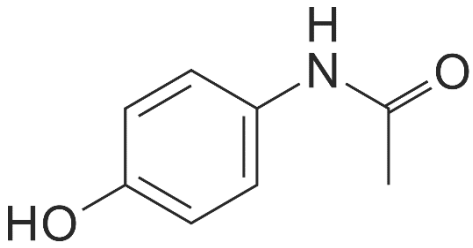

Figure 1.6. *The structure of paracetamol.*

from rapid to extremely slow, depending on the nature of the molecular structures, and there are no general rules for all polymorphic systems.

As mentioned above, when external conditions such as temperature or pressure are changed, polymorphic transformations can occur. Therefore, it is possible to distinguish between monotropic and enantiotropic systems by using thermal analytical techniques, such as Differential Scanning Calorimetry (DSC), to help us understand the relationship between polymorphs. In addition, DSC is also used to measure the melting points and the transformation temperature between different polymorphic forms.

As an example, we consider paracetamol (Figure 1.6), also called acetaminophen. According to the literature, there are three polymorphs of paracetamol, numbered I, II and III. The crystal structure of each polymorph has been determined.[105,106] Form I is stable at room temperature but has poor compressibility, while form II exhibits good compressibility but is not easy to isolate. Form III was reported to exist in 1982 but it is only recently determined (2009). That crystal structure was determined using high quality powder X-ray diffraction data by Perrin and co-workers.[107] Researchers have attempted to understand the relationships between the three polymorphs by DSC.[108,109] First of all, heating form I (the commercially available form) to 190 °C (the melting point of form I is 170 °C) followed by rapid cooling to 25 °C, produces an amorphous form. Heating the amorphous form to about 75 °C results in the formation of form III (form III can only prepared by this method). Further heating to around 140 °C causes form III to transform to form II and finally melts at 159 °C. From the results of DSC experiments,[108,109] the relationships among these three polymorphs is that form I is the most stable form and it is monotropic with respect to forms II and III; forms II and III are enantiotropically related, with the transition temperature at 140 °C.

1.2.3 Polymorphism in the Process of Crystallization from Solution

For a long time, it was quite difficult to understand why one polymorph is formed under certain conditions from solution, rather than another form. After long-term and detailed research work, scientists concluded that the preferential formation of a given polymorph under a particular set of experimental conditions depends largely on kinetic factors and the mechanism of the crystallization process.[110,111] In principle, the crystallization process of polymorphic systems involves three aspects: nucleation, crystal growth and the transformation from less stable forms to more stable forms. The processes of nucleation and crystal growth are controlled by kinetic factors. First of all, components aggregate into small clusters. These small clusters are unstable and are able to disperse into atoms, ions or molecules again; thus, at this stage, the process is reversible. As time goes on, these clusters become stable nuclei. Once the nuclei exceed a critical size, they finally grow into crystals. Therefore, the arrangement of components in the first batch of stable nuclei plays a key role in dictating the crystal structure (and hence the polymorph) of the crystal formed finally.

In general, all conditions involved in a specific crystallization process may affect the formation of specific polymorphs. These conditions include solvent effects,[112-114] additives, [115,116] temperature or pH values [117] as well as the crystallization methods.

1.2.4 Characterizations of Polymorphs

When a given compound has two or more polymorphs, the relationship among the different forms can be established using a combination of characterization techniques. Apart from DSC mentioned above, other analytical techniques used extensively are single-crystal X-ray diffraction (SCXRD), powder X-ray diffraction (PXRD), solid-state NMR, hot stage microscopy, etc.

SCXRD is the more powerful tool for polymorphic characterization as it can provide complete 3D structural information and atomic positions. However, sometimes it is not easy to obtain suitable single crystals for this technique. In such cases, PXRD becomes the alternative tool. PXRD is not only used for phase identification of different polymorphs but, nowadays, it is also used for structure determination. The details in this regard are given in chapter 2. Spectroscopic techniques, such as solid-state NMR, are very useful for characterization of polymorphs and can be used to study the different chemical environments of the nuclei in different polymorphs. In addition, hot stage

microscopy is used to determine the phase transition temperature (if one exists) and help to identify the changes in crystal shape. It should be noted that the techniques listed above are only a few the methods used for characterizing polymorphs. As technology evolves, new techniques will emerge in the future.

1.2.5 The Polymorphism in Co-Crystals

There is no doubt that, just like singe-component crystals, co-crystals are also able to exhibit polymorphism, i.e., different packing arrangements but with the same composition in the crystal structures. The phenomenon of polymorphism in single-component crystals has been recognized and studied for a long time and research in this regard is still ongoing. However, recently the subject of co-crystals has seized the attention of a great number of chemists. Few polymorphic co-crystal systems have been reported in the literature compared to single-component crystals and research on polymorphism in the case of co-crystals is still at a relatively early stage.

As discussed above, polymorphism is an important issue in the pharmaceutical industry in relation to human safety. Generally, drug products need to receive regulatory approval for only one particular crystal form or a specified polymorph by the relevant government agency in different countries (such as FDA in the U.S., Medicines and Healthcare Products Regulatory Agency (MHRA) in the U.K., or the European Medicines Agency for EU). If a new drug can exist in different solid forms that differ in their physicochemical properties (which, consequently, would affect the drug product performance or stability), then the appropriate solid form must be specified. Therefore, in the pharmaceutical industry, lots of money and time are being spent on this aspect every year. Similarly, polymorphism of co-crystals is also a crucial issue, if pharmaceutical co-crystals are to reach the pharmaceutical market. However, only recently, pharmaceutical researchers recognized the importance of co-crystals, and investigations regarding polymorphism of co-crystals are less frequent. Therefore, understanding the details of polymorphism of co-crystals and systematic studies regarding co-crystals are still evolving.

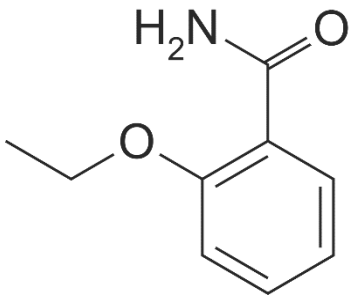

Figure 1.7. *The structure of ethenzamide.*

To date, only limited examples of polymorphic co-crystal systems have been reported in the literature. For example, Braga and co-workers reported a 1:1 co-crystal system of 4,4'-bipyridine and pimelic acid, which has three polymorphs.[118] Forms I and II both convert into form III at high temperature, with forms II and III being the thermodynamically stable forms at room temperature and high temperature, respectively. Moreover, based on the results from X-ray diffraction and solid-state NMR data, they concluded that no proton transfer takes place from the acid to the base. Halasz and co-workers discovered another 1:1 co-crystal system of 4,4'-bipyridine and 4-oxopimelic acid, which has two conformational polymorphs.[119] Form I was obtained by crystallization from ethanol, while form II was obtained from methanol. Form II can transform to form I by heating or by mechanochemical methods.

Ethenzamide (Figure 1.7), an analgesic drug, is used for the relief of fever, headaches and other minor pains. However, due to its poor water solubility, it is mainly used in combination with other ingredients, such as paracetamol, aspirin, caffeine and ibuprofen, etc. In order to improve its solubility in water and other physicochemical properties, several co-crystals of ethenzamide have been synthesized. Among these co-crystals, some exhibit polymorphism. For example, a 1:1 co-crystal of ethenzamide and gentisic acid has been reported by Aitipamula and co-workers, which has three polymorphs.[120] Form I was obtained by solution crystallization or solid-state grinding, while forms II and III were obtained only by solution crystallization. Forms II and III convert into form I by solid-state grinding. Apart from this co-crystal system, 1:1 co-crystal systems of ethenzamide with saccharin,[121] 3,5-dinitrobenzoic acid [122] and ethylmalonic acid [123] exhibit two polymorphs in each case.

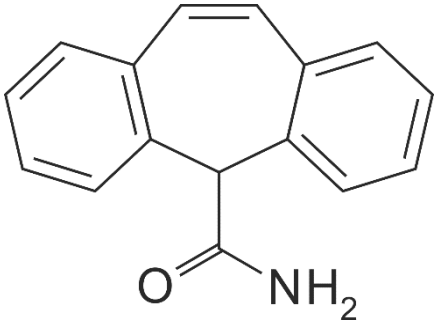

Figure 1.8. *The structure of carbamazepine.*

Another interesting example of a pharmaceutical substance which exhibits polymorphism in co-crystal systems is carbamazepine (Figure 1.8). For example, the 1:1 co-crystals of carbamazepine with nicotinamide,[124] saccharin[124] and isonicotinamide[125] have two polymorphs in each case, and a 2:1 co-crystal of carbamazepine/malonic acid has two polymorphs.[126] Other pharmaceutical co-crystals also exhibit polymorphism.[127-130] There is no doubt that, with the development of co-crystals, the number of polymorphic co-crystal systems will increase over time.

In practice, the process of searching for all different solid forms of a given compound is called polymorph screening. In principle, a comprehensive polymorph screening process is attempted to search for every solid form that can be prepared experimentally. In such a screening process, the number of preparation strategies should be as high as possible. However, due to limited budget and the current preparation strategies, no polymorph screening process can guarantee that all polymorphs of a given substance have been found. In fact, the process is still mainly based on a trial-and-error, case-by-case approach. There is no general method for finding all possible forms of a given molecule. As can be imagined, this process is often extremely time-consuming.

Due to the importance of polymorphism, scientists are attempting to develop models by using computer techniques to help predict the full range of polymorphs that can be formed by a given molecule. In the last decades, many theoretical approaches have been proposed and some successes were achieved.[101,131-136] These results are encouraging but, in the long run, there is still a lot of work needed to be done in order to achieve this goal.

1.3 The Purpose of the Thesis

As mentioned above, co-crystals have great potential applications in the pharmaceutical industry and a substantial amount of research has been done on this area. However, in practice, there are few commercial pharmaceutical co-crystals that have been approved for use in the pharmaceutical market. Therefore, this area still requires further investigation before co-crystals are able to be treated as a reliable technology in the pharmaceutical industry. In addition, polymorphism is an important issue in the pharmaceutical industry, as different polymorphs of a given API may affect the quality of the new drug product. During the development of a new drug, in order to ensure the required product quality, pharmaceutical companies have to spend substantial amounts of money and time to identify all polymorphic forms of the new drug. In the course of investigating pharmaceutical co-crystals, few polymorphic systems have been reported (as mentioned above), therefore, if pharmaceutical co-crystals are to be able to reach the market, understanding the details of polymorphism of pharmaceutical co-crystals is quite significant.

At present, most research on pharmaceutical co-crystals is related to a specific API, such as aspirin, paracetamol, or carbamazepine. That is to say, research on pharmaceutical co-crystals is still on a case by case basis. There is no general or systematic method for studying pharmaceutical co-crystals. Since the number of APIs is increasing every year and many substances can be used as coformers or excipients, there is no doubt that studying pharmaceutical co-crystals is extremely time-consuming. It is necessary to develop general and systematic approaches for studying pharmaceutical co-crystals. Among these API compounds, a number of commonly used drugs are aromatic compounds containing carboxylic acid functional groups, such as ibuprofen, aspirin, ketoprofen, etc. Through carboxylic acid groups, molecules of these drugs can co-crystalize with other excipients via hydrogen bonding.

Based on the importance of these drugs, we have attempted to develop a general co-crystallization strategy involving aromatic compounds containing carboxylic acid functional groups (trimesic acid) with two organic compounds containing amine functional groups (*tert*-butylamine and L-arginine), in order to investigate and demonstrate the structural diversity of these type of pharmaceutical co-crystals (in which one component is an API containing an aromatic ring and carboxylic acid

functional groups). We also used different co-crystallization conditions, including different solvents and different stoichiometric relationships between the components and different co-crystallization methods, to investigate the polymorphism in these co-crystal systems very comprehensively.

From the view point of crystal engineering, in the course of studying co-crystals, carboxylic acids and suitable N-containing compounds such as amides have been extensively investigated and the resulting co-crystals can form heteromeric systems with hydrogen-bonding patterns. Organic amines (NH_2R) are compounds with functional groups that contain a basic nitrogen atom with an electron lone pair. Obviously, amines also belong to N-containing compounds and can be used as hydrogen-bonding acceptors with carboxylic acids. In our present work, we focus on co-crystals of trimesic acid (TMA) with *tert*-butylamine (TBA) and co-crystals of trimesic acid with L-arginine, both of which are examples of carboxylic acid-amine heteromeric systems.

TMA is an important aromatic carboxylic acid and has attracted much attention because of its interesting structure. The TMA molecule has three carboxylic acid groups and can exist in the solid state in four different forms (corresponding to different levels of deprotonantion: H_3TMA, H_2TMA^-, $HTMA^{2-}$ and TMA^{3-}). Therefore, the structural diversity of co-crystals containing TMA is very interesting in our research, particularly with regard to the phenomenon of polymorphism. In Chapter 3, we present two polymorphic co-crystals of TMA and TBA. One is a solvated polymorphic system with 2:5:3 ratio of TMA, TBA and methanol; the other is a non-solvated polymorphic system with 2:3 ratio of TMA and TBA. Apart from these two polymorphic systems of TMA and TBA, we also discovered a series of solvates and hydrates of TMA and TBA with different ratios by using a series of solvents and crystallization methods. We discuss the structural diversity of the co-crystals of TMA and TBA in more detail in Chapter 4. In Chapter 5, we report and discuss the structures of co-crystals of TMA and L-arginine.

In addition, grinding methods have recently become a popular method for preparing pharmaceutical co-crystals; therefore, determining crystal structures directly from powder X-ray diffraction data has become a more important technique for characterization of co-crystals. Pillar[5]quinone is a potential molecule for molecular recognition and supramolecular host-guest chemistry. However, due to the fact that

large single-crystals of pillar[5]quinone cannot be prepared, the structure of pillar[5]quinone has not yet been reported. Therefore, in Chapter 6, we determined the structure of the co-crystal of pillar[5]quinone and 1,1,2,2-tetrachloroethane (solvent) directly from powder X-ray diffraction data.

Chapter 2 Experimental Techniques

2.1 Co-Crystallization Methods

Co-crystallization is the process of simultaneous crystallization of more than one component together into one crystal structure. According to the literature, there are a range of methods for the preparation of organic co-crystals. In general, the most common preparation methods are based on solution-state crystallization [137-140] and solid-state grinding.[50,141,142]

Solution methods are the simplest and commonest ways to prepare organic co-crystals and are easy to scale up for manufacturing in industry. In addition, co-crystals suitable for single-crystal X-ray diffraction can only be prepared through solution crystallization methods. Therefore, in the course of studying co-crystals, solution methods are the preferred way of synthesizing organic co-crystals. However, solution methods also have disadvantages. First, all components need to be suitably soluble in one solvent or mixture of solvents. Second, if the difference in solubility of the different components is large, the different components may crystallize separately. Third, in some cases, organic solvent molecules have been incorporated into crystal structures which causes crystals to be unstable at room temperature. Last, but not least, the processes of solution crystallization may be time-consuming and not environmentally-friendly.

Grinding methods are the alternative way to prepare organic co-crystals. These methods do not require the components to be soluble and, due to the absence of solvent or the use of only small amounts of solvent (so called liquid-assisted grinding), these methods are much more "green". Grinding methods are also generally quicker than solution methods. In addition, solid-state grinding may provide a way to synthesize new co-crystals which cannot be obtained by solution methods.[143]

Some researchers have attempted to prepare co-crystals containing the same components by both of these methods in order to compare the results.[121,144-149] These studies show that, in some cases, co-crystals obtained by grinding methods are the same as those from solution methods.[146,148] However, some co-crystals can only be obtained from one of the two methods.[121,147,148] For example, Aitipamula and co-workers[121] reported two polymorphs of the 1:1 co-crystal of ethenzamide and saccharin. Both

polymorphs could be obtained by slow evaporation from different solvents (methanol and acetonitrile). However, metastable form II was the only product from both neat grinding and solvent-assisted grinding. In other cases, co-crystals synthesized from the two methods are quite different.[145,149] For example, Trask and co-workers[149] attempted to synthesize co-crystals of caffeine with formic acid, acetic acid and trifluoroacetic acid via solid-state grinding and solution methods. Their results showed that, although some co-crystals can result from both methods, the co-crystals obtained from each method may have different stoichiometries. Furthermore, different co-crystal polymorphs can be obtained from each method. Therefore, in the course of studying co-crystals, employing more than one experimental method may result in the formation of a wider diversity of new co-crystals.

As research on organic co-crystals continues, apart from these two main methods, many other preparation techniques are emerging, such as the anti-solvent method,[150,151] reaction method,[152] co-crystallization assisted by ultrasound,[153,154] supercritical fluid method,[155,156] sublimation method,[128] slurry method,[157,158] and other strategies.[159-161]

2.1.1 Co-Crystallization from Solution

As mentioned above, the formation of co-crystals based on solution crystallization is very important. In general, solution methods for growing co-crystals mainly include slow evaporation and slow cooling. In order to grow co-crystals from solution successfully, we not only need to understand the intermolecular interactions among the components but, we also need to comprehend the co-crystallization process. In practice, the process of growing co-crystals from solution is quite complicated and many variables need to be considered in the process.

According to the classical view of crystal growth theory, the crystallization process from solution consists of two steps: nucleation and crystal growth.[162,163] First, at constant temperature and pressure, a number of small nuclei form from the components (ions and/or molecules). These nuclei are unstable and are able to disperse into their individual components again. As the solvent evaporates, these nuclei become stable and attain a critical size. Thus, the first, nucleation step is achieved. The next step is crystal growth. In this second stage, nuclei begin to grow and ultimately become the final crystals. This stage is affected by the nature of the solvent and any additives present.

In practice, preparing co-crystals of new components is based on experience. No general recipe exists. Therefore, a large number of different experimental conditions need to be tested for every system. Before trying to synthesize co-crystals from new materials, there are several important points to be aware of:

1. Pure materials should be used whenever possible as the impurities may affects the crystal growth.

2. The crystals obtained from solution do not necessarily contain all the solute components that are present in the solution. Thus, the crystals may contain just one component or may be a solvate of one component.

3. The process of co-crystallization may last over days, weeks or even months, so it is important to be patient and not to disturb the set up.

4. It is much better to leave the crystals in the liquor from which they have grown, particularly if there are solvent molecules incorporated into the crystal structures, as they may deteriorate on being removed from the mother liquor.

Slow evaporation is the simplest and the most important solution method for growing co-crystals. The process is to prepare a saturated or nearly saturated solution of all the components in a vial with a suitable solvent or mixture of solvents, then allow the solvent to evaporate undisturbed. Many co-crystals have been synthesized successfully by this method.[138,139,164-166]

As for crystallization of a single-component crystal, solvent selection is an important issue in the process of co-crystallization. Ideally, if all components have similar, moderate solubility in a specific solvent or mixture of solvents, then 1:1 co-crystals can be formed when equal molar components are dissolved in the solvent(s).[137] At present, the role of solvent in the formation of co-crystals is not fully understood. In some cases, changing the solvent will change the intermolecular interactions and cause different co-crystals to form. For example, in the course of studying co-crystals of 4-oxopimelic acid and 4,4-bipyridine, Halasz and co-workers[119] obtained two conformational polymorphs of a co-crystal with 1:1 molar ratio just by using different solvents (methanol and ethanol).

However, in some cases, slow evaporation of solvent may not lead to the formation of co-crystals. Instead, something else, such as a single-component crystal, a single-component solvate, a new polymorph of one component or mixtures of single-component crystal(s) and the co-crystal may form.[137,167,168] For example, Wenger and Bernstein[167] attempted to co-crystallize asparagine or glutamine with oxalic acid. Unexpectedly, they obtained two new hydrates of oxalic acid instead of co-crystals. In such cases, it is better to use non-equivalent component concentrations or to change the solvent system or even to try another co-crystallization method. In addition, co-crystals with the same components but different stoichiometries may be formed from different crystallization conditions (such as different solvents or different concentrations).[169,170]

Slow cooling is the most widely used scale-up crystallization method in the pharmaceutical industry. If co-crystals can be prepared by cooling crystallization, the same equipment used for conventional cooling crystallization can also be used for co-crystal crystallization. In theory, this method works well by following the rule: soluble hot and insoluble cold. This method for co-crystallization is carried out by preparing a saturated (or near saturated) solution of all components at a higher temperature, then slowly reducing the temperature. Some co-crystals have been prepared successfully by this method.[31,42,171-175] For example, Zhang and co-workers[171] reported a 2:1 co-crystal of theophylline and oxalic acid by cooling crystallization in a chloroform/methanol mixture (4:1, v:v). Sheikh and co-workers[176] demonstrated a generic, scalable, slow-cooling crystallization methodology for co-crystallization of carbamazepine/nicotinamide as a model system. This example shows that some techniques and equipment commonly used in single-component crystallization can also be used to control the process of co-crystallization with the desired benefits.

2.1.2 Co-Crystallization from Solid-State Grinding

The solid-state grinding method is not a new method for preparing co-crystals. In fact, the first reported organic co-crystal, quinhydrone, was obtained using solid-state grinding by Friedrich Wöhler in 1844[177]. In the past few decades, preparing co-crystals via grinding methods has become a more important topic due to the fact that these methods require no solvent or only a small amount of solvent compared to solution crystallization methods. As the process of producing drug products by solution methods in the pharmaceutical industry consumes a large amount of solvent and energy, leading

to environmental problems in the long run, scientists are trying to find new ways to improve this situation. Grinding methods are viewed as an effective and "green" way to prepare pharmaceutical co-crystals. In general, grinding methods include "neat" grinding (in the absence of solvent) and solvent-assisted grinding (in the presence of a small amount of solvent).

Neat grinding, also called dry grinding, consists of mixing two or more components together and grinding them manually, using a mortar and pestle, or mechanically, using an electrical mill, without any solvent. To date, many co-crystals have been successfully prepared by neat grinding.[121,142,178,179]

However, the mechanism of neat grinding remains poorly understood. Several mechanisms have been proposed for the process of neat grinding.[50,141,180] One of the recognized mechanisms is that neat grinding co-crystallization acts through molecular diffusion between the components. This mechanism requires that the components exhibit significant vapour pressures in the solid state. This mechanism was first proposed by Rastogi and co-workers in 1963[181] when they investigated the mechanism of the co-crystallization of hydrocarbons (naphthalene, phenanthrene and anthracene) with picric acid by neat grinding. In further studies, Rastogi and co-workers[182,183] monitored the reaction rates of co-crystals of picric acid with different aromatic compounds, further suggesting that both vapour and surface diffusion are important for the formation of these co-crystals. The role of grinding in these systems is to enhance the rate of surface diffusion of components and to make fresh reactive surfaces available.

Solvent-assisted grinding, also called liquid-assisted grinding or solvent-drop grinding, requires small amounts of an appropriate solvent added to the grinding mixture during grinding. Originally, the purpose of adding a small amount of solvent was to enhance the rate of co-crystal formation.[184] Therefore, the choice of solvent is important. It is required that at least a small portion of the original components can dissolve in the chosen solvent. Soon, it was found that the presence of a small amount of solvent, apart from increasing the rate of co-crystallization, could also provide benefits such as higher yield, higher crystallinity and control of the polymorphic outcome of co-crystallization.[185] One example is the co-crystallization of meloxicam with succinic and maleic acids,[186] which can be easily prepared by solvent-assisted grinding. Compared to the slow evaporation method, only a small amount of solvent is

used. If this method can be used widely for the preparation of pharmaceutical co-crystals, it would become much more efficient and environmentally friendly, and can save significant amounts of money and energy for pharmaceutical companies.

In general, in the course of liquid-assisted grinding, the liquid has a catalytic role. However, there is still no general explanation for the mechanism of solvent-assisted grinding and it varies from case to case. In some cases, the solvent is just a medium for molecular diffusion. In others, researchers suggest that the nature of the solvent may have a profound effect on the formation of the co-crystal. However, co-crystals prepared from neat grinding or solvent-assisted grinding are normally microcrystalline and are too small for structure determination by single-crystal X-ray diffraction. Sometimes, if we obtain microcrystals from grinding method, which cannot be crystallized directly from solution methods, then it is possible, using these microcrystals as seeds, to obtain large-size co-crystals by crystallization from solution.[149] In addition, due to the remarkable advances of the powder X-ray diffraction technique in recent years, we can employ the powder X-ray diffraction method to determine the crystal structure from the powder samples obtained directly from the grinding method.[187,188] Of course, structure determination from powder XRD data is enhanced by using information from other techniques, such as solid-state NMR. Even so, structure determination directly from powder XRD date remains more difficult compared to single-crystal X-ray diffraction methods.

2.1.3 Other Methods for Co-Crystallization

Since pharmaceutical co-crystals have attracted extensive attention in recent years, many new methods have appeared for pharmaceutical co-crystallization. For example, vapour diffusion is a good method for co-crystallization. It requires that all components have moderate solubility in one solvent and low solubility in another (the anti-solvent). Vapour diffusion is carried out by dissolving all components in the moderate solvent in a small glass bottle, which is placed inside a larger glass bottle that contains a small volume of the anti-solvent. The larger glass bottle is then sealed. Vapour from the anti-solvent will diffuse into the solution slowly, inducing crystals to grow in the solution. This method requires that the anti-solvent is more volatile than the solvent. For example, in this work, we used this method to prepare two polymorphs of a co-crystal system[189] composed of trimesic acid (TMA), *tert*-butylamine (TBA) and methanol with the stoichiometry $TMA_2TBA_5 \cdot (MeOH)_3$.

In the pharmaceutical industry, anti-solvent crystallization is an efficient way to control the particle size distribution of drug substances. Lee and co-workers [150,151] used anti-solvent crystallization to prepare co-crystals of saccharin with indomethacin and carbamazepine. In theory, the process is similar to vapour diffusion. The anti-solvent co-crystallization process is carried out by dissolving all components (saccharin with indomethacin or saccharin with carbamazepine) in methanol, then slowly adding purified water (the anti-solvent) to the solution using a peristaltic pump at room temperature over a period of about half an hour.

In practice, it is not possible to predict which method will work for a specific co-crystal system. If one method does not work or does not produce suitable crystals, adjusting the crystallization conditions such as the choice of solvents, temperature or method may be required. In general, the more crystallization conditions and methods that are used, the greater the potential to produce different new co-crystals or polymorphs. For example, Fucke and co-workers[174] reported, in the course of a study of piroxicam co-crystals, the formation of 46 co-crystals by using 20 different acids as co-crystal formers, five solvents and six crystallization techniques.

2.2 Characterization Methods for Co-Crystals

The goal of co-crystal characterization is to understand the physicochemical and crystallographic properties of the co-crystals. In general, co-crystals can be characterized by a wide variety of techniques, including single-crystal X-ray diffraction (SCXRD), powder X-ray diffraction (PXRD), differential scanning calorimetry (DSC), thermogravimetric analysis (TGA) and solid-state nuclear magnetic resonance (SSNMR).[190] As for single-component crystals, single-crystal X-ray diffraction is still the basic and best method for determining the crystal structure of co-crystals at the atomic level. However, it is not always easy to produce suitable, high-quality co-crystals for single-crystal X-ray diffraction, especially for co-crystals formed through grinding methods.

Originally, powder X-ray diffraction was just a tool used for phase identification of crystalline materials. Powder X-ray diffraction requires a small amount of powder. The data are much easier to record and it is also more convenient to identify phases from a recorded powder XRD pattern than using single-crystal XRD. In the case of co-crystals, from a recorded powder X-ray diffraction pattern, it is also easy to distinguish

whether a new co-crystal phase has been formed or not, owing to the fact that each compound has its own distinct powder XRD pattern. In addition, with the rapid development of powder X-ray diffraction techniques, using powder X-ray diffraction data for structure determination has become more and more routine.[191,192]

Apart from X-ray diffraction techniques, other methods of characterization also are available for co-crystals. DSC is a commonly used thermal method for determining the melting points, phase transitions and other properties of co-crystals. High-resolution solid-state NMR is another powerful technique for characterization of co-crystals. It is non-destructive and only requires a small amount of powder. It can provide detailed structural information about co-crystals and therefore it can be advantageous to use information from solid-state NMR to confirm details when carrying out structure determination from powder XRD data.

2.2.1 Single-Crystal X-ray Diffraction

A crystal is a solid material composed of atoms, ions or molecules that exhibit long range periodic order in three dimensions. X-ray diffraction is a powerful method for determination of crystal structure of crystalline materials, which involves determination of the unit cell parameters (the unit cell axis lengths *a*, *b* and *c* and the unit cell angles α, β and γ) and the atomic content of the unit cell [described by the atomic coordinates (x_1, y_1, z_1), (x_2, y_2, z_2), ⋯ (x_n, y_n, z_n)].

There is no doubt that single-crystal X-ray diffraction is the most unambiguous method for characterizing the structure of co-crystals at the atomic level, yielding detailed three-dimensional information such as bond lengths, bond angles and geometric properties of intermolecular interaction. If good single crystals can be prepared, single-crystal X-ray diffraction is the first choice for structure determination.

In 1895, German physicist Wilhelm Conrad Röntgen discovered X-rays. Subsequently, scientists began to explore the properties and applications of X-rays. X-rays are electromagnetic radiation of wavelength between *ca.* 1 Å to 100 Å, which is of similar order of magnitude to the periodic repeat distances in crystalline materials. This means that crystals can be used as a diffraction grating to scatter X-rays. In 1912, diffraction of X-rays by crystals was first observed, giving birth to X-ray diffraction and X-ray crystallography. In the same year, Sir W. L. Bragg developed Bragg's Law to explain the interference pattern of X-rays scattered by crystals.[193] In 1914, the first

structure (sodium chloride) was determined by single-crystal X-ray diffraction. After that, more and more structures of inorganic and organic compounds were solved by single-crystal X-ray diffraction. As a consequence, single-crystal X-ray diffraction has allowed scientists to better understand the three-dimensional structure of materials and intermolecular interactions in solid materials.

An X-ray diffraction measurement is based on constructive interference of monochromatic X-rays. Therefore, first of all, monochromatic X-rays are required. Usually, X-rays are produced by an X-ray tube. In the vacuum tube, a hot cathode (usually tungsten) releases electrons and these electrons were accelerated to a high velocity by a high voltage. These electrons then strike the anode (usually Cu or Mo), creating the X-rays. These continuous X-rays are then passed through a crystal monochromator, set to reflect one particular wavelength required for X-ray diffraction research.

Synchrotron radiation is another widely used X-rays source for X-ray diffraction research. A synchrotron is a type of particle accelerator. In a synchrotron, electrons are accelerated to a high speed close to the speed of light, and are then maintained at constant energy in a circular trajectory by a bending magnetic field. These higher intensity X-rays then pass through a crystal monochromator set to reflect the particular wavelength required. Compared to X-rays created from X-ray tubes, the X-rays generated by synchrotron radiation possess higher intensity and a broader spectrum. Therefore, researchers can select the specific wavelength required for their experiment. In addition, diffraction patterns obtained from synchrotron radiation have significantly higher resolution and improved signal-to-noise.

When monochromatic X-rays strike a crystal sample, the X-rays are scattered by their interaction with the electrons, producing constructive interference if the geometry of the scattering process satisfies Bragg's Law:

$$n\lambda = 2d_{hkl}\sin\theta\,. \tag{2.1}$$

Here, the variable d_{hkl} is the spacing between adjacent atomic layers for the lattice planes *hkl* in a crystal. For example, in the case of monoclinic system:

$$\frac{1}{d_{hkl}^2} = \frac{h^2}{a^2\sin^2\beta} + \frac{k^2}{b^2} + \frac{l^2}{c^2\sin^2\beta} - \frac{2hl\cos\beta}{ac\sin^2\beta}, \tag{2.2}$$

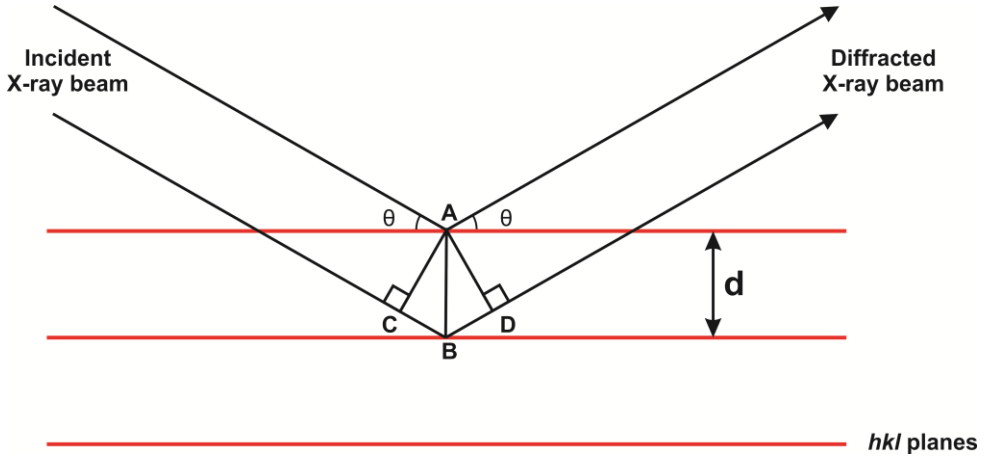

Figure 2.1. *The simplified derivation process of Bragg's Law*

Where, θ is the incident angle, n is the order of reflection (an integer), and λ is the wavelength of the beam. Bragg's Law is the fundamental equation of X-ray diffraction and provides a simple and convenient statement of the geometry of X-ray diffraction by crystals. The simplified derivation process of Bragg's law can been seen in Figure 2.1.

For constructive interference, the path difference between the waves scattered by electrons from adjacent lattice planes must be equal to an integer number of wavelengths, i.e.

$$\text{Path difference} = n\lambda = CB + BD. \tag{2.3}$$

According to the geometrical relationship shown in Figure 2.1, we can infer that

$$BC + BD = 2\,d_{hkl} \sin\theta. \tag{2.4}$$

Therefore, we can produce the equation of Bragg's law.

The aim of crystal structure determination is to determine the density of electrons ($\rho(\mathbf{r})$) in the crystal (where $\mathbf{r}$ is a vector in the unit cell), and to use the electron density map to calculate the actual real structure of the crystal. In order to create an electron density map, two pieces of information are needed: the amplitude and phase of the scattered X-rays. These two pieces of information can be expressed by a complex number, called the structure factor $F(\mathbf{H})$. The relationship between structure factor (reciprocal space vectors) and electron density (direct space vectors) can be illustrated by a mathematical operation called the Fourier transform, as follows:

$$F(\mathbf{H}) = |F(\mathbf{H})|\exp[i\alpha(H)] = \int \rho(\mathbf{r})\exp[2\pi i\,\mathbf{H}\cdot\mathbf{r}]d\mathbf{r}. \quad (2.5)$$

Here, **H** is the position vector in reciprocal space for the diffraction maximum (*hkl*) (i.e., **H** = *h* **a*** + *k* **b*** + *l* **c***), and **a***, **b*** and **c*** are the unit cell vectors in reciprocal space, while **r** is a position vector in direct space (i.e., **r** = *x* **a** + *y* **b** + *z* **c**), and **a**, **b** and **c** are the unit cell vectors in direct space. $|F(\mathbf{H})|$ is the amplitude and $\alpha(\mathbf{H})$ is the phase angle of the scattered X-ray corresponding to the diffraction maximum (*hkl*). The integration is performed over all vectors **r** in the unit cell.

Unfortunately, in an X-ray diffraction measurement, only the intensities of scattered X-ray beams are measured, which is related to the structure factor amplitude $|F(\mathbf{H})|$ (the intensities are proportional to the squares of the amplitudes). However, information on the phase angles cannot be obtained from experimental measurements. This is called the phase problem, which is the major problem in crystal structure determination. Since the diffraction pattern is the Fourier transform of the electron density, the electron density is the inverse Fourier transform of the diffraction pattern.

$$\rho(\mathbf{r}) = \frac{1}{V}\sum_{\mathbf{H}}|F(\mathbf{H})|\exp[i\alpha(\mathbf{H}) - 2\pi i\,\mathbf{H}\cdot\mathbf{r}], \quad (2.6)$$

where *V* is the volume of the unit cell, and the summation is over all vectors **H**. Thus, without the information about the phases, the inverse Fourier transform (Equation 2.6) cannot be performed. Researchers have developed several methods to recover information on the phases. The Patterson method and direct methods are the two major methods for recovering the phases in structure solution in small-molecule single-crystal X-ray diffraction data analysis.

The Patterson method was introduced in 1934.[194] As mentioned above, if we carry out an inverse Fourier transform of the structure factors (requiring both amplitudes and phases), we get the electron density map. However, if we carry out an inverse Fourier transform of the intensities from the measured data, the resulting map we get is called a Patterson map and is a map of the vectors between atoms. Using the Patterson method, it is possible to work out the positions of the atoms for small structures. If there are *n* atoms in the unit cell of the crystal, then there are n^2 interatomic vectors in the pattern map. Therefore, if *n* becomes larger, it is very difficult to solve the structure by

the Patterson method. In practice, it is mostly used for simple structures or structures containing a few 'heavy' atoms (i.e., atoms with high atomic numbers) as the Patterson map is dominated by the vectors between heavy atoms.

Due to the development of computer techniques, direct methods have become the most useful strategy for solving crystal structures.[195] Direct methods are mathematical methods to solve the phase problem that rely on the reasonable assumption that the electron density in the unit cell should be zero or positive everywhere in the unit cell. This creates certain relationships between the phases of sets of structure factors. These relationships can be used to deduce possible values for the phases. In general, direct methods employ such relationships with no previous knowledge about the crystal structure to solve the crystal structures. It is almost a trial and error process and often described as a "black box", because the process is automated by computers. In addition, the final structure from the direct methods calculation or Patterson method is only an initial approximation of the true structure and requires further refinement.

Space groups with screw axes, glide planes or centring result in diffraction patterns with certain reflections "missing" (i.e., the structure factor is zero). These are called systematic absences or systematic extinctions. The combination of the symmetry of the reciprocal lattice and the presence or absence of certain types of reflections is used to determine the space group of the crystal lattice. In a single-crystal X-ray diffraction experiment, the identification of systematic absences is done automatically by the data collection software on the diffractometer. However, during the process of crystal structure determination from powder X-ray diffraction data, in some cases, the systematic absences are not sufficiently decisive to differentiate between alternative space groups (for example, $P2_1$ and P2/m).

In general, single-crystal X-ray diffraction experiments involve three steps:

1. Growing a high quality single crystal large enough and with no significant cracks. Preferably, the size of crystal should be in the range 0.2 - 0.4 mm in the three directions of space because excessively small crystals are not suitable for single-crystal X-ray diffraction.

2. Collecting the X-ray diffraction data. First, a suitable crystal is fixed on the tip of a thin glass fibre using glue or in a loop including specific oil (for low

temperature experiments), which is then mounted on a goniometer head. The crystal is rotated through various angles with respect to the X-ray beam, producing a diffraction pattern. It is necessary to know the stability of the crystal. If the crystal is sensitive to air (mainly water) or unstable (solvate crystals) then special treatment is required. For example, if a crystal is sensitive to air, it can be sealed in a glass capillary. The glass is amorphous and thus does not affect the diffraction pattern. If the crystal is solvated and unstable at room temperature, we can collect the data at low temperature. In addition, data collection at low temperature can reduce the atomic mobility and thus enhance the diffraction intensities. Data is usually collected between 3° and 40° (2θ) and the process takes several hours, depending on the sample and the diffractometer. Usually, it is possible to determine the unit cell parameters from the first few images.

3. The 2D diffraction patterns are converted into a 3D model of the electron density by Fourier transformation. In this step, first of all, corrections of the measured intensities should be carried out. A common correction is the Lorentz-polarization correction. The Lorentz factor is related to the instrument geometry, whilst the polarization factor is due to the fact that the reflected X-rays are partially polarized. Another correction is for the absorption of X-rays by the crystal, particularly for crystals containing heavy atoms, since heavy atoms can strongly absorb X-rays. After corrections, the phase problem should be solved by direct methods or Patterson methods.

In the process of solving the phase problem, the structural model obtained is only approximate and has to be refined. Refinement is carried out by optimizing the fit between the observed and calculated intensities in the diffraction pattern. The refinement process includes adjustment of the positions of atoms and of anisotropic displacement parameters. When the following conditions are achieved, then the refinement is considered finished: a) the value of *R*-factor (*R*, Equation 2.7) and the weighted *R*-factor (R_w, Equation 2.8) are small enough. A value of *R* less than 5% is considered indicative of a good refined structure and high quality samples will result in *R* less than 2.5%. R_w is similar to *R* and the value of R_w is always higher than *R*. The *R*-factors are defined as

$$R = \frac{\sum \left| |F_o| - |F_c| \right|}{\sum |F_o|}, \tag{2.7}$$

$$R_w = \frac{\sum w \left| |F_o| - |F_c| \right|}{\sum w |F_o|}, \tag{2.8}$$

where $|F_o|$ is the observed structure factor amplitude, $|F_c|$ is the calculated structure factor amplitude and w is a weighting factor. b) The structural model is chemically reasonable. c) The estimated standard deviations for all parameters are sufficiently small. In practice, in the process of determining a small-molecule single crystal structure, the most widely used software for structure solution and refinement are SHELXS and SHELXL,[196] and these are called via the WinGX user interface.[197] Once the structure is refined, a standard file (CIF: crystal information file) containing all the information of the structure is created.

2.2.2 Powder X-ray Diffraction

Conventionally, powder X-ray diffraction is used as a rapid tool for phase identification of a crystalline material and if the sample is a mixture of more than one phase, in principle, all phases present can be identified due to each crystalline material having its own unique powder pattern. However, with recent developments of powder X-ray diffraction techniques, we can also use powder X-ray diffraction data for structure determination,[191] often combined with other techniques, such as high-resolution solid-state NMR.

Before carrying out structure determination from powder XRD data, a high quality powder XRD pattern should be recorded. There are two main ways to obtain high quality powder XRD data: conventional laboratory powder X-ray diffractometers and synchrotron X-ray diffractometers. Under normal conditions, powder XRD data obtained from a conventional laboratory powder X-ray diffractometer is already good enough for structure determination. However, in some cases, there are significant advantages to using synchrotron X-ray powder diffraction data. For example, sometimes, powder patterns recorded on conventional powder X-ray diffractometers suffer from peak overlap, a big issue for determination of unit cell parameters (see below). In contrast, the data recorded from a synchrotron source with higher resolution may make it possible to determine the unit-cell parameters successfully.[191,198] In

general, there are three stages for determination of crystal structures from powder X-ray diffraction data: [199-201] unit cell determination and space group assignment, structure solution and structure refinement.

The first stage is unit cell determination, also called "indexing". The process is carried out by using programs for automatic indexing, including: TREOR,[202] ITO,[203] or DICVOL,[204] which are incorporated into the program CRYSFIRE.[205] In practice, we use more than one program for indexing because these programs employ different methods for indexing and usually offer several different, possible sets of unit-cell parameters for a given set of powder XRD data. Normally, we pick out about 20 individual, non-overlapped peaks at low angles for indexing. The peaks in the high angle region cannot be trusted in this process due to extensive overlap.[206] Indexing is a very important step. If the correct unit cell cannot be found, then we cannot proceed to the next stage.

If the unit cell parameters have been determined, then the next task is the space group assignment. We use the program CHEKCELL[207] to assist in space group identification. Using the unit cell parameters obtained from indexing, the program CHEKCELL gives some suggested space groups. In the next stage, we use Le Bail profile fitting[208] to check all of these options in order to obtain the right space group, using the GSAS [209] software and its graphical user interface editor EXPGUI.[210] The Le Bail method fits the complete experimental powder XRD data by refinement of variables that include peak positions (including unit cell parameters and zero-point shift parameter), peak widths, peak shapes, background intensity distribution, and peak intensities. In the Le Bail fitting procedure, no structural model is used and the aim is to obtain reliable values of the variables that describe different features of the powder diffraction profile. In this case, the intensity data extracted from the powder XRD pattern are not used in the structure solution process. Instead, the determined values of variables that describe the features of the powder diffraction profile are required in order to construct the calculated powder diffraction pattern for the trial structure. In this stage, comparison of the experimental data with the calculated data is assessed by the whole-profile figure-of-merit, R_{wp}, which is defined as below (Equation 2.9). Following Le Bail fitting, the space group can be assigned by identifying the conditions for systematic absences in the intensity data. If the space group cannot be assigned uniquely,

structure solution calculations (the next stage) should be carried out in parallel for each of the possible space groups.

Before performing structure solution, the contents of the asymmetric unit must be established. By consideration of the unit cell volume, space group and density, the contents of the asymmetric unit can be established theoretically. High-resolution solid-state NMR can also be helpful for this purpose; for example, in some cases, solid-state ^{13}C NMR spectroscopy can be used to determine the number of independent molecules within the asymmetric unit.

The purpose of structure solution is to obtain a best approximation to the true structure. In this stage, we use the direct-space strategy for structure solution,[191] carried out using a genetic algorithm (GA) method[201,211,212] incorporated in the program EAGER.[195] The quality of trial structures is assessed by comparison between the calculated powder XRD pattern for the trial structure and the experimental powder XRD pattern. This comparison requires an appropriate *R*-factor. In our method, we use the weighted powder profile *R*-factor (R_{wp}), which is defined as

$$R_{wp} = \sqrt{\frac{\sum_i w_i \left(y_i - y_{ci}\right)^2}{\sum_i w_i {y_i}^2}}, \qquad (2.9)$$

where y_i is the intensity of the ith point in the experimental powder pattern, y_{ci} is the intensity of the ith point in the calculated powder pattern, and w_i is a weight factor for the ith point ($w_i = 1/y_i$).

In EAGER, a number of trial structures are initially generated randomly, defined by a set of structural variables. Each molecule is defined by its position in the unit cell (three coordinates), orientation with respect to the unit cell (three angles) and torsion angles. There are $6 + n$ variables for each molecule in the asymmetric unit, where n is the number of torsion angles. These trial structures evolve subject to rules and operations (mating, mutation and natural selection). The quality of each trial structure is assessed by comparing the calculated powder XRD pattern of each trial structure with the experimental powder XRD pattern as discussed above. New structures are generated by mating and mutation. In mating, a number of pairs of structures ("parents") are selected and new structures ("offspring") are generated by swapping structural

information between the two parents. In mutation, some structures are selected from the population and random changes are made to parts of their structure to create mutant structures. In the course of natural selection, only the structures with lowest R_{wp} are allowed to pass from one generation to the next generation. After a sufficiently large number of generations, a best trial structural solution will be generated in the population and this structure should be close to the true crystal structure. Therefore, this structure is taken as the starting structural model for the next stage of the structure determination process. A schematic flowchart illustrating the procedure for evolution of the population from one generation to the next generation in the genetic algorithm technique for structure solution is shown in Figure 2.2.

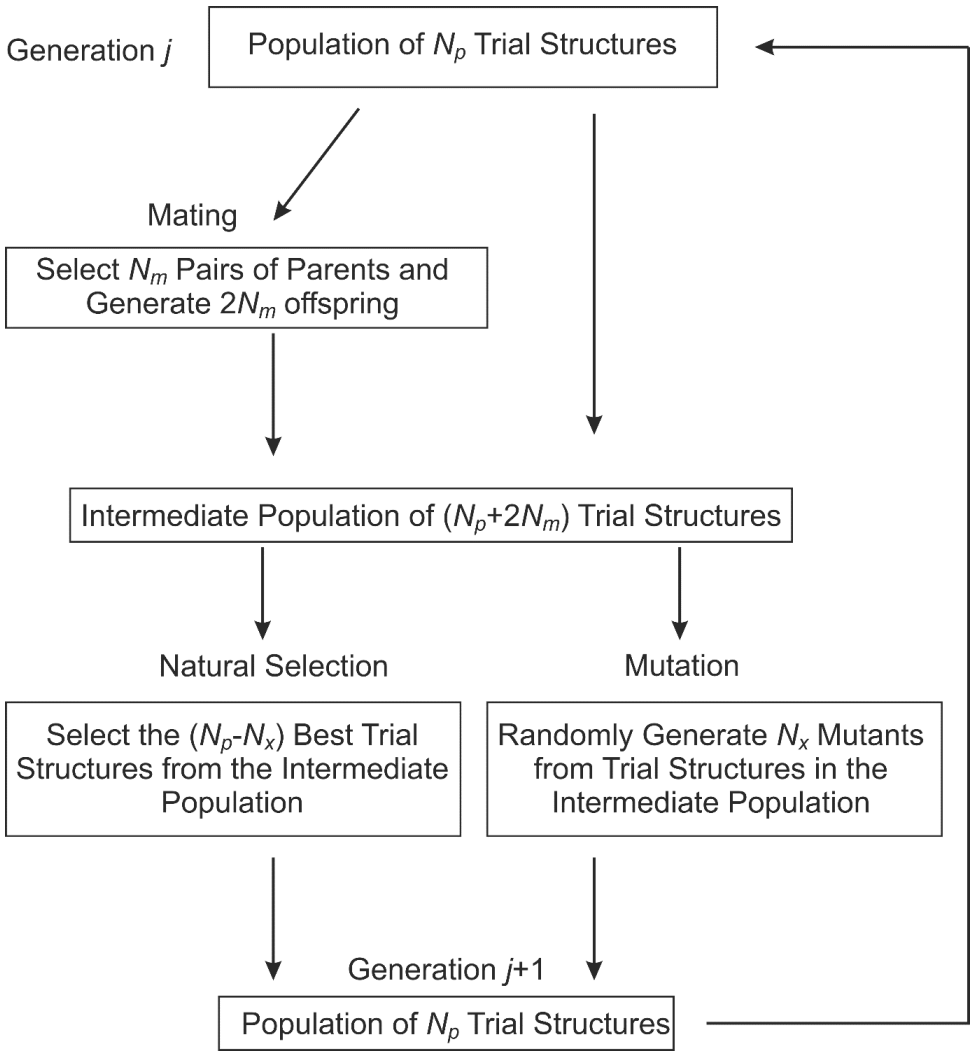

Figure 2.2. *Flow chart representing the evolution of the population from one generation (j) to the next generation (j + 1) in the genetic algorithm (GA) for powder structure solution.*

The structure with lowest R_{wp} in the final generation of the GA calculation is used as the starting structural model for Rietveld refinement,[213] which is carried out using the GSAS program. If the structural model from the structure solution calculation is a good approximation to the true structure, then a good quality structure may be obtained by Rietveld refinement. In Rietveld refinement, the atomic positions and atomic displacement parameters are adjusted. Thus, the constraints of planes (such as aromatic planes), bond lengths and bond angles are relaxed during Rietveld refinement. In terms of displacement parameters, U_{iso} values are refined and all atoms within the same molecule are generally set to the same value. For hydrogen atoms, the U_{iso} value is usually set to a value of 1.2 times that for the non-H atoms. In addition, if some molecules are considered to be disordered, the site occupancy can also be refined. During Rietveld refinement, the *R*-factor R_{wp} is used to assess the quality of fit between the experimental and calculated powder XRD patterns. In practice, Rietveld refinement may suffer from problems of instability. Therefore, it is necessary to use certain geometric restraints based on standard molecular geometries to ensure stable convergence of the refinement calculation. In addition, difference Fourier maps can be used in order to help Rietveld refinement and to check the correctness of the refined structural model. In general, the final structural parameters obtained from powder XRD data are not as accurate as structural parameters obtained from single-crystal XRD data. However, it is good enough for us to understand the arrangement of atoms and molecules in the crystal structure and the intermolecular interactions (such as hydrogen bonding).

In addition, structure solution will succeed only if the powder XRD pattern contains reliable information on the peak intensities. However, the existence of preferred orientation can significantly change the peak intensities and thus hinder the determination of the crystal structure from powder XRD data. When the crystallites are oriented preferentially in certain directions instead of randomly, preferred orientation arises. When the crystal shape is strongly anisotropic, such as long needles or flat plates, preferred orientation can be very severe. Since structure solution using the direct-space method starts with no knowledge of the correct structural model, the existence of preferred orientation can impose severe limitations on searching for an approximately correct structural model from scratch. Therefore, we need to address this problem during structure solution. The existence of preferred orientation can be detected by measuring the powder XRD pattern of the same sample in different types of sample

holder (e.g., capillary versus flat sample) or different measurement geometries (e.g., reflection versus transmission). If the sample exhibits preferred orientation, we need to re-prepare the sample in order to make sure that the sample is free of preferred orientation. Methods including repacking in a different sample holder (often the effects of preferred orientation are less severe using capillary than flat tape), regrinding (appropriate grinding can make the crystal morphology as isotropic as possible), recrystallization or mixing the powder sample with an amorphous material, such as starch.[214] When a sample without preferred orientation or only slight preferred orientation is obtained, it is used to record high quality powder XRD data for structure determination.

2.2.3 Thermal Analysis

Thermal analysis methods are well-known and commonly used techniques in many areas, such as pharmaceuticals, polymers, etc.[215] Differential scanning calorimetry (DSC) and thermogravimetric analysis (TGA) are the most commonly used and are distinguished from each other by the property measured: heat difference and the change in mass, respectively.

DSC investigates how the heat capacity of a material changes as the function of temperature under a controlled atmosphere. This information allows phase transitions (e.g., melting, glass transition, crystallization or decomposition) to be identified. DSC experiments are carried out in a chamber which consists of a sample holder and a reference holder. Usually, the sample is sealed inside a small aluminium pan and the reference is an empty pan and cover. The difference in heat flow to the sample and the reference is recorded as a function of temperature. Both the sample and reference are maintained at the same temperature throughout the experiment. The result of a DSC experiment is a plot of heat flux versus time or temperature. In DSC data, each peak corresponds to a specific thermal process, see Figure 2.3.

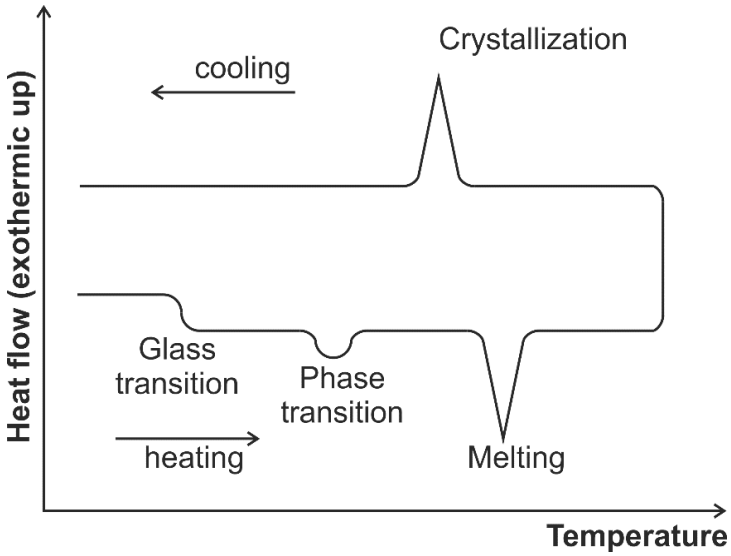

Figure 2.3. *A schematic DSC pattern with typical thermal processes.*

In general, in a DSC experiment, when the sample goes through a transformation, for example phase transition, more heat or less heat will need to flow to it to maintain the same temperature as the reference. Whether less heat or more heat flows to the sample will depend on whether the process is exothermic or endothermic. For example, when a sample melts, it requires more heat flowing into it, because melting is an endothermic phase transition. Similarly, when a sample undergoes an exothermic processes, such as crystallization, move heat is required. In addition, the glass transition is a very important property for amorphous materials. This process introduces a change in heat capacity and appears as a step change with respect to the baseline. By observing the difference in heat flow between the sample and reference, DSC can measure the amount of heat absorbed or released qualitatively and quantitatively. In order to obtain good data, we note that, in general, increasing the sample weight and/or increasing the rate of heating/cooling will increase the signal sensitivity, while lower sample weight and/or lower heating/cooling rates will increase the resolution.

TGA is a method that measures the mass change of a sample as a function of temperature under a controlled atmosphere. TGA is an extremely powerful thermal technique which can be used for studying several processes, including desorption, dehydration, decomposition, sublimation, etc. For example, in a decomposition TGA experiment, as the temperature increases, the components of the sample are gradually decomposed at different temperatures and the weight percentage of each resulting mass change can be precisely measured. Mass loss or percentage mass loss can be plotted as a

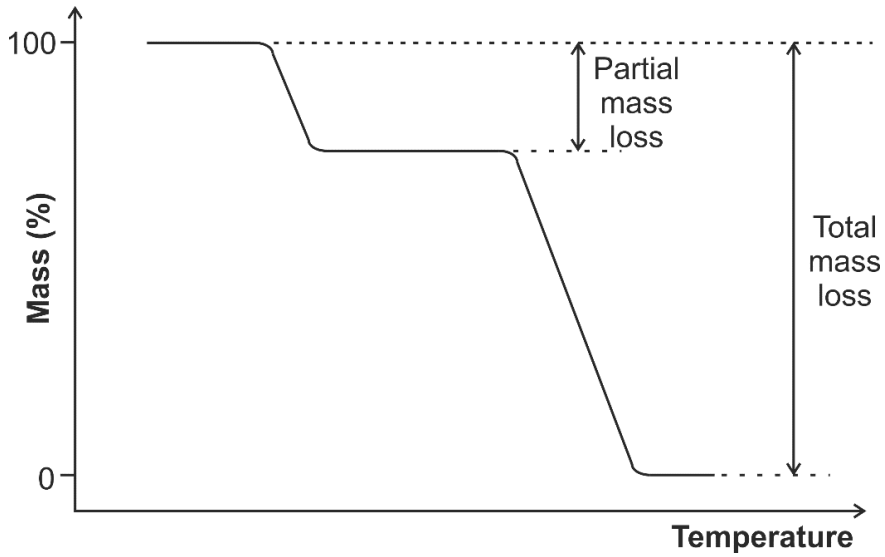

Figure 2.4. *A schematic TGA pattern illustrating partial mass loss (e.g., desolvation) followed by sample decomposition.*

function of temperature. From the TGA plot, we can analyse the decomposition behaviour of a given sample, see Figure 2.4.

2.2.4 Solid-State NMR

Solid-state NMR (SSNMR) is a powerful tool for characterization of solid materials and can provide detailed structural information due to the presence of anisotropic (directionally dependent) interactions. Anisotropic interactions have a substantial influence on the behaviour of nuclear spins. These interactions can be detected by solid-state NMR. However, in order to get high-resolution solid-state NMR spectra, a number of techniques/equipment are needed, including high-power ^{1}H decoupling, magic-angle spinning (MAS) and cross polarization (CP). In general, high-resolution SSNMR can provide the same type of information as that available from solution NMR.[216]

In solid-state NMR, nuclei in different chemical environments can give rise to different chemical shifts in the spectra and the position of these chemical shifts can be used to identify the structure of molecules. This kind of information is very useful in conjunction with determination of structure from powder XRD data. In practice, chemical shifts of nuclei are reported using δ values, which are usually expressed in parts per million (ppm). δ is defined as:

$$\delta = \frac{\nu_o - \nu_{TMS}}{\nu_s} \times 10^6 . \qquad (2.10)$$

Here, ν_o is the detected frequency, ν_{TMS} is the detected frequency of a reference substance (usually tetramethylsilane, (TMS)) and ν_s is the operating frequency of the spectrometer for the given type of Nucleus. The electron density, electronegativity of neighbouring groups and anisotropic induced magnetic field effects are the most important factors for influencing the value of the chemical shift. In general, electron density shields a nucleus from the external field, resulting in the chemical shift moving to an up-field position (lower δ value). A nucleus neighbouring an electronegative atom (such as I, Br, Cl, F) will have a reduced electron density and thus the chemical shift will move downfield (higher δ value). Electrons in π systems will interact with the external field which induces a magnetic field that causes anisotropy. The anisotropic induced magnetic field effects can be either shielded (lower δ value) or de-shielded (higher δ value), depending on the position of the nucleus.

From the number of the peaks in a ^{13}C SSNMR spectrum, in some cases, we can determine how many crystallographically distinct carbon atoms are present in the solid material and, thus, obtain information about the number of independent molecules in the asymmetric unit. In addition, for organic co-crystals composed of a carboxylic acid with organic base, powder X-ray diffraction cannot unambiguously determine whether proton transfer occurs from the acid to the base. ^{13}C SSNMR chemical shift analysis can help determine the protonation situation and hydrogen-bonding state of carboxylic acid and carboxylate groups.[217]

SSNMR can also be used to study molecular motions in solid materials using, for example, the CP/MAS experiment with dipolar dephasing. The aim of this kind of experiment is to simplify the high-resolution spectrum by removing signals that derive from any carbon atoms directly bonded to hydrogen (assuming a ^{13}C SSNMR experiment and the molecule is static). Thus, if a molecule contains carbon atoms directly bonded to hydrogen and the molecule is static, the peaks corresponding to these carbon atoms are absent in the spectrum recorded with dipolar dephasing compared to the spectrum recorded without dipolar dephasing. On the other hand, a molecule containing carbon atoms directly bonded to hydrogen that are mobile, or for a molecule containing carbon atoms not directly bonded to hydrogen (static or mobile), dipolar dephasing does not affect the intensity of the solid-state NMR signal. The basis of this experiment is simple: prepare sample as normal with CP (i.e., applying a 90° pulse to the ^{1}H channel of the spectrometer, then a spin-lock pulse is applied to the ^{1}H channel

and a contact pulse is applied to the ^{13}C channel in order to allow transference of magnetization from ^{1}H to ^{13}C nuclei (CP)). Then turn decoupling off (for ^{1}H channel), wait for an appropriate time (dipolar dephasing delay), decoupling on (for ^{1}H channel), acquiring the signal for the ^{13}C channel while performing ^{1}H decoupling to remove hetero-nuclear dipolar coupling. While the decoupling is turned off, the signal from any static carbon atoms strongly dipolar coupled to hydrogen will dephase faster than the signal derived from carbon atoms without coupling to hydrogen or mobile carbon atoms. If we choose the dipolar dephasing delay carefully, we can fully remove the signal from static carbon atoms that are directly bonded to hydrogen. Therefore, the resulting spectrum contains only signals from carbon atoms that are not directly bonded to hydrogen or mobile carbon atoms.

Chapter 3 Polymorphism of Co-Crystals of Trimesic Acid and *tert*-Butylamine

3.1 Introduction

Crystal engineering [218,219] of co-crystals concerns the design and synthesis of new molecular co-crystals with desired physicochemical properties based on the structure of the component molecules. The physicochemical properties of crystalline materials are influenced by the molecular arrangement in the crystal structure and the molecular arrangement is normally controlled by intermolecular interactions. Therefore, understanding intermolecular interactions in co-crystals is highly important. Among these intermolecular interactions,[220] hydrogen bonding, π-π stacking and van der Waals forces are the most influential. In particular, hydrogen bonding, due to its directionality and strength, is the most important tool for controlling the formation of organic co-crystals. Despite many successful co-crystallizations, it remains difficult to predict the crystal structure completely in advance, as the mechanism of co-crystallization is not fully understood. This is especially pertinent for organic co-crystals prepared by grinding methods.[221] Therefore, the field of crystal engineering still attracts many researchers.

Polymorphism is a very common phenomenon in nature. Due to different polymorphs having different physicochemical properties, it has potential applications in many industries, such as pharmaceuticals, dyes and pigments. In general, polymorphism is quite frequent in single-component crystals but, polymorphism in co-crystals and solvates is still a relatively rare phenomenon. In recent years, due to the subject of co-crystals becoming more and more important, research in polymorphism of co-crystals has gradually seized the attention of chemists and some polymorphic co-crystal systems have been reported in the literature.[118-120] In order to understand the details of polymorphism of co-crystals, research in this regard is still evolving.

Although it is very difficult to predict co-crystal structure in advance, selecting organic molecules with specific functional groups for preparing co-crystals with desired hydrogen bonding motifs may be possible. For example, organic compounds containing carboxylic acid functional groups have received significant attention due to their potential as hydrogen-bond donors to a variety of organic bases containing suitable N atoms which can act as hydrogen-bond acceptor, such as amides, pyridine and its

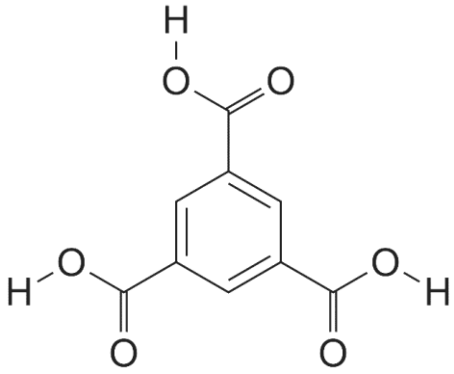

Figure 3.1. *The molecular structure of trimesic acid (TMA).*

derivatives.[57,60,61] Organic amines can also be used as a hydrogen bond acceptor with a carboxylic acid as the donor. Recently, the carboxylic acid-amine heteromeric system has drawn much attention.[222-224] In this chapter, we will present two novel polymorphic co-crystal systems containing acid-amine heteromers and analyse their crystal structures in terms of hydrogen bonding.

Trimesic acid (TMA), also known as benzene-1,3,5-tricarboxylic acid, is an important aromatic compound. It has attracted much attention because of its interesting molecular structure (Figure 3.1). TMA is a planar molecule with three carboxylic acid groups equally arranged around the benzene ring. It can exist in four forms in the solid state, depending on the degree of deprotonantion. For example, in the co-crystal of TMA and acetic acid,[225] TMA molecules exist in the form of neutral H_3TMA molecules, while in the co-crystal of TMA and N,N-dicyclohexylamine[226], TMA molecules are totally deprotonated and exist in the form of TMA^{3-} anions. The crystal structure of α-trimesic acid (the commercially available form) was determined by Duchamp and Marsh in 1969.[227] The basic motif of the α-TMA structure is a hydrogen-bonded, two-dimensional honeycomb (hexagonal) network. The main intermolecular interactions comprise the carboxylic acid dimer motif (graph set $R_2^2(8)$), arrangement of TMA molecules in a plane and interacting via this motif leads to a cavity of diameter of ~ 14 Å (Figure 3.2). However, these networks are not packed in a parallel, planar manner but as pleats with dihedral angles of about 70°. For the consideration of close packing, there is a triple concatenation of each network, leading to a triple interpenetration of each hexagonal hole. As TMA molecules can construct such honeycomb networks, they are often used as building blocks in the synthesis of hydrogen-bonded organic co-crystals [228-230] or metal-organic frameworks.[231-233] *Tert*-butylamine (TBA) (Figure 3.3) is an organic primary amine with a pK_a of 10.68,

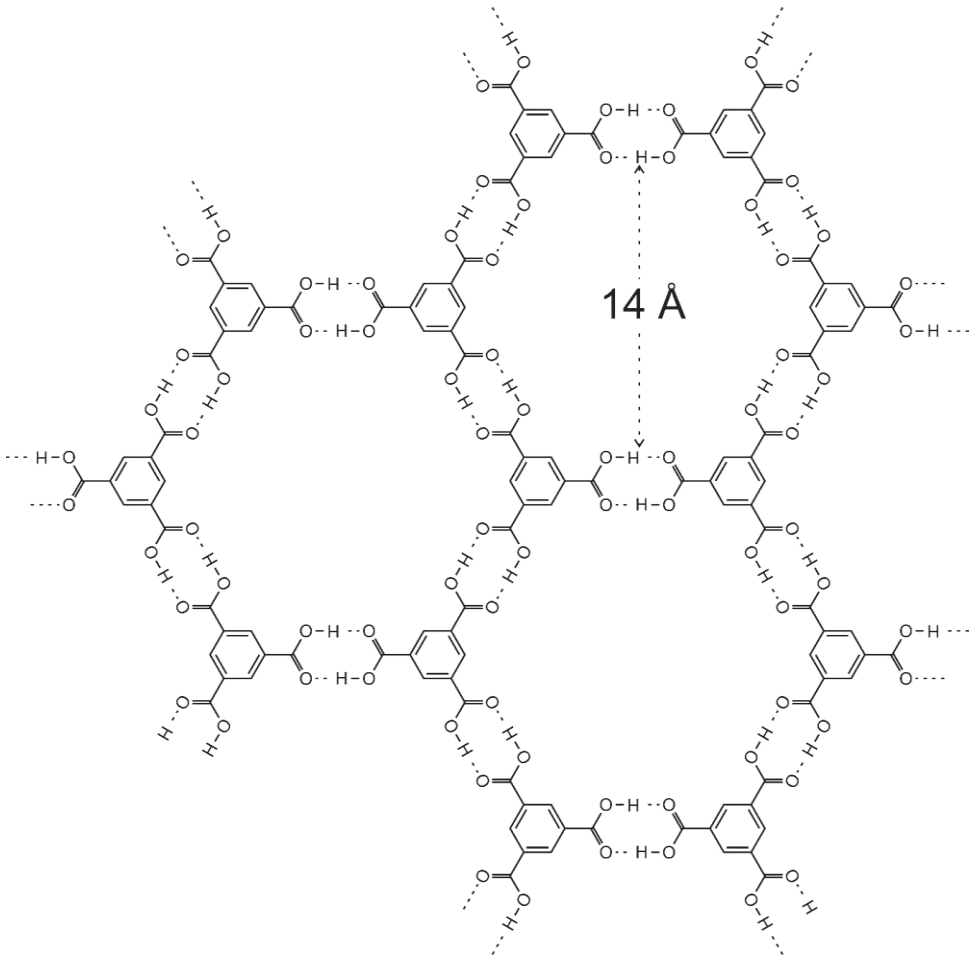

Figure 3.2. *The basic motif of the hydrogen-bonded hexagonal network in the crystal structure of α-TMA.*

indicating that it will exist almost always in the form of *tert*-butylammonium cations when interacting with carboxylic acid groups in aqueous solution or organic solvents. The geometry of the resulting *tert*-butylammonium cations is very interesting, as it can possesses a three-fold axis through the N–C bond with three identical N–H bonds that can act as strong hydrogen-bond donors. Therefore, it is possible to form geometrically well-defined hydrogen-bonding motifs. In addition, due to the steric effect of the *tert*-butyl group, the *tert*-butylammonium cation can only link with carboxylate groups through N–H···O hydrogen bonds when it co-crystallizes with carboxylic acids. As a whole, it is fascinating to investigate the co-crystal structures of TMA with TBA.

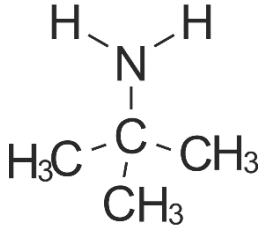

Figure 3.3. *The molecular structure of tert-butylamine (TBA).*

In the field of co-crystals, as mentioned before, the existence of polymorphism is not a common occurrence. However, molecules that possess multiple functional groups appear to be more likely to form polymorphs, because different hydrogen-bonding arrangements may arise between these functional groups in different polymorphs. In addition, molecules with several degrees of torsional freedom are also more prone to exhibit polymorphism due to the opportunity to exist in different conformers. The TMA molecule possesses three carboxylic acid groups with three torsional angles. Therefore, we expected that polymorphism might appear in organic co-crystals that containing the TMA molecule. In the course of studying co-crystals of TMA and TBA, we discovered that TMA and TBA form a series of co-crystals with different ratios, by using a series of solvents combined with different crystallization methods and different ratios of TMA and TBA in the crystallization solution. The resulting structural diversity of co-crystals of TMA and TBA in our research is very interesting, particularly with regard to the phenomenon of polymorphism. In this chapter, we present two novel polymorphic co-crystal systems of TMA and TBA. One is a solvated polymorphic system (with 2:5:3 ratio of TMA, TBA and methanol), which is particularly novel in having a large number of independent components in the asymmetric unit.[189] The other is a polymorphic co-crystal system with a 2:3 ratio of TMA and TBA. The other co-crystal structures of TMA and TBA discovered in this work are presented in the next chapter.

3.2 Polymorphism in Co-Crystals of $TMA_2TMA_5{\cdot}(MeOH)_3$

In crystallographic and structural chemistry, the number of independent molecules in the asymmetric unit is denoted by the parameter Z' and structures with high Z' (Z' = 2 to 4) are relatively common for systems with low symmetry, but structures with a value of Z' of more than four are extremely rare.[234] In recent years, the discovery of polymorphic systems with large numbers of independent molecules in the asymmetric unit has been become an interesting subject.[234-236] In our present work, we report the polymorphism of co-crystals of $TMA_2TBA_5{\cdot}(MeOH)_3$. The crystal structure of each polymorph is composed of ten independent molecules in the asymmetric unit. In the literature concerning polymorphic systems, there are very few examples comprising ten or more independent molecules in the asymmetric unit[237-239] and very few examples of co-crystals composed of three or more independent organic molecules. Therefore, polymorphism of co-crystals of $TMA_2TBA_5{\cdot}(MeOH)_3$ reported here can be considered very rare and interesting.

3.2.1 Synthesis and Structure Determination

The two polymorphs (denoted forms I and II) of $TMA_2TBA_5{\cdot}(MeOH)_3$ were prepared by vapour diffusion of anti-solvent into a solution of TMA and TBA in methanol. Vapour diffusion of acetone into a methanol solution containing TMA and TBA (TMA:TBA = 2:5, molar ratio in solution) at ambient temperature resulted, after a few days, in single crystals of form I. Vapour diffusion of ethanol into a methanol solution containing TMA and TBA (TMA:TBA = 2:5, molar ratio in solution) at ambient temperature resulted, after a few days, in single crystals of form II. The crystallization procedure to produce form II yielded monophasic samples, whereas our procedure to produce form I was frequently found to yield the concomitant formation of small amounts of form II.

Single-crystal X-ray diffraction data were collected at 150 K on a Nonius Kappa CCD diffractometer equipped with a molybdenum tube source ($\lambda = 0.71073$ Å). The crystal structures were solved (by direct methods) by SHELXS and refined using SHELXL.[196] Refinement of non-hydrogen atoms was carried out using anisotropic displacement parameters. All hydrogen atoms were located in difference Fourier maps and were added to the structural model according to idealized geometries. Refinement of hydrogen atoms was carried out using a riding model, with isotropic displacement parameter equal to 1.2 or 1.5 times the equivalent isotropic displacement parameter of the atom to which the hydrogen atom is bonded. Powder X-ray diffraction data were recorded on a Bruker D8 instrument ($CuK\alpha_1$; Ge monochromated; transmission geometry). Differential scanning calorimetry (DSC) data were measured on a TA Instruments Q100 using sealed aluminium pans and cooling rates between 1 and 20 °C min^{-1} under the N_2 atmosphere.

3.2.2 Structural Analysis and Discussion

The crystallographic parameters of the two polymorphs of $TMA_2TBA_5{\cdot}(MeOH)_3$, which have been determined from single-crystal X-ray diffraction, are summarized in Table 3.1 and the crystal structures of forms I and II are shown in Figures 3.4 and 3.5, respectively. In both forms of $TMA_2TBA_5{\cdot}(MeOH)_3$, the asymmetric unit comprises ten independent molecules: five $HTBA^+$ cations, one $HTMA^{2-}$ anion, one TMA^{3-} anion and three methanol molecules. For clarity, in this thesis, the abbreviations TMA and TBA in general refer to trimesic acid and *tert*-butylamine, respectively, without reference to the degree of protonation/deprotonantion. To indicate specifically the degree of

protonation/deprotonantion, we use TMA^{3-}, $HTMA^{2-}$, H_2TMA^- and H_3TMA to represent the different degrees of deprotonantion of TMA and we use $HTBA^+$ to represent the protonated TBA cation.

Table 3.1 The crystallographic parameters of forms I and II of $TMA_2TBA_5{\cdot}(MeOH)_3$

	Form I	Form II
Space Group	$P\bar{1}$	$P\bar{1}$
Temperature (K)	150 (2)	150 (2)
a/(Å)	10.3251(3)	10.2893(2)
b/(Å)	15.4590(4)	15.5312(2)
c/(Å)	17.7519(5)	17.6113(3)
α/(°)	69.964(2)	92.3960(10)
β/(°)	86.592(2)	106.2330(10)
γ/(°)	78.556(2)	100.9840(10)
V/(Å^3)	2608.96(13)	2639.14(8)
Z	2	2
R_1/(%)	4.88	5.39
R_{w2}/(%)	11.44	12.93

Table 3.2 The lattice parameters for the transformed unit cells of forms I and II of $TMA_2TBA_5{\cdot}(MeOH)_3$

	Form I	Form II
Space Group	$P\bar{1}$	$P\bar{1}$
a′/(Å)	20.2219(5)	20.1986(2)
b′/(Å)	19.9987(6)	21.7294(2)
c′/(Å)	10.3251(3)	10.2893(3)
α′/(°)	62.385(2)	83.640(1)
β′/(°)	48.527(2)	49.011(1)
γ′/(°)	85.268(2)	113.437(1)
Z	2	2

From the crystal structures of forms I and II, (see Figures 3.4a and 3.5a), we can see that, for each polymorph, the crystal structure comprises single hydrogen-bonded sheets with the planes of the TMA^{3-} and $HTMA^{2-}$ anions lying in the plane of the sheet and the $-N^+H_3$ groups of the $HTBA^+$ cations and the OH groups of the methanol molecules lying close to this plane as a result of intermolecular interactions (hydrogen bonding). The *tert*-butyl groups (TBA) and methyl groups (methanol) project outward from the sheets. For clarity, the three methyl groups of each *tert*-butyl group are omitted in the figures. The green dashed lines represent hydrogen bonds.

In order to compare these two polymorphic structures in more detail, we define a transformed unit cell (a', b' c') for each polymorph. The transformation relationship for form I is shown Equation 3.1 and for form II in Equation 3.2:

$$\begin{pmatrix} a' \\ b' \\ c' \end{pmatrix} = \begin{pmatrix} a \\ b \\ c \end{pmatrix} \bullet \begin{pmatrix} -1 & -1 & 0 \\ -1 & 0 & 1 \\ -1 & 0 & 0 \end{pmatrix} \tag{3.1}$$

$$\begin{pmatrix} a' \\ b' \\ c' \end{pmatrix} = \begin{pmatrix} a \\ b \\ c \end{pmatrix} \bullet \begin{pmatrix} 1 & -1 & 0 \\ 1 & 1 & 1 \\ 1 & 0 & 0 \end{pmatrix} \tag{3.2}$$

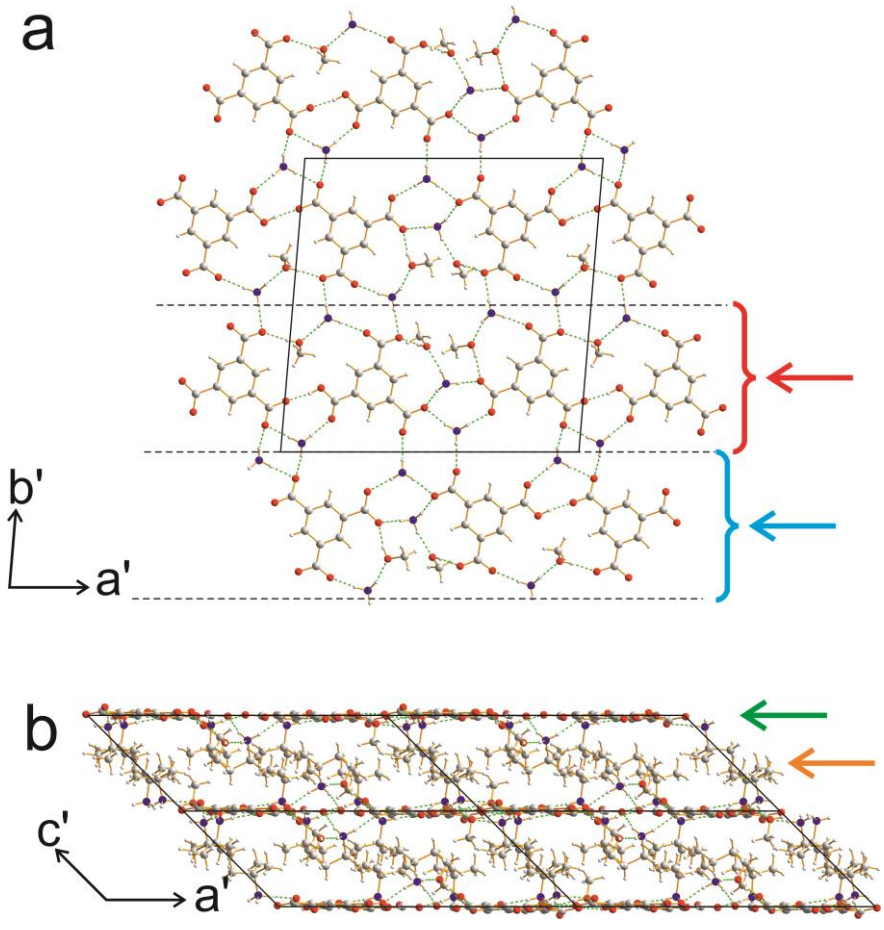

Figure 3.4. *Crystal structure of form I of the co-crystal of $TMA_2TBA_5{\cdot}(MeOH)_3$, viewed (a) perpendicular and (b) parallel to the plane of the hydrogen-bonded sheets. In (a), a single sheet is shown and the tert-butyl groups of the $HTBA^+$ cations are omitted for clarity. In (b), the green arrow indicates the hydrogen-bonded sheet and the orange arrow indicates the aliphatic region containing the methyl and tert-butyl groups.*

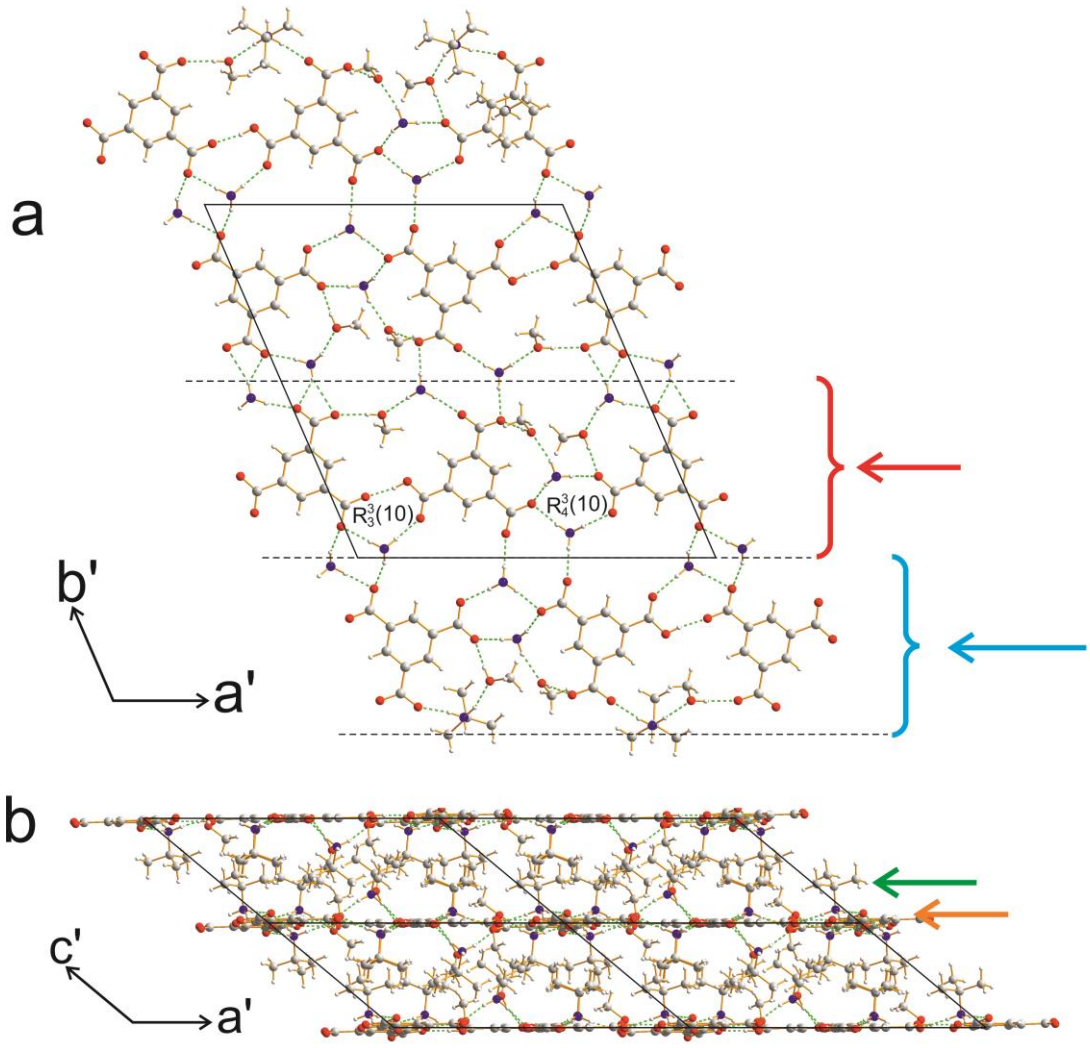

Figure 3.5. *Crystal structure of form II of the co-crystal of $TMA_2TBA_5{\cdot}(MeOH)_3$, viewed (a) perpendicular and (b) parallel to the plane of the hydrogen-bonded sheets. In (a), a single sheet is shown and the tert-butyl groups of the $HTBA^+$ cations are omitted for clarity. The unit cell shown is the transformed unit cell (a', b', c') defined in the text. In (b), the green arrow indicates the hydrogen-bonded sheet and the orange arrow indicates the aliphatic region containing the methyl and tert-butyl groups.*

Specifically, in the transformed unit cell, the a'-axis is parallel to the hydrogen-bonded ribbon motif that is common to forms I and II, the b'-axis is defined such that the a'b'-plane is parallel to the plane of the hydrogen-bonded sheet and the c'-axis is the periodic repeat vector between adjacent hydrogen-bonded sheets. The transformed unit cells (a', b', c') are shown in the plots of the crystal structures of form I (Figure 3.4) and form II (Figure 3.5). The lattice parameters for the transformed unit cells are summarized in Table 3.2.

From the crystal structures of forms I and II (Figures 3.4 and Figure 3.5), it is clear that there are both similar aspects and significant differences between these two structures, highlighted in particular by the overlay of the two structures in Figure 3.6. Specifically, within the sheets, forms I and II share a common hydrogen-bonded ribbon motif (parallel to the a'-axis of the transformed unit cell in each case), which runs horizontally in Figures 3.4a and 3.5a and is indicated as the region between the two dashed lines and marked by the red arrow (the symmetry related ribbon, generated by a crystallographic inversion centre, is indicated by the blue arrow in Figures 3.4a and 3.5a). From Figures 3.4b and 3.5b, we can see that the hydrogen-bonded sheets are stacked in a very similar manner that brings the *tert*-butyl groups and methyl groups together at the interface between adjacent sheets, with a similar perpendicular distance between the sheets in each polymorph (form I, 6.47 Å; form II, 6.55 Å).

In terms of $HTMA^{2-}$ and TMA^{3-} anions, the ribbon motif parallel to the a'-axis involves an alternation of the $HTMA^{2-}$ and TMA^{3-} anions along the ribbon. Within the $TMA^{3-}\cdots HTMA^{2-}\cdots TMA^{3-}$ repeat unit of these ribbons (periodic repeat distance along the ribbon: form I, a' = 20.22 Å; form II, a' = 20.22 Å), one $TMA^{3-}/HTMA^{2-}$ pair are linked by a direct O–H···O hydrogen bond involving the –COOH group of the $HTMA^{2-}$ anion and one of the $–COO^{-}$ groups of the TMA^{3-} anion, and the other two O atoms of these groups are bridged by an O···H–N–H···O hydrogen-bonding arrangement with an intervening $–N^{+}H_3$ group. Thus, this set of hydrogen bonds gives rise to a cyclic graph set $R_3^3(10)$.[55,56] The other $HTMA^{2-}/TMA^{3-}$ pair in the ribbon motif are linked by the interaction of a $–COO^{-}$ group from each of these anions with two intervening $–N^{+}H_3$ groups, which gives rise to a cyclic graph set $R_4^3(10)$. The primary difference between the structures of these two polymorphs lies in the relative disposition of adjacent ribbons of this type within the sheet and the nature of the hydrogen bonding between adjacent ribbons (Figure 3.6a, created by Dr Colan E. Hughes using the computer program Mathematica, constructed by aligning the a'-axes of forms I and II parallel to each other and by orienting the a'b'-planes of forms I and II parallel to each other) and some of these differences are highlighted by the yellow circles.

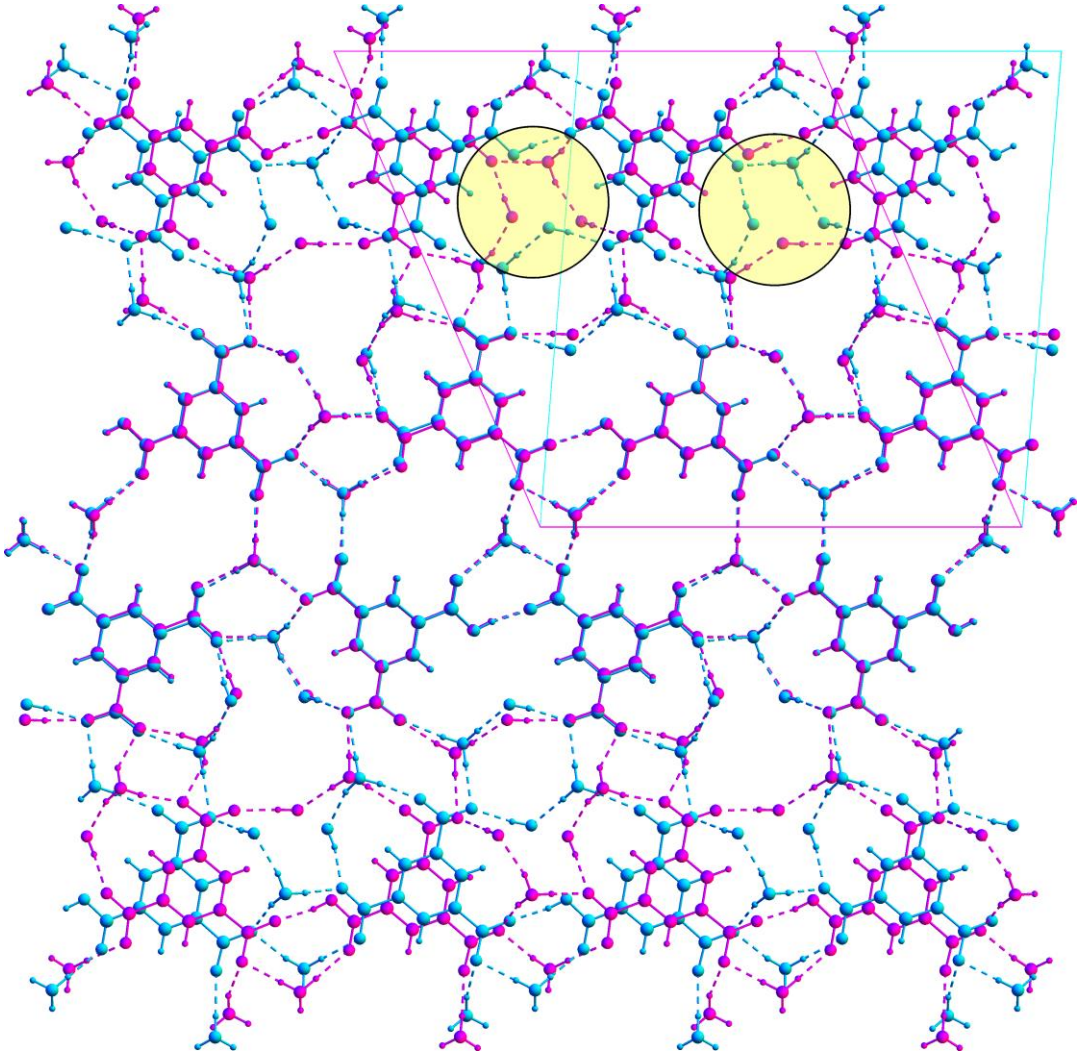

Figure 3.6a. *Overlay of the crystal structure of form I (cyan) and form II (magenta). The unit cell shown in each case is the transformed unit cell (a', b', c') defined in the text. The tert-butyl groups of the HTBA*$^{+}$ *are omitted for clarity.*

The hydrogen bonding involves the $–N^{+}H_3$ groups of $HTBA^{+}$ cations and the OH groups of methanol molecules located in the region between adjacent ribbons.

In terms of the $HTBA^{+}$ cations, for both polymorphs, all three N–H bonds in each independent $HTBA^{+}$ cation are used as donors in N–H···O hydrogen bonding to O atoms of the $HTMA^{2–}$ anion, the $TMA^{3–}$ anion or methanol molecules. With the exception of one specific N–H bond in form II (which forms a bifurcated hydrogen-bonding arrangement involving the two O atoms of a $–COO^{–}$ group of the $TMA^{3–}$ anion), all N–H···O hydrogen bonds involve a single O atom as the acceptor. In terms of methanol molecules, for each polymorph, the O–H bond in each independent methanol molecule is used both (i) as the donor in an O–H···O hydrogen bond with an O atom of the $HTMA^{2–}$ anion or the $TMA^{3–}$ anion as the acceptor and (ii) as the

acceptor in an N–H···O hydrogen bond with an N–H bond of an $HTBA^+$ cation as the donor.

In order to understand the relationships between these two polymorphs, we used DSC to investigate their relative stabilities as a function of temperature. However, we observed no transformations at room temperature or low temperature (down to –100 °C) for either polymorph. However, on standing in an ambient atmosphere, both polymorphs are highly susceptible to loss of methanol, resulting in the same crystalline phase in each case (Figure 3.6b). However, crystal structure determination of this new desolvated phase from powder X-ray diffraction data has not yet been successful.

3.3 Polymorphism of Co-Crystals of TMA_2TBA_3

As mentioned above and elsewhere (section 3.1), formation of carboxylic acid dimer interactions with the graph set $R_2^2(8)$ can yield an extensively hydrogen-bonded hexagonal network, as observed in the α-TMA crystal structure (Figure 3.2). Due to the low density, this kind of hexagonal network has potential as the structural basis of porous materials, the applications of which may be of particular interest. Similar extended hexagonal networks of TMA have also been found in co-crystals containing TMA molecules. However, due to the principle of close packing and space filling, interpenetration usually occurs in order to stabilize the structure.[229,240,241] However, it is also possible to avoid interpenetration by co-crystallizing TMA with a suitable

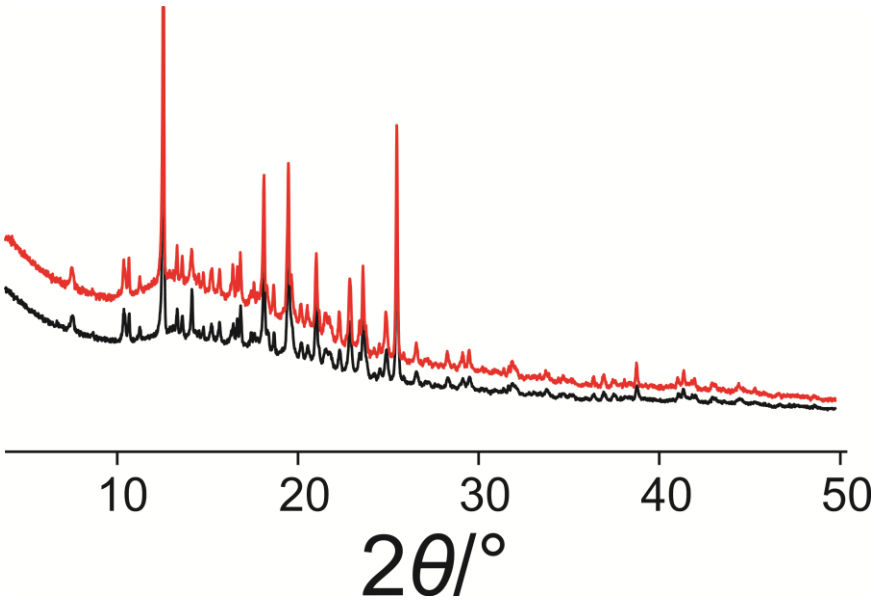

Figure 3.6b. *Powder X-ray diffraction pattern of the product on desolvation of form I (red) and form II (black) of co-crystal of $TMA_2TBA_5{\cdot}(MeOH)_3$*

molecule.[242-245] Here, we report two polymorphic structures of co-crystals of TMA_2TBA_3, both containing non-interpenetrated hydrogen-bonded hexagonal networks.

3.3.1 Synthesis and Structure Determination

The two polymorphs (denoted forms I and II) of TMA_2TBA_3 were prepared by vapour diffusion of anti-solvent into a solution of TMA and TBA in methanol. Vapour diffusion of ethanol or acetone into a methanol solution containing TMA and TBA (TMA:TBA = 2:3, molar ratio in solution) at ambient temperature resulted, after a few days, in single crystals of form I. Vapour diffusion of acetonitrile into a methanol solution containing TMA and TBA (TMA:TBA = 2:2.5, molar ratio in solution) at ambient temperature resulted, after a few days, in a mixture of crystals of form II and a second phase. The second phase was a methanol solvate with an asymmetric unit composed of two TMA molecules, two TBA molecules and one methanol molecule. We cannot distinguish this phase from form II by crystal shape or size. We left the mixture of crystals on the lab bench. After about two weeks, all the crystals of the methanol solvate became a white powder, allowing us to identify single crystals of form II of TMA_2TBA_3.

Single-crystal X-ray diffraction data were collected at 150 K on a Nonius Kappa CCD diffractometer equipped with a molybdenum tube source ($\lambda = 0.71073$ Å). The crystal structures were solved (by direct methods) by SHELXS and refined using SHELXL.[196] Refinement of non-hydrogen atoms was carried out using anisotropic displacement parameters. All hydrogen atoms were located in difference Fourier maps and were added to the structural model according to idealized geometries. Refinement of hydrogen atoms was carried out using a riding model, with isotropic displacement parameter equal to 1.2 or 1.5 times the equivalent isotropic displacement parameter of the atom to which the hydrogen atom is bonded. In addition, The H atoms of certain carboxylic acids are disordered and the refinement of each those H atoms are refined over two sites with totally occupancy equal to 1.

3.3.2 Structural Analysis and Discussion

The crystallographic parameters of the two polymorphs of TMA_2TBA_3, which have been determined from single-crystal X-ray diffraction, are summarized in Table 3.3 and the crystal structures of forms I and II are shown in Figures 3.7 and 3.8, respectively. In the case of form I, the space group is R3c, belonging to the

rhombohedral crystal system. This space group possesses high symmetry. Therefore, the asymmetric unit is composed of one independent $HTBA^+$ cation and two independent $(H_3TMA)_{1/3}$ units (denoted as TMA1 and TMA2). The H atoms of the carboxylic acids of TMA1 and TMA2 are disordered over two sites with occupancies 0.29 and 0.71.

Thus, this is equal to only one carboxylic acid group deprotonated, the charge between $HTBA^+$ cations and two independent $(H_3TMA)_{1/3}$ units is balanced. Form II crystallizes in the triclinic system with space group $P\bar{1}$ and an asymmetric unit comprising of five independent molecules: three independent $HTBA^+$ cations and two independent H_3TMA molecules (denoted as TMA3 and TMA4). The H atoms of the three carboxylic acids of TMA3 and TMA4 are disordered over two sites with the occupancies 0.36 and 0.64, 0.29 and 0.71, and 0.35 and 0.65. This is equal to three carboxylic acid groups of each two TMA molecules protonated, thus the charge is balanced in the asymmetric unit.

Table 3.3 The crystallographic parameters of forms I and II of TMA_2TBA_3

	Form I	Form II
Space Group	R3c	$P\bar{1}$
Temperature (K)	296 (2)	296 (2)
a/(Å)	16.7282(7)	7.3526(3)
b/(Å)	16.7282(7)	16.2289(6)
c/(Å)	21.1828(6)	16.4533(6)
α/(°)	90	118.901(4)
β/(°)	90	92.246(3)
γ/(°)	120	95.790(3)
V/(Å^3)	5133.5(5)	1701.26(13)
Z	18	2
R_1/(%)	4.21	5.17
R_{w2}*/(%)*	8.88	15.21

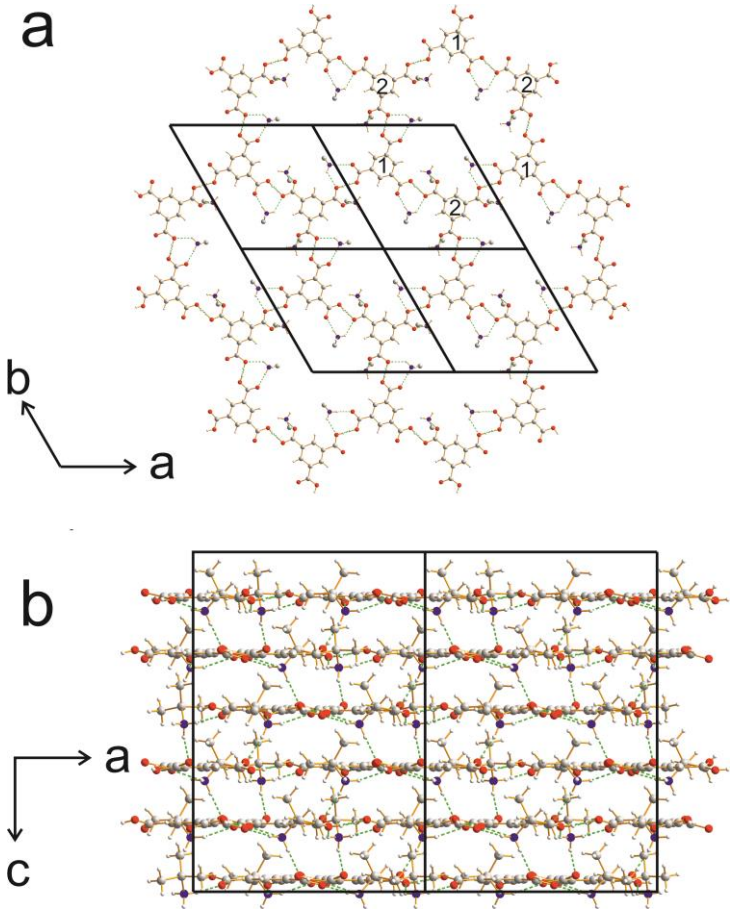

Figure 3.7. *(a) Hydrogen-bonding patterns of the hexagonal network in the flat sheets in the crystal structure of form I of co-crystal of* TMA_2TBA_3*, and (b) the complete crystal structure of form I.*

As shown in Figures 3.7 and 3.8, for each polymorph, the crystal structure comprises non-interpenetrated hydrogen-bonded hexagonal networks. In the case of form I, the crystal structure comprises two-dimensional sheets of hydrogen-bonded hexagonal networks with a cavity of diameter of *ca.*16.7 Å and all the sheets are packed parallel to the *ab*-plane, which runs in the plane of the paper in Figure 3.7b. Within each sheet, the three TMA1 molecules and three TMA2 molecules are linked alternately to each other and thus form a planar hexagonal ring. The rings of TMA1 and TMA2 lie in the plane of the sheet, while the $–N^+H_3$ groups of the $HTBA^+$ cations lie close to this plane linked by hydrogen bonding.

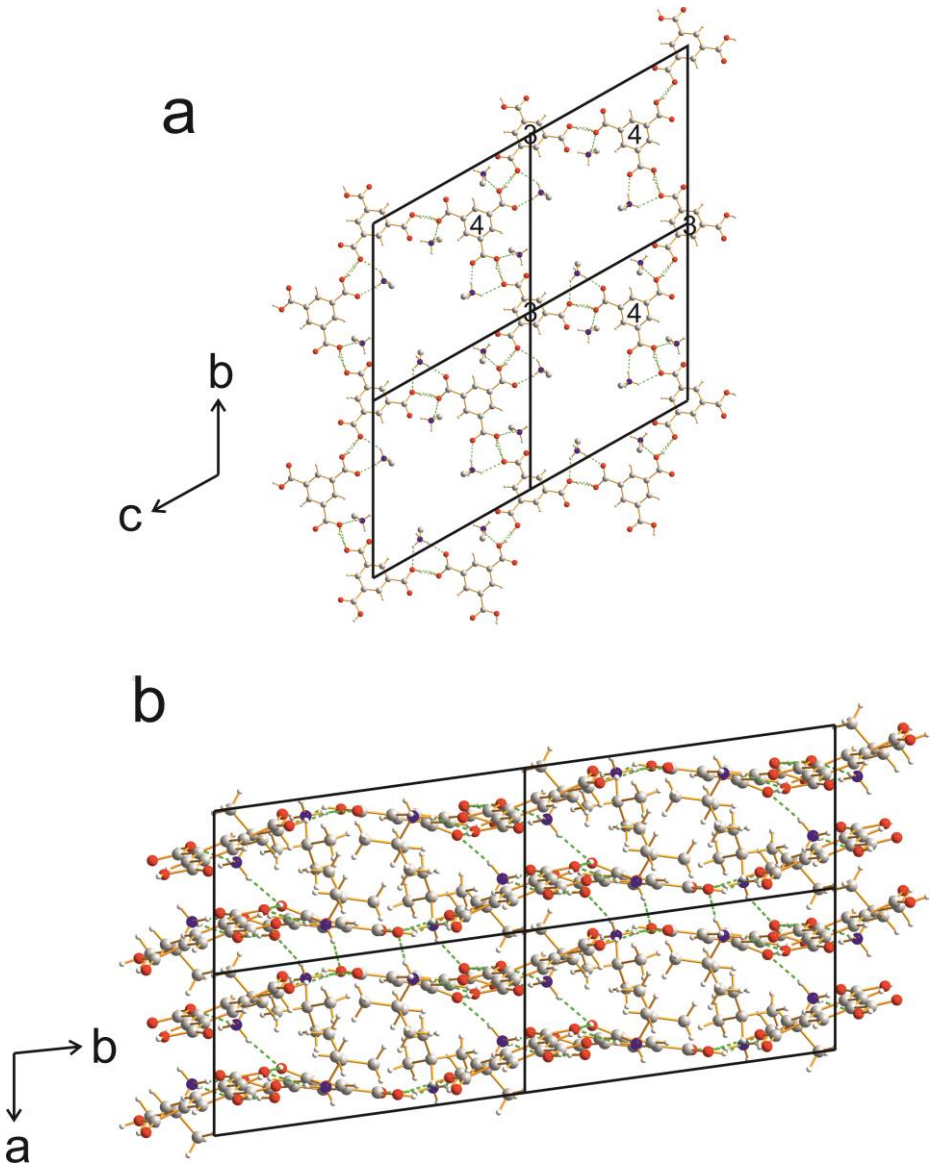

Figure 3.8. *(a) Hydrogen-bonding patterns of the hexagonal network in the corrugated sheets in the crystal structure of form II of co-crystal of* TMA_2TBA_3*. (b) The complete crystal structure of form II.*

For form II, the three TMA3 molecules and three TMA4 molecules are also alternately linked to each other to form hexagonal networks with the same size. However, the planes of the TMA3 and TMA4 molecules do not lie in the same plane. Therefore, the network is not planar but is instead corrugated; the $–N^+H_3$ groups of the $HTBA^+$ cations also lie close to these corrugated sheets and are linked to TMA1 and TMA2 by hydrogen bonding.

From Figures 3.7a and 3.8a, we can see that for both forms, each hexagonal ring is linked to six $HTBA^+$ cations through N–H···O hydrogen-bonding arrangements. Thus, seemingly, there are six $HTBA^+$ cations occupying each hexagonal ring. However, it is

not the true situation. As shown in Figures 3.9a and 3.9b, for both forms, within each hexagonal ring, there are only three $HTBA^+$ cations occupying the centre of each hexagonal ring and the other three $HTBA^+$ cations are linked to this hexagonal ring through hydrogen bond and are occupying the centre of the next hexagonal ring. In addition, for form I, the *tert*-butyl groups of all three $HTBA^+$ cations point below the plane of the hexagonal ring. For form II, the *tert*-butyl group of one $HTBA^+$ cation points below the plane of the hexagonal ring and the remaining *tert*-butyl groups of two $HTBA^+$ cations point above the plane of the hexagonal ring.

In terms of the TMA molecules, for each polymorph, there is only one type of cyclic hydrogen-bonding arrangement, corresponding to cyclic graph set $R_3^3(8)$. Specifically, for form I, due to its high symmetry, within every hexagonal ring, all TMA1/TMA2 pairs are identical. Each TMA1/TMA2 pair is linked by a direct O–H···O hydrogen bond involving one –COOH group of TMA1 and one –COOH group of TMA2. In this hydrogen bond, the O···O distance is 2.52 Å and the two H atoms between these two O atoms are disordered over two sites with occupancies 0.71 and 0.29. Therefore, we can consider that there is just one H atom shared between these two O atoms. The TMA1/TMA2 pair is also bridged by an O···H–N–H···O hydrogen-bonding arrangement with an intervening $–N^+H_3$ group of TBA. This set of hydrogen bonds gives rise to the cyclic graph set $R_3^3(8)$. However, in the case of form II, due to the

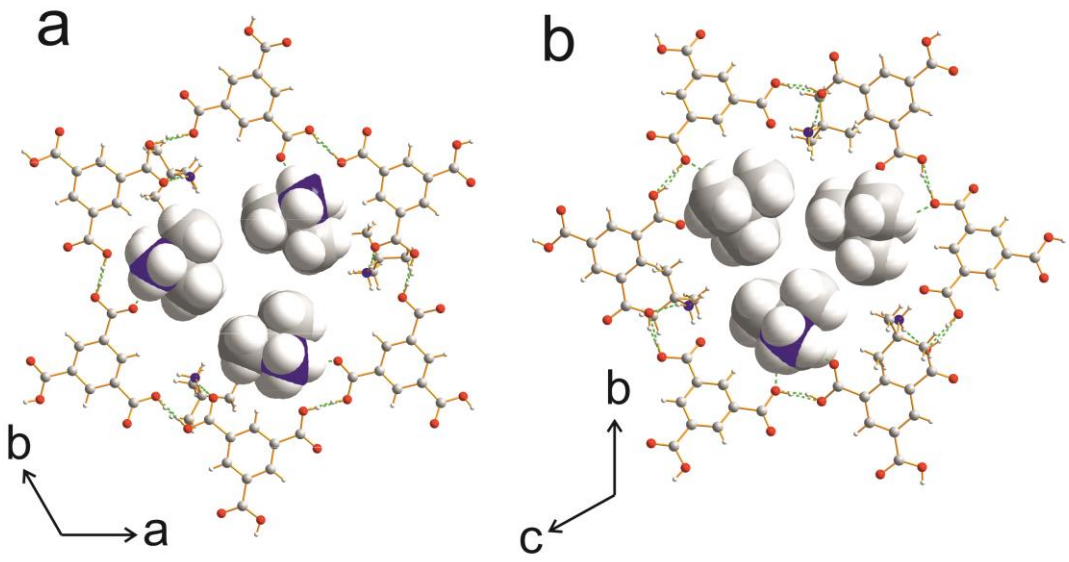

Figure 3.9. *(a) Three $HTBA^+$ cations occupying each hexagonal ring in form I of TMA_2TBA_3. (b) Three $HTBA^+$ cations occupying each hexagonal ring in form II of TMA_2TBA_3. The $HTBA^+$ cations are displayed in space-filling model.*

lower symmetry, within every hexagonal ring, the TMA3/TMA4 pairs are not exactly the same. There are three types of TMA3/TMA4 pair. In the three pairs, the O···O distances are 2.49 Å, 2.51 Å and 2.52 Å, respectively. In each O–H···O hydrogen bond, the H atom is disordered over two sites with occupancies 0.71 and 029, 0.65 and 0.35, and 0.64 and 0.36 (for the three pairs of TMA molecule). As in form I, there is just one H atom between each two O atoms. In a similar way as in form I, the TMA3/TMA4 pair is also bridged by an O···H–N–H···O hydrogen-bonding arrangement with an intervening $–N^{+}H_3$ group of TBA and thus forms the graph set $R_3^3(8)$.

In addition, for form I, all O atoms of TMA molecules are used as hydrogen-bond acceptors. However, in form II, all O atoms of TMA4 are used as hydrogen-bond acceptors to form hydrogen bonds but, three O atoms of TMA3 are used as hydrogen-bond acceptors and the other three O atoms of TMA3 do not form any hydrogen bonds. In order to compare the hexagonal rings formed in the two polymorphs, these are overlaid in Figure 3.10 (this figure was created by Dr Colan E. Hughes using the computer program Mathematica). From Figure 3.10, we can see that the sizes of these two hexagonal rings are almost the same, the primary difference is the relative disposition of carboxylic acid or carboxylate groups of each TMA molecule.

In terms of the $HTBA^{+}$ cations, for each polymorph, all three N–H bonds in each independent $HTBA^{+}$ cation are used as donors in N–H···O hydrogen bonds, linked with O atoms of TMA molecules as the acceptor. In each polymorph, two N–H bonds are linked to a TMA1/TMA2 pair (form I) or a TMA3/TMA4 pair (form II) to form graph set $R_3^3(8)$. Another N–H bond is linked to a TMA2 molecule (in form I) or a TMA4 molecule (in form II) in the adjacent layer, linking all hexagonal networks together. In

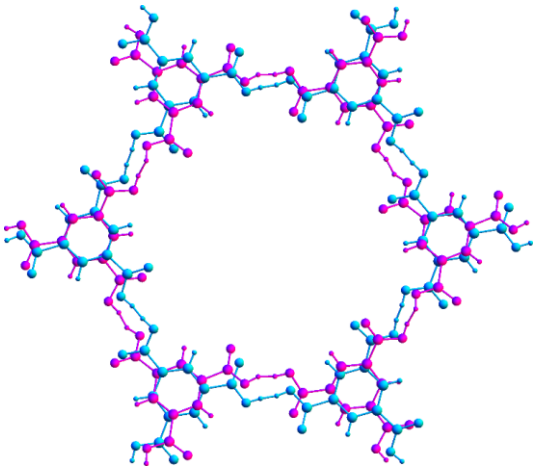

Figure 3.10. *Overlay of the hexagonal ring in form I (cyan) and form II (magenta).*

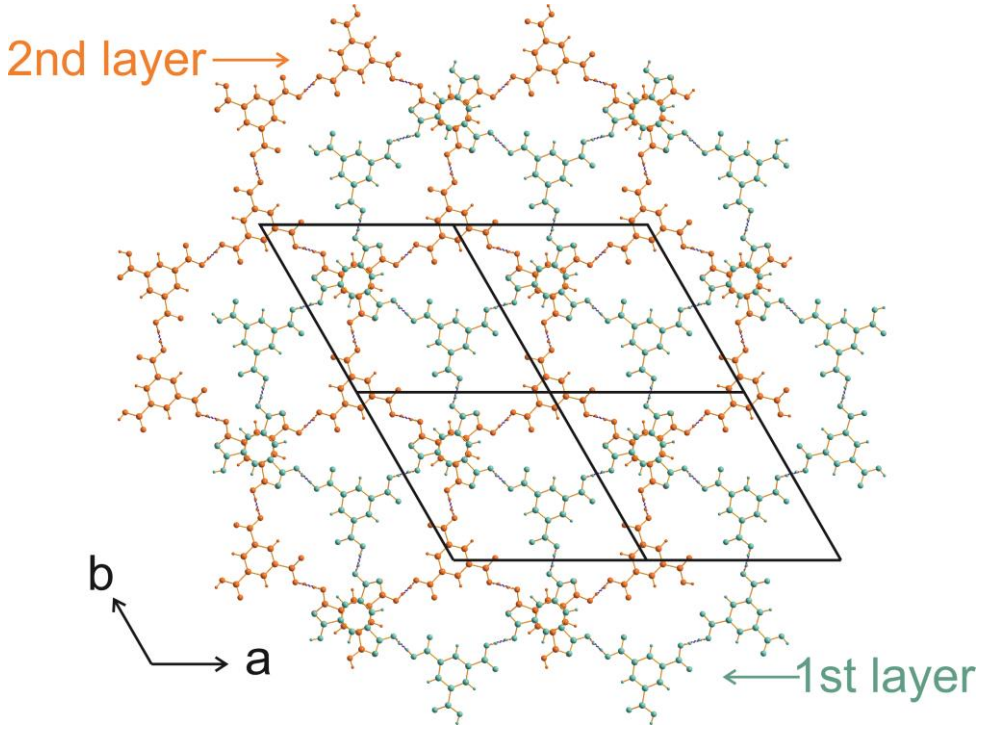

Figure 3.11. *Overlay of the hexagonal network layers (first layer: green; second layer: orange) in the crystal structure of form I of co-crystal of* TMA_2TBA_3.

addition, from the structure of form I, we can see that there are six individual layers of the hexagonal network along the c-axis in every unit cell. According to the symmetric relationship and symmetry operations, when the molecules of one layer are translated by $\frac{2}{3}a$ along the a-axis, then translated by $\frac{1}{3}b$ along the b-axis, followed by reflection in the *ab*-plane, we get a second layer of the hydrogen-bonded network (Figure 3.11). The same symmetry operation generates the other layers. In form II, there are two corrugated hexagonal networks (along the a-axis) in every unit cell, the second network generated by the crystallographic inversion centre.

3.4 Summary

Two polymorphic co-crystal systems containing TMA and TBA have been presented in this chapter. In the case of co-crystals of $TMA_2TBA_5{\cdot}(MeOH)_3$, the crystal structures of the two polymorphs both possess quite similar parallel 2D sheets but, the hydrogen-bonding pattern within these sheets shows subtle (but significant) differences. In the case of co-crystals of TMA_2TBA_3, despite the TMA molecules being partially deprotonated, both polymorphs still retain hexagonal networks and, due to the presence of TBA molecules, the hexagonal networks within both polymorphs are non-interpenetrated. However the network in form I is planar and while the network in form II is corrugated.

Chapter 4 Structural Analysis of Families of Co-Crystals of Trimesic Acid and *tert*-Butylamine

4.1 Introduction

The structural diversity of organic co-crystals is a very interesting phenomenon and has become a hot issue in recent years. In 1969, Duchamp and Marsh[246] determined the crystal structure of trimesic acid (TMA) and showed that TMA molecules can form hexagonal networks with triple interpenetration. This observation provided the basis for the design of organic porous materials and, since then, the TMA molecule has attracted considerable attention in crystal engineering. In the field of organic co-crystals, due to its symmetric molecular structure and its capability to form homo-dimers and hetero-dimers with a variety of functional groups (such as alcohols[247], carboxylic acids[225,241], pyridines[230,240,248] and organic amines[226,249]), trimesic acid has been widely studied and a wide range of organic co-crystals containing TMA molecules or deprotonated forms of TMA have been synthesized. It has been reported that organic co-crystals containing TMA molecules or deprotonated TMA anions are able to form a series of one-dimensional (1D), two-dimensional (2D) and three-dimensional (3D) frameworks, such as extended hexagonal networks with[240,248] or without[249] interpenetration. These interesting frameworks have shown versatile hydrogen-bonding patterns between carboxylic acid or carboxylate groups of pairs of TMA molecules, such as (Figure 4.1) typical acid-acid head-to-head $R_2^2(8)$, single-bridged $R_3^3(10)$ and double-bridged $R_4^4(12)$ dimer motif patterns.

Incorporation of solvent molecules,[250] such as methanol and water molecule,[251] into crystal structures is a wide-spread phenomenon in organic co-crystals. In such cases, the solvent molecules can usually be regarded as a nuisance because the presence of solvent molecules can render the crystals unstable. However, in some cases, the presence of solvent molecules is the key factor for successful crystallization. Solvent molecules in crystal structures may act as hydrogen-bond acceptors or donors to form three-dimensional networks and/or act as space fillers to stabilize channels or cavities within crystal structures. In addition to their value in fundamental academic study, solvates also have practical applications in industry, such as in the pharmaceutical industry. In many cases, a solvate of a given active pharmaceutical ingredient (API) may be chosen as the final commercial product if it is sufficiently stable and improves

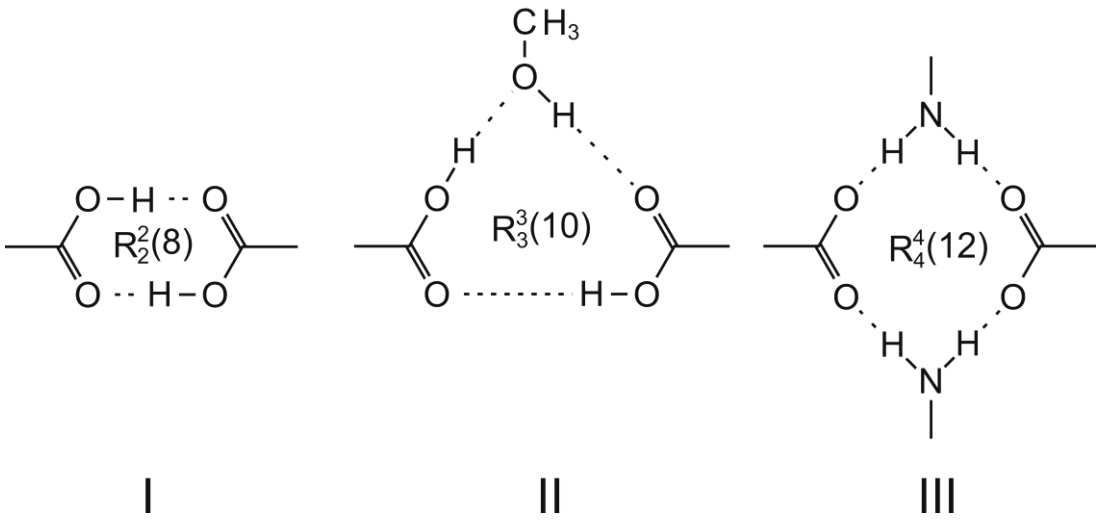

Figure 4.1. *Three common hydrogen-bonding motifs between two carboxylic acid or carboxylate groups. (I) Typical head-to-head* $R_2^2(8)$*, (II) single-bridged* $R_3^3(10)$ *and (III) double-bridged* $R_4^4(12)$.

the quality of the API. Specifically, about three-quarters of APIs can form hydrate crystal structures. The water molecule is very small and can often be accommodated at many positions in the crystal structure, partly as a result of the versatility of the water molecule to act both as a hydrogen bond donor and as a hydrogen bond acceptor. In addition, water is almost always present in the atmosphere, and in some cases it is quite easy for ambient water molecules to be incorporated into a crystal structure.

In the course of studying co-crystals of TMA and TBA, we discovered a series of co-crystals with different stoichiometries. The resulting structures contain diverse and interesting types of hydrogen-bonded networks, such as single-layered sheets, corrugated sheets, double-layered sheets and brick-wall networks. Most of these structures are solvates. In fact, incorporating solvent molecules into the crystal structures has been found to be quite common for this family of materials. It has been suggested[252] that the probability of forming a hydrate is particularly high when the components possess charged groups or polar groups, such as carbonyl (C=O), hydroxyl (OH) and primary amine (N–H) groups, which is exactly the case in the system of co-crystals of TMA and TBA. In these structures, the solvent molecules (alcohol or water) act as a "glue" via intermolecular hydrogen-bonding interactions between TMA and TBA molecules to form three-dimensional networks and/or as space fillers in order to stabilize empty channels or cavities formed by the TMA and TBA molecules.

It is well known that the goal of crystal engineering is to design and predict crystal structures based on knowledge of the molecular structures and the preferred modes of intermolecular interaction between the components. However, this task can be very complicated and far from predictable. However, "supramolecular synthons" based on hydrogen bonds can simplify this task to some extent, and this concept has been used extensively to facilitate the design of crystal structures. In order to identify common "synthons" that appear in the family of organic co-crystals of TMA and TBA, in this chapter we classify all the co-crystal structures of TMA and TBA into four families in accordance with their stoichiometry (TMA:TBA = 2:1, 1:1, 1:2 and 1:3) and then analyse the structural features of each family of co-crystals from the view point of hydrogen bonding with graph set notation, especially, concentrating on the hydrogen-bonding patterns between carboxylic acid or carboxylate groups of pairs of TMA molecules.

4.2 Structural Diversity of Solvatomorphs of TMA_2TBA_1

As mentioned above, water is all around us, and the formation of hydrate co-crystals is quite common. In the course of studying co-crystals of TMA and TBA, when the TMA:TBA stoichiometry is 2:1, we obtained four different types of hydrate (tri-hydrate, di-hydrate, mono-hydrate and hemi-hydrate), one methanol solvate and one anhydrous form by using different crystallization conditions and different crystallization methods. To the best of our knowledge, the existence of four different types of hydrate in the same family of organic co-crystals with the same stoichiometry is very rare.

4.2.1 Synthesis and Structure Determination

The crystallization process to form the tri-hydrate $TMA_2TBA_1 \cdot (H_2O)_3$ involved slow evaporation of a solution containing TMA and TBA (TMA:TBA = 2:1, molar ratio) in ethanol at room temperature. After a few days, the solution dried out, resulting in a white powder. Recrystallization of the powder in mixtures of ethanol and water (ethanol:water = 1:1, volume ratio), occasionally gave, after a few days, single crystals of the tri-hydrate. However, this process was quite difficult to reproduce. In the vast majority of cases, single crystals of the di-hydrate were obtained. Furthermore, single crystals of the tri-hydrate cannot be prepared directly by using ethanol and water as the crystallization solvent, as this results in the formation of di-hydrate single crystals.

The crystallization processes to form the di-hydrate $TMA_2TBA_1{\cdot}(H_2O)_2$ were as follows: (i) slow evaporation of a solution containing TMA and TBA (TMA:TBA = 2:1, molar ratio) in ethanol and water (ethanol:water = 3:1, 2:1, 1:1, 1:2 or 1:3, volume ratio) at room temperature; after a few days, single crystals of the di-hydrate were obtained; (ii) 1 mmol TBA dissolved in 10 ml water in a glass bottle, then slowly added this solution into 10 ml methanol solution containing TMA (1 mmol) at ambient temperature; the solution was then allowed to slowly evaporate, and after a few days single crystals of the di-hydrate were obtained; (iii) slow evaporation of a solution containing TMA and TBA (TMA:TBA = 2:1, molar ratio) in methanol and water (methanol:water = 5:1, 4:1, 3:1, 2:1, 1:1, 1:2, 1:3, 1:4 or 1:5, volume ratio) at ambient temperature; after a few days, single crystals of the di-hydrate were obtained.

The crystallization process to form anhydrous TMA_2TBA_1 involved dehydration of a sample of the di-hydrate in an oven at 100 °C for at least three days. This process produced a pure powder sample of anhydrous TMA_2TBA_1.

The crystallization process to form the mono-hydrate $TMA_2TBA_1{\cdot}(H_2O)_1$ involved the dissolution of a sample of the anhydrous form in methanol and water (methanol:water = 1:1, volume ratio), followed by slow evaporation. After a few days, single crystals of the mono-hydrate were obtained. However, the process was quite difficult to reproduce. In the vast majority of cases, single crystals of the di-hydrate were obtained.

The crystallization process to form the hemi-hydrate $TMA_4TBA_2{\cdot}(H_2O)_1$ involved heating a sample of the di-hydrate from room temperature to 200 °C, then cooling down to room temperature. This process was carried out in the DSC instrument, with the sample in a sealed aluminium pan with heating and cooling rates of 10 °C/min^{-1}. A powder sample of the hemi-hydrate was obtained.

The crystallization processes to form the methanol solvate $TMA_2TBA_1{\cdot}(MeOH)_1$ were as follows: (i) a solution containing TMA and TBA (TMA:TBA = 2:1, molar ratio) in methanol was allowed to evaporate slowly at room temperature; after a few days, single crystals of the methanol solvate were obtained; (ii) a hot methanol solution containing TMA and TBA (TMA: TBA = 2:1, molar ration) was prepared at 55 °C in a conical flask, followed by slow cooling from 55 °C to 25 °C in an incubator; single crystals of the methanol solvate were obtained.

All crystal structures (except the structures of the anhydrous form and the hemi-hydrate) described in this chapter were determined by single-crystal XRD at 150 K on a Nonius Kappa CCD diffractometer equipped with a molybdenum tube source (λ = 0.71073 Å). The crystal structures were solved (by direct methods) by SHELXS and refined using SHELXL.[196] Refinement of non-hydrogen atoms was carried out using anisotropic displacement parameters. All hydrogen atoms were located in difference Fourier maps and were added to the structural model according to idealized geometries. Refinement of hydrogen atoms was carried out using a riding model, with isotropic displacement parameter equal to 1.2 or 1.5 times the equivalent isotropic displacement parameter of the atom to which the hydrogen atom is bonded.

The crystal structures of the anhydrous form and the hemi-hydrate were determined directly from the powder XRD data. Firstly, high quality of powder X-ray diffraction pattern data were recorded for anhydrous form and hemi-hydrate sample at ambient temperature on a Bruker D8 instrument (CuKα_1; Ge monochromated; transmission geometry) with a tape sample holder (2θ range, 4 – 50°; total time, 48 hrs). Secondly, the powder XRD patterns of anhydrous form and hemi-hydrate were indexed by using program CRYSTFIRE, combined with the program CHEKCELL. The Le Bailing fitting using GSAS gave a good quality of fits with space groups $P2_1/a$ (for anhydrous form) and $P\bar{1}$ (for hemi-hydrate), respectively (Figure 4.2a and 4.2b). For the anhydrous form, a = 22.743 Å, b = 7.512 Å, c = 14.992 Å, β = 114.159°, (V = 2336.82 Å^3), R_{wp} = 2.17%, R_p = 1.69%. For the hemi-hydrate form, a = 15.071 Å, b = 21.503 Å, c = 7.391 Å, α = 90.319°, β = 89.99°, γ = 74.963°, (V = 2313.85 Å^3), R_{wp} = 1.85%, R_p = 1.43%.

Given the volume of the unit cell and consideration of density, for the anhydrous form, there are two TMA molecules and one TBA molecule in the asymmetric unit; for the hemi-hydrate form, there are four TMA molecules, two TBA molecules and one water molecule in the asymmetric unit. The refined unit cell and profile parameters obtained from the Le Bail fits were used in subsequent structure solution calculations. Structure solution was carried out using the direct-space genetic algorithm (GA) technique incorporated in the program EAGER[195] followed by Rietveld refinement[213]. In total, 16 independent GA calculations were carried out for each model and the GA calculation was allowed to evolve for 1000 generations for a population size of 100. In each generation, 10 mating operations and 50 mutation operations were carried out. The

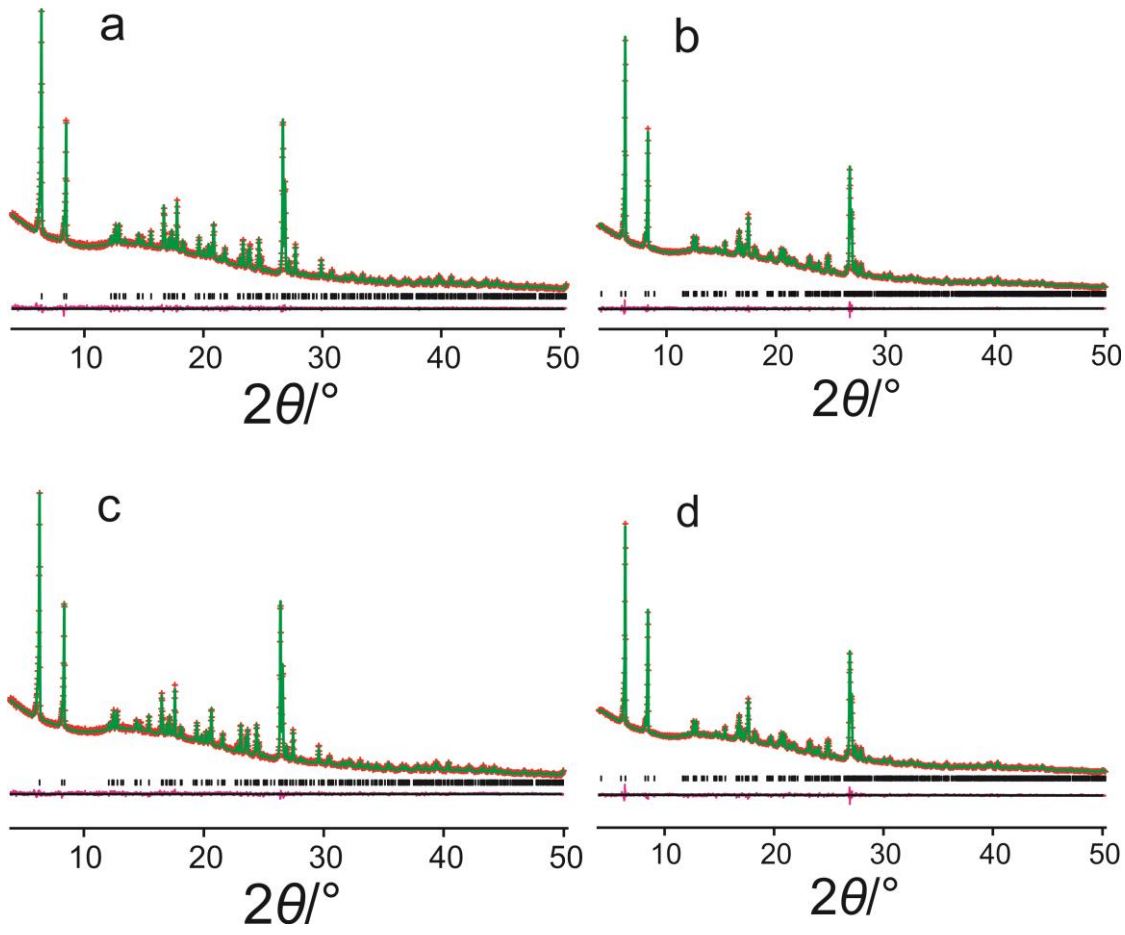

Figure 4.2. *Le Bail fits of anhydrous form (a) and hemi-hydrate (b) of co-crystal of TMA_2TBA_1; Rietveld Refinement of anhydrous form (c) and hemi-hydrate (d) of co-crystal of TMA_2TBA_1.*

results from all these structure solution calculations were assessed and evaluated to determine which model gives the best structure solution. In the Rietveld refinement, standard restraints were applied to bond lengths and bond angles, and planar restraints were applied to benzene rings and carboxylate groups. The structural model with lowest R_{wp} from GA calculation was used as the initial structural model for Rietveld refinement. The final Rietveld refinement gave good fits to the powder XRD data for both samples (for anhydrous form, R_{wp} = 2.34%, R_p = 1.81%; for hemi-hydrate, R_{wp} = 2.27%, R_p = 1.73%; Figure 4.2c and 4.2d), with the following refined parameters: for the anhydrous form, a = 22.7418 (6) Å, b = 7.5122 (1) Å, c = 14.9901 (4) Å, β = 114.1589 (20)°, (V = 2336.61 (10) Å^3); for the hemi-hydrate form, a = 15.0729 (4) Å, b = 21.5029 (6) Å, c = 7.3900 (1) Å, α = 90.336 (4)°, β = 90.021 (4)°, γ = 74.9580 (31)°, (V = 2313.08 Å^3). The details of the process for determination of crystal structures from powder XRD data are described in more detail in Chapters 5 and 6.

4.2.2 Structural Summary of Co-Crystals of TMA_2TBA_1

The relationships between these materials are summarized in Figure 4.2e. As shown in Figure 4.2, the di-hydrate $TMA_2TBA_1 \cdot (H_2O)_2$ is stable at room temperature in the open air. The other solvate co-crystals slowly transformed to the di-hydrate $TMA_2TBA_1 \cdot (H_2O)_2$ at room temperature. The crystallographic parameters of the six structures are summarized in Table 4.1 and the crystal structures are shown in Figures 4.3 to 4.12.

Table 4.1 Crystallographic parameters of co-crystals of TMA_2TBA_1.

	Tri-Hydrate	Di-Hydrate	Mono-Hydrate
Space group	$P2_1/n$	$P2_1/n$	$P2_1/n$
a/Å	6.7390(2)	15.2910(3)	15.2931(3)
b/Å	41.3370(12)	9.5020(2)	7.2592(1)
c/Å	9.5880(3)	16.9010(5)	21.5708(4)
α/°	90	90	90
β/°	106.763(1)	102.065(1)	104.885(2)
γ/°	90	90	90
V(Å^3)	2557.43(13)	2401.39(10)	2314.34
Z	4	4	4
Calculated Density (g/cm^3)	1.422	1.464	1.468
R_1/(%)	8.76	5.76	3.83
R_{w2}/(%)	17.27	13.37	10.62

	Hemi-Hydrate	Methanol Solvate	Anhydrous Form
Space group	$P\bar{1}$	$P\bar{1}$	$P2_1/a$
a/Å	15.0729(4)	6.8545(2)	22.7418(6)
b/Å	21.5029(6)	8.8246(2)	7.5122(1)
c/Å	7.3900(1)	20.0279(7)	14.9901(4)
α/°	90.336(4)	90.994(2)	90
β/°	90.021(4)	96.235(2)	114.1589(20)
γ/°	74.9580(31)	94.409(2)	90
V(Å^3)	2313.08	1200.32(6)	2336.61(10)
Z	2	2	4
Calculated Density (g/cm^3)	1.443	1.451	1.403
R_1/(%)	/	3.83	/
R_{w2}/(%)	/	10.62	/

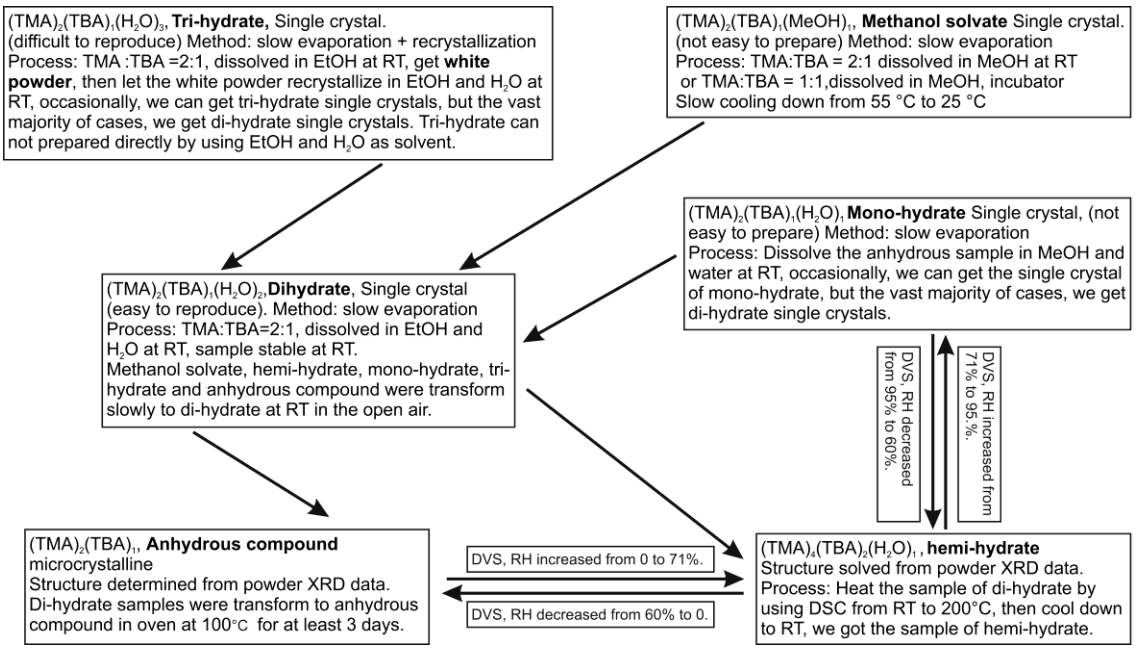

Figure 4.2e. *The relationships between solvatomorphs of co-crystals of TMA_2TBA_1. In this figure, DVS stands for dynamic vapor sorption. RH stands for relative humilities.*

These six crystal structures can be classified into three categories in accordance with their structural features. Thus, the structure of the di-hydrate comprises double-layered sheets without interpenetration (Figure 4.3), the structures of the tri-hydrate and methanol solvate are interpenetrated by two different sets of ribbons (Figure 4.6) and the remaining three structures are self-interpenetrated by one set of ribbons (Figure 4.10).

4.2.3 Structural Analysis of the Di-Hydrate of TMA_2TBA_1

The crystal structure of the di-hydrate $TMA_2TBA_1 \cdot (H_2O)_2$ is monoclinic with space group $P2_1/n$ and the asymmetric unit is composed of five independent molecules: one H_3TMA molecule, one H_2TMA^- anion, one $HTBA^+$ cation and two water molecules. The structure (Figure 4.3) does not form the typical honeycomb network but, instead comprises double-layered sheets which are linked by intervening water molecules and $HTBA^+$ cations via hydrogen bonding. The distance between two adjacent sheets is about 3.5 Å and the distance between adjacent $HTBA^+$ cations is about 10.4 Å. The double-layered sheets are stacked in an offset manner.

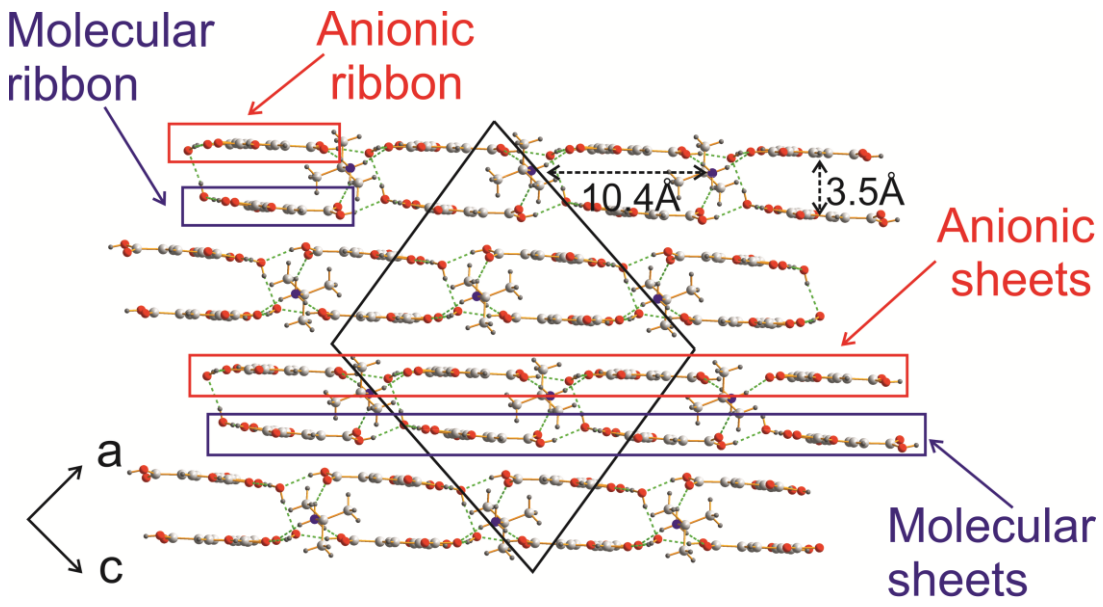

Figure 4.3. *Double-layered sheets in the crystal structure of the di-hydrate of* $TMA_2TBA_1 \cdot (H_2O)_2$.

In Figure 4.4, the two types of sheet are shown. One sheet is formed by H_2TMA^- anions (denoted as the anionic sheet) and the other sheet is formed by H_3TMA molecules (denoted as the molecular sheet). Both sheets are not exactly flat. The anionic and molecular sheets both comprise hydrogen-bonded ribbon motifs (ribbons parallel to the b-axis). These ribbons are indicated by the region between the two dashed lines in Figure 4.4. We note that adjacent H_2TMA^- anionic ribbons do not lie in the same plane but are slightly offset (the offset between adjacent anionic ribbons is 0.40 Å). It is for this reason that the anionic sheet is not entirely flat (Figure 4.3). The same situation exists for the molecular sheets (the offset between adjacent molecular ribbons is 0.77 Å). The distance between a pair of anionic/molecular ribbons is 3.5 Å (Figure 4.3).

From Figure 4.4a, we can see that, within an anionic ribbon, adjacent H_2TMA^- anions are linked by a direct O–H···O hydrogen bond involving an OH group of one H_2TMA^- anion and an O atom of one $–COO^-$ group of another H_2TMA^- anion, and the other two O atoms of these groups are bridged by an O···H–O–H···O hydrogen-bonding arrangement with an intervening water molecule, resulting in the cyclic graph set $R_3^3(10)$. In this hydrogen-bonding arrangement, the water molecule provides two hydrogen bond donors within the sheet. Between two adjacent anionic ribbons, adjacent H_2TMA^- anions from each ribbon are double-bridged by the intervening water molecule and an $–N^+H_3$ group, forming a cyclic hydrogen-bonding ring (graph set $R_4^3(10)$). These two graph sets are marked in Figure 4.4a.

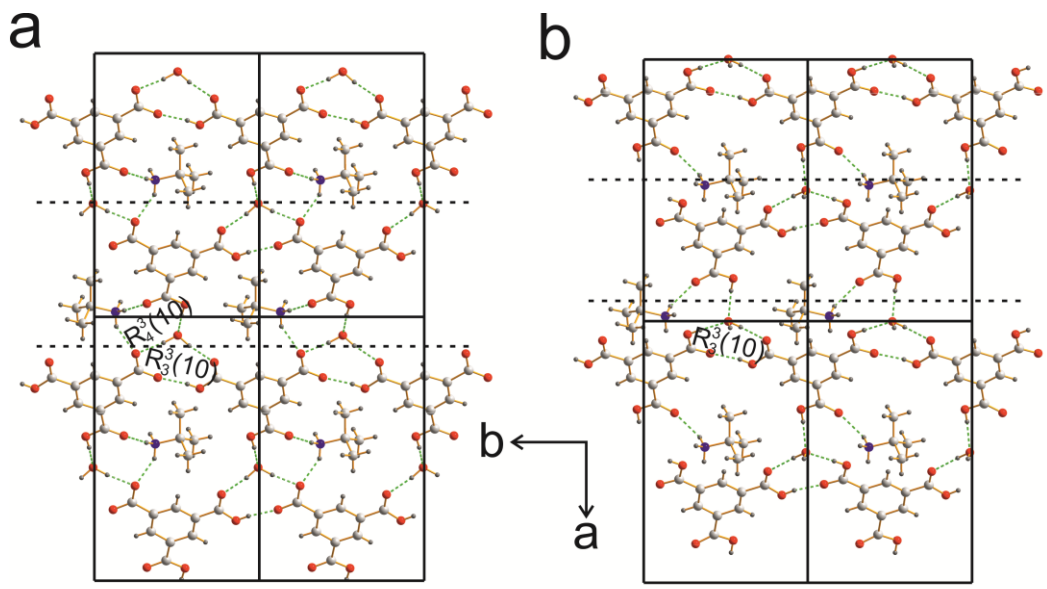

Figure 4.4. *(a) Anionic sheet and (b) molecular sheet of the crystal structure of the di-hydrate.*

Within a molecular ribbon (Figure 4.4b), a slightly different cyclic hydrogen-bonding arrangement (graph set $R_3^3(10)$) is formed between –COOH groups of adjacent TMA molecules and an intervening water molecule, which acts as both hydrogen bond acceptor and donor. Thus, the functionalities of the water molecules in the anionic and molecular sheets are not the same. Between adjacent molecular ribbons, an OH group of –COOH of a TMA molecule (denoted TMA1) of one ribbon is linked to two other TMA molecules (denoted TMA2 and TMA3) of another ribbon via O–H(TMA1)···O–H (water)···O (TMA2) and O–H (TMA1)···O (water)···O–H (TMA3) hydrogen-bonding arrangements with no cyclic hydrogen-bonding ring formed, due to the intervening $HTBA^+$ cation linking to only one adjacent TMA molecule through O···H–N^+ hydrogen bonding.

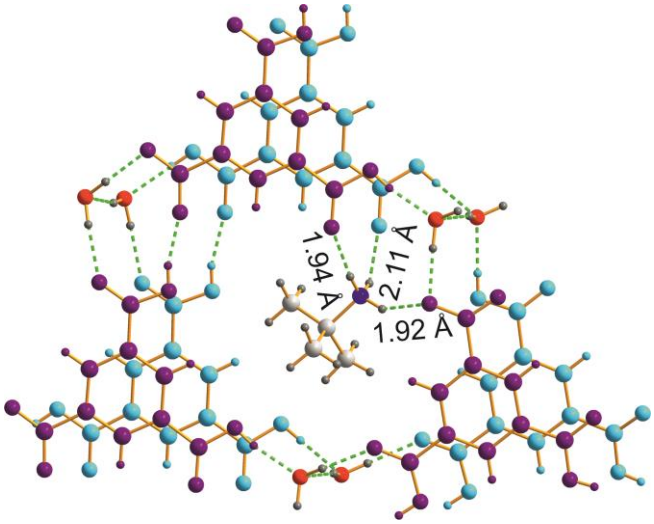

Figure 4.5. *Cavity formed by double-layered anionic (purple) and molecular (cyan) sheets in the structure of the di-hydrate.*

As shown in Figure 4.5, within both anionic and molecular sheets, groups of three adjacent H_2TMA^- anions and H_3TMA molecules form a hydrogen-bonded triangular ring (graph set $R_5^5(28)$) involving three intervening water molecules. The two triangular rings in adjacent sheets are parallel to each other but, slightly offset, and are linked to each other through the three intervening water molecules, which gives rise to a cavity. One $HTBA^+$ cation occupies the centre of the cavity and the $HTBA^+$ cation is linked to one H_3TMA molecule through O···H–N^+ hydrogen bonds and linked to two H_2TMA^- anions through another two O···H–N^+ hydrogen bonds. In order to balance the charge of the H_2TMA^- anions, the –N^+H_3 group of the $HTBA^+$ cation is close to the anionic sheet. Thus, the distance from the N atom of the –N^+H_3 groups to the anionic sheet is slightly shorter than the distance to the molecular sheet. These three hydrogen bonds are marked in Figure 4.5 and the distances (H···O) are 1.94 Å, 1.92 Å and 2.11 Å. In this structure, all water molecules act as bridges, providing two hydrogen bond donors and two hydrogen bond acceptors to link H_2TMA^- anions and H_3TMA molecules together to form a 3D network.

4.2.4 Structural Comparison Between the Tri-Hydrate and the Methanol Solvate of TMA_2TBA_1.

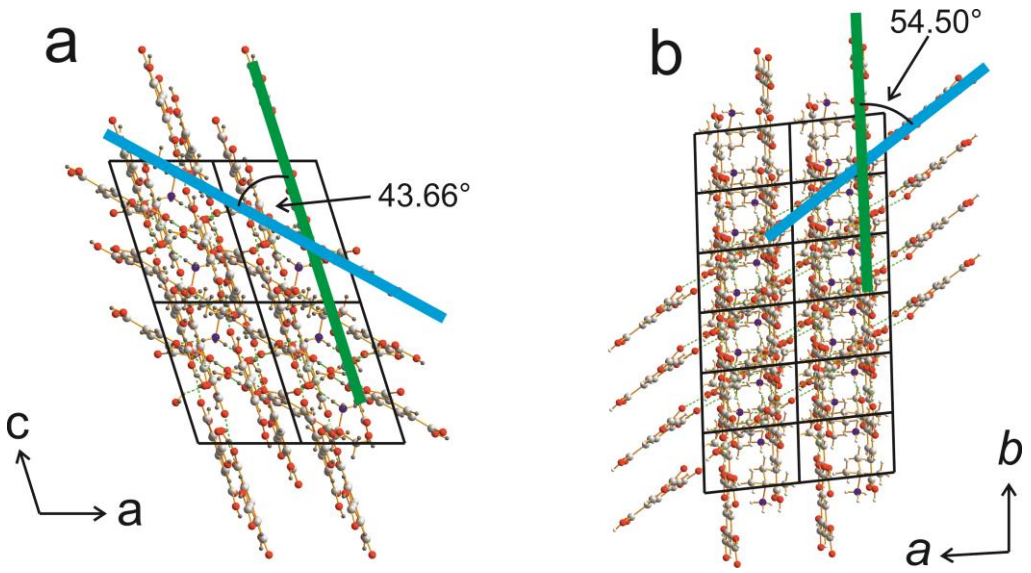

Figure 4.6. *Interpenetrated structures of (a) the tri-hydrate and (b) the methanol solvate. For clarity, the blue & green lines represent two different sets of ribbons.*

The tri-hydrate $TMA_2TBA_1 \cdot (H_2O)_3$ is monoclinic with space group $P2_1/n$ and the asymmetric unit is composed of one neutral H_3TMA molecule, one H_2TMA^- anion, one $HTBA^+$ cation and three water molecules. The methanol solvate $TMA_2TBA_1 \cdot (MeOH)_1$ is triclinic with space group $P\bar{1}$ and the asymmetric unit is composed of one neutral H_3TMA molecule, one H_2TMA^- anion, one $HTBA^+$ cation and one methanol molecule.

These two crystal structures (Figures 4.6a and 4.6b) are both constructed from two sets of parallel ribbons which interpenetrate each other at angles of 43.66° (tri-hydrate) and 54.50° (methanol solvate). In both structures (Figure 4.7), $HTBA^+$ cations and solvent molecules occupy the space between ribbons and act as a "glue" to link these ribbons together to form three-dimensional networks. In both structures (Figures 4.8 and 4.9), one ribbon is formed by H_2TMA^- anions (denoted ribbon I, Figures 4.8a and 4.9a) and the other ribbon is formed by H_3TMA molecules (denoted ribbon II, Figures 4.8b and 4.9b). In the structure of the tri-hydrate (Figure 4.8a), within ribbon I, adjacent H_2TMA^- anions are linked directly on one side by the typical carboxylic acid dimer head-to-head hydrogen-bonding motif (graph set $R_2^2(8)$), whilst on the other side, the $-COO^-$ group and the second –COOH group of each H_2TMA^- anion link to each other via two intervening water molecules to form a large hydrogen-bonding ring, with graph set $R_4^4(20)$. In the structure of the methanol solvate (Figure 4.9a), two adjacent H_2TMA^- anions are linked directly not only by the head-to-head carboxylic acid dimer motif but also by direct hydrogen bonding between the $-COO^-$ group of one H_2TMA^- anion and the second –COOH group of the other H_2TMA^- anion, forming graph set $R_2^2(16)$.

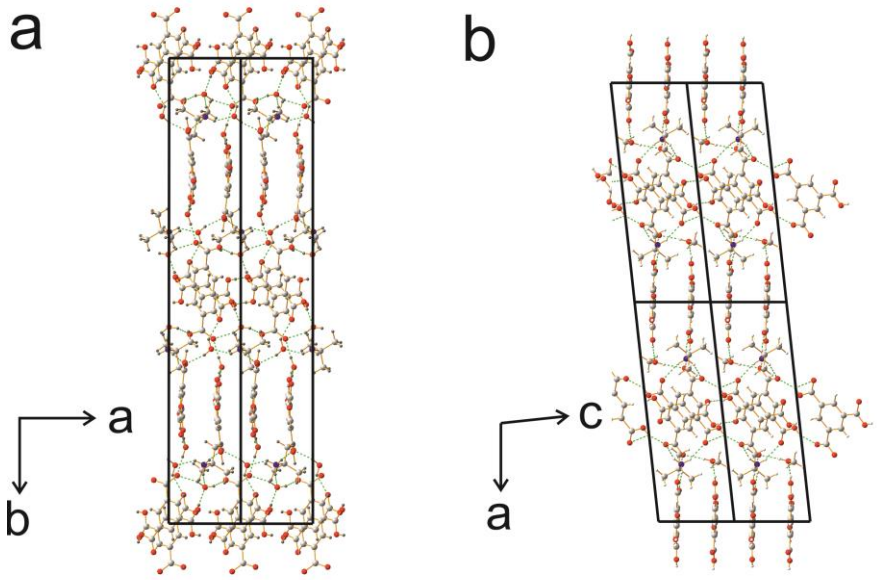

Figure 4.7. *Structures of (a) the tri-hydrate and (b) the methanol solvate.*

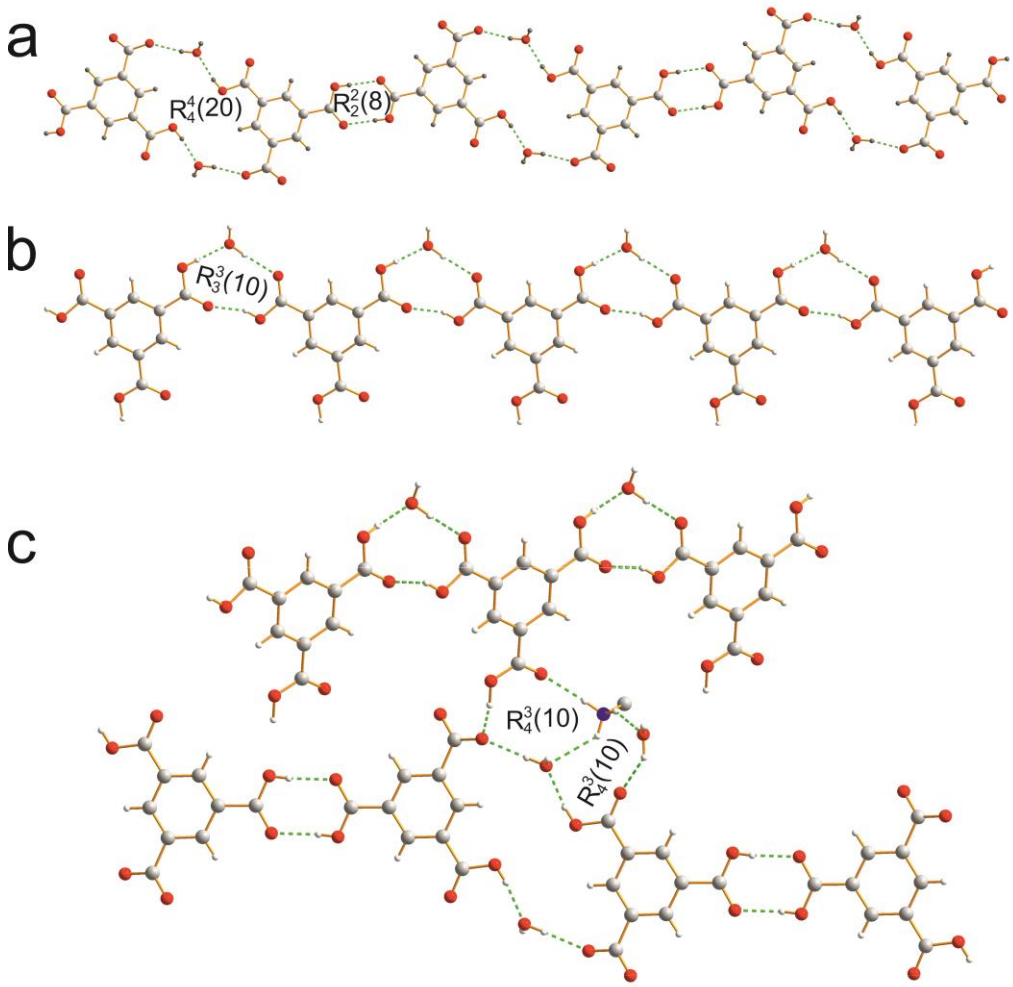

Figure 4.8. *Two types of ribbon, (a) type I and (b) type II in the crystal structure of the tri-hydrate and (c) the hydrogen-bonding patterns formed between these two ribbons.*

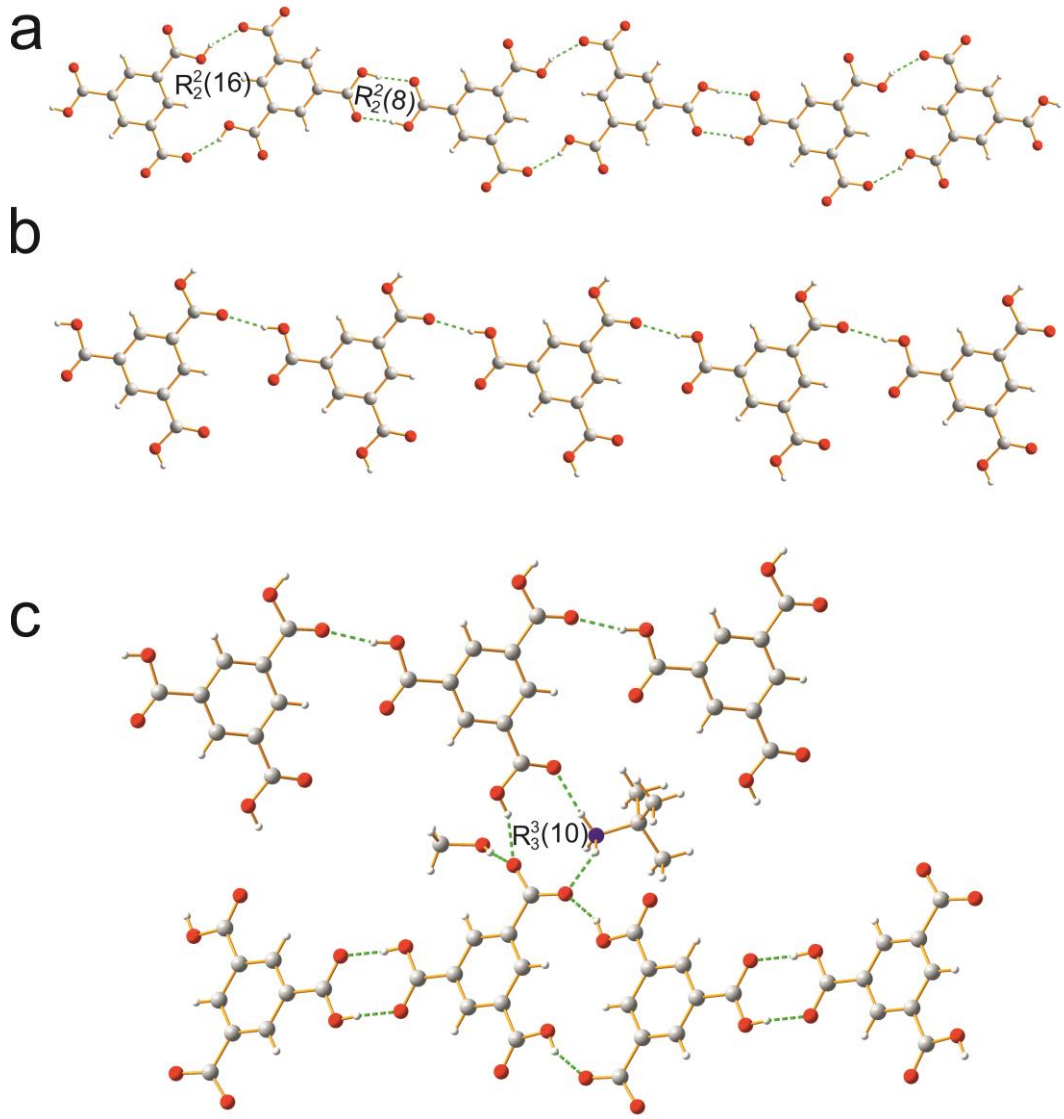

Figure 4.9. *Two types of ribbon (a) type I and (b) type II in the methanol solvate and (c) the hydrogen-bonding patterns formed between these two ribbons.*

In the case of ribbon II for the tri-hydrate (Figure 4.8b), one H_3TMA molecule is linked to an adjacent H_3TMA molecule by a direct O–H···O hydrogen bond and by an intervening water molecule, giving rise to the cyclic graph set $R_3^3(10)$. As discussed above (section 4.2.3), this hydrogen-bonding motif is also observed in the structure of the di-hydrate (Figure 4.4b). However, in the structure of the methanol solvate (Figure 4.9b), the ribbons formed by H_3TMA molecules are different. Adjacent H_3TMA molecules are linked directly only by a single O···H–O hydrogen bond and no cyclic hydrogen- bonding arrangement is formed.

In the crystal structure of the tri-hydrate (Figure 4.8c), the two types of ribbon are linked together by a direct O···H–O hydrogen bond and via two intervening water

molecules and the $-N^+H_3$ group of the $HTBA^+$ cation, giving rise to two graph sets $R_4^3(10)$. This situation is quite different from the two graph sets $R_4^3(10)$ and $R_3^3(10)$ observed in the structure of the di-hydrate (Figure 4.4a). By comparison, in the methanol solvate (Figure 4.9c), the two sets of ribbons are linked directly by an O···H–O hydrogen bond and are bridged by the $-N^+H_3$ group of one $HTBA^+$ cation, forming a cyclic hydrogen-bonding arrangements with graph set $R_3^3(10)$.

In both structures, all three N–H bonds of the $HTBA^+$ cation act as hydrogen bond donors and each methanol molecule in the methanol solvate acts both as a hydrogen bond donor (bonding to one H_2TMA^- anion) and as a hydrogen bond acceptor (bonding to one H_3TMA molecule). However, the methanol molecule is not involved in any cyclic hydrogen-bonding arrangement. In the structure of the tri-hydrate, there are three independent water molecules. The functionality of each water molecule is quite different. One water molecule (Figure 4.8a) is hydrogen bonded to two H_2TMA^- anions to form graph set $R_4^4(20)$. The second water molecule (Figure 4.8b) is hydrogen bonded to two H_3TMA molecules to form graph set $R_3^3(10)$. The third water molecule (Figure 4.8c) is hydrogen bonded to a $HTBA^+$ cation and a H_2TMA^- anion to form graph set $R_4^3(10)$, with the intervention also of the first water molecule.

4.2.5 Structural Comparison Between the Mono-Hydrate, Hemi-Hydrate and Anhydrous Form of TMA_2TBA_1

The mono-hydrate and the anhydrous form are monoclinic with space groups $P2_1/n$ and $P2_1/a$, respectively. The asymmetric unit of the mono-hydrate and the anhydrous form comprise one neutral H_3TMA molecule, one H_2TMA^- anion, one $HTBA^+$ cation and, in the mono-hydrate, one water molecule. The hemi-hydrate is triclinic with space group $P\bar{1}$ and the asymmetric unit is composed of two neutral H_3TMA molecules, two H_2TMA^- anions, two $HTBA^+$ cations and one water molecule. All three crystal structures (Figure 4.10) are constructed from sheets of parallel ribbons which interpenetrate with symmetry copies at angles of 51.96° (mono-hydrate), 52.45° (hemi-hydrate) and 53.97° (anhydrous form). Furthermore, the TMA ribbons in each structure are essentially the same (Figure 4.11).

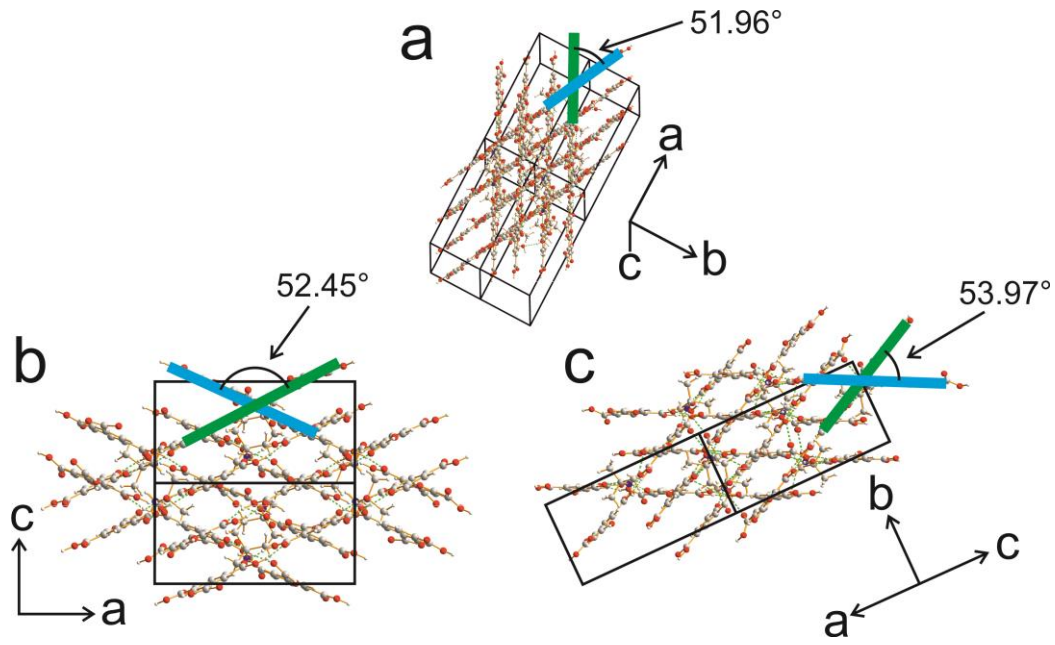

Figure 4.10. *Self-interpenetrated structures of (a) the mono-hydrate, (b) the hemi-hydrate and (c) anhydrous TMA_2TBA_1. For clarity, the blue & green lines represent two different sets of ribbons.*

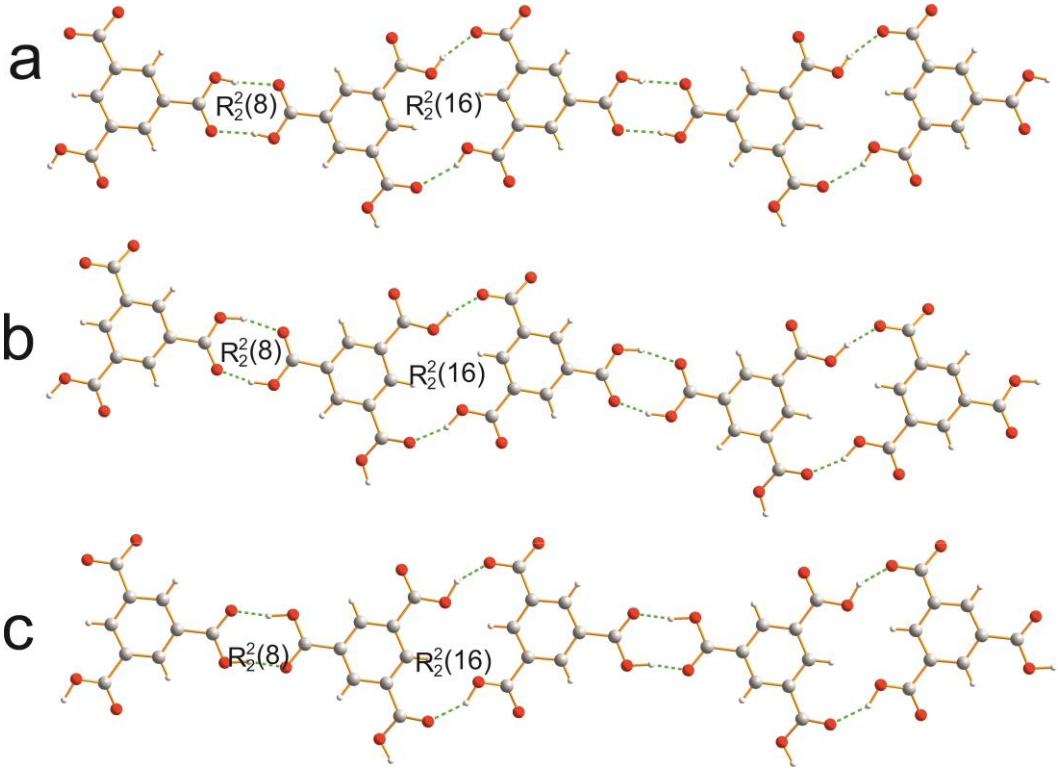

Figure 4.11. *The common ribbon motif in the structures of (a) the mono-hydrate (b) the hemi-hydrate and (c) anhydrous TMA_2TBA_1. For clarity, the blue & green lines are represent two different sets of ribbons.*

As shown in Figure 4.11, the common ribbon in each structure involves an alternation of H_2TMA^- anions and H_3TMA molecules. Within the common ribbon, one H_2TMA^-/H_3TMA pair is linked on one side directly by the typical carboxylic acid dimer head-to-head hydrogen-bonding motif (graph set $R_2^2(8)$), whilst on the other side, the $–COO^-$ group of one H_2TMA^- anion and the –COOH group of the H_3TMA molecule are linked directly, giving rise to the graph set $R_2^2(16)$. As shown in Figure 4.12, in all three structures, adjacent interpenetrated ribbons are linked together by a direct O···H–O hydrogen bond. The major difference between the three structures is that, in the mono-hydrate (Figure 4.12a), adjacent interpenetrated ribbons are also linked by an intervening $HTBA^+$ anion to form a cyclic hydrogen-bonded ring, described by graph set $R_4^4(12)$. The water molecule acts as a hydrogen bond acceptor, linked to the adjacent $HTBA^+$ anion through O···H–N hydrogen bonding. In the structure of the hemi-hydrate and the anhydrous form (Figure 4.12b and 4.12c), there is no cyclic hydrogen bonding formed between the two interpenetrated ribbons.

4.2.6 Summary

When the stoichiometric ratio between TMA and TBA is 2:1, we obtained six different co-crystals. The crystal structures exhibit aspects of structural similarity as

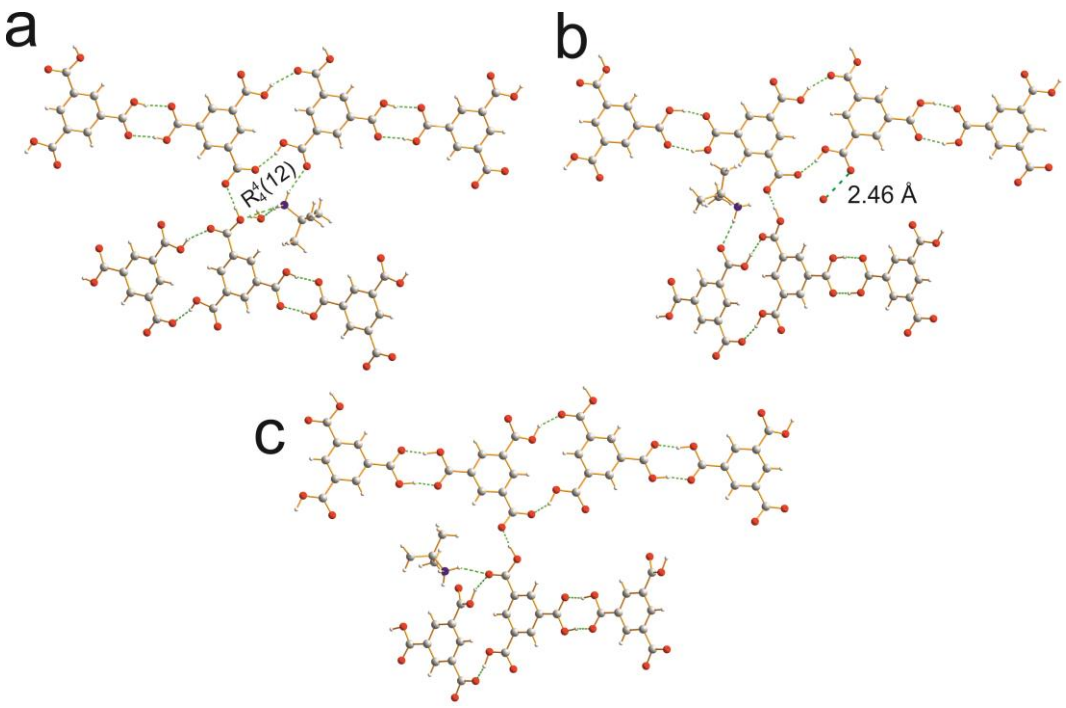

Figure 4.12. *The hydrogen-bonding patterns formed between two interpenetrated ribbons in the structures of (a) the mono-hydrate (b) the hemi-hydrate and (c) anhydrous TMA_2TBA_1.*

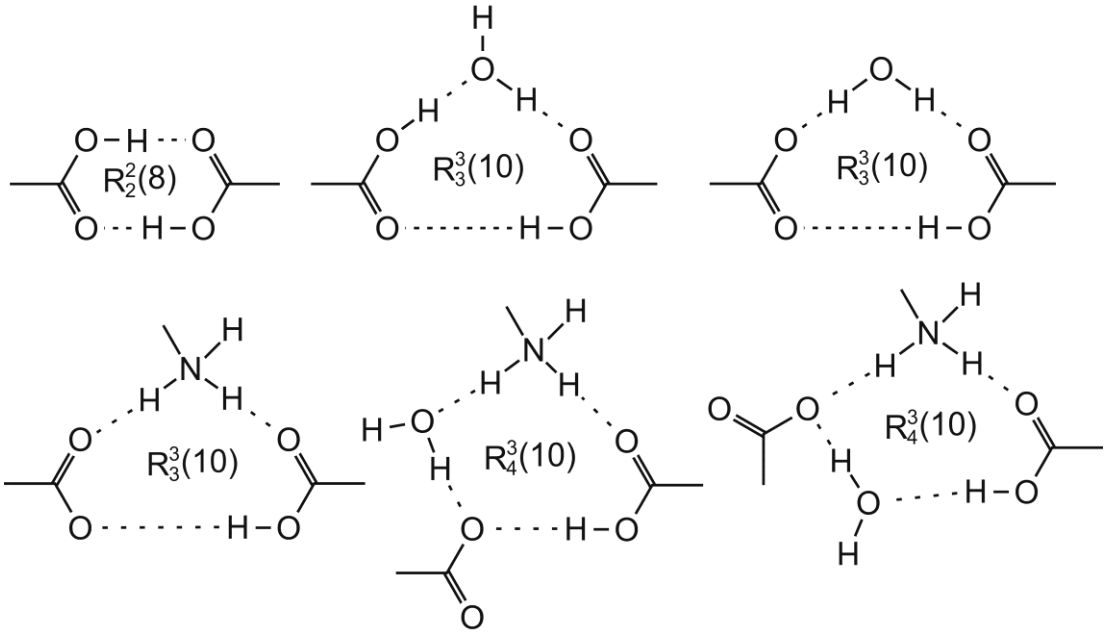

Figure 4.13. *The hydrogen-bonding motifs exhibit in the family of co-crystals of* TMA_2TBA_1

well as significant structural diversity. Thus, one structure comprises double-layered sheets and the other five structures comprise single hydrogen-bonded ribbons with interpenetration. With the participation of $HTBA^+$ cations and solvent molecules, the –COOH and $–COO^–$ groups of adjacent H_3TMA molecules and $H_2TMA^–$ anions form different types of extended hydrogen-bonding patterns (Figure 4.13). Specifically, between adjacent TMA molecules, apart from the typical carboxylic acid dimer head-to-head hydrogen-bonding motif (graph set $R_2^2(8)$), three different single-bridged cyclic hydrogen-bonding motifs $R_3^3(10)$, one single-bridged cyclic hydrogen-bonding motif $R_4^3(10)$ and one double-bridged cyclic hydrogen-bonding motif $R_4^3(10)$ are observed in this family of co-crystals of TMA and TBA.

4.3 Solvatomorphs of TMA_1TBA_1

When the stoichiometric ratio between TMA and TBA is 1:1, we obtained three different crystal structures, comprising one non-solvated material, one methanol solvate and one ethanol solvate, by using different crystallization conditions and methods. All three crystal structures may be described in terms of non-interpenetrated brick-wall networks. To the best of our knowledge, TMA has been used extensively to form honeycomb networks in organic co-crystals, while brick-wall networks of TMA molecules in organic co-crystals are not common[245].

4.3.1 Synthesis and Structure Determination

The crystallization processes to form the methanol solvate $TMA_2TBA_2 \cdot (MeOH)_1$ were as follows: (1) a solution containing TMA and TBA (TMA:TBA = 1:1, molar ratio) in methanol was allowed to evaporate slowly at room temperature. After a few days, the solution dried out in air, and no large single crystals were formed (just microcrystalline materials of the methanol solvate were formed). By recrystallization from methanol and water and allowing it evaporate slowly at room temperature (1:1, volume ratio), after a few days, single crystals of the methanol solvate were obtained. (2) Crystallization was carried out by vapour diffusion of acetone (or acetonitrile) into a solution of TMA and TBA (TMA:TBA = 1:1, molar ratio) in methanol at room temperature; after a few days, single crystals of the methanol solvate were obtained.

The crystallization process to form the ethanol solvate $TMA_1TBA_1 \cdot (EtOH)_{0.25}$ involved vapour diffusion of hexane, acetone or acetonitrile into an ethanol solution containing TMA and TBA (TMA:TBA = 2:1) at ambient temperature. After a few days, single crystals of the ethanol solvate were obtained.

The crystallization process to form the non-solvated material TMA_1TBA_1 involved vapour diffusion of acetonitrile into a methanol and *iso*-propanol (7:1, volume ratio) solution of TMA and TBA (4:3, molar ratio) at room temperature. After a few days, needle crystals were formed (a mixture of the methanol solvate and the non-solvated material). These crystals were left in the open air for a few days. The methanol solvate became a white powder. However, some crystals were still transparent and these crystals were the non-solvated material. Since the morphologies of the methanol solvate and non-solvated material are both needles, we could not distinguish them by their morphology.

Single-crystal X-ray diffraction data for these three structures were collected at 150 K on a Nonius Kappa CCD diffractometer equipped with a molybdenum tube source ($\lambda = 0.71073$ Å). The crystal structures were solved (by direct methods) by SHELXS and refined using SHELXL. Refinement of non-hydrogen atoms was carried out using anisotropic displacement parameters. All hydrogen atoms were located in difference Fourier maps and were added to the structural model according to idealized geometries. Refinement of hydrogen atoms was carried out using a riding model, with

isotropic displacement parameter equal to 1.2 or 1.5 times the equivalent isotropic displacement parameter of the atom to which the hydrogen atom is bonded.

4.3.2 Structural Analysis and Discussion

The crystallographic parameters of these three structures are summarized in Table 4.2 and the crystal structures are shown in Figures 4.14 and 4.15.

Table 4.2 Crystallographic parameters of three co-crystals of TMA_1TBA_1.

	Non-Solvate	Methanol Solvate	Ethanol Solvate
Asymmetric unit	TMA_1TBA_1	$TMA_2TBA_2{\cdot}(MeOH)_1$	$TMA_1TBA_1{\cdot}(EtOH)_{0.25}$
Crystal system	Orthorhombic	Orthorhombic	Orthorhombic
Space group	Pnma	$Pn2_1a$	Pnma
a/Å	6.7096(2)	6.6455(2)	6.7024(2)
b/Å	18.4261(4)	18.4347(5)	18.4663(4)
c/Å	24.8287(5)	24.7661(5)	24.8273(6)
V(Å^3)	3036.62(13)	3034.04(14)	3072.84(14)
Z	8	4	8
Calculated Density (g/cm^3)	1.226	1.310	1.266
R_1/(%)	4.63	5.85	9.60
R_{w2}/(%)	13.58	14.48	28.37

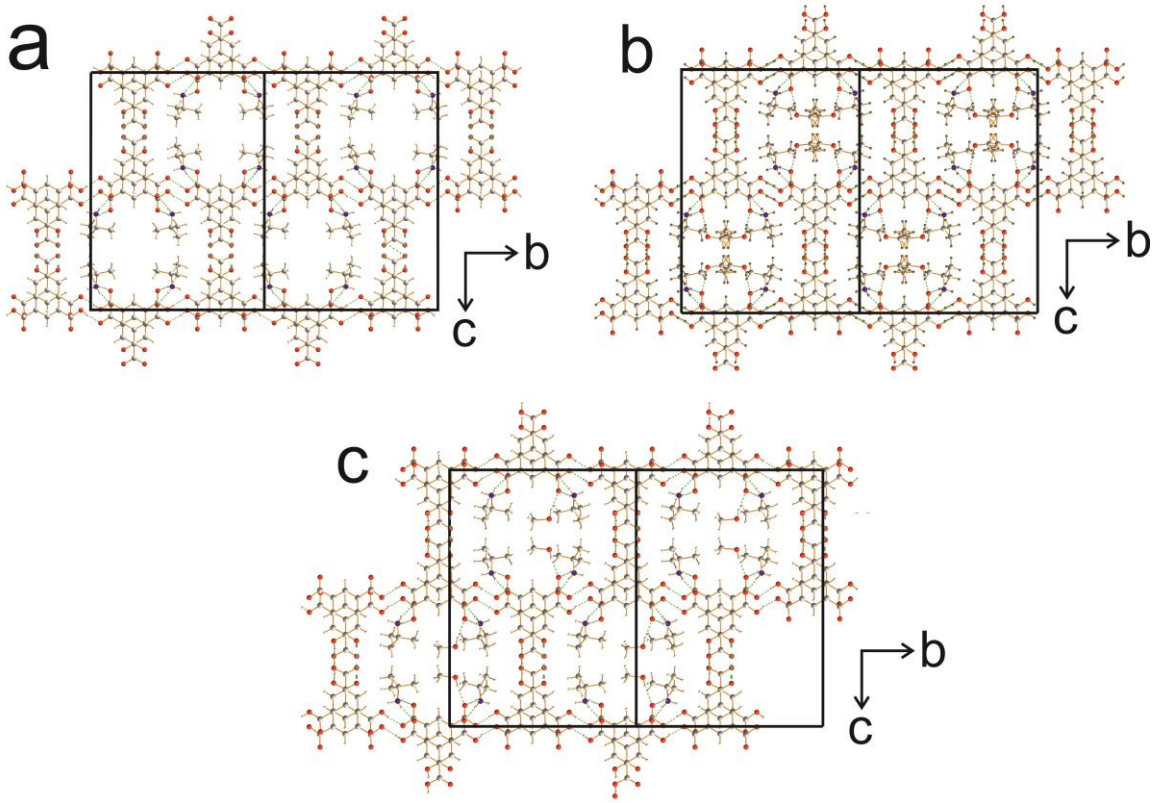

Figure 4.14. *The crystal structures of (a) the non-solvated material (b) the ethanol solvate and (c) the methanol solvate.*

From Figure 4.14 and Table 4.2, we can see that all three co-crystal structures are very similar. Firstly (Table 4.2), all of these materials are orthorhombic although with different space groups (for the non-solvated material and ethanol solvate, the space group is Pnma; for the methanol solvate, the space group is $Pn2_1a$) and the unit cell parameters and volumes are quite similar. In addition, all of these structures comprise $HTBA^+$ cations and H_2TMA^- anions. Secondly (Figure 4.14), all of these structures are composed of two-dimensional, brick-wall networks instead of hexagonal network sheets, which are generated by six adjacent H_2TMA^- anions through $–COOH\cdots–COO^-$ hydrogen bonding. This hydrogen-bonding arrangement creates almost the same size of cavities with dimensions of 16.2 × 11.1 Å in each structure, which is comparable with the cavities observed in the crystal structure of pure α-trimesic acid (14 × 14 Å). Third, in every cavity in all three structures, there are four $HTBA^+$ cations and, due to the symmetry of each structure, the positions of all four $HTBA^+$ cations are symmetry related.

We note that, in all three structures, some of the H atoms of the carboxylic acid groups of the H_2TMA^- anions are partially deprotonated, representing disorder in the hydrogen-bonding arrangement (with partial occupancy of certain H sites). Part of the reason for the disorder of the H atoms over two sites with the same occupancies is a consequence of the high symmetry of the space group. In every brick-wall network ring (Figure 4.14), two typical carboxylic acid dimer head-to-head hydrogen-bonding motifs (graph set $R_2^2(8)$) remain intact through hydrogen bonding involving these disordered H atoms of one carboxylic group of adjacent TMA molecules.

Investigating these three structures in more detail, we can see that, in each structure (Figure 4.15a to c), adjacent brick-wall network sheets pack with a small offset to produce a channel along the a-axis, which runs through the brick-wall cavities. The distance between adjacent sheets is 3.35 Å (for the non-solvated structure), 3.32 Å (for the methanol solvate structure) and 3.35 Å (for the ethanol solvate structure). In each structure, the channel is occupied by four symmetrically arranged $HTBA^+$ cations. Two N–H groups of each $HTBA^+$ cation are linked to adjacent brick-wall network sheets through $N–H\cdots O$ hydrogen bonds. The distances between pairs of N atoms in every cavity are slightly different (Figure 4.15). For example, for all three structures, viewing along the b-axis, the distances between pairs of N atoms are 8.10 Å, 8.13 Å and 8.20 Å,

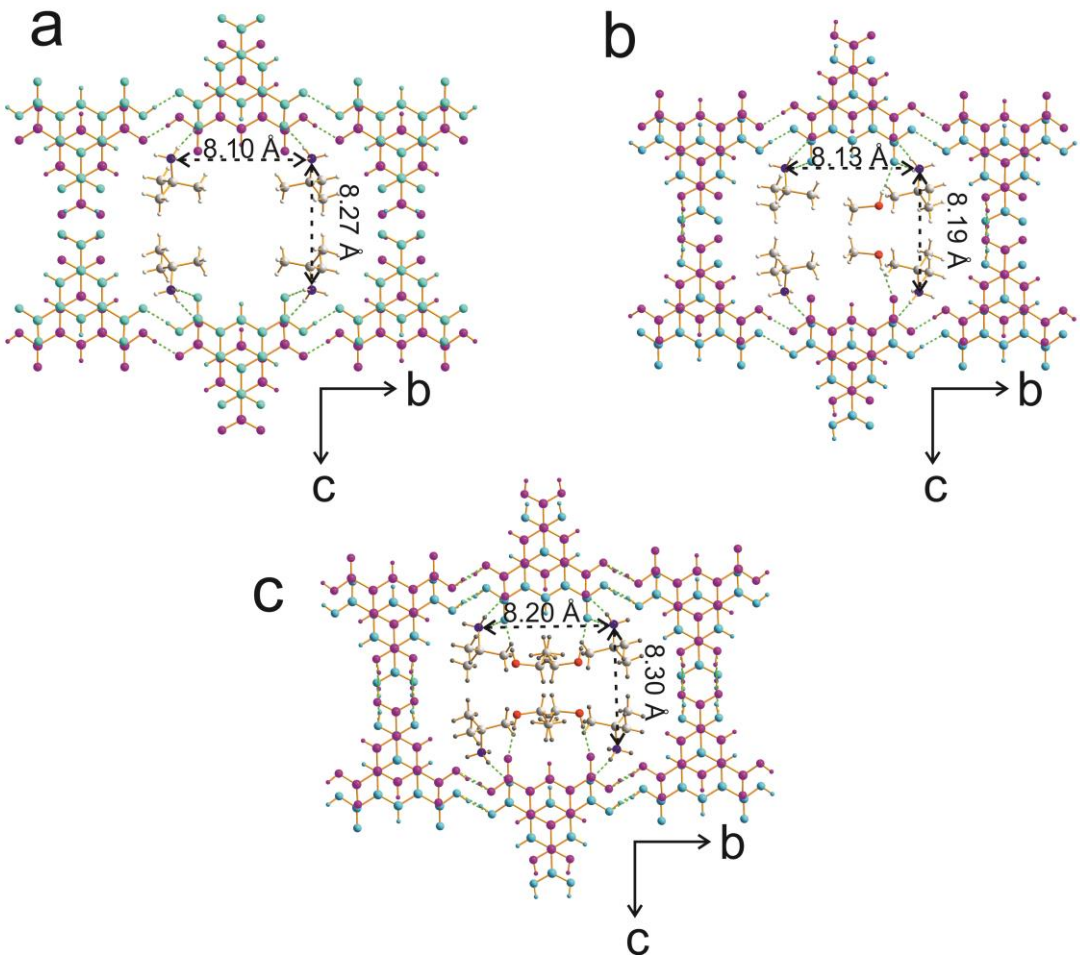

Figure 4.15. *The brick-wall network motifs in the crystal structures of (a) the non-solvated material, (b) the ethanol solvate and (c) the methanol solvate.*

respectively; viewing along the c-axis, the distances between pairs of N atoms are 8.27 Å, 8.19 Å and 8.30 Å, respectively. In the case of the ethanol solvate (Figure 4.15c), apart from four $HTBA^+$ cations, disordered ethanol molecules are also trapped in the centre of the channel, filling the void space not occupied by the $HTBA^+$ cations. The ethanol molecule is disordered over four positions with the same occupancies (0.25:0.25:0.25:0.25). The ethanol molecule is linked to an adjacent H_2TMA^- anion through an O (TMA)···H–O (ethanol) hydrogen bond, with an O···H distance of 1.91 Å and an O···O distance of 2.74 Å. In the case of the methanol solvate (Figure 4.15b), in addition to the $HTBA^+$ cations, there are two ordered methanol molecules (symmetry related) trapped in the centre of the channel and the methanol molecule is linked to an adjacent TMA molecule through an O (TMA)···H–O (methanol) hydrogen bond and the O···H distance is 2.01 Å. In the structure of the non-solvated material, the cavities of the channels are empty (apart from $HTBA^+$ cations).

4.3.3 Summary

When the stoichiometric ratio between TMA and TBA is 1:1, we obtained three different co-crystals and each structure comprises non-interpenetrated brick-wall networks. Apart from the typical carboxylic acid dimer head-to-head hydrogen-bonding motif (graph set $R_2^2(8)$), there is no new cyclic hydrogen-bonding motif formed in this family of co-crystals.

4.4 Solvatomorphs of TMA_1TBA_2

In the course of studying co-crystals of TMA and TBA, when the stoichiometric ratio of TMA to TBA is 1:2, we obtained six solvated co-crystals by using different solvents and different crystallization methods. The co-crystals contain the following solvents: methanol, ethanol, *iso*-propanol, *iso*-butanol, 2-methyl-2-butanol (TAA) and 1,4-butanediol (BDO), and the ratio of TMA:TBA:solvent is 1:2:1 in each case except the BDO solvate (in the BDO solvate, the ratio of TMA:TBA:BDO is 4:8:3.5). Initially, we attempted to crystallize co-crystals without solvent at this stoichiometric ratio between TMA and TBA by using different types of alcohol. However, it turned out that incorporating alcohol molecules into the structure is a key factor in the formation of the structures reported here.

4.4.1 Synthesis and Structure Determination

The crystallization process to form the methanol solvate $TMA_1TBA_2{\cdot}(MeOH)_1$ involved dissolving TMA and TBA (1:2, molar ratio) in methanol, followed by stirring for 1 hour, then vapour diffusion of hexane into this solution at room temperature. After a few days, single crystals were obtained.

The crystallization processes to form the ethanol solvate $TMA_1TBA_2{\cdot}(EtOH)_1$ were as follows: (1) Vapour diffusion of acetone into an ethanol solution containing TMA and TBA (2:1) at ambient temperature; after a few days, single crystals of the ethanol solvate were obtained. (2) A solution of TMA and TBA (1:2, molar ratio) in ethanol and methanol (4:1, volume ratio) was evaporated slowly at ambient temperature; after a few days, single crystals were obtained.

The crystallization process to form the *iso*-propanol solvate $TMA_1TBA_2{\cdot}(iso\text{-propanol})_1$ involved slow evaporation of a solution of TMA and TBA

(1:2, molar ratio) in methanol and *iso*-propanol (1:1, volume ratio) at ambient temperature. After a few days, single crystals were obtained.

The crystallization process to form the *iso*-butanol solvate $TMA_1TBA_2{\cdot}(iso\text{-butanol})_1$ involved slow evaporation of a solution of TMA and TBA (1:2, molar ratio) in methanol and *iso*-butanol (1:1, volume ratio) at room temperature. After a few days, single crystals were obtained.

The crystallization process to form the TAA solvate $TMA_1TBA_2{\cdot}(TAA)_1$ involved slow evaporation of a solution of TMA and TBA (1:2, molar ratio) in methanol and TAA (1:1, volume ratio) at ambient temperature. After a few days, single crystals were obtained.

The crystallization process to form the BDO solvate $TMA_4TBA_8{\cdot}(BDO)_{3.5}$ involved slow evaporation of a solution of TMA and TBA (1:2, molar ratio) in methanol and BDO (6:1, volume ratio) at room temperature. After a few days, single crystals were obtained.

Single-crystal X-ray diffraction data for these three structures were collected at 150 K on a Nonius Kappa CCD diffractometer equipped with a molybdenum tube source ($\lambda = 0.71073$ Å). The crystal structures were solved (by direct methods) by SHELXS and refined using SHELXL. Refinement of non-hydrogen atoms was carried out using anisotropic displacement parameters. All hydrogen atoms were located in difference Fourier maps and were added to the structural model according to idealized geometries. Refinement of hydrogen atoms was carried out using a riding model, with isotropic displacement parameter equal to 1.2 or 1.5 times the equivalent isotropic displacement parameter of the atom to which the hydrogen atom is bonded.

4.4.2 Structural Summary of the Co-Crystals of TMA_1TBA_2

The relationships between these solvated co-crystals are summarized in Figure 4.16. As shown in Figure 4.16, all these solvates are unstable at room temperature in the open air, the process of desolvation would give rise to the mixed sample of TMA_2TBA_3 and $TMA_1TBA_3{\cdot}(H_2O)_{4.5}$.The crystallographic parameters of the six solvate structures are summarized in Table 4.3 and the crystal structures are shown in Figures 4.17 to 4.23.

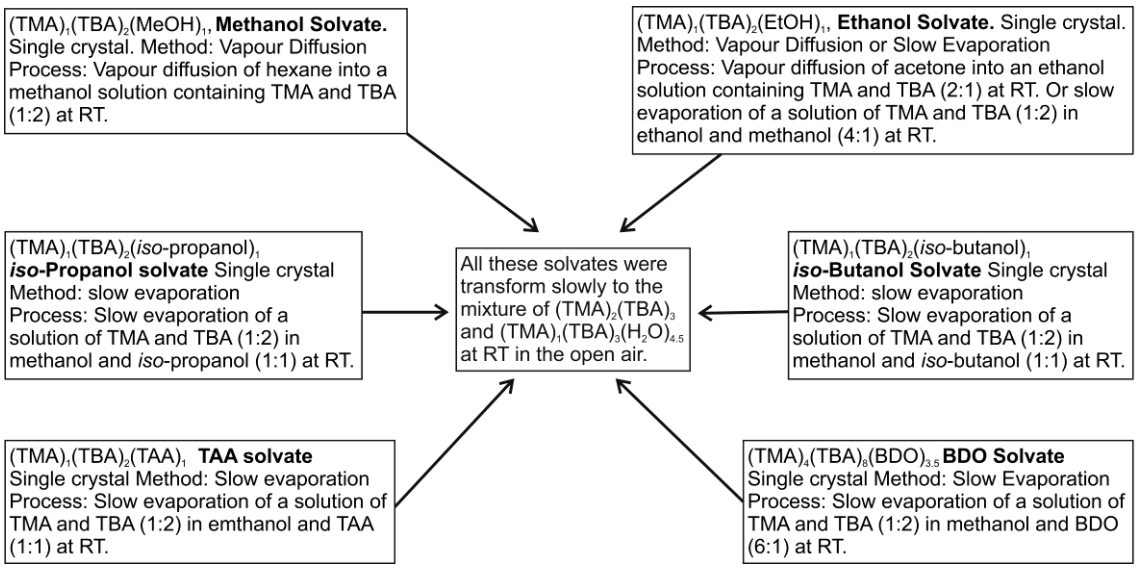

Figure 4.16. *The relationships between solvatomorphs of co-crystals of TMA_1TBA_2.*

Table 4.3 The crystallographic parameters for solvates of TMA_1TBA_2

	Methanol Solvate	Ethanol Solvate	*iso*-Propanol Solvate
Space group	$P2_1/c$	Pbca	Pbca
a/Å	8.6137(3)	12.9364(2)	13.1597(2)
b/Å	15.4335(3)	17.8528(5)	18.0482(5)
c/Å	16.9968(6)	20.2683(5)	20.1787(5)
α/°	90	90	90
β/°	104.108(1)	90	90
γ/°	90	90	90
V(Å^3)	2191.39(12)	4680.98(19)	4792.62(19)
Z	4	8	8
Calculated Density (g/cm^3)	1.177	1.142	1.154
R_1/(%)	8.07	6.41	6.03
R_{w2}/(%)	20.66	14.99	14.24

	iso-Butanol Solvate	TAA Solvate	BDO Solvate
Space group	$Pna2_1$	$Pna2_1$	$P2_1/c$
a/Å	12.1189(4)	12.2728(3)	16.4207(4)
b/Å	12.6727(4)	12.4920(3)	21.8182(6)
c/Å	16.4727(3)	16.5334(5)	27.9872(6)
α/°	90	90	90
β/°	90	90	101.187(2)
γ/°	90	90	90
V (Å^3)	2529.86(12)	2534.77(12)	9836.46(42)
Z	4	4	4
Density (g/cm^3)	1.130	1.165	1.206
R_1/(%)	6.83	7.54	9.69
R_{w2}/(%)	17.98	15.42	24.94

From Table 4.3, we can see that these six structures can be classified into three categories according to their space groups. The ethanol and *iso*-propanol solvates are orthorhombic with space group Pbca. The *iso*-butanol and TAA solvates are orthorhombic with space group $Pna2_1$. The methanol and BDO solvates are monoclinic with space group $P2_1/c$. In the structures of the methanol, ethanol, *iso*-propanol, *iso*-butanol and TAA solvates, the asymmetric unit comprises four independent molecules: one $HTMA^{2-}$ anion, two $HTBA^{+}$ cations and one solvent molecule. However, in the structure of the BDO solvate, the asymmetric unit comprises of four $HTMA^{2-}$

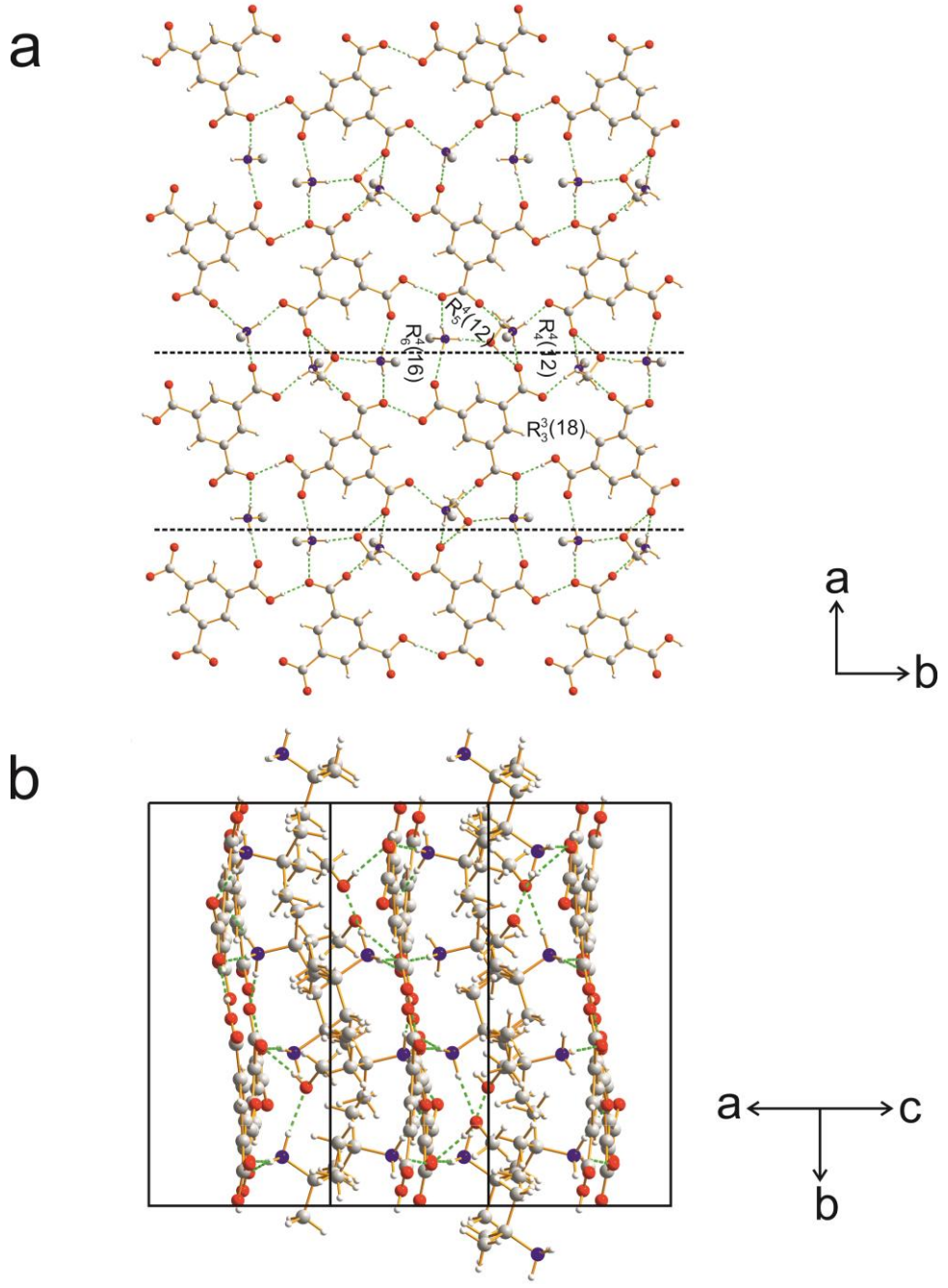

Figure 4.17. *(a) Hydrogen-bonding patterns in the corrugated sheets and (b) the complete crystal structure of the methanol solvate.*

anions, eight $HTBA^+$ cations and three and a half independent solvent molecules (three independent whole molecules of BDO and a half independent molecule of BDO).

In addition, from Figures 4.17b to 4.22b, we can see that these six structures can be classified into three categories according to their structural features. For the methanol, ethanol and *iso*-propanol solvates, the crystal structures comprise similar, single hydrogen-bonded corrugated sheets. For the *iso*-butanol and TAA solvates, the crystal

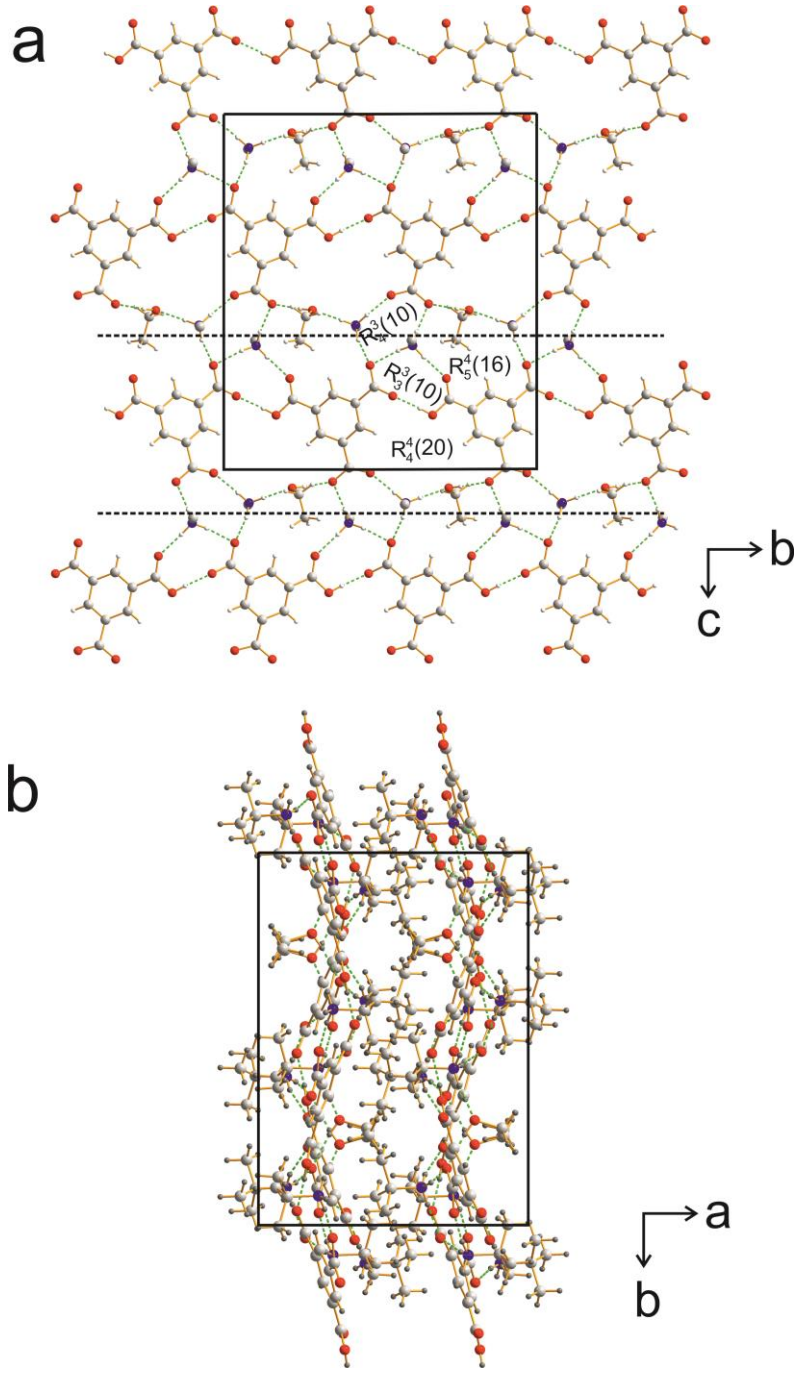

Figure 4.18. *(a) Hydrogen-bonding patterns in the corrugated sheets and (b) the complete crystal structure of the ethanol solvate.*

structures comprise single hydrogen-bonded flat sheets. For the BDO solvate, the crystal structure also comprises single hydrogen-bonded sheets, which are almost but not exactly flat, as the planes of all the $HTMA^{2-}$ anions do not lie exactly in the same plane. These sheets actually give rise to channels, containing the BDO solvent molecules. In all six structures, the $-N^{+}H_3$ groups of the $HTBA^{+}$ cations and the OH groups of the solvent molecules lie close to the sheets of $HTMA^{2-}$ anions, and are engaged in hydrogen bonding. The *tert*-butyl groups (TBA) and alkyl groups of the solvents project outwards from the sheets. For clarity, the three methyl groups of the *tert*-butyl groups are omitted in the figures.

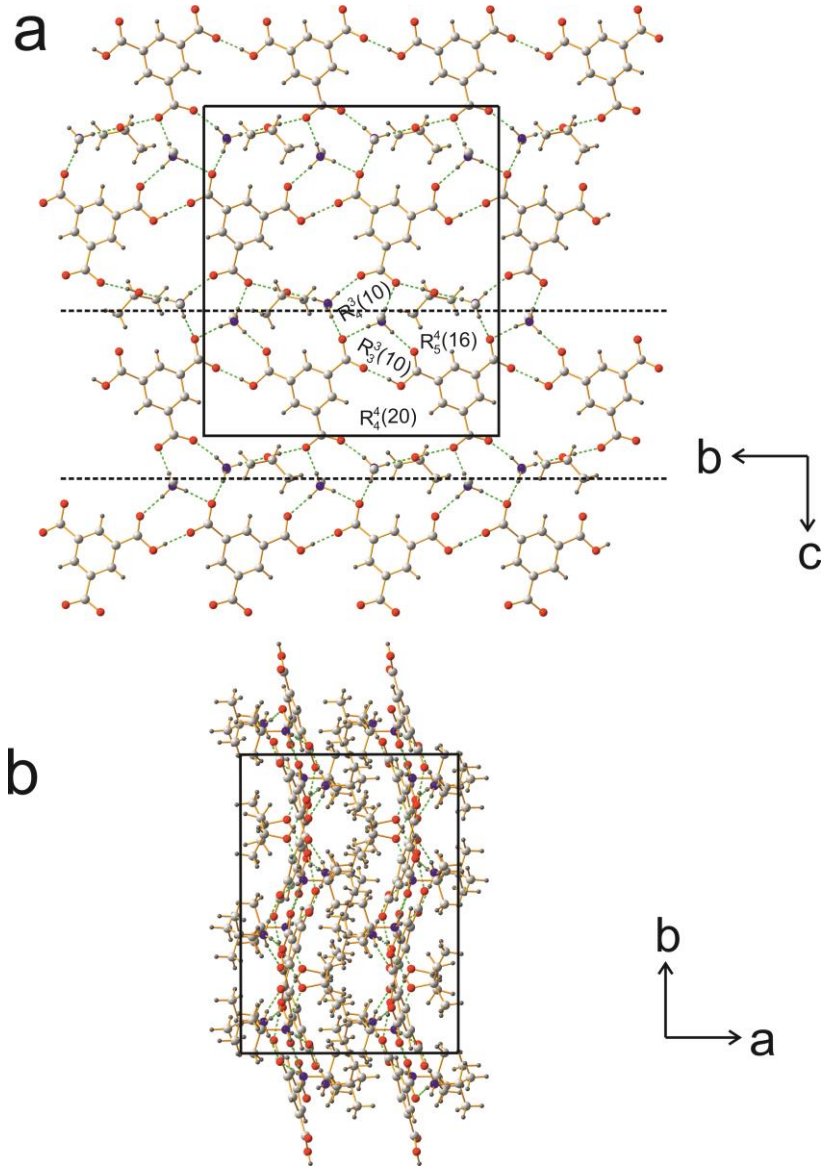

Figure 4.19. *(a) Hydrogen-bonding patterns in the corrugated sheet in the crystal structure of the iso-propanol solvate TMA_1TBA_2·(iso-propanol), and (b) the complete crystal structure of iso-propanol solvate.*

4.4.3 Structural Comparison Between the Methanol Solvate, the Ethanol Solvate and the iso-Propanol Solvate of TMA_1TBA_2

As shown in Figures 4.17 to 4.19, within the corrugated sheet, each structure has a similar hydrogen-bonded ribbon motif, which runs parallel to the b-axis in each case. These ribbons are indicated as the region between the two dashed lines.

For the ethanol and *iso*-propanol solvates (Figures 4.18a and 4.19a), within the ribbon motif, adjacent $HTMA^{2-}$ anions are linked by a direct O–H···O hydrogen bond and are bridged by an intervening $-N^+H_3$ group, forming a common cyclic hydrogen-bonding motif with graph set $R_3^3(10)$. Furthermore, these two $HTMA^{2-}$ anions are also linked to each other by an intervening $-N^+H_3$ group and the OH group of a solvent molecule to form a large common cyclic hydrogen-bonding motif with graph set $R_4^4(20)$. In the ribbon motif of the methanol solvate (Figure 4.17a), adjacent $HTMA^{2-}$ anions are linked by a direct O–H···O hydrogen bond but, there is no cyclic hydrogen-bonding motif involving these two groups. Instead, a large cyclic hydrogen-bonding motif with graph set $R_3^3(18)$ forms between these two $HTMA^{2-}$ anions and an intervening $-N^+H_3$ group.

For the ethanol and *iso*-propanol solvates (Figures 4.18a and 4.19a), adjacent ribbons are linked by two common cyclic hydrogen-bonded rings, described by graph sets $R_4^3(10)$ and $R_5^4(16)$. However, the methanol solvate (Figure 4.17a) has a different arrangement. Between two adjacent ribbons, three new cyclic hydrogen-bonded rings, described as $R_4^4(12)$, $R_5^4(12)$ and $R_6^4(16)$, are formed.

4.4.4. Structural Comparison Between the iso-Butanol and the 2-Methyl-2-Butanol Solvates of TMA_1TBA_2

As shown in Figures 4.20a and 4.21a, these two solvates possess flat hydrogen-bonded sheets and their structures are quite similar. Specifically, within the sheet, both structures have almost the same hydrogen-bonded zigzag ribbons, which run along the c-axis and are indicated as the region between the two dashed zigzag lines. The hydrogen-bonded sheets are stacked in a very similar manner (Figures 4.20b and 4.21b) that causes the *tert*-butyl groups and the alkyl groups of the solvent to come together at the interface between adjacent sheets, with a similar perpendicular distance (6.34 Å and 6.26 Å) between the sheets in each structure.

In both structures (Figures 4.20a and 4.21a), within the zigzag ribbon, adjacent $HTMA^{2-}$ anions are linked together by a direct O–H···O hydrogen bond and by an intervening $-N^{+}H_3$ groups of $HTBA^{+}$ cation to form the cyclic graph set $R_3^3(10)$, as in the structures of the ethanol and *iso*-propanol solvates. Adjacent zigzag ribbons are linked by the interaction of one $-COO^{-}$ group from each of $HTMA^{2-}$ anion with two intervening $-N^{+}H_3$ groups, which gives rise to the same cyclic graph set $R_4^3(10)$ as that observed in the ethanol and *iso*-propanol solvates.

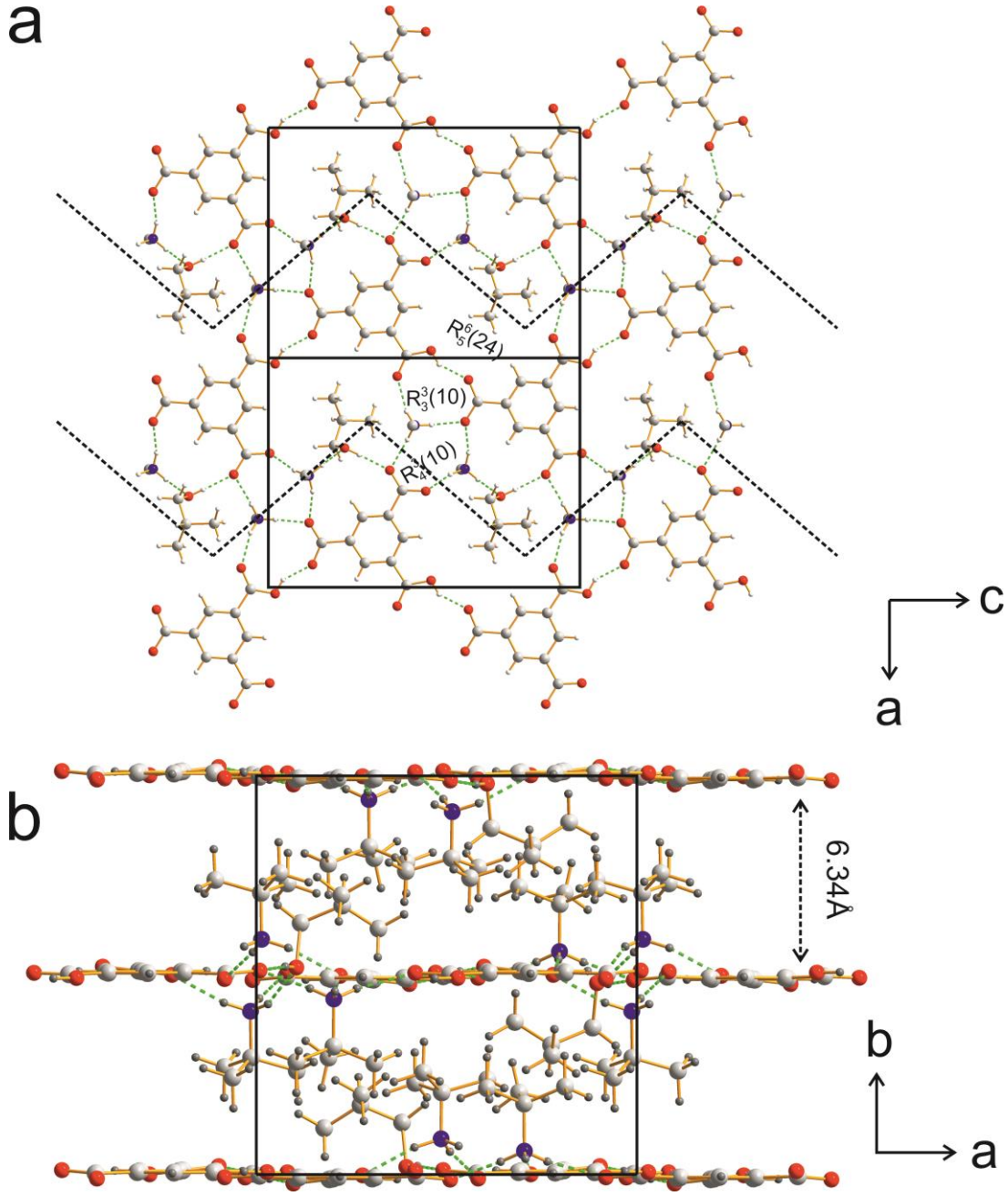

Figure 4.20. *(a) Hydrogen-bonding patterns of zigzag ribbon in the sheet s and (b) the complete crystal structure of the iso-butanol solvate.*

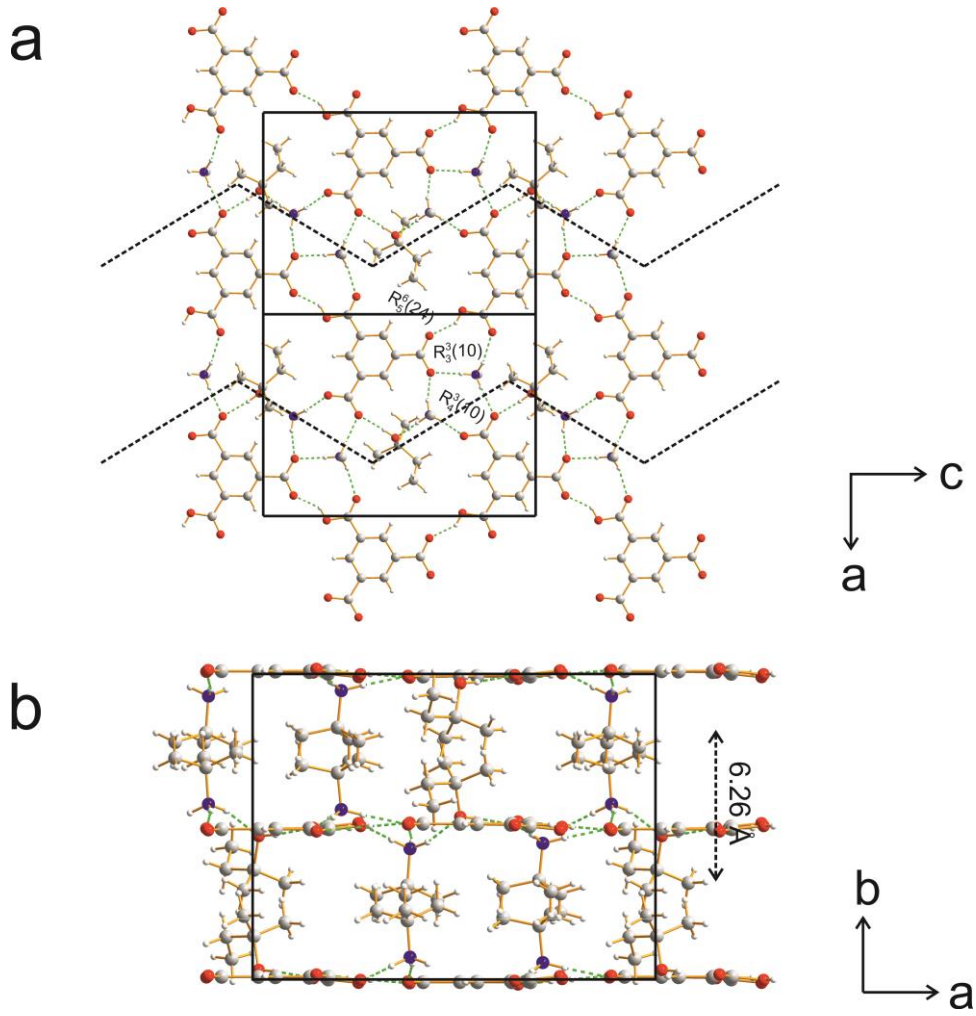

Figure 4.21. *(a) Hydrogen-bonding patterns of zigzag ribbon in the sheet in the crystal structure of the TAA solvate and (b) the complete crystal structure.*

In addition, within every sheet, three adjacent $HTMA^{2-}$ anions are linked together via two intervening $-N^+H_3$ groups forming a large cyclic hydrogen-bonding motif (graph set $R_5^6(24)$). One solvent molecule (*iso*-butanol or TAA) occupies the centre of this hydrogen-bonded ring. The solvent molecule is linked to one $HTMA^{2-}$ anion through an O ($HTMA^{2-}$)···H–O (solvent) hydrogen bond and linked to one $-N^+H_3$ group of a $HTBA^+$ anion through an O (solvent)···H–N ($HTBA^+$) hydrogen bond.

4.4.5. Structural Analysis of the 1,4-Butanediol Solvate of TMA_1TBA_2

From Figure 4.22, we can see that, in the structure of BDO solvate, the $HTMA^{2-}$ anions form approximately flat sheets. These sheets and BDO solvent molecules form two types of channel with cavities of dimensions *ca.* 7.4 Å × 9.3 Å and *ca.*7.0 Å × 5.5 Å, and the $HTBA^+$ cations occupy these channels.

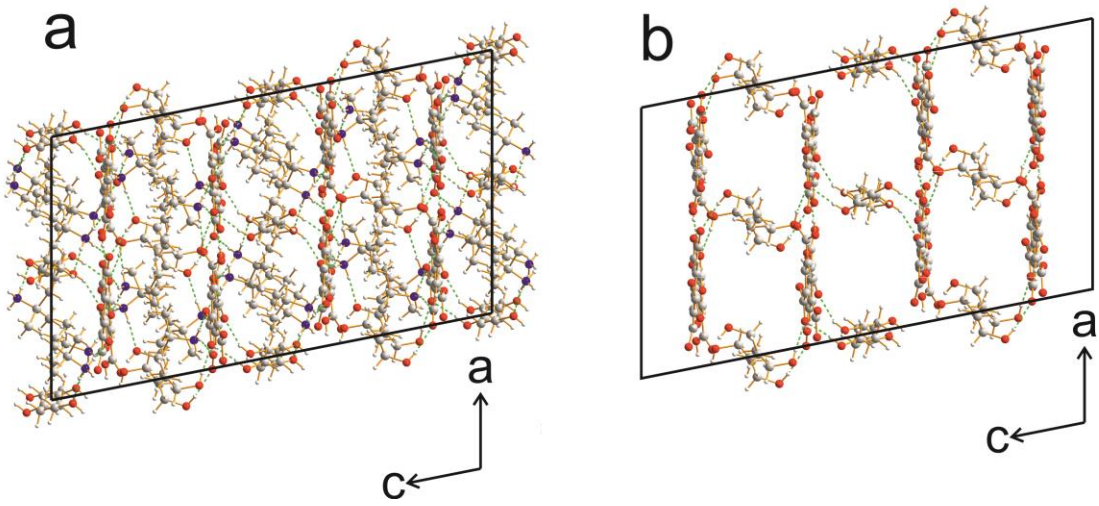

Figure 4.22. *(a) Crystal structure of the BDO solvate $TMA_4TBA_8{\cdot}(BDO)_{3.5}$ and (b) two types of channel formed by $HTMA^{2-}$ anions and solvent molecules.*

The BDO solvate is monoclinic with space group $P2_1/c$ and the asymmetric unit comprises four independent $HTMA^{2-}$ anions (denoted A_1 to A_4), eight independent $HTBA^+$ cations (denoted N_1 to N_8) and three and a half independent solvent molecules (denoted S_1 to S_4). As the solvent molecule has two OH groups, the OH groups of each solvent molecule are denoted S_{ia} and S_{ib}, i = 1 to 4.

As shown in Figure 4.23, within each sheet, there are two types of zigzag ribbons (denoted ribbons I and II), which run along the a-axis. The ribbon I motif involves an alternation of the A_2 and A_1 anions in a zigzag and the ribbon II motif involves an alternation of the A_3 and A_4 anions in a zigzag. Within ribbon I, each A_2/A_1 anion pair is linked by a direct O–H···O hydrogen bond and forms a cyclic hydrogen-bonding ring through an intervening $–N^+H_3$ group of the N_4 cation, which gives rise to graph set $R_3^2(8)$. The A_2 anion and the A_1 anion are also bridged by an intervening $–N^+H_3$ group of the N_3 cation and OH bond S_{1b} of the molecule to form a cyclic hydrogen-bonded ring with graph set $R_4^4(16)$. On the other side, the A_1 anion and another A_2 anion are bridged by an intervening $–N^+H_3$ group of the N_7 cation and OH bond S_{4b} of the solvent, forming another cyclic hydrogen-bonded motif with graph set $R_4^4(16)$.

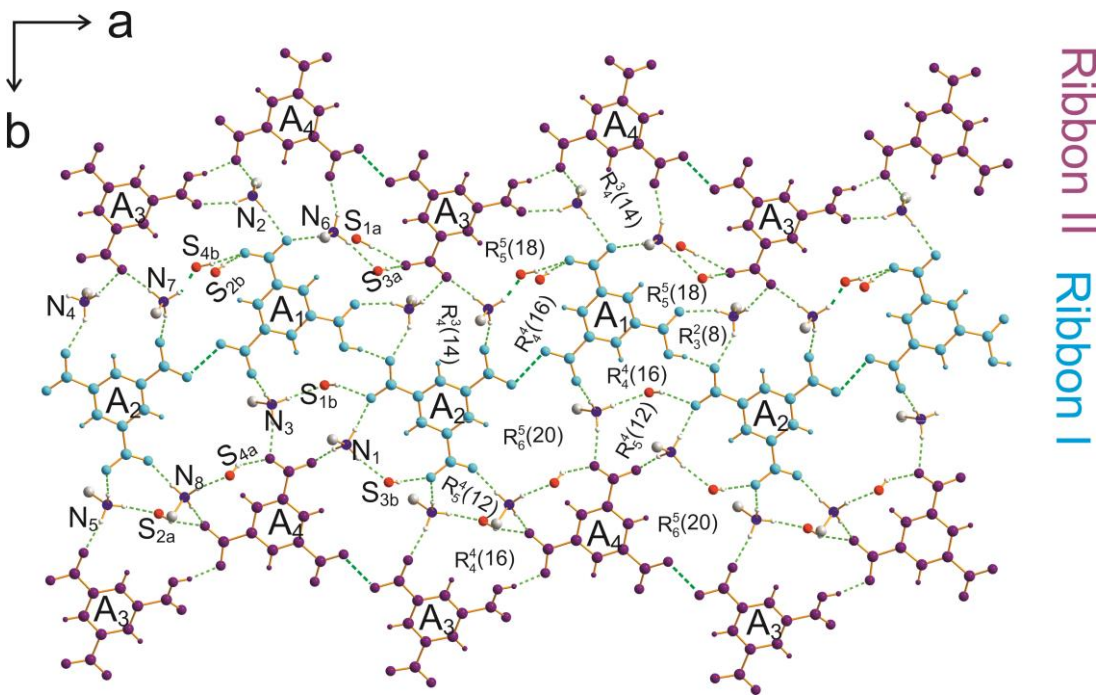

Figure 4.23. *The hydrogen-bonding patterns of ribbon I (cyan) and ribbon II (purple) in the BDO solvate* $TMA_4TBA_8 \cdot (BDO)_{3.5}$.

Within ribbon II, the same graph set $R_3^2(8)$ is formed between each A_3/A_4 anion pair, involving the intervening $-N^+H_3$ group of the N_2 cation. In addition, as for each A_2/A_1 anion pair, two hydrogen-bonded rings with graph sets $R_4^4(16)$ are also formed for each A_3/A_4 anion pair. One ring involves an A_3/A_4 anion pair and the intervening $-N^+H_3$ group of the N_6 cation and the OH group S_{3a} of the solvent and the other involves an A_3/A_4 anion pair with the intervening $-N^+H_3$ group of the N_5 cation and the OH group S_{2a} of the solvent.

Between these two types of ribbons, seven different cyclic hydrogen-bonded rings arise. The graph set descriptors for all these rings are marked in Figure 4.23 and are described as follows: (i) $R_5^5(18)$, involving the A_1 and A_3 anions, the N_2 and N_7 cations and the S_{4b} solvent molecule; (ii) another $R_5^5(18)$, involving the A_1 anion, another A_3 anion, the N_4 and N_6 cations and the S_{3a} solvent molecule; (iii) $R_4^3(14)$, involving the A_1 and A_4 anions, the N_2 and N_6 cations; (iv) another $R_4^3(14)$ involving the A_2 and A_3 cations, the N_4 and N_7 cations; (v) $R_5^4(12)$, involving the A_2 and A_4 anions, the N_5 and N_8 cations and the S_{2a} solvent molecule; (vi) $R_6^5(20)$, involving the A_1, A_2 and A_4 anions, the N_3 and N_8 cations and the S_{3b} solvent molecule; (vii) $R_6^5(20)$, involving the A_2, A_4 and A_5 anions, the N_1 and N_5 cations and the S_{3b} solvent molecule.

In terms of the $HTBA^+$ cations, for all six solvates, all three N–H bonds in each independent $HTBA^+$ cation are engaged as donors in N–H···O hydrogen bonds to O atoms of the $HTMA^{2-}$ anion or a solvent molecule. In terms of the solvent molecules, the O–H bond of each independent solvent molecule is used both (i) as the donor in an O–H···O hydrogen bond with an O atom of the $HTMA^{2-}$ anion as the acceptor, and (ii) as the acceptor in an N–H···O hydrogen bond with an N–H bond of an $HTBA^+$ cation as the donor.

4.4.6 Summary

When the stoichiometric ratio between TMA and TBA is 1:2, we obtained six solvate co-crystals, with each structure comprising hydrogen-bonded sheets. Analysis of these six crystal structures indicates that the specific hydrogen-bonding motifs formed are quite sensitive to the crystallization solvent. In these six solvate structures, the typical carboxylic acid dimer head-to-head hydrogen-bonding motif (graph set $R_2^2(8)$) does not appear between carboxylic acid groups of the H_2TMA^- anions. However, several new hydrogen-bonding patterns are observed (Figure 4.24). Specifically, in addition to graph set $R_3^3(10)$ (a common cyclic hydrogen-bonding motif already observed in the family of co-crystals of TMA_2TBA_1), one new single-bridged cyclic

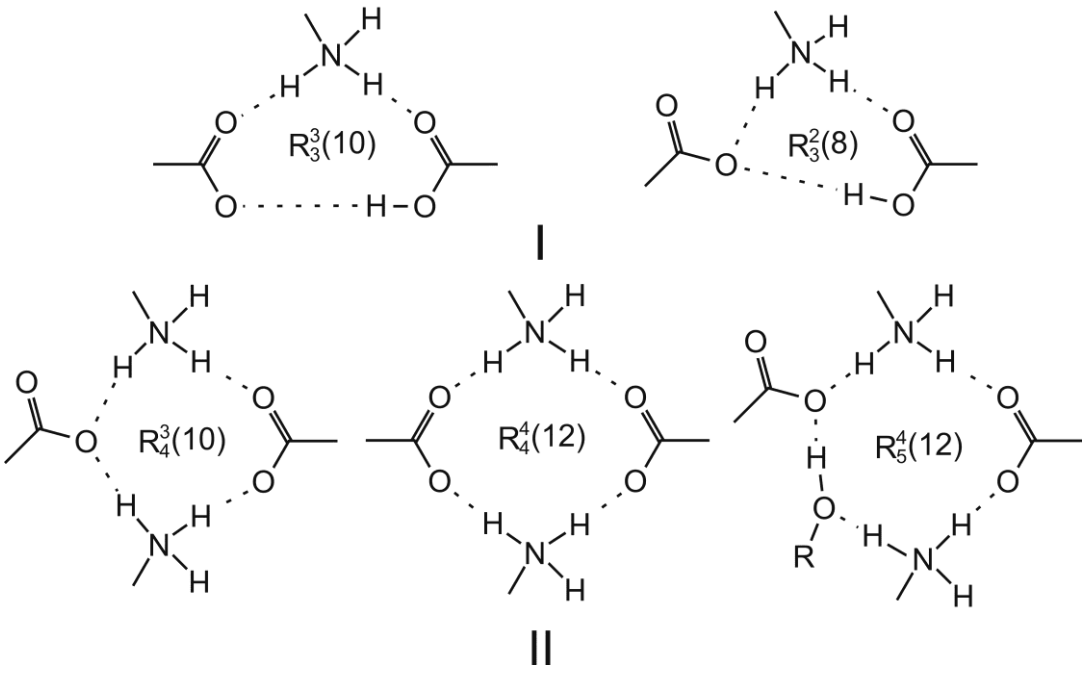

Figure 4.24. *The hydrogen-bonding motifs observed in the family of co-crystals of TMA_1TBA_2 (I) single-bridged graph sets $R_3^3(10)$ and $R_3^2(8)$; (II) double-bridged graph sets $R_4^3(10)$, $R_4^4(12)$ and $R_5^4(12)$.*

hydrogen-bonding motif $R_3^2(8)$ and three new double-bridged cyclic hydrogen-bonding motifs $R_4^3(10)$, $R_4^4(12)$ and $R_5^4(12)$ are formed in this family of co-crystals.

4.5 Solvatomorphs of TMA_1TBA_3

When the stoichiometric ratio of TMA to TBA is 1:3, we obtained five different co-crystals of TMA_1TBA_3 by using different crystallization conditions and different crystallization methods. Clearly, the H_3TMA molecules are totally deprotonated (i.e., TMA^{3-}) in these co-crystals, and thus the resulting crystal structures are devoid of any type of acid-acid hydrogen bonding. In these structures, the carboxylate groups of the TMA^{3-} anions are bridged by the OH groups of the solvent molecules or the N^+H_3 groups of the $HTBA^+$ cations.

4.5.1 Synthesis and Structure Determination

The crystallization process to form the mixed di-methanol/mono-hydrate $TMA_1TBA_3{\cdot}(MeOH)_2(H_2O)_1$ involved slow evaporation of a methanol solution containing TMA and TBA (1:3 molar ratio). After a few days, single crystals were obtained.

The crystallization process to form the methanol solvate $TMA_1TBA_3{\cdot}(MeOH)_2$ involved vapour diffusion of ethanol into a methanol solution containing TMA and TBA (1:3, molar ratio) at ambient temperature. After a few days, single crystals were obtained.

The crystallization process to form the BDO solvate $TMA_1TBA_3{\cdot}(BDO)_1$ involved slow evaporation of a methanol and BDO (9:1, volume ratio) solution containing TMA and TBA (1:3, molar ratio). After a few days, single crystals were obtained.

The crystallization process to form the di-hydrate $TMA_1TBA_3{\cdot}(H_2O)_2$ involved slow evaporation of a solution of TMA and TBA (1:3, molar ratio) in ethanol and methanol (2:1, volume ratio) at ambient temperature. After a few days, single crystals were obtained.

The crystallization processes to form the sesquin-hydrate $TMA_1TBA_3{\cdot}(H_2O)_{4.5}$ were as follows: (i) a water solution containing TMA and TBA (1:3, molar ratio) at ambient temperature was allowed to evaporate slowly at ambient temperature; after a

few weeks, single crystals were obtained; (ii) a solution of TMA and TBA (1:3, molar ratio) in methanol and ethanol (1:1, volume ratio) at ambient temperature was allowed to evaporate slowly at ambient temperature; after a few weeks, single crystals were obtained; (iii) an experiment was carried out involving vapour diffusion of acetone into a solution of TMA and TBA (1:3, molar ratio) in ethanol and water (5:1, volume ratio) at ambient temperature; after a few days, single crystals were obtained.

Single-crystal X-ray diffraction data were collected at 150 K on a Nonius Kappa CCD diffractometer equipped with a molybdenum tube source ($\lambda = 0.71073$ Å). The crystal structures were solved (by direct methods) by SHELXS and refined using SHELXL.[196] Refinement of non-hydrogen atoms was carried out using anisotropic displacement parameters. All hydrogen atoms were located in difference Fourier maps and were added to the structural model according to idealized geometries. Refinement of hydrogen atoms was carried out using a riding model, with isotropic displacement parameter equal to 1.2 or 1.5 times the equivalent isotropic displacement parameter of the atom to which the hydrogen atom is bonded.

4.5.2 Structural Summary of Co-Crystals of TMA_1TBA_3

The relationships between these five solvated co-crystals are summarized in Figure 4.25. As shown in Figure 4.25, the sesquin-hydrate $TMA_1TBA_3{\cdot}(H_2O)_{4.5}$ is the most stable material at room temperature in the open air, the other four solvates would slowly lose solvent molecules (methanol or BDO molecules) which were incorporated into their structures (desolvation) and absorb water molecules from the atmosphere, transforming to the sesquin-hydrate $TMA_1TBA_3{\cdot}(H_2O)_{4.5}$. The crystallographic parameters are summarized in Table 4.4 and the crystal structures are shown in Figures 4.26 to 4.32.

From Table 4.4 and Figures 4.26 to 4.32, we can see that these five structures can be classified into three categories according to the types of solvent molecules. If only alcohol molecules (methanol or BDO, Figures 4.26 and 4.27) are incorporated into the structure, the crystal structure comprises single hydrogen-bonded corrugated sheets. If both alcohol and water molecules (Figure 4.28) are incorporated into the structure, the crystal structure comprises single hydrogen-bonded sheets that are approximately flat. If

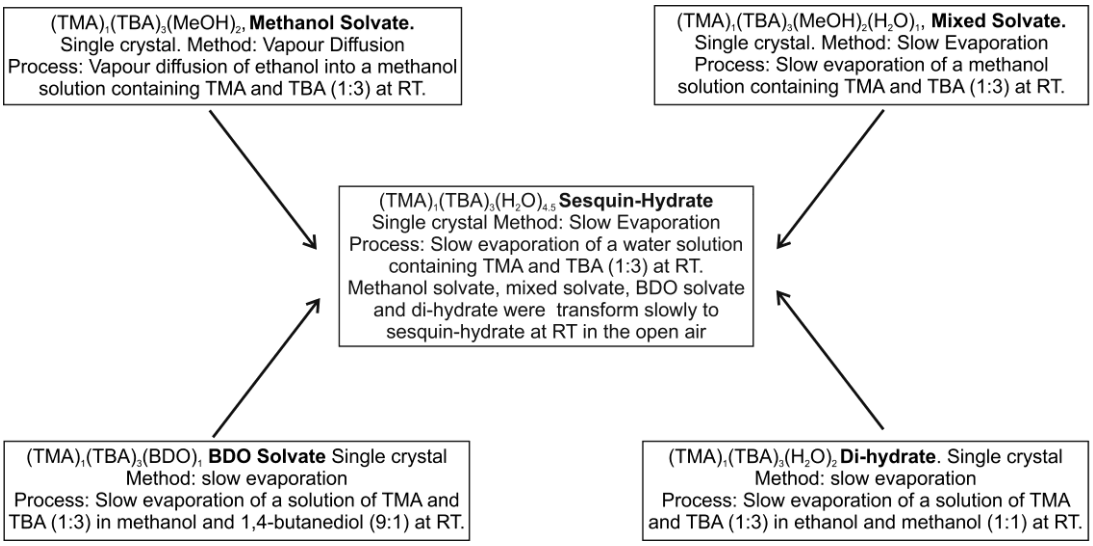

Figure 4.25. *The relationships between solvatomorphs of co-crystals of TMA_1TBA_3.*

Table 4.4 The crystallographic parameters of solvates of TMA_1TBA_3

	Mixed Solvate	Sesquin-Hydrate	Methanol Solvate
Space group	$P\bar{1}$	Pbca	$P2_1/n$
a/Å	12.4168(3)	14.2800(2)	9.0451(2)
b/Å	14.7844(4)	21.5449(4)	19.4603(6)
c/Å	17.3285(5)	38.2318(7)	17.2206(5)
α/°	84.555(2)	90	90
β/°	88.500(2)	90	100.029(2)
γ/°	69.781(2)	90	90
V(Å^3)	2971.51(14)	11762.44(35)	2984.86(14)
Z	2	8	4
Calculated Density (g/cm^3)	1.142	1.153	1.098
R_1/(%)	/	6.52	8.46
R_{w2}/(%)	16.1	15.26	20.98

	Di-Hydrate	BDO Solvate
Space group	$P2_1$	$P2_1/n$
a/Å	8.9845(2)	9.1626(3)
b/Å	20.9121(6)	19.3079(11)
c/Å	14.1487(4)	17.4446(8)
α/°	90	90
β/°	97.894(2)	98.561(2)
γ/°	90	90
V(Å^3)	2633.13(12)	3051.75(25)
Z	2	4
Calculated Density (g/cm^3)	1.174	1.131
R_1/(%)	9.62	9.69
R_{w2}/(%)	15.43	24.94

only water molecules (Figures 4.29 and 4.31) are incorporated into the structure, the crystal structure comprises single hydrogen-bonded flat ribbons that are stacked alternately in a slightly offset manner. In all five structures, the $–N^+H_3$ groups of the $HTBA^+$ cations and the OH groups of the alcohol solvent molecules or water molecules lie close to the $TMA^{3–}$ sheets or ribbons due to hydrogen bonding. The *tert*-butyl groups of the $HTBA^+$ cations and the alkyl groups of the alcohol solvent molecules project outward from the sheets.

4.5.3 Structural Comparison Between the Methanol, Mixed Methanol/Water and 1,4-Butanediol Solvates of TMA_1TBA_3

The methanol and BDO solvates are monoclinic and have the same space group, $P2_1/n$. In the crystal structure of the methanol solvate, the asymmetric unit comprises one $TMA^{3–}$ anion, three $HTBA^+$ cations and two methanol molecules. One methanol

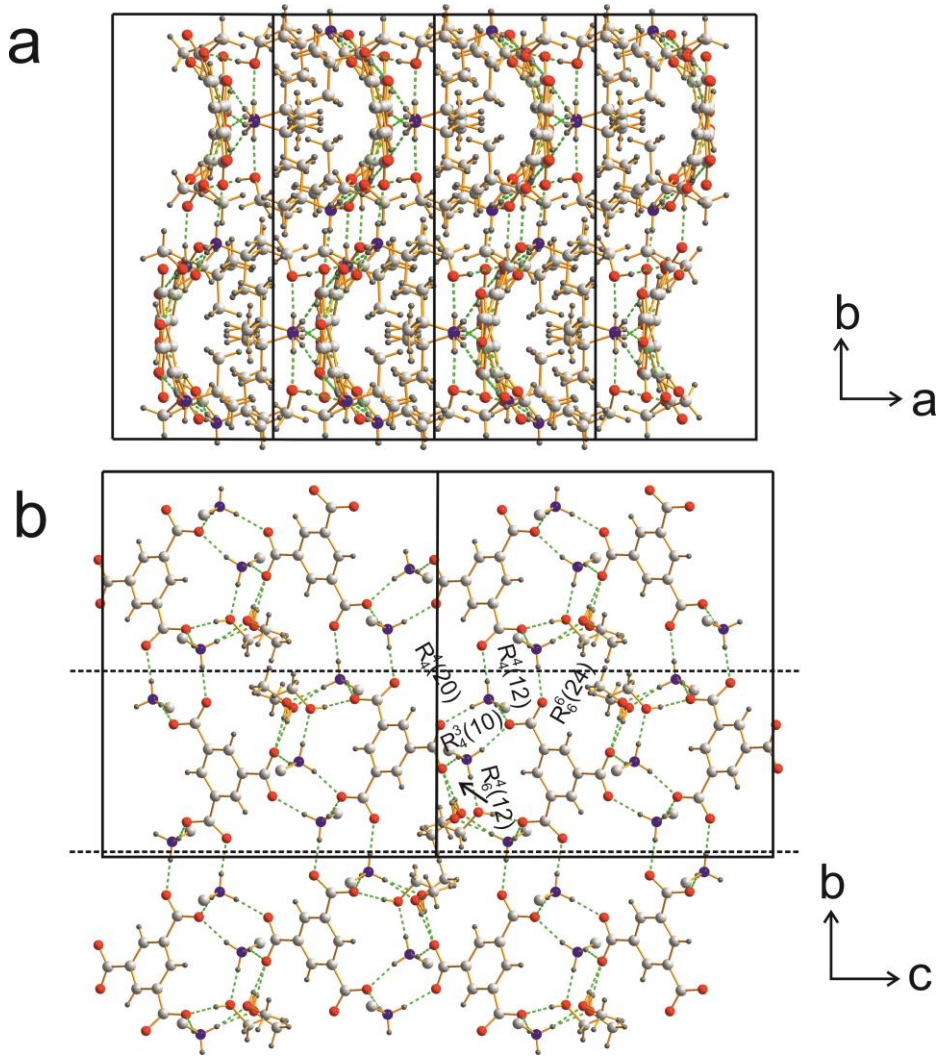

Figure 4.26. *(a) Crystal structure of the methanol solvate and (b) the hydrogen-bonding pattern in a single sheet.*

molecule is disordered over two sites with occupancies 0.49 and 0.51. In the crystal structure of the BDO solvate, the asymmetric unit comprises one TMA^{3-} anion, three $HTBA^{+}$ cations and two half solvent units (due to the two half solvent units on special positions, the other two half solvent units can be created by symmetry operation (inversion centre). For the mixed solvate, the asymmetric unit comprises 12 independent molecules: two TMA^{3-} anions, six $HTBA^{+}$ cations, four methanol molecules and two water molecules. The structure is triclinic with space group $P\bar{1}$. The crystal structures of these three solvates (Figures 4.26 to 4.28) have both similarities and differences, which are explained below. In the crystal structure of each of these solvates, the sheets contain a single hydrogen-bonded ribbon motif, which runs parallel to the c-axis in each case. These ribbons are indicated as the region between the two dashed lines in each case.

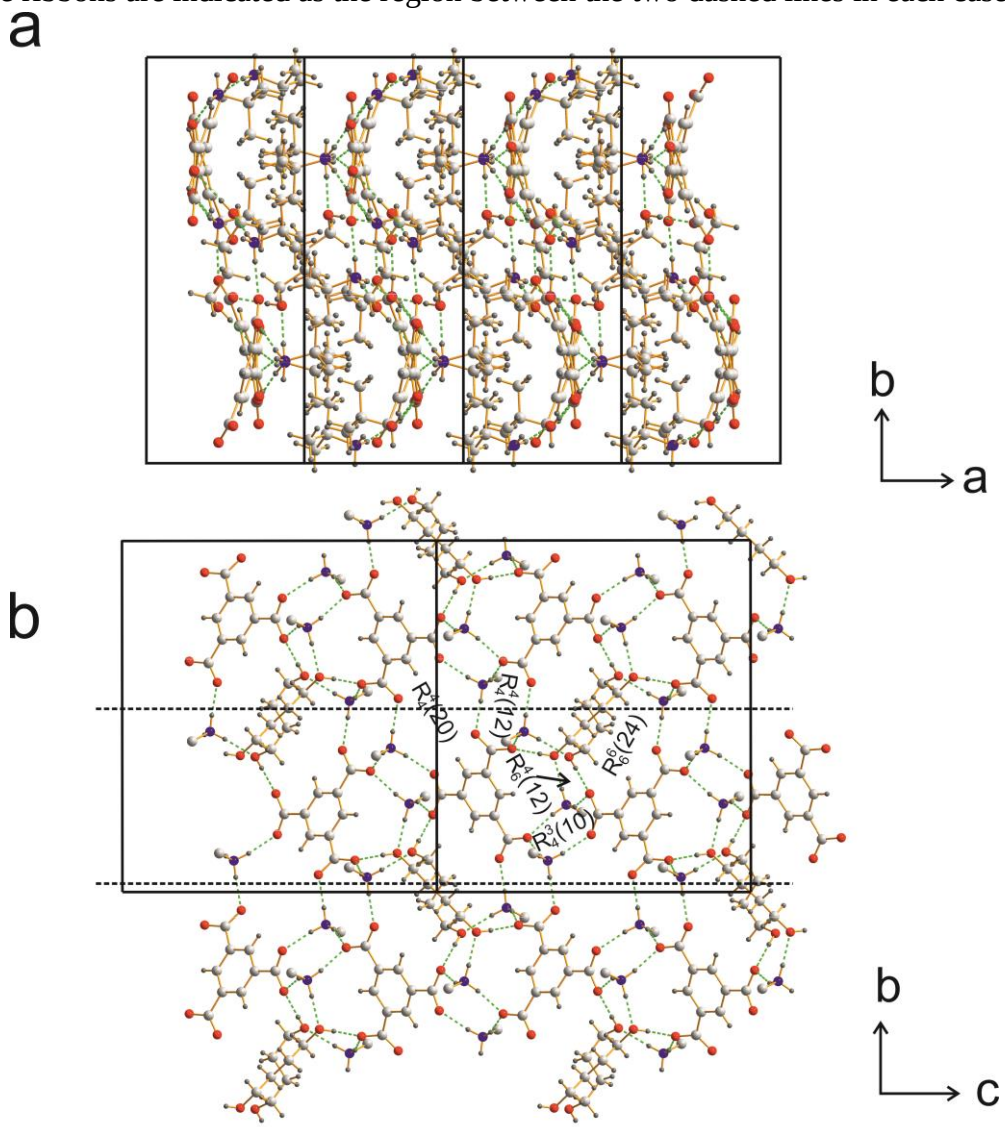

Figure 4.27. *(a) Crystal structure of the BDO solvate $TMA_1TBA_3{\cdot}(BDO)_1$ and (b) the hydrogen-bonding patterns of the corrugated sheet.*

For all three structures, pairs of adjacent TMA^{3-} anions are not linked to each other directly (as a consequence of total deprotonation, the TMA^{3-} anion has no hydrogen bond donors) but are double-bridged by intervening $-N^{+}H_3$ groups of $HTBA^{+}$ cations and O–H bonds of solvent molecules. For both single-component solvates (Figures 4.26b and 4.27b), within each ribbon, one $-COO^{-}$ group of TMA^{3-} anion is linked to the $-COO^{-}$ group of an adjacent TMA^{3-} anion by two O···H–N–H···O hydrogen-bonding arrangements, giving rise to a cyclic hydrogen-bonding ring with graph set $R_4^3(10)$. For one of the $-COO^{-}$ groups, each O atom receives one N–H···O hydrogen bond whereas for the other $-COO^{-}$ group, one O atom receives two N–H···O hydrogen bonds. These two anions are also double-bridged by two O···H–N–H···O–H···O hydrogen-bonding arrangements involving an intervening

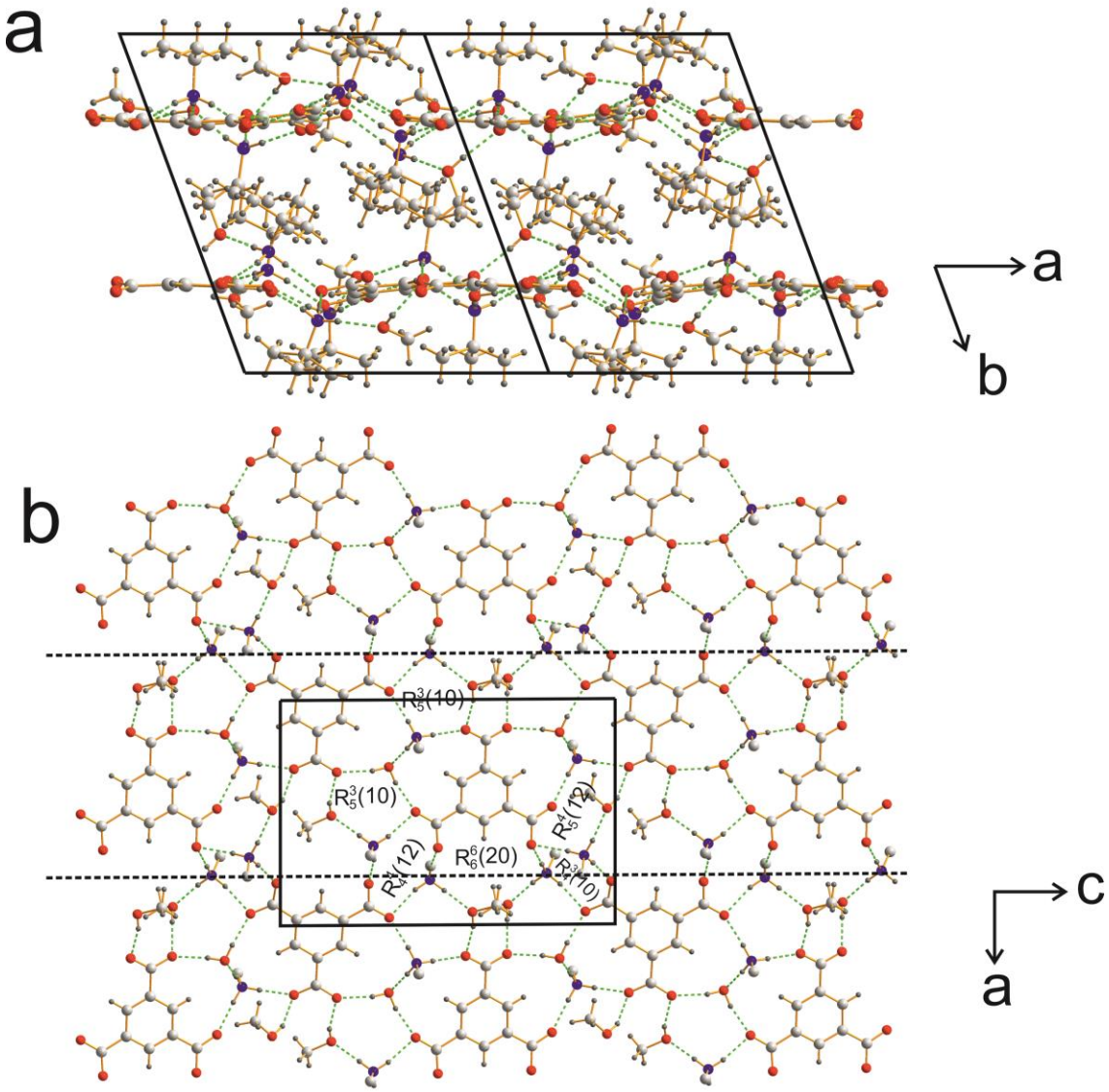

Figure 4.28. *(a) Crystal structure of the mixed solvate $TMA_1TBA_3{\cdot}(H_2O)_2(MeOH)_1$ and (b) the hydrogen-bonding patterns of the corrugated sheets*

–N^+H_3 group and an intervening OH group of a methanol (or BDO) molecule, corresponding to graph set $R_6^4(12)$.

In the structure of the mixed solvate (methanol hydrate, Figure 4.28b), within the hydrogen-bonded ribbon, the hydrogen-bonding arrangements are totally different and more complicated. All the hydrogen-bonding patterns within this structure are marked in Figure 4.28b. Adjacent TMA^{3-} anions are double-bridged by three different cyclic hydrogen-bonding rings: (i) an $R_5^3(10)$ cyclic arrangement, involving one –COO^- group of each TMA^{3-} anion, one intervening –N^+H_3 group, the OH group of one methanol molecule and both OH groups of one water molecule; (ii) another $R_5^3(10)$ cyclic arrangement, involving one –COO^- group of each TMA^{3-} anion, two intervening –N^+H_3 groups and the OH bond of one methanol molecule; and (iii) an $R_5^4(12)$ cyclic arrangement involving one –COO^- group of each TMA^{3-} anion, two intervening –N^+H_3 groups and the OH bond of one methanol molecule.

For the solvates containing only methanol and BDO as the solvent component (Figures 4.26b and 4.27b), adjacent ribbons are linked indirectly by three different cyclic hydrogen-bonding arrangements: (i) an $R_4^4(12)$ ring, involving one –COO^- group of each TMA^{3-} anion and two intervening –N^+H_3 groups; (ii) an $R_4^4(20)$ ring, involving two –COO^- groups of each TMA^{3-} anion and two intervening –N^+H_3 groups on one side; (iii) an $R_6^6(24)$ ring, involving two –COO^- groups of each TMA^{3-} anion and two intervening –N^+H_3 groups on the other side. It is interesting to note that either two methanol molecules (one of which is disordered) or one BDO molecule occupy the cavities formed by the cyclic graph set $R_6^6(24)$, while the cavities formed by cyclic graph set $R_4^4(20)$ are empty. For the mixed solvate (methanol hydrate, Figure 4.28b), adjacent ribbons are linked indirectly by three cyclic hydrogen-bonding arrangements: (i) an $R_4^4(12)$ ring, comprising the same hydrogen-bonding arrangement discussed above for the pure solvate; (ii) an $R_4^3(10)$ ring, involving one –COO^- group of each TMA^{3-} anion and two intervening–N^+H_3 groups, and (iii) an $R_6^6(20)$ ring, involving one –COO^- group of one TMA^{3-} anion, two –COO^- groups of another TMA^{3-} anion, two intervening –N^+H_3 groups and the OH bonds of two methanol molecules.

4.5.4. Structural Comparison Between the Di-Hydrate and Sesquin-Hydrate of TMA_1TBA_3

For the di-hydrate and the sesquin-hydrate $TMA_1TBA_3 \cdot (H_2O)_{4.5}$, the asymmetric unit is composed of two TMA^{3-} anions, six $HTBA^+$ cations and four or nine water

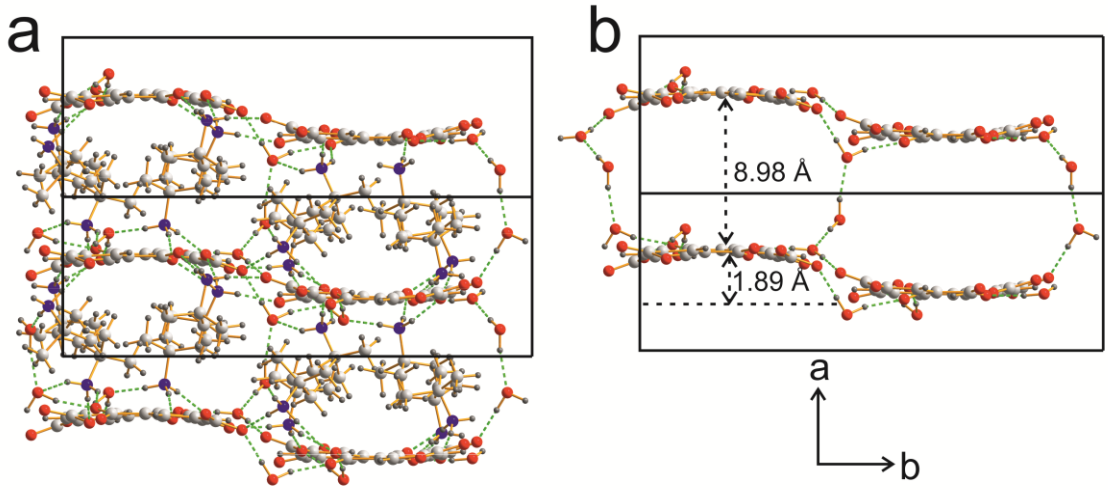

Figure 4.29. *(a) Crystal structure of the di-hydrate and (b) channel formed by TMA and water molecules.*

molecules, respectively. Although the structures of these two hydrates are described by different crystal systems (the di-hydrate is monoclinic with space group $P2_1$ and the sesquin-hydrate $TMA_1TBA_3{\cdot}(H_2O)_{4.5}$ is orthorhombic with space group Pbca), the crystal structures of these two hydrates share several similar aspects (Figures 4.29 to 4.32).

Both structures (Figures 4.29 and Figure 4.31) comprise one-dimensional hydrogen-bonded ribbons, which are stacked parallel to the a-axis in each case (the distances between adjacent parallel ribbons along the a-axis are 8.98 Å (di-hydrate, Figure 4.29b) and 7.21 Å (the sesquin-hydrate $TMA_1TBA_3{\cdot}(H_2O)_{4.5}$), Figure 4.31b) and adjacent ribbons are linked together by $HTBA^+$ cations and water molecules with a slight offset along the a-axis (the offset is about 1.89 Å (di-hydrate, Figure 4.29b) and 1.81 Å (the sesquin-hydrate $TMA_1TBA_3{\cdot}(H_2O)_{4.5}$), Figure 4.31b). In both structures (Figures 4.29b and 4.31b), water molecules act as both hydrogen bond acceptors and donors to link all TMA^{3-} anions together to form a channel, which is occupied by $HTBA^+$ cations. From Figures 4.29 and 4.31, we can see that the ribbons run horizontally along the c-axis.

In the crystal structure of the di-hydrate (Figure 4.30), the ribbons are zigzag and there are four different cyclic hydrogen-bonded rings between adjacent TMA^{3-} anions within the ribbon: (i) an $R_4^2(8)$ cyclic arrangement involving one $–COO^-$ group from each of two adjacent TMA^{3-} anions and two intervening $–N^+H_3$ groups; (ii) another $R_4^2(8)$ cyclic arrangement involving one $–COO^-$ group from each of two adjacent

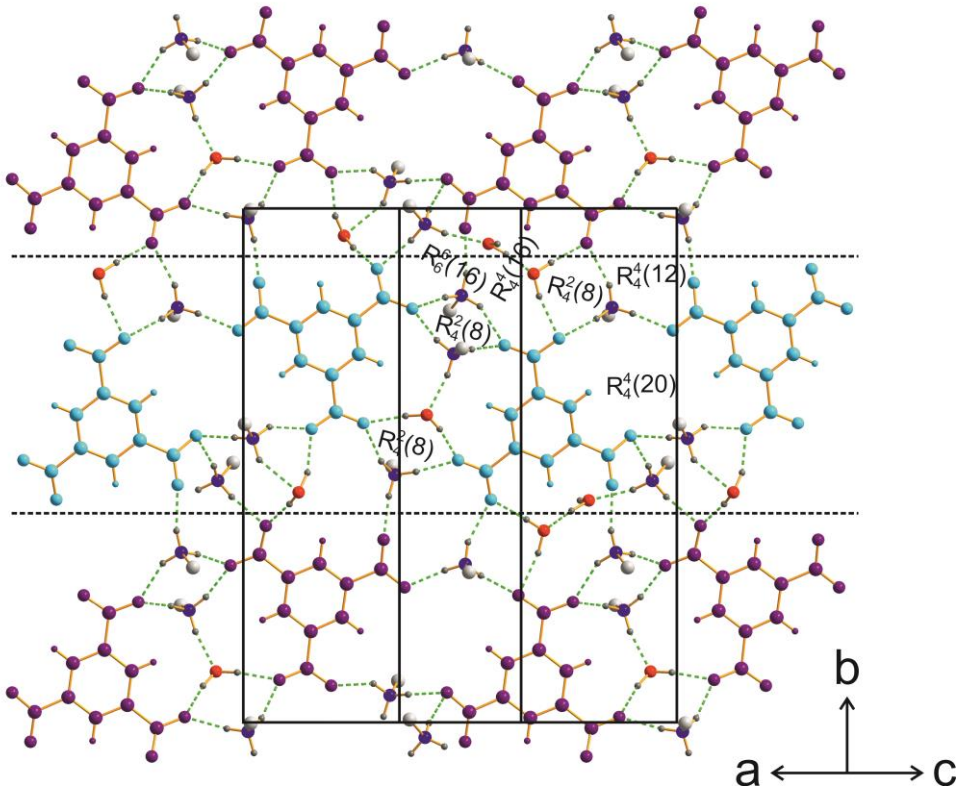

Figure 4.30. *Hydrogen-bonding patterns of the zigzag ribbons in the crystal structure of the di-hydrate* $TMA_1TBA_3\cdot(H_2O)_2$.

TMA^{3-} anions, one intervening $-N^+H_3$ group and the OH bond of one water molecule. These two cyclic hydrogen-bonding arrangements are also observed in the crystal structure of the sesquin-hydrate $TMA_1TBA_3\cdot(H_2O)_{4.5}$ (Figure 4.32); (iii) a double-bridged cyclic arrangement with graph set $R_6^6(16)$, involving two intervening $-N^+H_3$ groups and two water molecules.

This hydrogen-bonding ring is very rare in the structures studied here. On one side, an intervening $-N^+H_3$ group acts as a bridge to link two O atoms of adjacent TMA^{3-} anions through O···H–N–H···O hydrogen bonds; however, on the other side, one

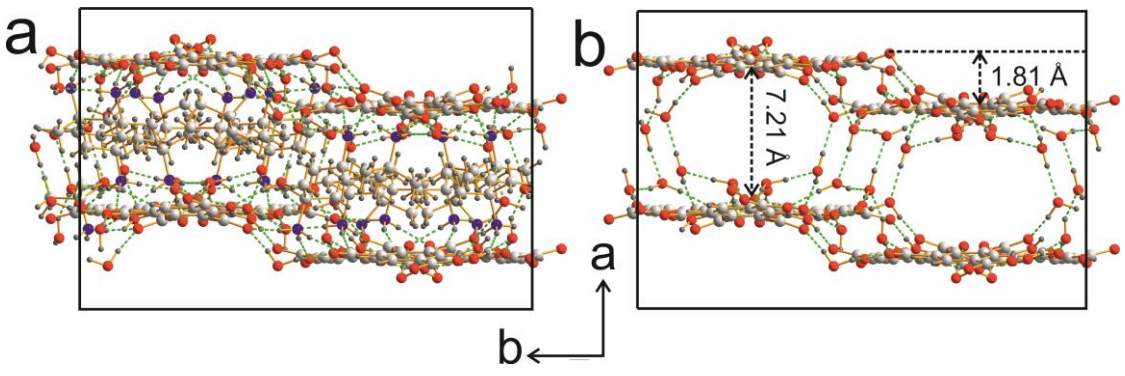

Figure 4.31. *(a) Crystal structure of the sesquin-hydrate* $TMA_1TBA_3\cdot(H_2O)_{4.5}$ *and (b) the channel formed by TMA molecules and water molecules.*

intervening–N^+H_3 group and two water molecules are linked together to act as another bridge to link another two O atoms of adjacent TMA^{3-} anions through an O···H–N–H···O–H···O–H···O hydrogen-bonding arrangement; and (iv) an $R_4^4(20)$ cyclic arrangement involving two $–COO^-$ groups of each two adjacent TMA^{3-} anions and two intervening $–N^+H_3$ groups.

In the structure of the sesquin-hydrate $TMA_1TBA_3\cdot(H_2O)_{4.5}$, (Figure 4.32), within the zigzag ribbon, there are five different cyclic hydrogen-bonding rings formed between pairs of adjacent TMA^{3-} anions. (i) and (ii) are the common arrangement with graph sets $R_4^2(8)$ discussed above for the di-hydrate. (iii) an $R_4^3(10)$ cyclic arrangement involving one $–COO^-$ group of each two adjacent TMA^{3-} anions and two intervening $–N^+H_3$ groups; (iv) an $R_5^4(12)$ cyclic arrangement involving one $–COO^-$ group of each two adjacent TMA^{3-} anions, one intervening $–N^+H_3$ group and two water molecules.

In this double-bridged hydrogen-bonding arrangement, one bridge is an intervening $–N^+H_3$ group, while the other bridge comprises two water molecules which are linked together through O (TMA^{3-})···H–O–H (water)···O–H (water)···O (TMA^{3-}) hydrogen-bond arrangement; (v) a double-bridged cyclic arrangement with graph set $R_7^5(14)$. In this complicated hydrogen-bonding arrangement, one bridge involves O (TMA^{3-})···H–N–H ($HTBA^+$)···O–H (water)···O (TMA^{3-}) hydrogen bonds and the other bridge involves O (TMA^{3-})···H–O (water)···H–N–H ($HTBA^+$)···O–H (water)···O (TMA^{3-}) hydrogen bonds. In these two structures, we can see that the water molecules participate actively in the cyclic hydrogen-bonding arrangements.

For the di-hydrate (Figure 4.30), adjacent ribbons are double-bridged by three different cyclic hydrogen-bonding arrangements: (i) $R_4^2(8)$, (ii) $R_4^4(12)$, and (iii) $R_4^4(16)$. For the sesquin-hydrate $TMA_1TBA_3\cdot(H_2O)_{4.5}$ (Figure 4.32), adjacent ribbons are bridged by four different cyclic hydrogen-bonding arrangements: (i) $R_4^3(10)$, (ii) $R_4^4(12)$, (iii) a double-bridged arrangement with graph set $R_5^4(16)$ involving one intervening $–N^+H_3$ group and two water molecules acting as bridges. In this double-bridged hydrogen-bonding arrangement, one bridge involves O···H–O–H···O hydrogen bonds and the other involves O (TMA^{3-})···H–N–H ($HTBA^+$)···O–H (water)···O (TMA^{3-}) hydrogen bonds. (iv) A double-bridged graph set $R_6^4(18)$ involves four water molecules acting as bridges; one bridge involves O (TMA^{3-})···H–O–H (water)···O (TMA^{3-})

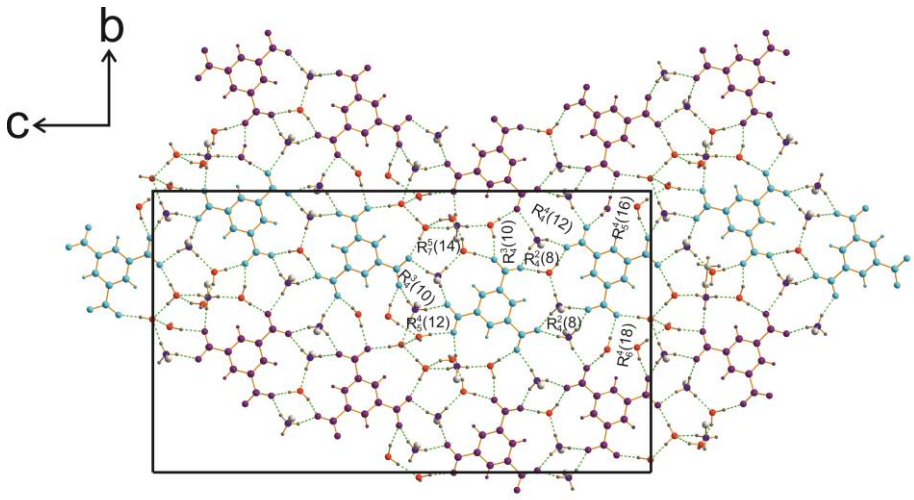

Figure 4.32. *Hydrogen-bonding patterns of the two zigzag ribbons in the crystal structure of the hydrate* $TMA_1TBA_3 \cdot (H_2O)_{4.5}$.

hydrogen bonds and the other more complicated and longer bridge involves O (TMA^{3-})···H–O–H (water)···O (water)···O–H (water)···O (TMA^{3-}) hydrogen bonds. The latter bridge involving three water molecules is quite uncommon in organic hydrate structures. Comparing the cyclic hydrogen-bonding arrangements observed in the di-hydrate and sesquin-hydrate, it is clear that there are four common cyclic graph sets: two different cyclic graph sets $R_4^2(8)$ arrangements, one $R_4^3(10)$ arrangement and one $R_4^4(12)$ arrangement which exist in both structures.

For all five structures, all three N–H bonds in each $HTBA^+$ cation are used as donors in N–H···O hydrogen bonding to O atoms of the TMA^{3-}anions or solvent molecules as hydrogen bond acceptors. The O–H group in each solvent molecule is used both (i) as the donor in an O–H (solvent)···O (TMA^{3-}) hydrogen bond, and (ii) as the acceptor in an N^+–H ($HTBA^+$)···O (solvent) hydrogen bond.

4.5.5 Summary

When the stoichiometric ratio between TMA and TBA is 1:3, we obtained five co-crystals of TMA and TBA. In these five crystal structures, due to the TMA molecules being fully deprotonated, there is no direct hydrogen bonding between adjacent TMA^{3-} anions. Pairs of adjacent carboxylate groups are double-bridged by OH groups of solvent molecules and/or by $–N^+H_3$ groups of $HTBA^+$ cations. The specific hydrogen-bonding motifs formed are quite sensitive to the particular solvents incorporated into the structure (methanol and BDO) and the number of water molecules. Apart from double-bridged graph sets $R_4^3(10)$, $R_4^4(12)$ and $R_5^4(12)$, there are another nine new double-

bridged cyclic graph sets (Figure 4.33) observed in this family of co-crystals of TMA and TBA.

4.6 Summary

In conclusion, the range and diversity of structures and compositions of co-

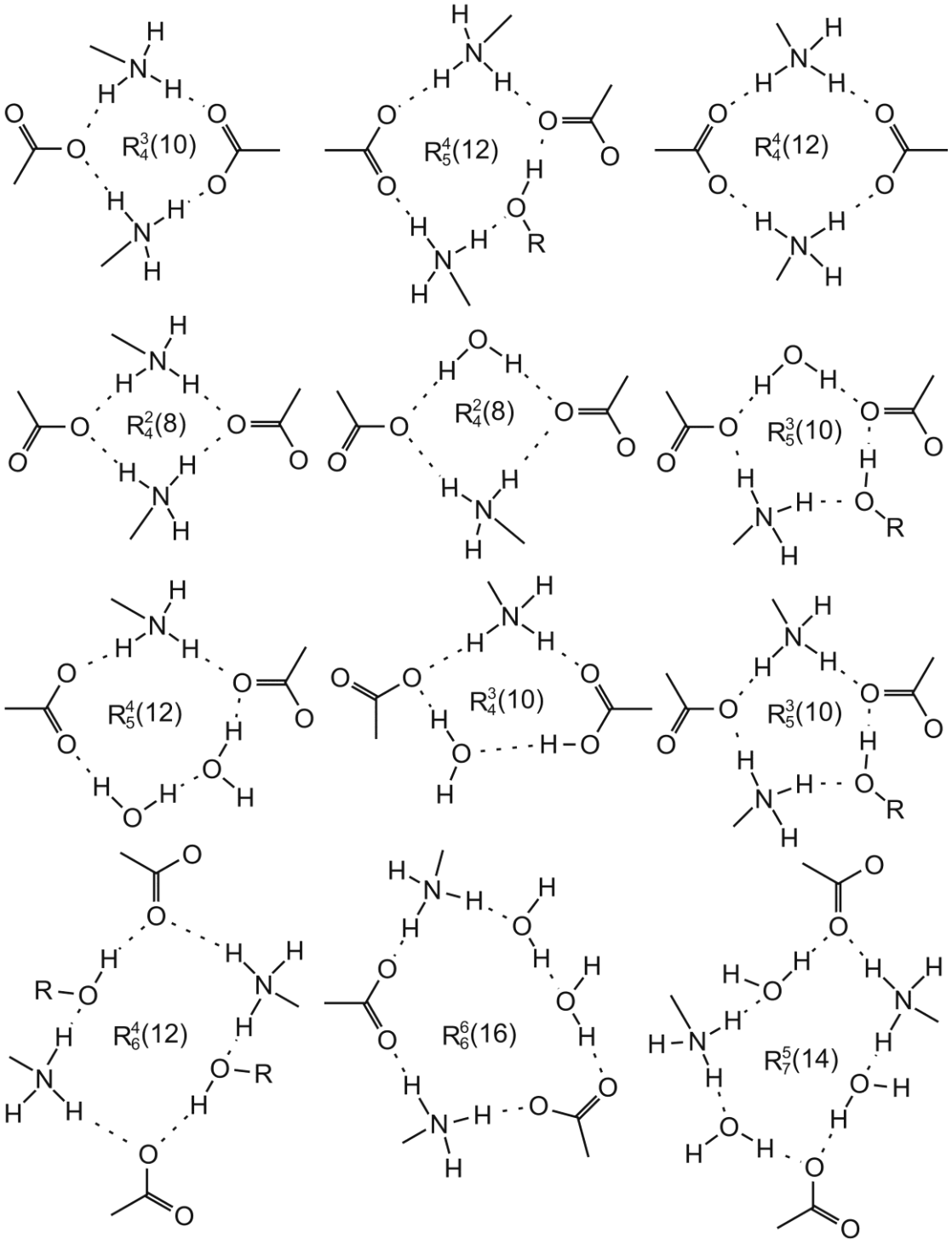

Figure 4.33. *Double-bridged hydrogen-bonding motifs observed in the family of co-crystals of TMA_1TBA_3.*

crystals of TMA and TBA is very uncommon. Adjusting the stoichiometric ratio between TMA and TBA and the types of solvent used gives rise to a broad range of totally different crystal structures, such as a structure comprising double-layered sheets $TMA_2TBA_1 \cdot (H_2O)_2$, single hydrogen-bonded flat sheets $TMA_1TBA_2 \cdot (\textit{iso}\text{-butanol})_1$, single hydrogen-bonded corrugated sheets $TMA_1TBA_2 \cdot (MeOH)_1$), a structure with interpenetration $TMA_2TBA_1 \cdot (H_2O)_3$ and a structure comprising brick-wall networks $TMA_2TBA_2 \cdot (MeOH)_1$. Furthermore, the formation of hydrogen-bonding motifs are quite sensitive to the stoichiometric ratio between TMA and TBA and the crystallization solvents. In general, we have observed several recurrent "supramolecular synthons" in the family of co-crystals of TMA and TBA (see Figures 4.13, 4.24 and 4.33).

Chapter 5 Co-Crystals of L-Arginine and Trimesic Acid, with Structure Determination Directly from Powder X-Ray Diffraction Data

5.1 Introduction

Amino acids are a class of materials containing not only a proton donor group (–COOH) but also a proton acceptor group ($–NH_2$). Designing and preparing new organic nonlinear optical (NLO) materials involving amino acids with low cost and high efficiency is a hot issue for scientists.[253,254] L-arginine (Figure 5.1) (L-Arg) is one of the 20 genetically encoded amino acids and is the most basic amino acid. Due to its basic nature, it can form co-crystals with many different types of acids. The discovery of a mono-hydrate co-crystal of L-arginine and phosphoric acid[255], which showed high nonlinear optical (NLO) properties, has attracted a great deal of attention and led to significant interest in co-crystals containing L-arginine molecules. Due to its potential applications for NLO materials, a series of co-crystals of L-arginine with different types of inorganic or organic acids[256-262] have been prepared and their structural, physical and optical properties have been investigated.

L-Arginine is a chiral molecule with several conformational degrees of freedom and may be prone to exhibiting polymorphism when co-crystallized with other molecules. Therefore, in the course of studying the co-crystallization of TMA and L-arginine, we expected that polymorphic co-crystals might appear as in the case of the co-crystals of TMA and TBA. We attempted to prepare single crystals of TMA and L-arginine by different co-crystallization methods. However, no large single crystals were prepared successfully. Instead, four types of microcrystalline TMA and L-arginine co-crystals have been discovered, which are designated as phase 1 to phase 4. The powder XRD patterns are shown in Figure 5.2.

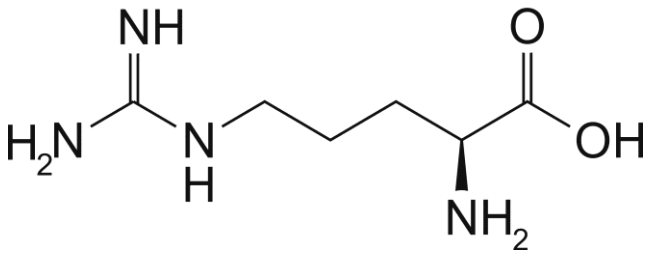

Figure 5.1. *Molecular structure of L-arginine.*

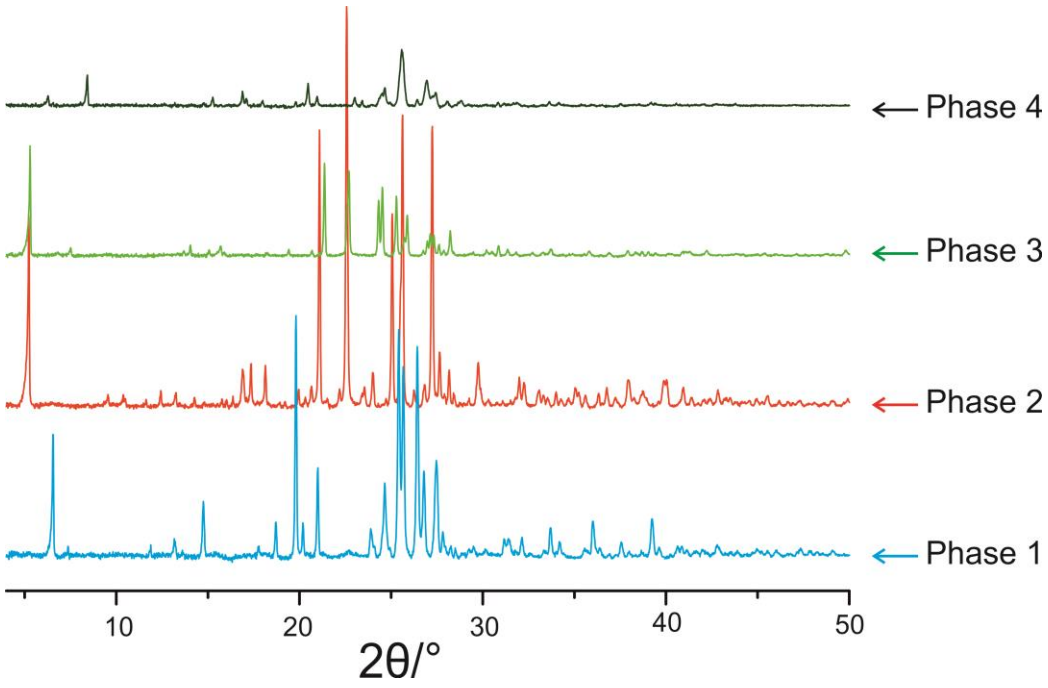

Figure 5.2. *The powder XRD patterns of Phase 1 to Phase 4 of co-crystal of TMA and L-arginine.*

We could not determine the crystal structures of these materials by single-crystal XRD methods because no large single crystals of these samples were produced. However, due to the recent advances in structure determination from PXRD data, especially the development of the direct-space strategy, researchers are able to determine the structures of organic materials (microcrystalline) with moderate complexity (small molecules) from PXRD data, sometimes in conjunction with other techniques.[263-268] In this chapter, the crystal structures of two co-crystals of TMA and L-arginine (phase 1 and phase 2) are determined directly from PXRD data, while the structure determination of the other two phases is currently in progress. We present the results from structure determination of phases 1 and 2 from PXRD data, and analyse the structures of these co-crystals of TMA and L-arginine.

5.2 Synthesis

In the course of studying organic co-crystals of TMA and L-arginine, we prepared four distinct microcrystalline phases from this family of co-crystals. Each powder sample can be produced by several different methods and the processes are as follows.

The crystallization processes to form phase 1 were as follows: (1) TMA (1 mmol) was dissolved in *iso*-propanol (5 ml) and water (5 ml). Separately, L-arginine (1.5 mmol)

was dissolved in water (2 ml). These two solutions were then mixed together, stirring for 15 minutes, then the solution was allowed to slowly evaporate at room temperature. After about two weeks, a white precipitate appeared in the solution. The solution was filtered and the precipitates were allowed to dry out, producing a microcrystalline sample of phase 1. (2) TMA (1 mmol) was dissolved in ethanol (10 ml) and water (2 ml). Separately, L-arginine (1 mmol) was dissolved in water (2 ml). These two solutions were then mixed together, stirring for about 15 minutes, then the solution was allowed to slowly evaporate at room temperature. After a few weeks, a microcrystalline sample of phase 1 was obtained.

The crystallization processes to form phase 2 were as follows: (1) TMA (1 mmol) was dissolved in ethanol (10 ml) and water (5 ml). Separately, L-arginine (1 mmol) was dissolved in water (5 ml) and 1,4-dioxane (5 ml). These two solutions were then mixed together, stirring for 15 minutes, then the solution was allowed to slowly evaporate at room temperature. After about two weeks, a microcrystalline sample of phase 2 was obtained. (2) L-arginine (0.5 mmol) and TMA (1 mmol) was dissolved in DMSO (2 ml), ethanol (4 ml) and water (3 ml), stirring for 15 minutes, then the solution was allowed to slowly evaporate at room temperature. After a few weeks, a microcrystalline sample of phase 2 was obtained. (3) L-arginine (1.5 mmol) was dissolved in ethanol (2 ml) and water (2 ml). Separately, TMA (1 mmol) was dissolved in water (2 ml) and ethanol (4 ml). These solutions were then mixed together in a conical flask and the solution was heated to 55 °C, followed by placing the conical flask into an incubator and slowly cooling from 55 °C to 20 °C. A microcrystalline sample of phase 2 was obtained.

The crystallization processes to form phase 3 were as follows: (1) L-arginine (0.5 mmol) was dissolved in methanol (1 ml) in a small glass bottle, then a solution of 1,4-dioxane (2 ml) and water (0.5 ml) containing TMA (0.5 mmol) was slowly added into the glass bottle and sealed with a cap. After a few weeks, a microcrystalline sample of phase 3 was obtained. (2) L-arginine (2 mmol) was dissolved in water (6 ml). Separately, TMA (1 mmol) was dissolved in ethanol (4 ml). These two solutions were then mixed together, with stirring for 15 minutes, then the solution was allowed to slowly evaporate at room temperature. After about two weeks, a microcrystalline sample of phase 3 was obtained. (3) L-arginine (2 mmol) was dissolved in water (3 ml). Separately, TMA (1 mmol) was dissolved in *iso*-propanol (5 ml) and water (7 ml). These two solutions were then mixed together, with stirring for 15 minutes, then the

solution was allowed to slowly evaporate at room temperature. After about two weeks, a microcrystalline sample of phase 3 was obtained. (4) TMA (0.5 mmol) was dissolved in methanol (1 ml) and THF (1 ml) in a small glass bottle, then a solution of water (1 ml) containing L-arginine (0.5 mmol) was slowly added to this glass bottle and sealed with a cap. After a few weeks, a microcrystalline sample of phase 3 was obtained.

The crystallization processes to form phase 4: (1) TMA (1 mmol) was dissolved in *iso*-propanol (5 ml) and water (7 ml). Separately, L-arginine (0.5 mmol) was dissolved in water (3 ml). These two solutions were then mixed together, with stirring for 15 minutes, then the solution was allowed to slowly evaporate at room temperature. After about two weeks, a microcrystalline sample of phase 4 was obtained. (2) TMA (1 mmol) and L-arginine (2 mmol) were dissolved in water (5 ml), then the solution was allowed to slowly evaporate at room temperature. After a few weeks, a microcrystalline sample of phase 4 was obtained.

5.3 Structure Determination

The powder XRD data for phase 1 to phase 4 were recorded on a Bruker D8 instrument in transmission mode using Ge-monochromated CuKα1 radiation. (2θ: 4–50, total time 48 hrs). Samples were mixed with starch (2:1, mass ratio) and contained within glass capillaries to reduce the effects of preferred orientation in each case.

5.3.1 Structure Determination of Phase 1

For phase 1, the powder XRD pattern was indexed successfully by using the TREOR[202] and ITO[203] codes, which are incorporated into the program CRYSFIRE[205], combined with the program CHEKCELL[207]. The Le Bailing fitting[208] using GSAS[209] software and its graphical user interface editor EXPGUI[210] gave a good quality of fit with space groups $P2_1$ and P2 (Figure 5.3a, space group: $P2_1$, a = 26.8480(11) Å, b = 13.3480(5) Å, c = 3.7442(2) Å, β = 88.8447(16)°, V = 1341.53(17) Å^3, R_{wp} = 1.30%, R_p = 0.98%. Figure 5.3b, space group P2: a = 26.8492(10) Å, b = 13.3484(5) Å, c = 3.7444(2) Å, β = 88.8419(15)°, V = 1341.69(14) Å^3, R_{wp} = 1.30%, R_p = 0.98%). Thus, both space groups are possible, and the true space group cannot be assigned uniquely at this stage. Therefore, structure solution calculations were carried out in parallel using these two possible space groups in the next stage.

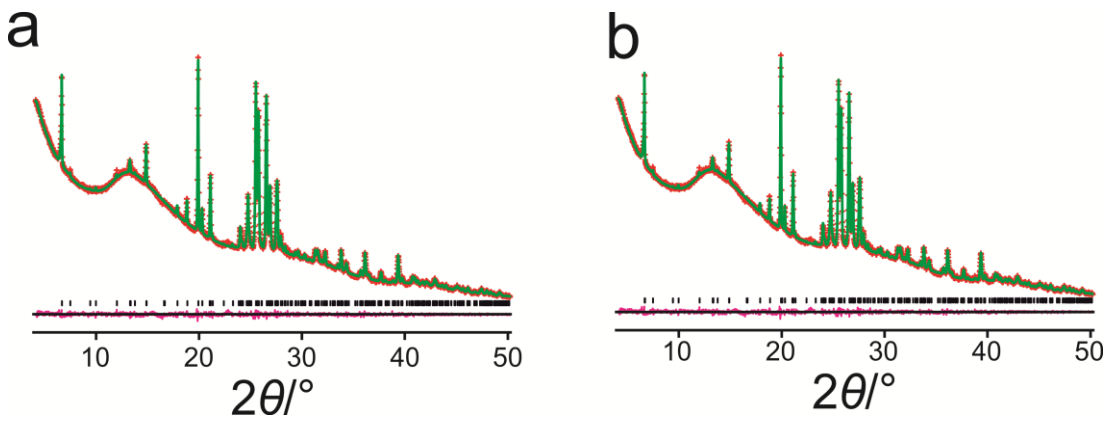

Figure 5.3. *Le Bail profile fitting for phase 1 with (a) $P2_1$ and (b) P2.*

From the solution ^{1}H NMR spectrum, we know that the molar ratio of L-arginine to TMA in this sample is 1:2. Given the volume of the unit cell and consideration of the density of the sample, we infer that there are four TMA molecules and two L-arginine molecules in the unit cell and the calculated density is 1.47 g cm^{-3}. Therefore, for space groups P2 and $P2_1$, there are two TMA molecules and one L-arginine molecule in the asymmetric unit. The refined unit cell parameters and profile parameters obtained from the Le Bail fits and space groups P2 and $P2_1$ were used in the structure solution calculations.

Structure solution was carried out using the direct-space genetic algorithm[191] (GA) technique incorporated in the program EAGER[195]. Two input models were used in the structure solution calculations, representing the two different space groups $P2_1$ and P2. For each input model, there are three fragments: two fragments are TMA molecules and the third fragment is the L-arginine molecule. In each fragment, the TMA molecule was defined by a total of nine structural variables (three positional variables, three orientational variables and three torsion angle variables) and the L-arginine molecule was defined by a total of twelve structural variables (three positional variables, three orientational variables and six torsion angles). Hence, each model is represented by a total of 30 structural variables. In total, 16 independent GA calculations were carried out for each model and the GA calculation was allowed to evolve for 1000 generations for a population size of 100. In each generation, 10 mating operations and 50 mutation operations were carried out. The results from all these structure solution calculations were assessed and evaluated to determine which model gives the best structure solution.

The results from the structure solution calculations show that, for space group P2, one structural model has lowest R_{wp} but this structural model is unreasonable, because all molecules are linked together (in fact, all structural models with space group P2 obtained from the GA calculations are unreasonable). For space group $P2_1$, the structural models obtained from the GA calculations are reasonable. Therefore, the structural model with lowest R_{wp} for space group $P2_1$ was used as the initial structural model for Rietveld refinement[213], which was carried out using the GSAS program. In the Rietveld refinement, initially, the TMA molecule was modelled as H_2TMA^- anions and the carboxylic acid group of the L-arginine molecule was modelled as deprotonated (carboxylate group) and the $–NH_2$ of the L-arginine molecule was modelled as protonated ($–N^+H_3$ group). Standard restraints were applied to bond lengths and bond angles, and planar restraints were applied to benzene rings, carboxylate groups, carboxylic acid groups and guanidinium groups. As the refinement progressed, these restraints were gradually relaxed. In the process of refinement, the isotropic displacement parameters were refined as a common value for all atoms within the same molecule. The value of isotropic displacement parameter for all hydrogen atoms were set to 1.2 times that of the non-H atoms in the same molecule. After the initial Rietveld refinement, the calculated powder XRD pattern did not fit the experimental powder pattern satisfactorily with R_{wp} = 3.67% (Figure 5.4a).

With the help of difference Fourier maps, we could see that some electron density in the crystal had not been included in the structural model. Considering the solvent (water) and the density of the sample, we concluded that there are one or two water molecules in the asymmetric unit (corresponding to calculated densities of 1.51 g cm^{-3} and 1.56 g cm^{-3}, respectively). Therefore, the initial input models as discussed above for structure solution are not correct, and these input models were modified by adding one more or two water molecules in the asymmetric unit, representing two new input models for structure solution calculations. In these two input models, one or two more fragments, which represent one or two water molecules, were introduced and the other conditions were kept the same as those discussed above. The structure solution calculations using the program EAGER were then carried out again.

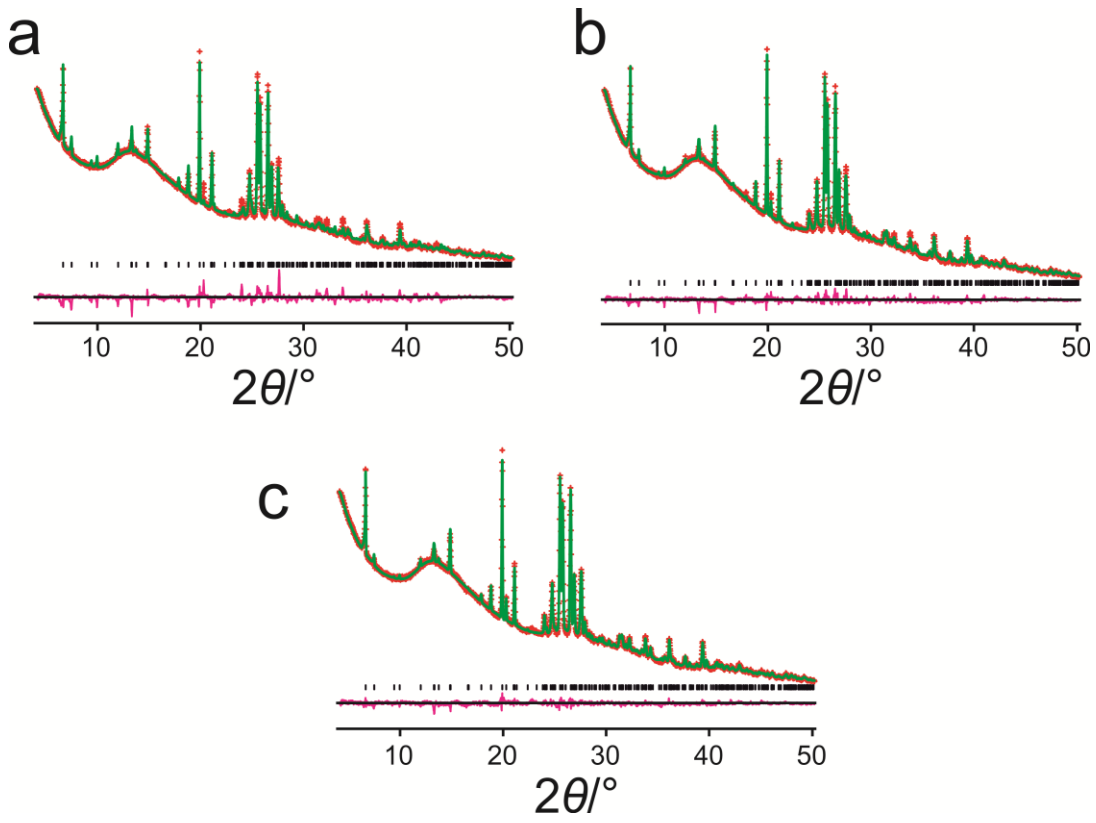

Figure 5.4. *Rietveld refinements for phase 1 for the models with (a) no water, (b) one water molecule and (c) two water molecules in the asymmetric unit.*

The results from structure solution indicated that the model with two water molecules in the asymmetric unit had the lowest R_{wp} and the structural model was reasonable. We performed Rietveld refinement with this model, exploring the process as described above. This refinement led to a good fit with the experimental powder XRD data (R_{wp} = 1.78%, R_p = 1.27%, Figure 5.4c). In addition, in order to make sure that the model with one water molecule in the asymmetric unit does not lead to a superior final refinement, we also performed Rietveld refinement with the structural model containing one water molecule in the asymmetric unit. As expected, this model did not give as good a fit to the experimental powder XRD data (R_{wp} = 2.41%, R_p = 1.68%, Figure 5.4b). The final Rietveld refinement for the structural model containing two water molecules gave the following data: $P2_1$; a = 26.8430(21) Å, b = 13.3445(9) Å, c = 3.7441(3) Å, β = 88.8585(24)°; V = 1340.91(30) Å^3, R_{wp} = 1.78%, R_p = 1.27%.

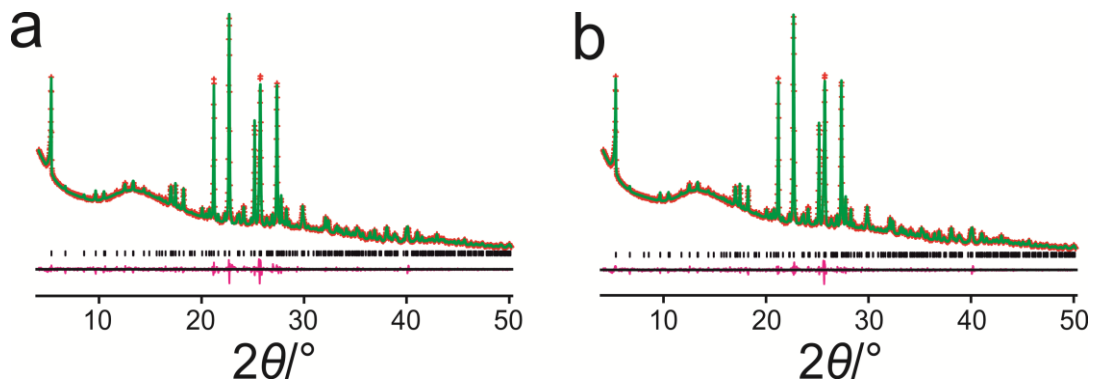

Figure 5.5. *Le Bail profile fitting for phase 2 with (a) $P222_1$ and (b) P222.*

5.3.2 Structure Determination of Phase 2

The powder XRD pattern of phase 2 was indexed by using program CRYSFIRE, giving the following unit cell parameters in an orthorhombic system: a = 16.84 Å, b = 13.34 Å, c = 11.06 Å (V = 2484.7 Å^3), with $P222_1$ as the best estimated space group. However, profile-fitting did not give a good quality of fit (Figure 5.5a). We then used the simplest space group in the orthorhombic system, P222, for Le Bail fitting. The resulting fit was still not good (Figure 5.5b). Therefore, we lowered the symmetry to monoclinic (The powder pattern of phase 2 was indexed again by using program CRYSFIRE and combined with the program CHEKCELL). When the space group was assigned as P2 and $P2_1$ with the unit cell parameters: a = 13.342 Å, b = 11.057 Å, c = 16.844 Å, β = 90.133° (V = 2484.7 Å^3), Le Bail fitting gave a good quality of fit (Figure 5.6a, space group P2, a = 13.3277(3) Å, b = 11.0393(2) Å, c = 16.8182(4) Å, β = 90.1354(17)°, V = 2474.43(13) Å^3, R_{wp} = 1.55%, R_p = 1.17%. Figure 5.6b, space group $P2_1$, a = 13.3299(3) Å, b = 11.0393(2) Å, c = 16.8175(4) Å, β = 90.1388(18)°, V = 2474.74(13) Å^3, R_{wp} = 1.58%, R_p = 1.18%).

From the solution ^{1}H NMR spectrum, we determined the molar ratio between L-arginine and TMA is 1:1. Thus, we deduced that there are six TMA molecules and six L-arginine molecules in the unit cell and the calculated density is 1.54 g cm^{-3}. Thus, there are three TMA molecules and three L-arginine molecules in the asymmetric unit for space group P2 and $P2_1$. The refined unit cell parameters and profile parameters obtained from the Le Bail fits and space groups P2 and $P2_1$ were used in the structure solution calculation.

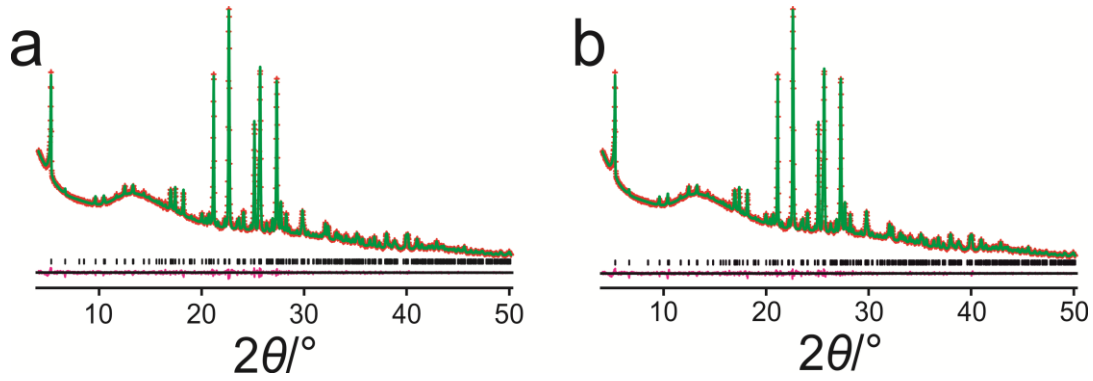

Figure 5.6. *Le Bail profile fitting for phase 2 with (a) P2 and (b) $P2_1$.*

Structure solution calculations were carried out using the program EAGER. Two input models were used in the structure solution calculations. For each input model, there were six fragments: three fragments were TMA molecules and the remaining three fragments were L-arginine molecules. In each fragment, the TMA molecule was defined by a total of nine structural variables and the L-arginine molecule was defined by a total of twelve structural variables. Hence, each model was represented by a total of 63 structural variables. The other conditions were kept the same as phase 1.

From the structure solution calculations, the lowest R_{wp} was obtained for space group $P2_1$, and the structural model is reasonable. When the space group is P2, the structural model has the second lowest R_{wp} and is also reasonable. First, the structural model with lowest R_{wp} with space group $P2_1$ was used as the initial structural model for Rietveld refinement. This refinement led to a good fit with the experimental powder XRD data (R_{wp} = 2.42%, R_p = 1.71%, Figure 5.7a). In order to make sure that the model with space group P2 is not correct, we also performed Rietveld refinement with the structural model for this space group. As expected, this model did not give as good a fit to experimental powder XRD data (R_{wp} = 3.47%, R_p = 2.30%, Figure 5.7b). The final Rietveld refinement for the structural model with space group $P2_1$ gave the following data: a = 13.3271(4) Å, b = 11.0393(3) Å, c = 16.8183(6) Å, β = 90.1491(27)°, V = 2474.34(20) $Å^3$, R_{wp} = 2.42%, R_p = 1.71%.

5.3.3 Structure Determination of Phases 3 and 4

The powder XRD pattern of phase 3 was indexed successfully by using program CRYSFIRE and combined with the program CHEKCELL, giving the following unit cell parameters in an monoclinic system: a = 17.17 Å, b = 3.81 Å, c = 13.34 Å, β = 104.7°, with P2 and $P2_1$ as the best estimated space group. The Le Bail fitting gave

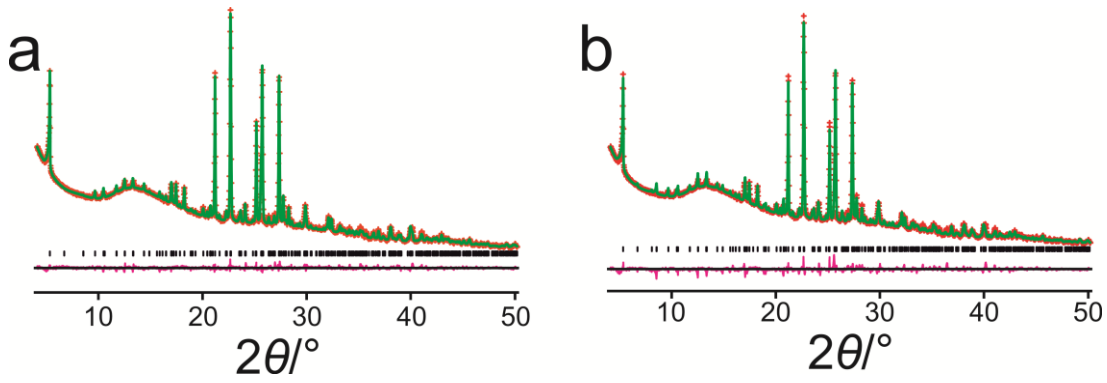

Figure 5.7. *Rietveld refinement for phase 2 with (a) $P2_1$ and (b) P2.*

a good quality of fit for space groups P2 and $P2_1$ (Figures 5.8a: P2, a = 17.1675(7) Å, b = 3.8101(5) Å, c = 13.3367(5) Å, β = 104.7039(18)°, V = 843.77(8) Å^3, R_{wp} = 2.12%, R_p = 1.60%. Figure 5.8b: $P2_1$, a = 17.1672(6) Å, b = 3.8099(2) Å, c = 13.3370(6) Å, β = 104.7035(19)°, V = 843.75(9) Å^3, R_{wp} = 2.13%, R_p = 1.61%).

From the solution ^{1}H NMR spectrum, the molar ratio of L-arginine to TMA is 1:1 was established. With two TMA molecules and two L-arginine molecules in the unit cell, the calculated density is 1.51 g cm^{-3}. Thus, there is one TMA molecule and one L-arginine molecule in the asymmetric unit for space groups P2 and $P2_1$. Structure solution calculations were carried out using the program EAGER. Two input models were used in the structure solution calculations. For each input model, there were two fragments: one fragment was the TMA molecule and the other fragment was the L-arginine molecule. The TMA molecule was defined by nine structural variables and the L-arginine molecule was defined by twelve structural variables. Hence, each model was represented by a total of 21 structural variables. The other conditions were kept the same as phase 1.

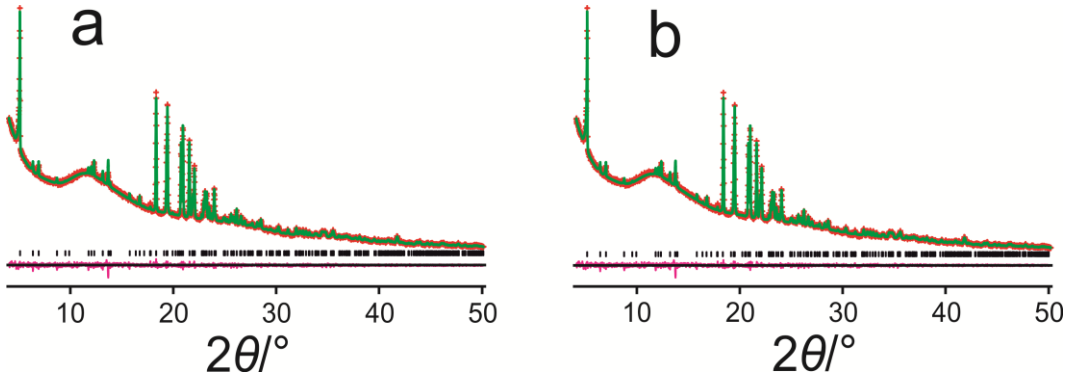

Figure 5.8. *Le Bail profile fitting for phase 3 with (a) P2 and (b) $P2_1$.*

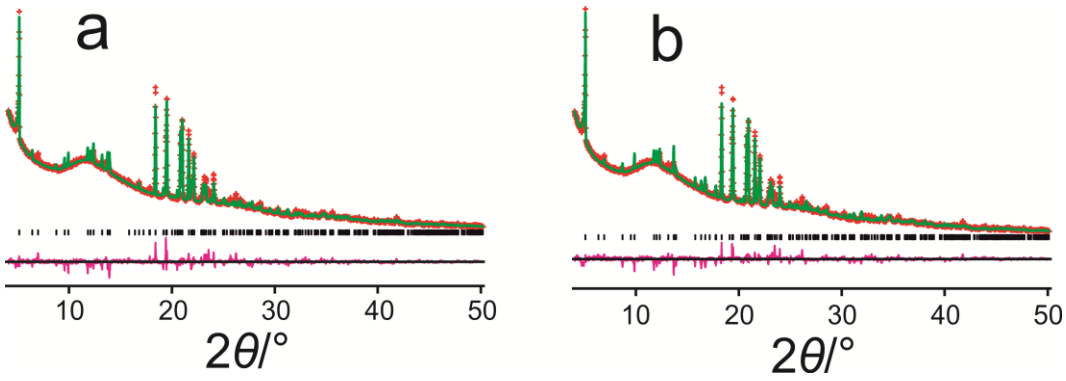

Figure 5.9. *Rietveld refinement for phase 3 with (a) P2 and (b) $P2_1$.*

Using the structural models giving the structure solution with lowest R_{wp} for space groups P2 and $P2_1$, the Rietveld refinement did not lead to a good fit (space group P2: R_{wp} = 4.58%, R_p = 2.97%, Figure 5.9a; space group $P2_1$: R_{wp} = 4.34%, R_p = 2.87%, Figure 5.9b). Therefore, we lowered the symmetry to triclinic. (The powder pattern of phase 3 was indexed again by using program CRYSFIRE and combined with the program CHEKCELL). Since L-arginine is a chiral molecule, the achiral space group $P\bar{1}$ is ruled out, thus the space group was assigned as P1 with the unit cell parameters: a = 3.81 Å, b = 13.34 Å, c = 17.17 Å, α = 104.70°, β = 90.13°, γ = 90.04°, V = 843.9 Å^3. Le Bail fitting gave a good quality of fit (Figure 5.10a, space group P1, a = 3.8104(1) Å, b = 13.3370(4) Å, c = 17.1673(5) Å, α = 104.7018(18)°, β = 89.9990(31)°, γ = 90.037(4)°, V = 843.87(6) Å^3, R_{wp} = 2.15%, R_p = 1.61%).

Structure solution calculations were carried out in the program EAGER again. For this input model, there were four fragments: two fragments were TMA molecules and the other two fragments were L-arginine molecules. The TMA molecule was defined by a total of nine structural variables and the L-arginine molecule was defined by a total of twelve structural variables. Hence, this model was represented by a total of 42 structural variables. The other conditions were kept the same as discussed above. The structural model with lowest R_{wp} was used as the initial model for Rietveld refinement. However, this refinement did not lead to an acceptable fit (R_{wp} = 4.51%, R_p = 2.96%, Figure 5.10b). The structure determination of this phase is currently in progress.

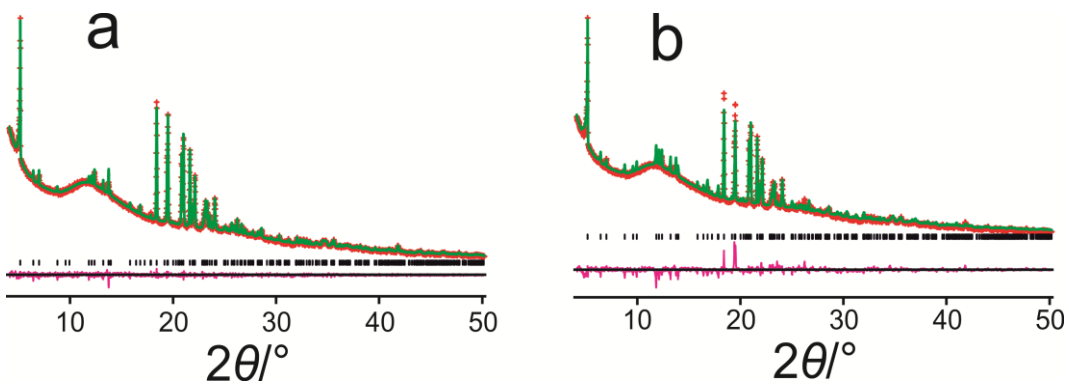

Figure 5.10.*(a) Le Bail profile fitting and (b) Rietveld refinement for phase 3.*

For phase 4, it was quite difficult to reproduce this sample and the quality of powder XRD pattern was not good enough (due to peak overlap), we could not index this powder XRD pattern at this stage. Thus, we could not carry out structure solution calculation in the program EAGER and could not determine the structure of phase 4 from PXRD data.

5.4 Results and Discussion

5.4.1 Structural Analysis of Phase 1

As mentioned above, there are two TMA molecules (denoted as TMA1 and TMA2), one L-arginine molecule and two water molecules in the asymmetric unit of phase 1. Thus, the formula of phase 1 is $(TMA)_2$ $(L\text{-}Arg)_1 \cdot (H_2O)_2$. The structure of phase 1 is shown in Figure 5.11. In the crystal structure, all TMA molecules are present as H_2TMA^{2-} anions and the carboxylic acid group of L-arginine molecule is not deprotonated (present as the –COOH group)and the $–NH_2$ group is protonated (i.e., the $–N^+H_3$ group). Viewed along the c-axis, the crystal structure comprises two types of TMA ribbons, which lie parallel to the b-axis (these two ribbons are denoted as ribbon I and ribbon II, indicated within a green rectangle in Figure 5.11). Ribbon I is formed by TMA1 molecules and ribbon II is formed by TMA2 molecules. The L-arginine molecules line up to occupy the space between these two types of TMA ribbons and are linked to adjacent TMA ribbons directly through O (TMA)···H–O (L-Arg) hydrogen bonds and N–H (L-Arg)···O (TMA) hydrogen bonds or indirectly via intervening water molecules.

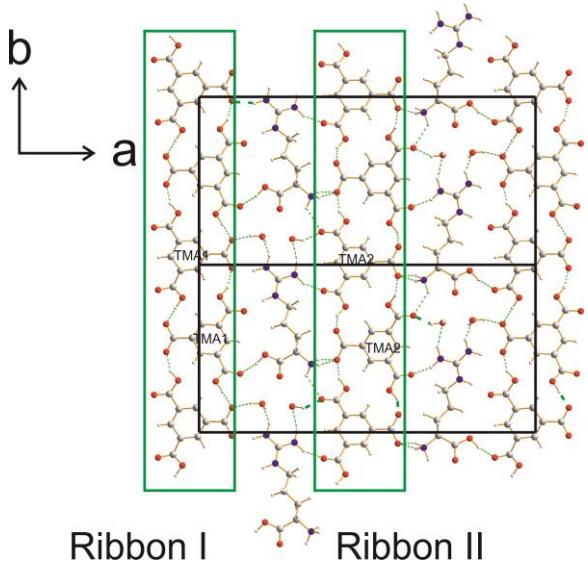

Figure 5.11. *Two types of TMA ribbons (ribbon I and ribbon II) in the crystal structure of phase 1, viewed along the* c*-axis.*

Viewed along the a-axis separately (Figures 5.12a and 5.12b), we can see that these two types of TMA ribbons are almost the same and both are corrugated instead of flat. For both types of ribbons (Figures 5.12a and 5.12b), each TMA molecule in one ribbon is linked to an adjacent TMA molecule directly by an O···H–O hydrogen bond (in ribbon I, the distance of O···H and O···O is 1.72 Å and 2.71 Å and in ribbon II, the distance of O···H and O···O is 1.57 Å and 2.51 Å). Adjacent ribbons are also linked together through an O···H–O hydrogen bond (in ribbon I, the distance of O···H and O···O is 1.57 Å and 2.51 Å and in ribbon II, the distance of O···H and O···O is 1.58 Å and 2.51 Å). Thus, all ribbons I are linked together and there are no cyclic hydrogen-bonding arrangements observed in ribbon I (the same situation for ribbon II).

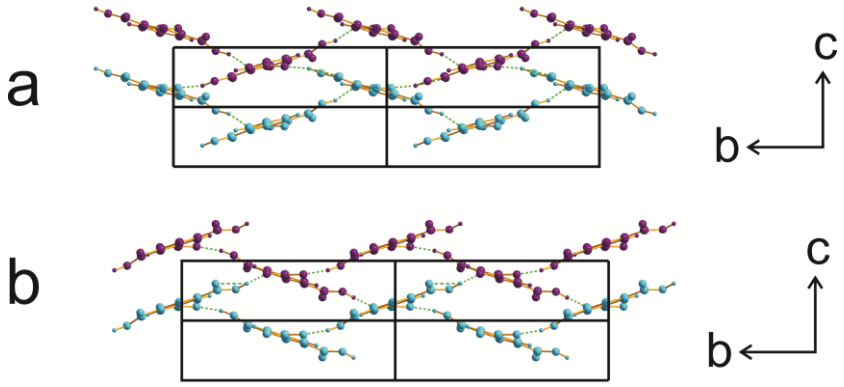

Figure 5.12. *Two types of TMA ribbons (a) ribbon I and (b) ribbon II in the crystal structure of phase 1, viewed along the* a*-axis.*

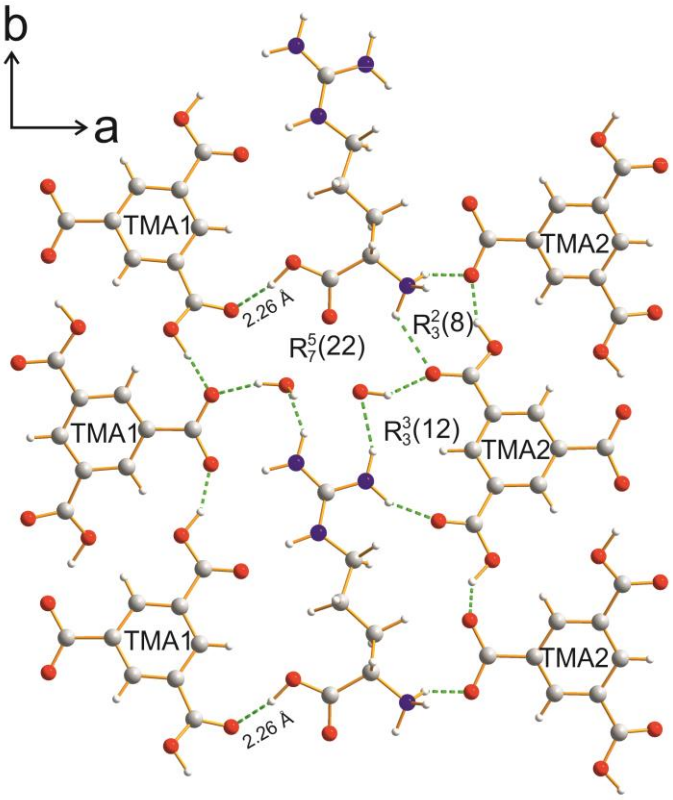

Figure 5.13. *Hydrogen-bonding arrangements between L-Arg molecules and TMA molecules in the structure of phase 1.*

In terms of the L-arginine molecule, as shown in Figure 5.13, for each L-arginine molecule, on one side, the –COOH group of the L-arginine molecule is linked to one TMA1 molecule directly through an O–H···O hydrogen bond (the distance of H···O and O···O in this hydrogen bond is 2.26 Å and 3.12 Å) and one $–NH_2$ group of the guanidinium group is linked to another TMA1 molecule through an N–H···O–H (water)···O hydrogen-bonding arrangement involving one intervening water molecule. On the other side of the L-arginine molecule, the $–N^+H_3$ group of the L-arginine is linked to two TMA2 molecules through two N–H···O hydrogen bonds (in these two hydrogen bonds, the distances of N···O is 2.96 Å and 2.68 Å and a cyclic hydrogen-bonding $R_3^2(8)$ arrangement forms between them. Another $–NH_2$ group of the

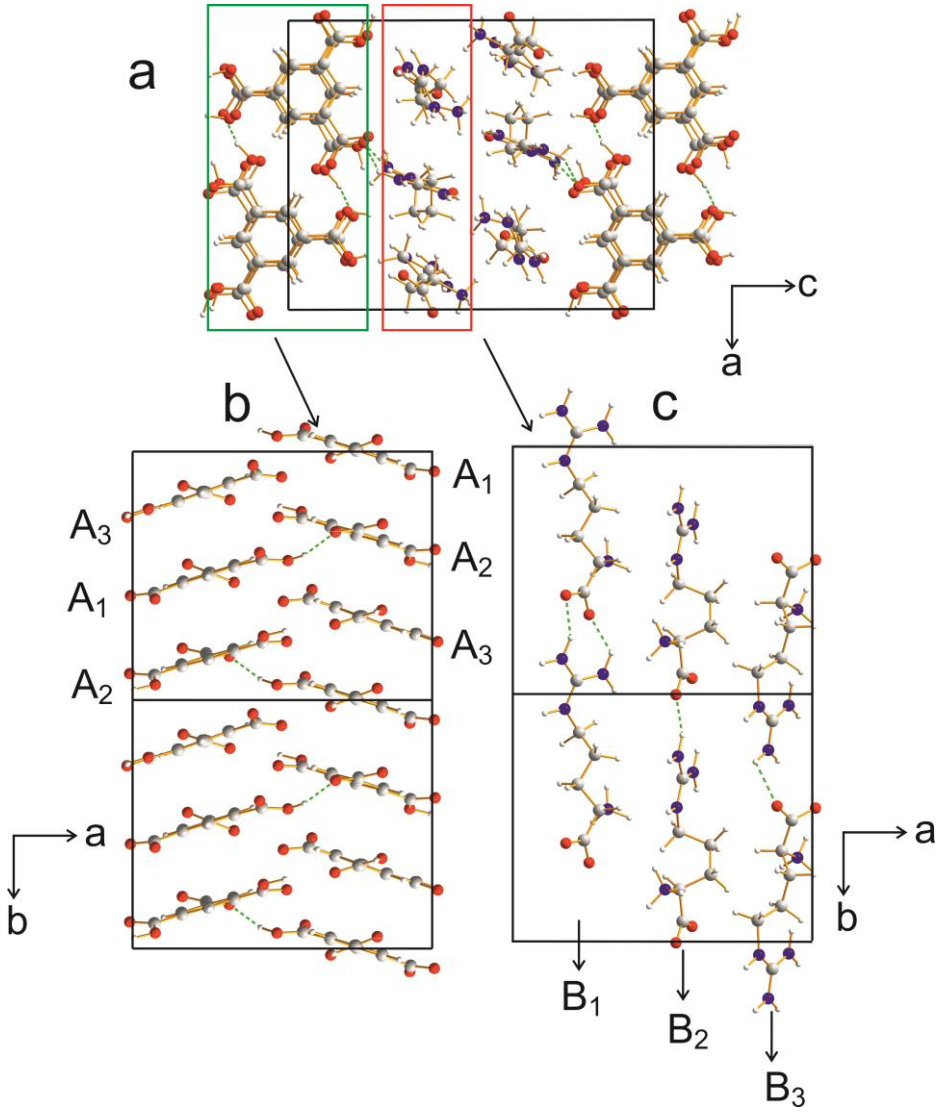

Figure 5.14. *(a) The complete crystal structure of phase 2, viewed along the b-axis. (b) Two types of TMA pillars and (c) Three types of strands of L-arginine molecule in the crystal structure of phase 2, viewed along the c-axis.*

guanidinium group is linked to one TMA2 molecule involving one intervening water molecule, which give rise to graph set $R_3^3(12)$. In this cyclic hydrogen-bonding arrangement, on one side, the $–NH_2$ group of the guanidinium group is linked to a TMA2 molecule directly through an N–H···O hydrogen bond, on other side, the $–NH_2$ group is linked to a TMA2 molecule via an intervening water molecule through an N–H···O–H···O hydrogen bond. In addition, it is noted that there is a large cyclic hydrogen-bonding ring, which involves two TMA1 molecules, two water molecules, two L-arginine molecules and one TMA2 molecule, giving rise to graph set $R_7^5(22)$.

5.4.2 Structural Analysis of Phase 2

In the structure of phase 2, there are three independent TMA molecules (A_1, A_2, and A_3) and three independent L-arginine molecules (B_1, B_2 and B_3) in the asymmetric unit. Thus, the formula of phase 2 is $(TMA)_1$ $(L\text{-}Arg)_1$. The structure of phase 2 is shown in Figure 5.14, in the crystal structure, all TMA molecules are present as H_2TMA^{2-} anions and the carboxylic acid group of L-arginine molecule is deprotonated and present as the $–COO^-$ group and the $–NH_2$ group is protonated and present as the $–N^+H_3$ group.

As show in Figure 5.14a, viewed along the b-axis, there are two types of TMA pillars and three types of L-arginine strands. The TMA molecules are stacked in the sequence A_1, A_2, A_3, A_1, A_2, A_3,… with two different dispositions to form two types of TMA pillars, which both lie parallel to the b-axis (Figure 5.14b, viewing along the c-axis). Next to the TMA pillars, there are three lined different types of L-arginine strand (Figure 5.14c, strand B_1, B_2 and B_3) in turn. These three strands are also parallel to the b-axis (viewing along the c-axis). Within the strand B_1, adjacent B_1 molecules are linked together by two N–H···O hydrogen-bonding arrangements involving two $–NH_2$ groups of the guanidinium group of one B_1 molecule and the $–COO^-$ group of another B_1 molecule, which gives rise to a hydrogen-bonding arrangement with graph set $R_2^2(8)$. The distances (hydrogen bond lengths) between these two H···O hydrogen bonds within this strand are 1.948 Å and 1.985 Å, and the distance of N···O are 2.867 Å and 2.719 Å. Within each of the strands B_2 and B_3, there is only one N–H···O hydrogen bond involving one $–NH_2$ of the guanidinium group of one B_2 (or B_3) molecule and the $–COO^-$ group of another B_2 (or B_3) molecule, and the distance (hydrogen bond lengths) between H···O hydrogen bonds is 1.846 Å (or 2.295 Å) and the distances of N···O are 2.811 Å or (2.859 Å).

The hydrogen-bonding arrangements between TMA molecules and L-arginine molecules in the crystal structure of phase 2 are shown in Figure 5.15 (viewed along (-5 2 0)), i.e. firstly, view along the a-axis, then rotate the structure with about 26° along the a-axis in order to show the TMA molecules clearly). One A_2 molecule is linked to an A_1 molecule and an A_3 molecule through two O (A_2)···H–O (A_1 or A_3) hydrogen bonds to form a short TMA ribbon. On one side, one B_1 molecule of the B_1 strand is linked to an A_2 molecule through an N–H···O hydrogen bond and the distance (hydrogen bond length) of H···O is 1.967 Å and the distance of N···O is 2.70 Å. On the other side, one

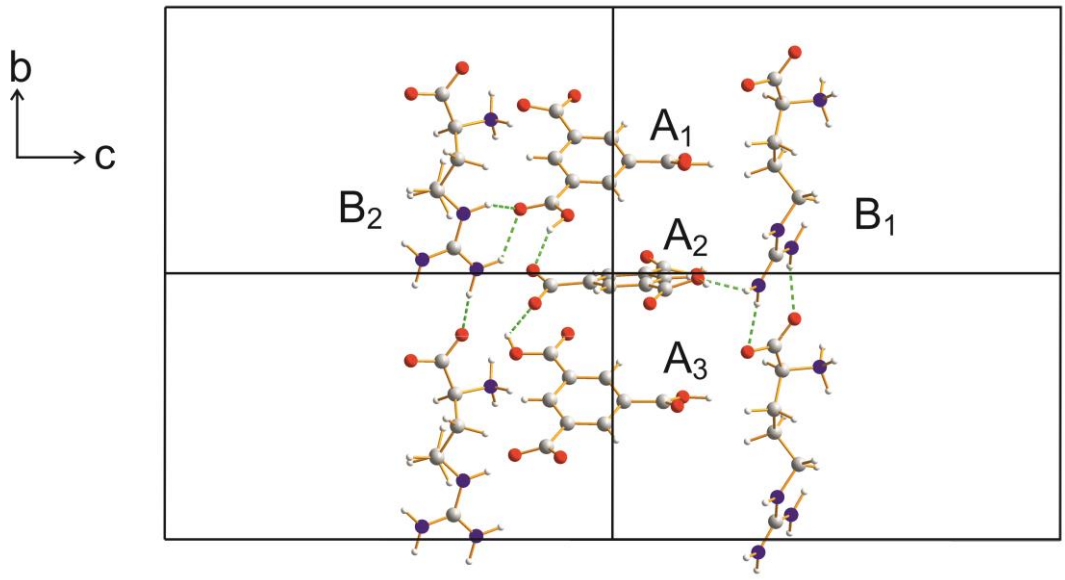

Figure 5.15. *Hydrogen-bonding arrangements between TMA molecules and L-arginine molecules of phase 2, viewed towards plane* $(\bar{5}20)$.

B_2 molecule of the B_2 strand is linked to the A_1 molecule through two N–H···O hydrogen bonds, forming a hydrogen-bonding arrangement with graph set $R_2^1(6)$. The distance (hydrogen bond lengths) of these two H···O hydrogen bonds are 1.934 Å and 2.109 Å and the distances of N···O are 2.758 Å and 2.885 Å. The B_3 molecules in the strand B_3 is not linked to any TMA molecules.

5.5 Summary

In conclusion, in the course of studying co-crystals of TMA and L-arginine, we obtained four new solid phases and the structures of two co-crystals of TMA and L-arginine have been determined directly from powder XRD data. One co-crystal is composed of two TMA molecules, one L-arginine molecule and two water molecules in the asymmetric unit, whereas the co-crystal is composed of three TMA molecules and three L-arginine molecules in the asymmetric unit. The process of structure determination from powder XRD data is presented in this chapter, demonstrating that PXRD analysis is a reliable alternative for structural analysis when the single-crystal XRD method cannot be used.

Chapter 6 Co-Crystal of Pillar[5]quinone and 1,1,2,2,-Tetrachloroethane, with Structure Determination Directly from Powder X-Ray Diffraction Data

6.1 Introduction

Pillar[*n*]arenes[269-272] are a new class of macrocyclic molecular compound composed of hydroquinone units linked by methylene groups at the *para* positions (Figure 6.1a). Due to their symmetrical, pillar-like structures and potential applications in host-guest chemistry, pillar[*n*]arenes and their derivatives have attracted considerable attention.[273,274] To date, pillar[n]arenes (n = 5 - 10) have been synthesized. However, due to the low yields (1 - 2%) of pillar[n]arenes (n = 7 - 10), currently most research involving pillar[*n*]arenes has been focused on pillar[5]arene and pillar[6]arene and their derivatives, especially pillar[5]arene and its derivatives.[275-279] It has been reported that partial or full functionalization of pillar[5]arenes with different functional groups can change their physicochemical properties (such as solubility), leading to different potential applications in various areas.[280-283]

Pillar[5]quinone (P[5]Q), the oxidation product of pillar[5]arene, was synthesized for the first time in 2009.[271] P[5]Q is composed of five *p*-benzoquinones linked by methylene groups at the *para* positions (Figure 6.1b). In theory, the structure of the P[5]Q molecule should have a symmetrical pillar-shaped framework with two equally sized cavity portals. These features make P[5]Q interesting and useful in host-guest chemistry. Therefore, understanding the detailed crystal structure properties of P[5]Q is very important. Lao and Yu[284] investigated the thermodynamic properties and electronic structure of P[5]Q by computational studies and the results of their calculations suggested that P[5]Q undergoes significant intramolecular charge transfer upon the electronic excitation from the HOMO to the LUMO, owing to the large difference in electron distributions between the HOMO to the LUMO.

Furthermore, they also suggested that P[5]Q is a promising material for trapping anionic halogens through anion-π interactions[285] in the interior cavity of P[5]Q. Significantly, π-π interactions and cation-π interactions are well known to play a key role in chemistry and biological sciences, such as crystal engineering, protein structures and DNA structures. However, non-covalent interactions between π-acidic aromatic

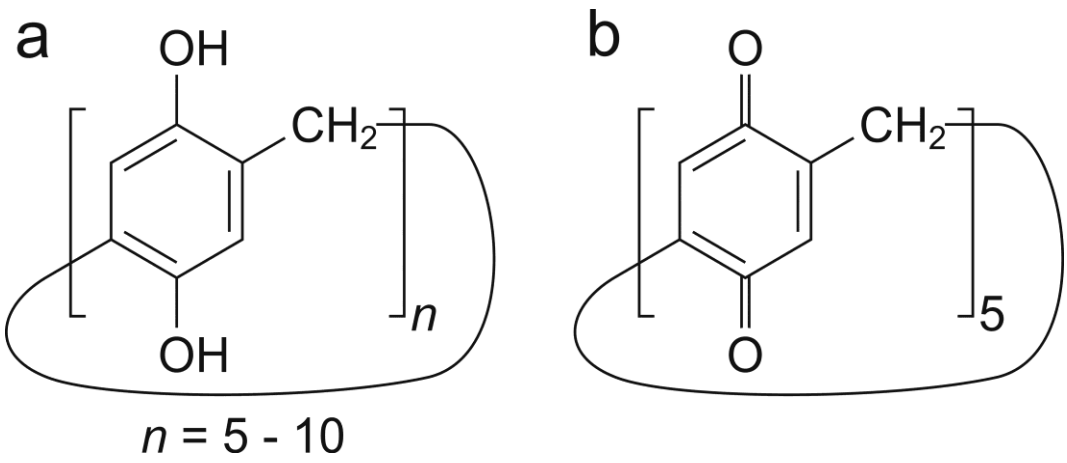

Figure 6.1. *(a) Molecular structure of pillar[n]arenes. (b) Molecular structure of pillar[5]quinone.*

systems and anions, namely anion-π interactions, have been largely ignored by scientists due to their seemingly counterintuitive nature. In 2002, scientists[286] established that anion-π interactions really exist and are energetically favourable, and subsequently anion-π interactions have attracted much attention.[287-290] It has been reported[291,292] that 1,4-benzoquinone has a large electron affinity, which makes 1,4-benzoquinone very efficient as an electron acceptor. Therefore, as P[5]Q is composed of five 1,4-benzoquinone moieties, it is anticipated that P[5]Q can interact with anions in the interior cavity through anion-π interactions. In order to understand the structural properties of P[5]Q in more detail and to confirm the expectations inferred from computational studies, chemists attempted to prepare P[5]Q in the form of a crystalline solid. However, to date, large single crystals of P[5]Q have not been prepared, and the structural properties of P[5]Q have not been determined by single-crystal X-ray diffraction techniques. Fortunately, using powder X-ray diffraction for structure solution (the direct-space strategy), we can carry out the structure determination of P[5]Q instead by powder X-ray diffraction data, combined with other techniques such as high-resolution solid-state NMR. Given the importance of P[5]Q in host-guest chemistry, the aim of this chapter is to determine the co-crystal structure of P[5]Q with 1,1,2,2-tetrachloroethane directly from powder X-ray diffraction data.

6.2 Experimental

A yellow-coloured, fluffy, microcrystalline sample of co-crystals of P[5]Q with 1,1,2,2-tetrachloroethane (TCE) was produced by our collaborators in India (Gangadhar J. Sanjayan, CSIR-National Chemical Laboratory). A high-quality powder XRD pattern of this sample was recorded on a Bruker D8 instrument (Ge-monochromated CuKα_1

radiation) using a tape sample holder. The powder XRD data were recorded in transmission mode (2θ range: 4 - 50°, total time: 48 h). Differential scanning calorimetry (DSC) data were measured on a TA Instruments Q100 using sealed aluminium pans and cooling rates between 1 and 20 °C min^{-1}. Variable-temperature powder XRD data were recorded from 90 K to 300 K (90 K, 100 K, 150 K, 200 K, 250 K, 295 K and 300 K) using synchrotron X-ray powder diffraction at the Diamond Light Source. (Beam-line I11, High resolution powder diffraction, λ = 0.826607(2) Å). The sample was loaded within a capillary sample holder and step-scanned in 2θ steps of 0.001° with total scan time of 1800 s for each experiment). High-resolution solid-state ^{13}C NMR experiments were carried out at the EPSRC UK National Solid-State NMR Service at the University of Durham. Spectra were recorded at ambient temperature on a spectrometer operating at a ^{13}C Larmor frequency of 100.562 MHz, with MAS at 8 kHz. Spectra were recorded both using the standard $^{1}H \rightarrow ^{13}C$ CPMAS pulse sequence and using the $^{1}H \rightarrow ^{13}C$ CPMAS pulse sequence with a dipolar dephasing delay of 50 μs between the ^{1}H excitation pulse and CP.

6.3 Structure Determination from Powder XRD Data

The powder XRD pattern was indexed by using the TREOR[202] and ITO[203] codes, which are incorporated into the program CRYSFIRE.[205] Combined with the program CHEKCELL[207], the following unit cell in an orthorhombic system was obtained: a = 18.794 Å, b = 15.258 Å, c = 6.914 Å (V = 1982.8 $Å^3$), and the best estimated space groups given by program CHEKCELL were I222 and Immm. Le Bail fitting[208] was then used to check these space groups using the GSAS[209] software and the graphical user interface editor EXPGUI.[210] However, a good quality of Le Bail fit was not obtained for either of these space groups (Figure 6.2a and 6.2b). We then used the simplest space group in the orthorhombic system, P222, for Le Bail fitting. The resulting fit was still not good quality (Figure 6.2c), suggesting that the orthorhombic system is not correct. Therefore, we lowered the symmetry to monoclinic. The space group was assigned as P2, $P2_1$, Pm, P2/m, P2/n, $P2_1/m$ or $P2_1/n$, with the unit cell parameters: a = 18.771 Å, b = 15.250 Å, c = 6.905 Å, β = 89.736° (V = 1976.6 $Å^3$). Le Bail fitting gave a good quality of fit for all these space groups (Figure 6.3a - 6.3g). Thus, the space group could not be assigned uniquely on the basis of systematic absences alone at this stage and, all these seven possible space groups were considered in parallel for structure solution in the next stage.

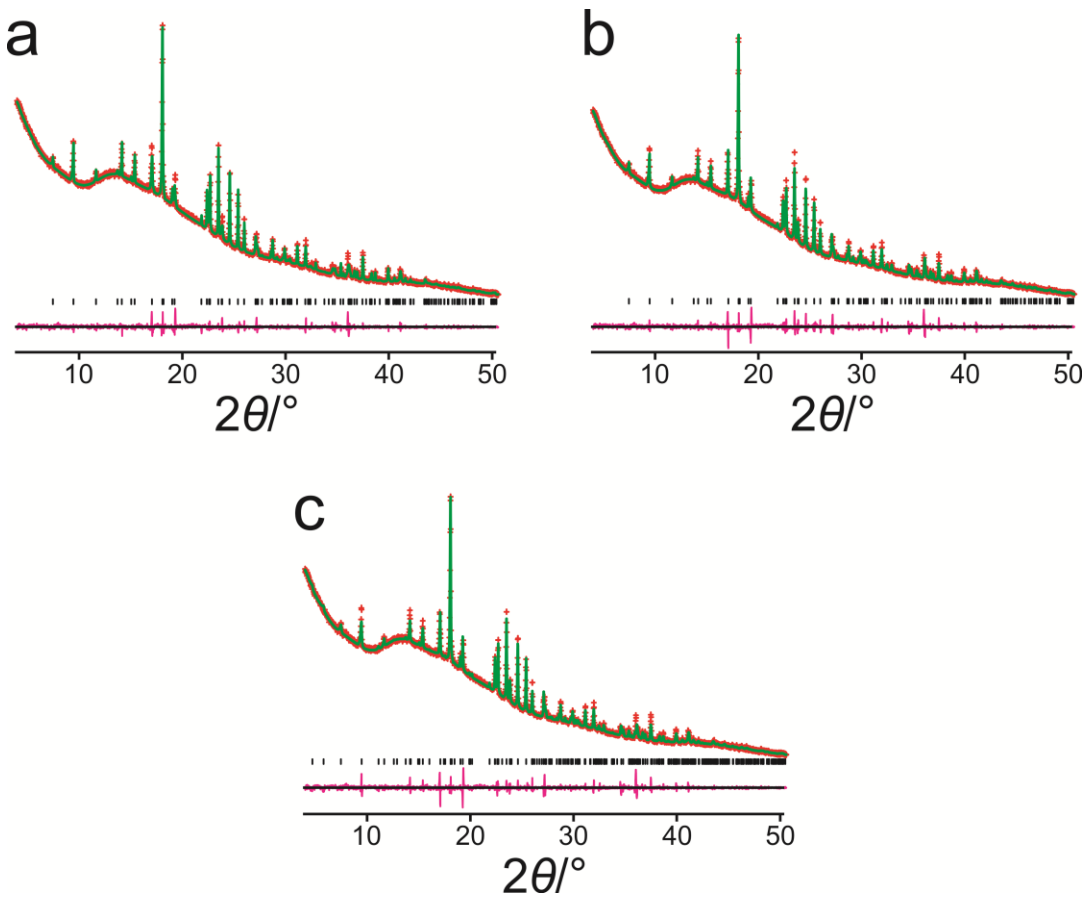

Figure 6.2. *Le Bail profile fitting for space groups (a) I222, (b) Immm and (c) P222.*

Given the volume of the unit cell and consideration of the density of the material, there are two P[5]Q molecules and four TCE molecules in the unit cell and the calculated density is 1.57 g cm^{-3}. Therefore, if the space groups is P2, $P2_1$ or Pm, there is one P[5]Q molecule and two TCE molecules in the asymmetric unit; if the space group is P2/m, P2/n, $P2_1/m$ or $P2_1/n$, there is one half a P[5]Q molecule and one TCE molecule in the asymmetric unit. The refined unit cell parameters and profile parameters obtained from the Le Bail fits for space groups P2, $P2_1$, Pm, P2/m, P2/n, $P2_1/m$ and $P2_1/n$ were used in the structure solution calculations.

Structure solution calculations were carried out using the direct-space genetic algorithm (GA)[191] technique incorporated in the program EAGER.[195] A total of seven input models were used in the structure solution calculations, representing the seven different space group. For space groups P2, $P2_1$ and Pm, the input model comprised four fragments: two half P[5]Q molecules and two TCE molecules. The reason for two half P[5]Q molecules rather than one independent P[5]Q molecule were used in these cases was to confirm whether the P[5]Q molecule can form a pentagonal ring and whether the five 1,4-benzoquinone moieties can link each other by methylene groups at the *para*

positons. Each half P[5]Q molecule was defined by a total of six structural variables (three positional variables and three orientational variables) and each TCE molecule was defined by a total of seven structural variables: three positional variables, three orientational variables and one torsional angle variable. Hence, these structure solution calculations involved a total of 26 structural variables. For P2/m, P2/n, $P2_1/m$ and $P2_1/n$, each input model comprised three fragments: one fragment was a half P[5]Q molecule and each of the other two fragments was a half TCE molecule. The half P[5]Q molecule was defined by six structural variables and each half TCE molecule was defined by six structural variables. Hence, these structure solution calculations involved a total of 18 structural variables. In total, 16 independent GA calculations were carried out for each space group and the GA calculation was allowed to evolve for 1000 generations with a population size of 100. In each generation, 10 mating operations and 50 mutation operations were carried out. The results from all these structure solution calculations were assessed and evaluated to determine which space group gives the best structure solution.

The results from the structure solution calculations indicated that the lowest R_{wp} was obtained for space group $P2_1$, and this best structure solution was structurally reasonable. In this model, the two half P[5]Q molecules formed into one complete P[5]Q molecule. For space group P2/n, the structure solution with the second lowest R_{wp} is obtained, with two half P[5]Q molecules (related to each other by the 2-fold axis) forming into one complete P[5]Q molecule. However, one of TCE molecules is not formed correctly in this space group. In the remaining five space groups, the two half P[5]Q molecules do not form a complete P[5]Q molecule correctly. Therefore, the structure solution with lowest R_{wp} obtained in the GA calculations with space group $P2_1$ was used as the initial structural model for Rietveld refinement,[213] which was carried out using the GSAS program. In the Rietveld refinement, standard restraints were applied to bond lengths and bond angles, and planar restraints were applied to each quinone ring. As the refinement progressed, these restraints were gradually relaxed. In the process of refinement, the isotropic displacement parameters were refined. The value of U_{iso} for all atoms within the same molecule were set to the same value. All hydrogen atoms were set to a value of 1.2 times that of the non-H atoms. However, the initial Rietveld refinement did not lead to an acceptable quality of fit, with acceptable discrepancies between the experimental and calculated powder XRD patterns (R_{wp} = 1.82%, Figure 6.4a).

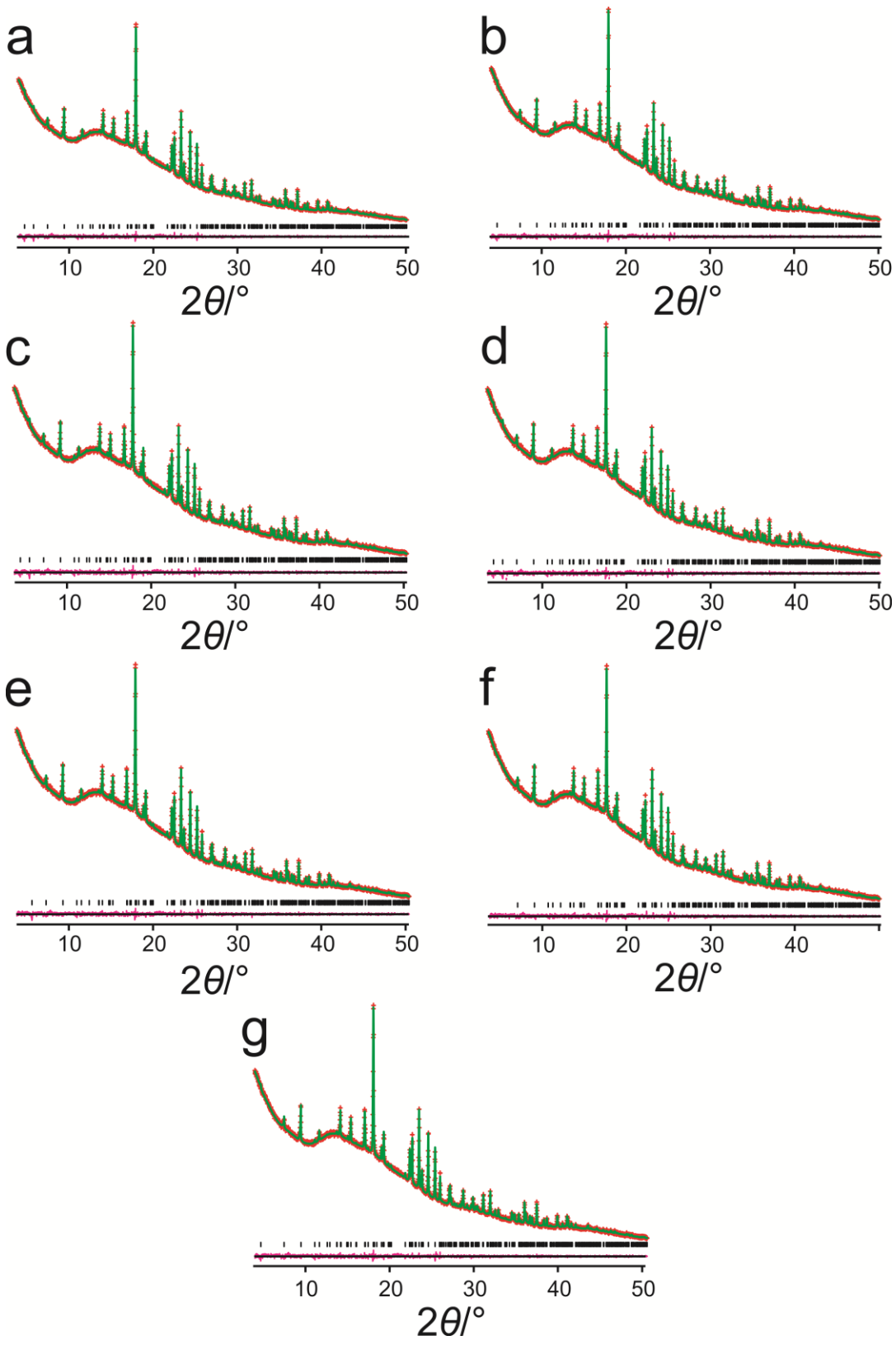

Figure 6.3. *Le Bail profile fitting for space groups (a) P2, (b) $P2_1$, (c) Pm, (d) P2/m, (e) P2/n, (f) $P2_1/m$ and (g) $P2_1/n$.*

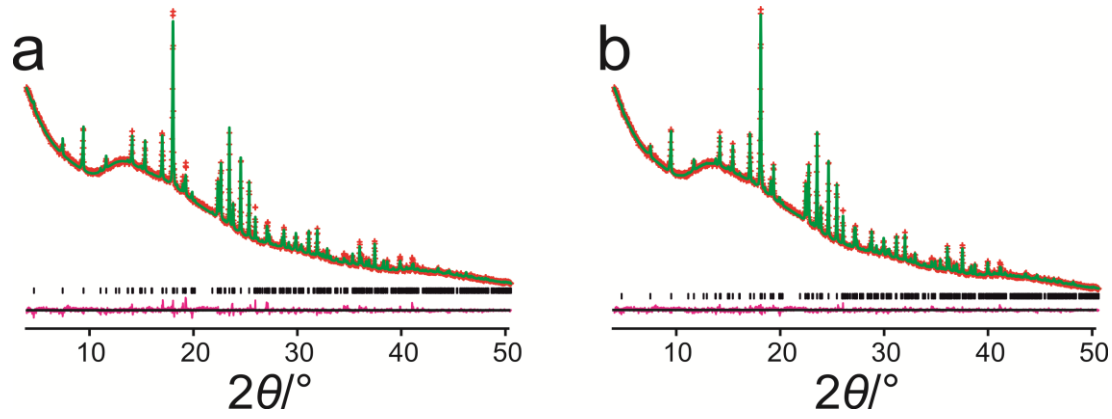

Figure 6.4. *Rietveld refinements for the models with (a) two ordered solvent molecules and (b) one ordered and one disordered solvent molecule.*

With the help of difference Fourier maps, we noticed that there were significant discrepancies in electron density associated with one of the TCE molecule, suggesting that this molecule may be disordered. To confirm this suggestion, we performed a CP/MAS ^{13}C SSNMR experiment with dipolar dephasing to investigate the possible motion of the TCE molecules. The solid-state ^{13}C NMR spectra are shown in Figure 6.5. In the solid-state ^{13}C NMR spectrum recorded without a dephasing delay (Figure 6.5a), we can see two isotropic peaks at 75.14 ppm and 73.53 ppm assigned to the carbon atoms of TCE. Thus, there are two different types of TCE molecules in the solid state. Then we performed the solid-state ^{13}C NMR experiment with a dephasing delay of 50.0 μs. The peak at 75.14 ppm is missing from the resulting spectrum (Figure 6.5b), with just one peak at 73.62 ppm. Comparing these two spectra, we conclude that the peak at 75.14 ppm corresponds to a static TCE molecule and the peak at 73.53 ppm (present in the spectrum recorded without a dephasing delay) or 73.62 ppm (present in the spectrum recorded with a dephasing delay of 50.0 μs) corresponds to a mobile TCE molecule. These results indicate that one TCE molecule in the asymmetric unit is mobile, representing dynamic disorder. From these solid-state ^{13}C NMR spectra, we can conclude that there are two TCE molecules in the asymmetric unit and one molecule is dynamic and the other molecule is static.

Therefore, the initial input models as discussed above for structure solution are not optimal, and modifications to the input model are required to enable one of TCE molecules to be disordered. Thus, we set up a new input model with space group $P2_1$ for structure solution calculations. In this input models, one TCE molecule is now represented by two components each with occupancy of a half.

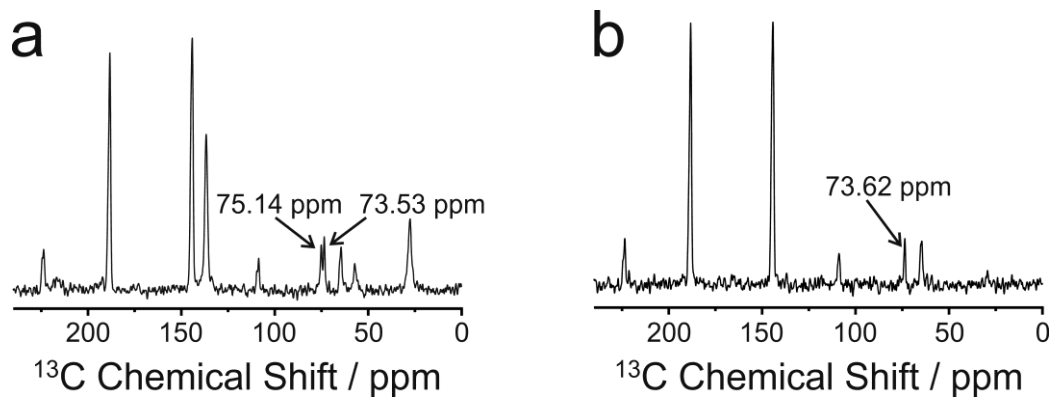

Figure 6.5. *Solid-state ^{13}C NMR spectrum of P[5]Q·TCE$_2$ (a) without dephasing delay and (b) with a dephasing delay of 50.0 μs.*

Other conditions were kept the same as discussed above. The structure solution calculations in the program EAGER were carried out again.

The results from structure solution indicated that the best structure solution with the lowest R_{wp} was structurally reasonable. In this model, the two half P[5]Q molecules formed into one complete P[5]Q. We performed Rietveld refinement for the new structure solution with the lowest R_{wp}, and the occupancies for the two TCE molecules with partial occupancies were allowed to refine, subject to the total occupancy being equal to 1. This time the refinement led to a good fit with the experimental powder XRD data (R_{wp} = 1.29%, Figure 6.4b). The final Rietveld refinement gave the following data: $P2_1$; a = 18.7699(5) Å, b = 15.2490(5) Å, c = 6.9056(2) Å, β = 89.7436(19)°, V = 1976.52(15) Å^3, R_{wp} = 1.29%, R_p = 0.99%; the two TCE are disordered over two sites with occupancies 0.577(18):0.423(18).

6.4 Results and Discussion

From the structure of P[5]Q·TCE$_2$ (Figure 6.6b, viewed along the c-axis) we can see that, due to the packing arrangement of P[5]Q molecules, there are two types of channel along the c-axis: pentagonal channels formed by the internal cavities of each P[5]Q molecule (denoted by channel I) and channels formed by the region of space between groups of four adjacent P[5]Q molecules (denoted by channel II). The ordered TCE molecules occupy channel II and the disordered TCE molecules occupy channel I. From Figure 6.6a (view along the b-axis), we can see that, in channel I, the disordered TCE molecules occupy the space between two adjacent P[5]Q molecules, instead of the internal cavities of the P[5]Q molecules. This is because the volume of one TCE

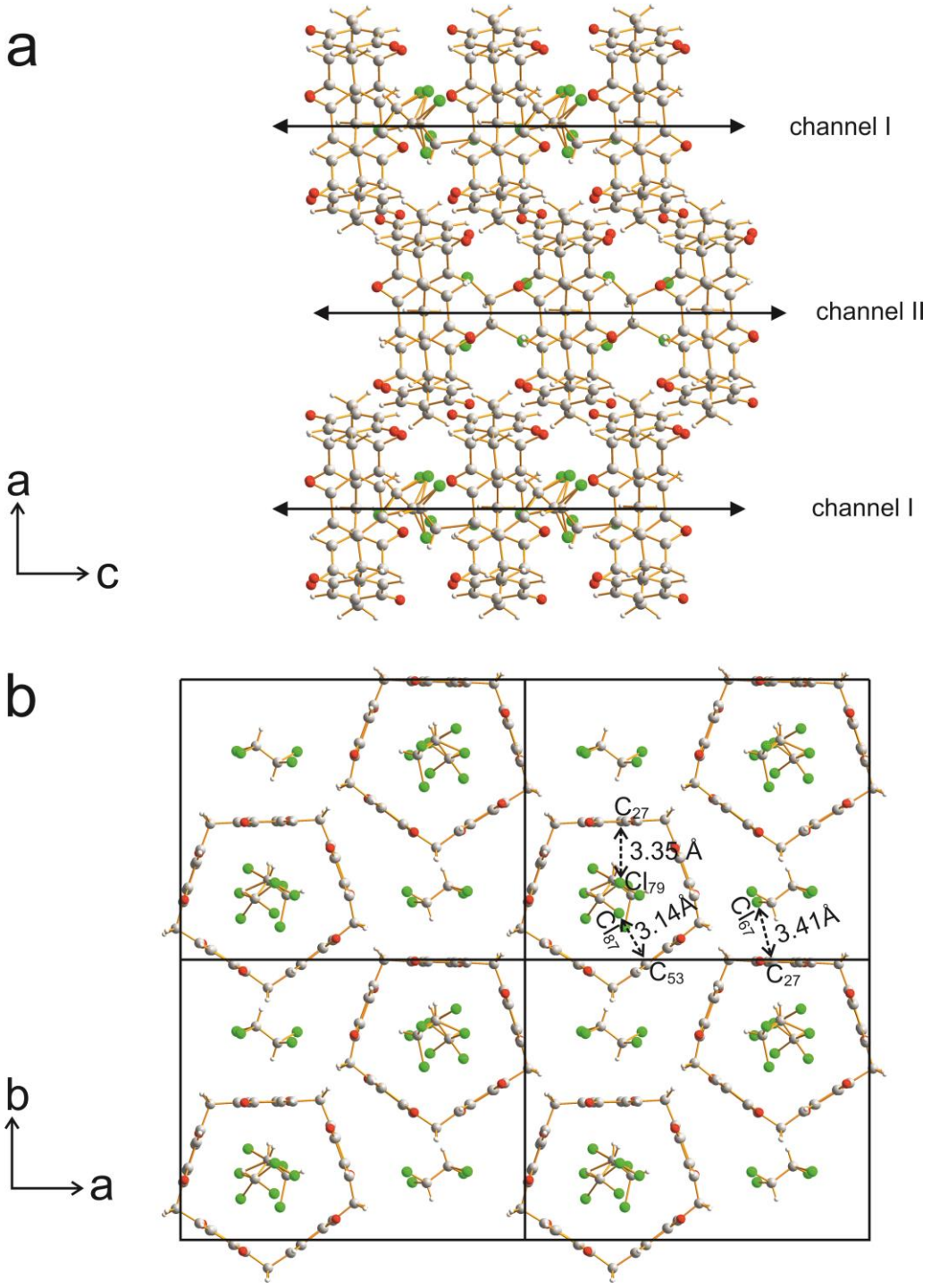

Figure 6.6. *(a) Two types of channels (channel I and channel II) in the crystal structure of P[5]Q·TCE₂, and (b) the complete crystal structure of P[5]Q·TCE₂.*

molecule is larger than the volume of the cavity inside the P[5]Q molecule. The ordered TCE molecules filled the void formed by groups of four P[5]Q molecules.

Investigating the crystal structure in more detail, we note that each P[5]Q molecule is not based on a perfect pentagonal ring, as the five angles (the angle refers to the dihedral angle between two adjacent 1,4-benzoquinone moieties) and the lengths of

the five sides (the length refers to the distance between two adjacent methylene groups) in the pentagon are not the same. Specifically, the five angles are 113.6°, 108.6°, 117.8°, 110.4° and 106.3°, and the lengths of the five sides are 5.96 Å, 5.88 Å, 5.93 Å, 6.00 Å and 5.99 Å.

In addition, due to the lack of hydrogen bond donors, there is no hydrogen bonding between P[5]Q molecules and TCE molecules. However, as mentioned above, from computational studies, researchers have inferred that P[5]Q can interact with anions (e.g. Cl^-) in the interior cavity through anion-π interactions. From the crystal structure of the cocrystal of P[5]Q with TCE, we can see that, in channel I, due to the volume of TCE being larger than the internal cavity of P[5]Q, the whole TCE molecule cannot be located within the cavity of P[5]Q (Figure 6.7a). However, one Cl atom of each disordered TCE molecule does penetrate within the internal cavity of P[5]Q (Figure 6.7b).

As shown in Figure 6.6b, the shortest distances between the two "included" Cl atoms (Cl_{79} and Cl_{87}) and the C atoms (C_{27} and C_{53}) of adjacent 1,4-benzoquinone are 3.14 Å ($Cl_{87}\cdots C_{53}$) and 3.35 Å ($Cl_{79}\cdots C_{27}$), respectively. The shortest distances from these two "included" Cl atoms to the plane of the adjacent 1,4-benzoquinone moiety are 3.35 Å and 3.10 Å. According to the criterion of anion-π interactions[285] (the distance from anion to carbon atom distances is less than or equal to the sum of van der Waals radii plus 0.8 Å), the sum of van der Waals radii of C and Cl is 3.45 Å, so the distance between the "included" Cl atoms and the C atom of P[5]Q (3.14 Å and 3.35 Å) should be less than 4.25 Å. Thus, the two Cl atoms of the disordered TCE molecules in channel I can be considered to be bound to the P[5]Q molecules through anion-π type interactions. In channel II, the shortest distance between the Cl (Cl_{67}) atom of the ordered TCE molecule and the C (C_{27}) atom of the adjacent 1,4,-benzoquinone moiety is 3.41 Å and the distance of Cl_{67} to the plane of this 1,4-benzoquione moiety is 3.21 Å. Therefore, there is also an anion-π type interaction between them.

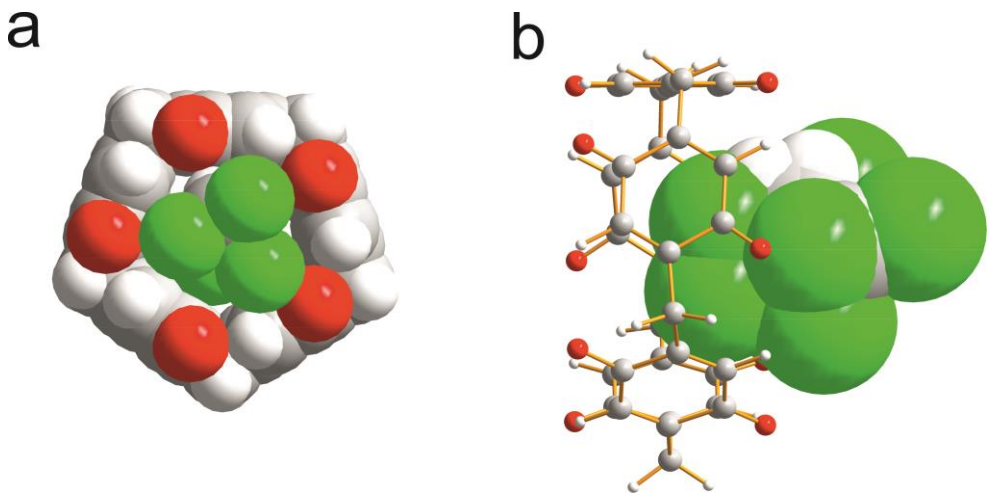

Figure 6.7. *(a) Space-filling structure of one TCE molecule in front of a P[5]Q molecule. (b) One Cl atom of each dynamically disordered TCE molecule penetrates the internal cavity of a P[5]Q molecule.*

Since two TCE molecules in the asymmetric unit are disordered over two sites at room temperature, we expected that, at lower temperatures, the disordered molecules might become ordered. Therefore, we investigated the thermal properties of this sample by using DSC and variable-temperature powder XRD. However, even when we cooled the sample slowly from room temperature down to –160 °C (113 K) with different cooling rates (cooling rates between 1 and 20 °C min^{-1}) by DSC, no phase transition was observed. Likewise, the powder XRD patterns (synchrotron data) recorded at 295 K, 250 K, 200 K, 150 K, 100 K and 90 K showed no evidence for a phase transition.

6.5 Summary

In conclusion, we have determined the crystal structure of P[5]Q·TCE_2 directly from powder XRD data. In the asymmetric unit, there is one P[5]Q molecule, one ordered TCE molecule and one disordered TCE molecule (disordered over two sites with occupancies 0.577(18):0.423(18). The final refined parameters are as follows: $P2_1$; a = 18.7699 (5) Å, b = 15.2490 (5) Å, c = 6.9056 (2) Å, β = 89.7436 (19)°; V = 1976.52 (15) $Å^3$, R_{wp} = 1.29%, R_p = 0.99%. One Cl atom of each TCE molecule may be considered to be bound to an adjacent P[5]Q molecule through an anion-π type interaction.

Chapter 7 Conclusions and Future Work

7.1 Conclusions

Due to the importance of organic co-crystals in the pharmaceutical industry, in this thesis we focused on the preparation and investigations of two types of co-crystal system. One system comprises organic co-crystals of TMA and TBA, which exhibits astonishing structural diversity based on the stoichiometric ratios between TMA and TBA, particularly with regard to the phenomenon of polymorphism. The other system comprises co-crystals of TMA and L-arginine.

In the course of study of co-crystals of TMA and TBA, we discovered that they form a series of co-crystals with different molar ratios, by using a series of solvents combined with different crystallization methods and different ratios of TMA and TBA in the crystallization solution. The structural diversity observed for the co-crystals in this system is quite uncommon. In chapter 3, we reported two novel polymorphic co-crystal systems of TMA and TBA. One is a solvated polymorphic system (with 2:5:3 ratio of TMA, TBA and methanol), which is particularly novel in having a large number of independent components in the asymmetric unit in each of the polymorphs. The other is a polymorphic co-crystal system with a 2:3 ratio of TMA and TBA. In the case of co-crystals of $TMA_2TBA_5 \cdot (MeOH)_3$, the crystal structures of the two polymorphs both have quite similar parallel 2D sheets but the hydrogen-bonding pattern within these sheets shows subtle (but significant) differences. In the case of co-crystals of TMA_2TBA_3, despite the TMA molecules being partially deprotonated, both polymorphs still retain hexagonal networks and, due to the presence of TBA molecules, the hexagonal networks within both polymorphs are non-interpenetrated. However, the network in form I is planar while the network in form II is corrugated.

In addition to the phenomenon of polymorphism of co-crystals of TMA and TBA, the structural diversity of other co-crystals of TMA and TBA is discussed in chapter 4. In this chapter, all co-crystals of TMA and TBA are classified into four families based on the stoichiometric ratio between TMA and TBA, and the structural features of each family are investigated from the viewpoint of hydrogen bonding. Adjusting the stoichiometric ratio between TMA and TBA and the types of solvent used gives rise to a broad range of totally different crystal structures, such as a structure comprising double-

layered sheets ($TMA_2TBA_1 \cdot (H_2O)_2$), single hydrogen-bonded flat sheets ($TMA_1TBA_2 \cdot (iso\text{-Butanol})_1$), single hydrogen-bonded corrugated sheets ($TMA_1TBA_2 \cdot (MeOH)_1$), a structure with interpenetration ($TMA_2TBA_1 \cdot (H_2O)_3$) and a structure comprising brick-wall networks ($TMA_2TBA_2 \cdot (MeOH)_1$). That is to say, the hydrogen-bonding motifs formed in these co-crystals are quite sensitive to the stoichiometric ratios between TMA, TBA and the crystallization solvents used in each co-crystal.

In the course of studying co-crystals of TMA and L-arginine, we attempted to prepare single crystals of TMA and L-arginine by different co-crystallization methods. However, no large single crystals were prepared successfully. Instead, four types of microcrystalline co-crystals materials containing TMA and L-arginine were discovered. Since determining crystal structures directly from powder X-ray diffraction data has become an increasingly important technique for characterization of co-crystals, in chapters 5 and 6 we demonstrate the processes of structure determination of co-crystals of TMA and L-arginine (chapter 5) and the co-crystal of pillar[5]quinone and 1,1,2,2-tetrachloroethane (chapter 6) from powder X-ray diffraction data. The process of structure determination from powder X-ray diffraction data is presented in these two chapters, demonstrating that powder X-ray diffraction analysis is a reliable alternative for structural analysis when single-crystal X-ray diffraction cannot be used.

7.2 Future Work

In the course of studying the co-crystals of TMA and L-arginine, we discovered four different phases and the structures of only two phases were determined from powder X-ray diffraction data. In the future, we could focus on the other two phases. In addition, in order to obtain good quality powder X-ray diffraction data for structure determination, which cannot obtained easily from solution crystallization or to obtain new phases of co-crystals of TMA and L-arginine, we could use solid-state grinding methods to prepare co-crystals of TMA and L-arginine.

In the course of studying polymorphic co-crystals of $TMA_2TBA_5 \cdot (MeOH)_3$, we discovered that, under an ambient atmosphere, both polymorphs were highly susceptible to loss of methanol, resulting in the same crystalline phase in each case. In the future, we could try to determine the structure of this new desolvated phase from powder X-ray diffraction data.

References

[1] G. R. Desiraju, *CrystEngComm*, **5**, 466-467 (2003)

[2] J. D. Dunitz, *CrystEngComm*, **5**, 506-506 (2003)

[3] C. B. Aakeroy and D. J. Salmon, *CrystEngComm*, **7**, 439-448 (2005)

[4] M. J. Zaworotko, *Cryst. Growth Des.*, **7**, 4-9 (2007)

[5] N. Shan and M. J. Zaworotko, *Drug Discov. Today*, **13**, 440-446 (2008)

[6] J. Lu, Y.-P. Li, J. Wang, Z. Li, S. Rohani and C.-B. Ching, *J. Cryst. Growth*, **335**, 110-114 (2011)

[7] H. G. Brittain, *Cryst. Growth Des.*, **12**, 1046-1054 (2011)

[8] A. D. Bond, *CrystEngComm*, **9**, 833-834 (2007)

[9] L. Kux, *Federal Register*, 75551-75552 (2011)

[10] S. Aitipamula, R. Banerjee, A. K. Bansal, K. Biradha, M. L. Cheney, A. R. Choudhury, G. R. Desiraju, A. G. Dikundwar, R. Dubey, N. Duggirala, P. P. Ghogale, S. Ghosh, P. K. Goswami, N. R. Goud, R. K. R. Jetti, P. Karpinski, P. Kaushik, D. Kumar, V. Kumar, B. Moulton, A. Mukherjee, G. Mukherjee, A. S. Myerson, V. Puri, A. Ramanan, T. Rajamannar, C. M. Reddy, N. Rodriguez-Hornedo, R. D. Rogers, T. N. G. Row, P. Sanphui, N. Shan, G. Shete, A. Singh, C. C. Sun, J. A. Swift, R. Thaimattam, T. S. Thakur, R. K. Thaper, S. P. Thomas, S. Tothadi, V. R. Vangala, P. Vishweshwar, D. R. Weyna and M. J. Zaworotko, *Cryst. Growth Des.*, **12**, 4290-4291 (2012)

[11] Guidance for Industry: Regulatory Classification of Pharmaceutical Co-Crystals, U.S. Department of Health and Human Services - Food and Drug Administration, Silver Spring, MD, 2013.

[12] B. R. Bhogala, S. Basavoju and A. Nangia, *CrystEngComm*, **7**, 551-562 (2005)

[13] D. A. Haynes, W. Jones and W. D. S. Motherwell, *CrystEngComm*, **8**, 830-840 (2006)

[14] S. L. Childs, G. P. Stahly and A. Park, *Mol. Pharm.*, **4**, 323-338 (2007)

[15] M. K. Stanton and A. Bak, *Cryst. Growth Des.*, **8**, 3856-3862 (2008)

[16] S. Mohamed, D. A. Tocher, M. Vickers, P. G. Karamertzanis and S. L. Price, *Cryst. Growth Des.*, **9**, 2881-2889 (2009)

[17] C. B. Aakeroy, M. E. Fasulo and J. Desper, *Mol. Pharm.*, **4**, 317-322 (2007)

[18] J. Kastelic, Z. Hodnik, P. Sket, J. Plavec, N. Lah, I. Leban, M. Pajk, O. Planinsek and D. Kikelj, *Cryst. Growth Des.*, **10**, 4943-4953 (2010)

[19] G. P. Stahly, *Cryst. Growth Des.*, **9**, 4212-4229 (2009)

[20] A. Gavezzotti, *Curr. Opin. Solid State Mater. Sci.*, **1**, 501-505 (1996)

[21] H. Thakuria, B. M. Borah, A. Pramanik and G. Das, *J. Chem. Cryst.*, **37**, 807-816 (2007)

[22] H. G. Brittain, *Cryst. Growth Des.*, **12**, 5823-5832 (2012)

[23] J. Geng, T. Tao, S.-J. Fu, W. You and W. Huang, *Dyes and Pigments*, **90**, 65-70 (2011)

[24] D.-K. Bucar, S. Filip, M. Arhangelskis, G. O. Lloyd and W. Jones, *CrystEngComm*, **15**, 6289-6291 (2013)

[25] F. Pan, M. S. Wong, V. Gramlich, C. Bosshard and P. Gunter, *J. Am. Chem. Soc.*, **118**, 6315-6316 (1996)

[26] K. S. Huang, D. Britton, M. C. Etter and S. R. Byrn, *J. Mater. Chem.*, **7**, 713-720 (1997)

[27] C. A. Ellis, E. R. T. Tiekink and J. Zukerman-Schpector, *J. Chem. Cryst.*, **38**, 513-517 (2008)

[28] S.-J. Kwon, O. P. Kwon, M. Jazbinsek, V. Gramlich and P. Guenter, *Chem. Comm.*, 3729-3731 (2006)

[29] V. Krishnakumar, M. Rajaboopathi and R. Nagalakshmi, *Physica B*, **407**, 1119-1123 (2012)

[30] H. M. Ratajczak, I. Bryndal, I. Ledoux-Rak and A. J. Barnes, *J. Mol. Struct.*, **1047**, 310-316 (2013)

[31] K. Hoogsteen, *Acta Cryst.*, **16**, 907-916 (1963)

[32] S. Shavitt and R. H. Fazio, *Pers. Soc. Psychol. B*, **17**, 507-516 (1991)

[33] A. K. H. Hirsch, M. S. Alphey, S. Lauw, M. Seet, L. Barandun, W. Eisenreich, F. Rohdich, W. N. Hunter, A. Bacherc and F. Diederich, *Org. Biomol. Chem.*, **6**, 2719-2730 (2008)

[34] D. M. Bender, J. Q. Bao, A. H. Dantzig, W. D. Diseroad, K. L. Law, N. A. Magnus, J. A. Peterson, E. J. Perkins, Y. W. J. Pu, S. M. Reutzel-Edens, D. M. Remick, J. J. Starling, G. A. Stephenson, R. K. Vaid, D. Y. Zhang and J. R. McCarthy, *J. Med. Chem.*, **52**, 6958-6961 (2009)

[35] A. Bak, A. Gore, E. Yanez, M. Stanton, S. Tufekcic, R. Syed, A. Akrami, M. Rose, S. Surapaneni, T. Bostick, A. King, S. Neervannan, D. Ostovic and A. Koparkar, *J. Pharm. Sci.*, **97**, 3942-3956 (2008)

[36] K. Shiraki, N. Takata, R. Takano, Y. Hayashi and K. Terada, *Pharm. Res.*, **25**, 2581-2592 (2008)

[37] G. Bruni, M. Maietta, L. Maggi, P. Mustarelli, C. Ferrara, V. Berbenni, C. Milanese, A. Girella and A. Marini, *J. Pharm. Sci.*, **102**, 4079-4086 (2013)

[38] N. Schultheiss and A. Newman, *Cryst. Growth Des.*, **9**, 2950-2967 (2009)

[39] A. V. Trask, W. D. S. Motherwell and W. Jones, *Cryst. Growth Des.*, **5**, 1013-1021 (2005)

[40] S. Jung, J. Lee and I. W. Kim, *J. Cryst. Growth*, **373**, 59-63 (2013)

[41] R. Thakuria, A. Delori, W. Jones, M. P. Lipert, L. Roy and N. Rodriguez-Hornedo, *Int. J. Pharm.*, **453**, 101-125 (2013)

[42] M. B. Hickey, M. L. Peterson, L. A. Scoppettuolo, S. L. Morrisette, A. Vetter, H. Guzmán, J. F. Remenar, Z. Zhang, M. D. Tawa, S. Haley, M. J. Zaworotko and Ö. Almarsson, *Eur. J. Pharm. Biopharm.*, **67**, 112-119 (2007)

[43] P. Vishweshwar, J. A. McMahon, J. A. Bis and M. J. Zaworotko, *J. Pharm. Sci.*, **95**, 499-516 (2006)

[44] N. Blagden, M. de Matas, P. T. Gavan and P. York, *Adv. Drug. Deliver. Rev.*, **59**, 617-630 (2007)

[45] S. Mirza, J. Heinamaki, I. Miroshnyk and J. Yliruusi, *Eur. J. Pharm. Sci.*, **34**, S16-S17 (2008)

[46] T. Friščič and W. Jones, *J. Pharm. Pharmacol.*, **62**, 1547-1559 (2010)

[47] N. Qiao, M. Li, W. Schlindwein, N. Malek, A. Davies and G. Trappitt, *Int. J. Pharm.*, **419**, 1-11 (2011)

[48] D. P. Elder, R. Holm and H. L. de Diego, *Int. J. Pharm.*, **453**, 88-100 (2013)

[49] H. G. Brittain, *J. Pharm. Sci.*, **102**, 311-317 (2013)

[50] A. Delori, T. Friščič and W. Jones, *CrystEngComm*, **14**, 2350-2362 (2012)

[51] E. Arunan, G. R. Desiraju, R. A. Klein, J. Sadlej, S. Scheiner, I. Alkorta, D. C. Clary, R. H. Crabtree, J. J. Dannenberg, P. Hobza, H. G. Kjaergaard, A. C. Legon, B. Mennucci and D. J. Nesbitt, *Pure Appl. Chem.*, **83**, 1637-1641 (2011)

[52] T. Steiner, *Angew. Chem. Int. Ed.*, **41**, 48-76 (2002)

[53] G. R. Desiraju, *Acc. Chem. Res.*, **24**, 290-296 (1991)

[54] H. Adams, K. D. M. Harris, G. A. Hembury, C. A. Hunter, D. Livingstone and J. F. McCabe, *Chem. Comm.*, 2531-2532 (1996)

[55] M. C. Etter, J. C. Macdonald and J. Bernstein, *Acta Cryst. B*, **46**, 256-262 (1990)

[56] M. C. Etter, *Acc. Chem. Res.*, **23**, 120-126 (1990)

[57] T. Sugiyama, J. B. Meng and T. Matsuura, *J. Mol. Struct.*, **611**, 53-64 (2002)

[58] R. D. B. Walsh, M. W. Bradner, S. Fleischman, L. A. Morales, B. Moulton, N. Rodriguez-Hornedo and M. J. Zaworotko, *Chem. Comm.*, 186-187 (2003)

[59] C. B. Aakeroy, A. M. Beatty and B. A. Helfrich, *J. Am. Chem. Soc.*, **124**, 14425-14432 (2002)

[60] S. Jin, W. Zhang, L. Liu, D. Wang, H. He, T. Shi and F. Lin, *J. Mol. Struct.*, **991**, 1-11 (2011)

[61] S. Jin, L. Liu, D. Wang and J. Guo, *J. Mol. Struct.*, **1005**, 59-69 (2011)

[62] P. Vishweshwar, A. Nangia and V. M. Lynch, *Cryst. Growth Des.*, **3**, 783-790 (2003)

[63] H. Y. Ando, L. Dehaspe, W. Luyten, E. Van Craenenbroeck, H. Vandecasteele and L. Van Meervelt, *Mol. Pharm.*, **3**, 665-674 (2006)

[64] P. T. A. Galek, L. Fabian, W. D. S. Motherwell, F. H. Allen and N. Feeder, *Acta Cryst. B*, **63**, 768-782 (2007)

[65] A. Delori, P. T. A. Galek, E. Pidcock, M. Patni and W. Jones, *CrystEngComm*, **15**, 2916-2928 (2013)

[66] G. M. Day, T. G. Cooper, A. J. Cruz-Cabeza, K. E. Hejczyk, H. L. Ammon, S. X. M. Boerrigter, J. S. Tan, R. G. Della Valle, E. Venuti, J. Jose, S. R. Gadre, G. R. Desiraju, T. S. Thakur, B. P. van Eijck, J. C. Facelli, V. E. Bazterra, M. B. Ferraro, D. W. M. Hofmann, M. A. Neumann, F. J. J. Leusen, J. Kendrick, S. L. Price, A. J. Misquitta, P. G. Karamertzanis, G. W. A. Welch, H. A. Scheraga, Y. A. Arnautova, M. U. Schmidt, J. van de Streek, A. K. Wolf and B. Schweizer, *Acta Cryst. B*, **65**, 107-125 (2009)

[67] T. S. Thakur and G. R. Desiraju, *Cryst. Growth Des.*, **8**, 4031-4044 (2008)

[68] A. J. Cruz-Cabeza, G. M. Day and W. Jones, *Chem. Eur. J.*, **14**, 8830-8836 (2008)

[69] D. W. M. Hofmann and T. Lengauer, *J. Mol. Struct.*, **474**, 13-23 (1999)

[70] J. Kendrick, F. J. J. Leusen, M. A. Neumann and J. van de Streek, *Chem. Eur. J.*, **17**, 10736-10744 (2011)

[71] K. B. Landenberger and A. J. Matzger, *Cryst. Growth Des.*, **10**, 5341-5347 (2010)

[72] C. A. Hunter and J. K. M. Sanders, *J. Am. Chem. Soc.*, **112**, 5525-5534 (1990)

[73] M. L. Waters, *Curr. Opin. Chem. Biol.*, **6**, 736-741 (2002)

[74] C. A. Hunter, K. R. Lawson, J. Perkins and C. J. Urch, *J. Chem. Soc., Perkin Trans. 2*, 651-669 (2001)

[75] A. K. Tewari and R. Dubey, *Bioorg. Med. Chem.*, **16**, 126-143 (2008)

[76] B. Sarma, L. S. Reddy and A. Nangia, *Cryst. Growth Des.*, **8**, 4546-4552 (2008)

[77] C. R. P. G. S. Prosser, *Nature*, **187**, 1021-1021 (1960)

[78] A. P. West, S. Mecozzi and D. A. Dougherty, *J. Phys. Org. Chem.*, **10**, 347-350 (1997)

[79] J. H. Williams, *Acc. Chem. Res.*, **26**, 593-598 (1993)

[80] M. Baldrighi, G. Cavallo, M. R. Chierotti, R. Gobetto, P. Metrangolo, T. Pilati, G. Resnati and G. Terraneo, *Mol. Pharm.*, **10**, 1760-1772 (2013)

[81] D. Cincic, T. Friscic and W. Jones, *Chem. Eur. J.*, **14**, 747-753 (2008)

[82] S. Tothadi and G. R. Desiraju, *Chem. Comm.*, **49**, 7791-7793 (2013)

[83] F. Wöhler and V. Liebig, *J. Ann. Pharm.*, **3**, 249-282 (1832)

[84] J. M. Robertson and A. R. Ubbelohde, *Proc. Roy. Soc. London A*, **167**, 0122-0135 (1938)

[85] J. B. Nanubolu, B. Sridhar, V. S. P. Babu, B. Jagadeesh and K. Ravikumar, *CrystEngComm*, **14**, 4677-4685 (2012)

[86] A. R. Sheth, S. Bates, F. X. Muller and D. J. W. Grant, *Cryst. Growth Des.*, **4**, 1091-1098 (2004)

[87] P. Sanphui, N. R. Goud, U. B. R. Khandavilli, S. Bhanoth and A. Nangia, *Chem. Comm.*, **47**, 5013-5015 (2011)

[88] J. Y. Khoo, U. V. Shah, M. Schaepertoens, D. R. Williams and J. Y. Y. Heng, *Powder Technol.*, **236**, 114-121 (2013)

[89] J. Lu, X.-J. Wang, X. Yang and C.-B. Ching, *Cryst. Growth Des.*, **7**, 1590-1598 (2007)

[90] T. Gelbrich, D. E. Braun, A. Ellern and U. J. Griesser, *Cryst. Growth Des.*, **13**, 1206-1217 (2013)

[91] K. M. Lutker, R. Quinones, J. Xu, A. Ramamoorthy and A. J. Matzger, *J. Pharm. Sci.*, **100**, 949-963 (2010)

[92] P. J. Wheatley, *J. Chem. Soc.*, **S**, 6036-6048 (1964)

[93] P. Vishweshwar, J. A. McMahon, M. Oliveira, M. L. Peterson and M. J. Zaworotko, *J. Am. Chem. Soc.*, **127**, 16802-16803 (2005)

[94] M. R. Hauser, L. Zhakarov, K. M. Doxsee and T. Li, *Cryst. Growth Des.*, **8**, 4428-4431 (2008)

[95] S. Long, S. Parkin, M. Siegler, C. P. Brock, A. Cammers and T. Li, *Cryst. Growth Des.*, **8**, 3137-3140 (2008)

[96] I. Barsky and J. Bernstein, *CrystEngComm*, **10**, 669-674 (2008)

[97] B. D. Sharma, *J. Chem. Educ.*, **64**, 404-407 (1987)

[98] A. Gavezzotti, *J. Pharm. Sci.*, **96**, 2232-2241 (2007)

[99] Guideline on Test Procedures and Acceptance Criteria for New Veterianary Drug Substances and New Medicinal Products: Chemical Substances, European Medicines Agency, London, 2005.

[100] B. R. Jali and J. B. Baruah, *Cryst. Growth Des.*, **12**, 3114-3122 (2012)

[101] K. R. Back, R. J. Davey, T. Grecu, C. A. Hunter and L. S. Taylor, *Cryst. Growth Des.*, **12**, 6110-6117 (2012)

[102] S. Long, S. Parkin, M. A. Siegler, A. Cammers and T. Li, *Cryst. Growth Des.*, **8**, 4006-4013 (2008)

[103] A. Nangia, *Acc. Chem. Res.*, **41**, 595-604 (2008)

[104] G. R. Desiraju, *Cryst. Growth Des.*, **8**, 3-5 (2008)

[105] M. Haisa, S. Kashino, R. Kawai and H. Maeda, *Acta Cryst. B*, **32**, 1283-1285 (1976)

[106] T. N. Drebushchak and E. V. Boldyreva, *Z. Kristallogr.*, **219**, 506-512 (2004)

[107] M.-A. Perrin, M. A. Neumann, H. Elmaleh and L. Zaske, *Chem. Comm.*, 3181-3183 (2009)

[108] J. C. Burley, M. J. Duer, R. S. Stein and R. M. Vrcelj, *Eur. J. Pharm. Sci.*, **31**, 271-276 (2007)

[109] S. Gaisford, A. B. M. Buanz and N. Jethwa, *J. Pharm. Biomed. Anal.*, **53**, 366-370 (2010)

[110] M. Kitamura, *J. Cryst. Growth*, **237**, 2205-2214 (2002)

[111] A. Llinas and J. M. Goodman, *Drug Discov. Today*, **13**, 198-210 (2008)

[112] W. S. Wang, M. D. Aggarwal, J. Choi, T. Gebre, A. D. Shields, B. G. Penn and D. O. Frazier, *J. Cryst. Growth*, **198**, 578-582 (1999)

[113] R. C. Kelly and N. Rodriguez-Hornedo, *Org. Process Res. Dev.*, **13**, 1291-1300 (2009)

[114] M. Alleso, F. Van Den Berg, C. Cornett, F. S. Jorgensen, B. Halling-Sorensen, H. L. De Diego, L. Hovgaard, J. Aaltonen and J. Rantanen, *J. Pharm. Sci.*, **97**, 2145-2159 (2008)

[115] K. R. Prasad, A. Chandrakumar, A. G. Dikundwar and T. N. G. Row, *CrystEngComm*, **12**, 3452-3454 (2010)

[116] J. M. Rubin-Preminger and J. Bernstein, *Cryst. Growth Des.*, **5**, 1343- 1349 (2005)

[117] A. F. Fioritto, S. N. Bhattachar and J. A. Wesley, *Int. J. Pharm.*, **330**, 105- 113 (2007)

[118] D. Braga, G. Palladino, M. Polito, K. Rubini, F. Grepioni, M. R. Chierotti and R. Gobetto, *Chem. Eur. J.*, **14**, 10149-10159 (2008)

[119] I. Halasz, M. Rubčić, K. Užarević, I. Dilović and E. Meštrović, *New J. Chem.*, **35**, 24-27 (2011)

[120] S. Aitipamula, P. S. Chow and R. B. H. Tan, *CrystEngComm*, **11**, 1823-1827 (2009)

[121] S. Aitipamula, P. S. Chow and R. B. H. Tan, *CrystEngComm*, **11**, 889-895 (2009)

[122] S. Aitipamula, P. S. Chow and R. B. H. Tan, *Cryst. Growth Des.*, **10**, 2229-2238 (2010)

[123] S. Aitipamula, P. S. Chow and R. B. H. Tan, *CrystEngComm*, **12**, 3691-3697 (2010)

[124] W. W. Porter, III, S. C. Elie and A. J. Matzger, *Cryst. Growth Des.*, **8**, 14-16 (2008)

[125] J. H. ter Horst and P. W. Cains, *Cryst. Growth Des.*, **8**, 2537-2542 (2008)

[126] W. Limwikrant, A. Nagai, Y. Hagiwara, K. Higashi, K. Yamamoto and K. Moribe, *Int. J. Pharm.*, **431**, 237-240 (2012)

[127] S. Aitipamula, A. B. H. Wong, P. S. Chow and R. B. H. Tan, *CrystEngComm*, **14**, 8193-8198 (2012)

[128] M. D. Eddleston, S. Sivachelvam and W. Jones, *CrystEngComm*, **15**, 175-181 (2013)

[129] N. Schultheiss, M. Roe and S. X. M. Boerrigter, *CrystEngComm*, **13**, 611-619 (2011)

[130] A. V. Trask, W. D. S. Motherwell and W. Jones, *Chem. Comm.*, 890-891 (2004)

[131] A. Asmadi, J. Kendrick and F. J. J. Leusen, *Phys. Chem. Chem. Phys.*, **12**, 8571-8579 (2010)

[132] H. C. S. Chan, J. Kendrick and F. J. J. Leusen, *Phys. Chem. Chem. Phys.*, **13**, 20361-20370 (2011)

[133] M. D. Eddleston, K. E. Hejczyk, E. G. Bithell, G. M. Day and W. Jones, *Chem. Eur. J.*, **19**, 7874-7882 (2013)

[134] J. Kendrick, G. A. Stephenson, M. A. Neumann and F. J. J. Leusen, *Cryst. Growth Des.*, **13**, 581-589 (2013)

[135] A. Gavezzotti, *CrystEngComm*, 343-347 (2002)

[136] R. G. Della Valle, E. Venuti, A. Brillante and A. Girlando, *J. Phys. Chem. A*, **112**, 6715-6722 (2008)

[137] R. A. Chiarella, R. J. Davey and M. L. Peterson, *Cryst. Growth Des.*, **7**, 1223-1226 (2007)

[138] S. G. Fleischman, S. S. Kuduva, J. A. McMahon, B. Moulton, R. D. B. Walsh, N. Rodriguez-Hornedo and M. J. Zaworotko, *Cryst. Growth Des.*, **3**, 909-919 (2003)

[139] T. Rager and R. Hilfiker, *Cryst. Growth Des.*, **10**, 3237-3241 (2010)

[140] A. Jayasankar, L. S. Reddy, S. J. Bethune and N. Rodríguez-Hornedo, *Cryst. Growth Des.*, **9**, 889-897 (2009)

[141] S. L. James, C. J. Adams, C. Bolm, D. Braga, P. Collier, T. Friščič, F. Grepioni, K. D. M. Harris, G. Hyett, W. Jones, A. Krebs, J. Mack, L. Maini, A. G. Orpen, I. P. Parkin, W. C. Shearouse, J. W. Steed and D. C. Waddell, *Chem. Soc. Rev.*, **41**, 413-447 (2012)

[142] S. Karki, T. Friščič, W. Jones and W. D. S. Motherwell, *Mol. Pharm.*, **4**, 347-354 (2007)

[143] A. O. Patil, D. Y. Curtin and I. C. Paul, *J. Am. Chem. Soc.*, **106**, 348-353 (1984)

[144] W. Somphon and K. J. Haller, *J. Cryst. Growth*, **362**, 252-258 (2013)

[145] A. Shevchenko, I. Miroshnyk, L.-O. Pietilä, J. Haarala, J. Salmia, K. Sinervo, S. Mirza, B. van Veen, E. Kolehmainen, Nonappa and J. Yliruusi, *Cryst. Growth Des.*, **13**, 4877-4884 (2013)

[146] J. Lu and S. Rohani, *Org. Process Res. Dev.*, **13**, 1269-1275 (2009)

[147] M. C. Etter, S. M. Reutzel and C. G. Choo, *J. Am. Chem. Soc.*, **115**, 4411-4412 (1993)

[148] M. C. Etter and D. A. Adsmond, *J. Chem. Soc. Chem. Comm.*, 589-591 (1990)

[149] A. V. Trask, J. van de Streek, W. D. S. Motherwell and W. Jones, *Cryst. Growth Des.*, **5**, 2233-2241 (2005)

[150] I.-C. Wang, M.-J. Lee, S.-J. Sim, W.-S. Kim, N.-H. Chun and G. J. Choi, *Int. J. Pharm.*, **450**, 311-322 (2013)

[151] M.-J. Lee, N.-H. Chun, I.-C. Wang, J. J. Liu, M.-Y. Jeong and G. J. Choi, *Cryst. Growth Des.*, **13**, 2067-2074 (2013)

[152] N. Rodríguez-Hornedo, S. J. Nehru, K. F. Seefeldt, Y. Pagan-Torres and C. J. Falkiewicz, *Mol. Pharm.*, **3**, 362-367 (2006)

[153] T. Friščič, S. L. Childs, S. A. A. Rizvi and W. Jones, *CrystEngComm*, **11**, 418-426 (2009)

[154] S. Aher, R. Dhumal, K. Mahadik, A. Paradkar and P. York, *Eur. J. Pharm. Sci.*, **41**, 597-602 (2010)

[155] L. Padrela, M. A. Rodrigues, S. P. Velaga, A. C. Fernandes, H. A. Matos and E. G. de Azevedo, *J. Supercrit. Fluids*, **53**, 156-164 (2010)

[156] L. Padrela, M. A. Rodrigues, S. R. Velaga, H. A. Matos and E. G. de Azevedo, *Eur. J. Pharm. Sci.*, **38**, 9-17 (2009)

[157] N. Takata, K. Shiraki, R. Takano, Y. Hayashi and K. Terada, *Cryst. Growth Des.*, **8**, 3032-3037 (2008)

[158] F. L. F. Soares and R. L. Carneiro, *Cryst. Growth Des.*, **13**, 1510-1517 (2013)

[159] E. Lu, N. Rodríguez-Hornedo and R. Suryanarayanan, *CrystEngComm*, **10**, 665-668 (2008)

[160] R. S. Dhumal, A. L. Kelly, P. York, P. D. Coates and A. Paradkar, *Pharm. Res.*, **27**, 2725-2733 (2010)

[161] D. J. Berry, C. C. Seaton, W. Clegg, R. W. Harrington, S. J. Coles, P. N. Horton, M. B. Hursthouse, R. Storey, W. Jones, T. Friščič and N. Blagden, *Cryst. Growth Des.*, **8**, 1697-1712 (2008)

[162] P. G. Vekilov, *Nanoscale*, **2**, 2346-2357 (2010)

[163] P. R. Unwin, *Farad. Discuss.*, **136**, 409-416 (2007)

[164] Y.-H. Luo and B.-W. Sun, *Cryst. Growth Des.*, **13**, 2098-2106 (2013)

[165] J. A. Bis, O. L. McLaughlin, P. Vishweshwar and M. J. Zaworotko, *Cryst. Growth Des.*, **6**, 2648-2650 (2006)

[166] C. B. Aakeröy, I. Hussain and J. Desper, *Cryst. Growth Des.*, **6**, 474-480 (2006)

[167] M. Wenger and J. Bernstein, *Mol. Pharm.*, **4**, 355-359 (2007)

[168] P. K. Thallapally, R. K. R. Jetti, A. K. Katz, H. L. Carrell, K. Singh, K. Lahiri, S. Kotha, R. Boese and G. R. Desiraju, *Angew. Chem. Int. Ed.*, **43**, 1149-1155 (2004)

[169] C. C. Seaton, A. Parkin, C. C. Wilson and N. Blagden, *Cryst. Growth Des.*, **9**, 47-56 (2009)

[170] T. Leyssens, G. Springuel, R. Montis, N. Candoni and S. Veesler, *Cryst. Growth Des.*, **12**, 1520-1530 (2012)

[171] S. Zhang and A. C. Rasmuson, *CrystEngComm*, **14**, 4644-4655 (2012)

[172] Z. Q. Yu, P. S. Chow and R. B. H. Tan, *Cryst. Growth Des.*, **10**, 2382-2387 (2010)

[173] D. M. Croker, R. J. Davey, A. C. Rasmuson and C. C. Seaton, *Cryst. Growth Des.*, **13**, 3754-3762 (2013)

[174] K. Fucke, S. A. Myz, T. P. Shakhtshneider, E. V. Boldyreva and U. J. Griesser, *New J. Chem.*, **36**, 1969-1977 (2012)

[175] S. J. Nehm, B. Rodríguez-Spong and N. Rodríguez-Hornedo, *Cryst. Growth Des.*, **6**, 592-600 (2006)

[176] A. Y. Sheikh, S. A. Rahim, R. B. Hammond and K. J. Roberts, *CrystEngComm*, **11**, 501-509 (2009)

[177] F. Wöhler, *Annalen Chem. Pharm.*, **51**, 145-163 (1844)

[178] A. Jayasankar, A. Somwangthanaroj, Z. J. Shao and N. Rodríguez-Hornedo, *Pharm. Res.*, **23**, 2381-2392 (2006)

[179] M. R. Caira, L. R. Nassimbeni and A. F. Wildervanck, *J. Chem. Soc., Perkin Trans. 2*, 2213-2216 (1995)

[180] T. Friščič and W. Jones, *Cryst. Growth Des.*, **9**, 1621-1637 (2009)

[181] R. P. Rastogi, P. S. Bassi and S. L. Chadha, *J. Phys. Chem.*, **67**, 2569-2573 (1963)

[182] R. P. Rastogi and N. B. Singh, *J. Phys. Chem.*, **72**, 4446-4449 (1968)

[183] R. P. Rastogi and N. B. Singh, *J. Phys. Chem.*, **70**, 3315-3324 (1966)

[184] N. Shan, F. Toda and W. Jones, *Chem. Comm.*, 2372-2373 (2002)

[185] T. Friščič and W. Jones, *Farad. Discuss.*, **136**, 167-178 (2007)

[186] S. A. Myz, T. P. Shakhtshneider, K. Fucke, A. P. Fedotov, E. V. Boldyreva, V. V. Boldyrev and N. I. Kuleshova, *Mendeleev Commun.*, **19**, 272-274 (2009)

[187] E. Y. Cheung, S. J. Kitchin, K. D. M. Harris, Y. Imai, N. Tajima and R. Kuroda, *J. Am. Chem. Soc.*, **125**, 14658-14659 (2003)

[188] B. M. Kariuki, P. Calcagno, K. D. M. Harris, D. Philp and R. L. Johnston, *Angew. Chem. Int. Ed.*, **38**, 831-835 (1999)

[189] Y. Yan, C. E. Hughes, B. M. Kariuki and K. D. M. Harris, *Cryst. Growth Des.*, **13**, 27-30 (2013)

[190] F. G. Vogt, J. S. Clawson, M. Strohmeier, A. J. Edwards, T. N. Pham and S. A. Watson, *Cryst. Growth Des.*, **9**, 921-937 (2009)

[191] K. D. M. Harris, M. Tremayne and B. M. Kariuki, *Angew. Chem. Int. Ed.*, **40**, 1626-1651 (2001)

[192] W. I. F. David, K. Shankland and N. Shankland, *Chem. Comm.*, 931-932 (1998)

[193] C. Hammond, The Basics of Crystallography and Diffraction, Oxford University Press, Oxford, 2009.

[194] A. L. Patterson, *Phys. Rev.*, **46**, 0372-0376 (1934)

[195] D. Albesa-Jové, B. M. Kariuki, S. J. Kitchin, L. Grice, E. Y. Cheung and K. D. M. Harris, *ChemPhysChem*, **5**, 414-418 (2004)

[196] G. Sheldrick, *Acta Cryst. A*, **64**, 112-122 (2008)

[197] L. Farrugia, *J. Appl. Cryst.*, **32**, 837-838 (1999)

[198] M. Tremayne, B. M. Kariuki and K. D. M. Harris, *Angew. Chem. Int. Ed.*, **36**, 770-772 (1997)

[199] K. D. M. Harris and M. Tremayne, *Chem. Mater.*, **8**, 2554-2570 (1996)

[200] K. D. M. Harris and E. Y. Cheung, *Chem. Soc. Rev.*, **33**, 526-538 (2004)

[201] K. D. M. Harris, R. L. Johnston and B. M. Kariuki, *Acta Cryst. A*, **54**, 632-645 (1998)

[202] P. E. Werner, L. Eriksson and M. Westdahl, *J. Appl. Cryst.*, **18**, 367-370 (1985)

[203] J. W. Visser, *J. Appl. Cryst.*, **2**, 89-95 (1969)

[204] A. Boultif and D. Louër, *J. Appl. Cryst.*, **24**, 987-993 (1991)

[205] R. A. Shirley, CRYSFIRE, Suite of Programs for Indexing Powder Diffraction Patterns, University of Surrey, 2002.

[206] B. M. Kariuki, S. A. Belmonte, M. I. McMahon, R. L. Johnston, K. D. M. Harris and R. J. Nelmes, *J. Synchrotron Radiat.*, **6**, 87-92 (1999)

[207] J. Laugier and B. Bochu, CHEKCELL: A Powder Indexing Suite, Software Performing Automatic Cell/Space Group Determination, Collaborative Computational Project Number 14 (CCP14), *Laboratoire des Materiaux et du Genie Physique de l'Ecole Superieure de Physique de Grenoble*, France, 2000

[208] A. Le Bail, H. Duroy and J. L. Fourquet, *Mat. Res. Bull.*, **23**, 447- 452 (1988)

[209] A. C. Larson and R. B. V. Dreele, *Los Alamos National Laboratory Report LAUR*, 86-748 (2004)

[210] B. H. Toby, *J. Appl. Cryst.*, **34**, 210-213 (2001)

[211] B. M. Kariuki, H. Serrano-González, R. L. Johnston and K. D. M. Harris, *Chem. Phys. Lett.*, **280**, 189-195 (1997)

[212] S. Habershon, E. Y. Cheung, K. D. M. Harris and R. L. Johnston, *Chem. Phys. Lett.*, **390**, 394-398 (2004)

[213] R. A. Young, The Rietveld Method, Oxford University Press, Oxford, 1993.

[214] E. Y. Cheung, K. D. M. Harris and B. M. Foxman, *Cryst. Growth Des.*, **3**, 705-710 (2003)

[215] D. Giron, *J. Therm. Anal. Cal.*, **68**, 335-357 (2002)

[216] D. C. Apperley, R. K. Harris and P. Hodgkinson, Solid-State NMR: Basic Principles and Practice, Momentum Press, New York, 2012.

[217] J. S. Clawson, F. G. Vogt, J. Brum, J. Sisko, D. B. Patience, W. Dai, S. Sharpe, A. D. Jones, T. N. Pham, M. N. Johnson and R. C. P. Copley, *Cryst. Growth Des.*, **8**, 4120-4131 (2008)

[218] G. M. J. Schmidt, *Pure Appl. Chem.*, **27**, 647-678 (1971)

[219] J. C. Macdonald and G. M. Whitesides, *Chem. Rev.*, **94**, 2383-2420 (1994)

[220] K. Biradha, *CrystEngComm*, **5**, 374-384 (2003)

[221] S. L. James, C. J. Adams, C. Bolm, D. Braga, P. Collier, T. Friscic, F. Grepioni, K. D. M. Harris, G. Hyett, W. Jones, A. Krebs, J. Mack, L. Maini, A. G. Orpen, I. P. Parkin, W. C. Shearouse, J. W. Steed and D. C. Waddell, *Chem. Soc. Rev.*, **41**, 413-447 (2012)

[222] T. Steiner, *Acta Cryst. B*, **57**, 103-106 (2001)

[223] A. Ballabh, D. R. Trivedi and P. Dastidar, *Cryst. Growth Des.*, **5**, 1545-1553 (2005)

[224] A. Ballabh, T. K. Adalder and P. Dastidar, *Cryst. Growth Des.*, **8**, 4144-4149 (2008)

[225] I. Goldberg and J. Bernstein, *Chem. Comm.*, 132-134 (2007)

[226] R. E. Melendez, C. V. K. Sharma, M. J. Zaworotko, C. Bauer and R. D. Rogers, *Angew. Chem. Int. Ed.*, **35**, 2213-2215 (1996)

[227] D. J. Duchamp and R. E. Marsh, *Acta Cryst. B*, **25**, 5-19 (1969)

[228] C. V. K. Sharma, C. B. Bauer, R. D. Rogers and M. J. Zaworotko, *Chem. Comm.*, 1559-1560 (1997)

[229] T. R. Shattock, P. Vishweshwar, Z. Q. Wang and M. J. Zaworotko, *Cryst. Growth Des.*, **5**, 2046-2049 (2005)

[230] F. A. A. Paz and J. Klinowski, *CrystEngComm*, **5**, 238-244 (2003)

[231] O. M. Yaghi, G. M. Li and H. L. Li, *Nature*, **378**, 703-706 (1995)

[232] O. M. Yaghi, H. L. Li and T. L. Groy, *J. Am. Chem. Soc.*, **118**, 9096-9101 (1996)

[233] D. P. Cheng, M. A. Khan and R. P. Houser, *Inorg. Chem.*, **40**, 6858-6859 (2001)

[234] J. W. Steed, *CrystEngComm*, **5**, 169-179 (2003)

[235] K. M. Anderson, M. R. Probert, A. E. Goeta and J. W. Steed, *CrystEngComm*, **13**, 83-87 (2011)

[236] K. M. Anderson, A. E. Goeta and J. W. Steed, *Cryst. Growth Des.*, **8**, 2517-2524 (2008)

[237] H. S. Shieh, L. G. Hoard and C. E. Nordman, *Acta Cryst. B*, **38**, 2411-2419 (1982)

[238] D. A. Parrish, J. R. Deschamps, R. D. Gilardi and R. J. Butcher, *Cryst. Growth Des.*, **8**, 57-62 (2008)

[239] A. S. Batsanov, J. C. Collings, R. M. Ward, A. E. Goeta, L. Porres, A. Beeby, J. A. K. Howard, J. W. Steed and T. B. Marder, *CrystEngComm*, **8**, 622-628 (2006)

[240] C. V. K. Sharma and M. J. Zaworotko, *Chem. Comm.*, 2655-2656 (1996)

[241] P. Vishweshwar, D. A. Beauchamp and M. J. Zaworotko, *Cryst. Growth Des.*, **6**, 2429-2431 (2006)

[242] F. H. Herbstein, M. Kapon and G. M. Reisner, *J. Incl. Phenom. Macro. Chem.*, **5**, 211-214 (1987)

[243] S. V. Kolotuchin, P. A. Thiessen, E. E. Fenlon, S. R. Wilson, C. J. Loweth and S. C. Zimmerman, *Chem. Eur. J.*, **5**, 2537-2547 (1999)

[244] O. Ermer and J. Neudorfl, *Helv. Chim. Acta*, **84**, 1268-1313 (2001)

[245] S. Bhattacharya and B. K. Saha, *Cryst. Growth Des.*, **11**, 2194-2204 (2011)

[246] D. J. Duchamp and R. E. Marsh, *Acta Cryst. B*, **B 25**, 5-19 (1969)

[247] S. H. Dale, M. R. J. Elsegood and S. J. Richards, *Chem. Comm.*, 1278-1279 (2004)

[248] R. Santra, N. Ghosh and K. Biradha, *New J. Chem.*, **32**, 1673-1676 (2008)

[249] D. J. Plaut, K. M. Lund and M. D. Ward, *Chem. Comm.*, 769-770 (2000)

[250] C. H. Gorbitz and H. P. Hersleth, *Acta Cryst. B*, **56**, 526-534 (2000)

[251] H. D. Clarke, K. K. Arora, H. Bass, P. Kavuru, T. T. Ong, T. Pujari, L. Wojtas and M. J. Zaworotko, *Cryst. Growth Des.*, **10**, 2152-2167 (2010)

[252] L. Infantes, J. Chisholm and S. Motherwell, *CrystEngComm*, **5**, 480-486 (2003)

[253] G. Bhagavannarayana, B. Riscob and M. Shakir, *Mater. Chem. Phys.*, **126**, 20-23 (2011)

[254] M. Prakash, D. Geetha and M. L. Caroline, *Physica B*, **406**, 2621-2625 (2011)

[255] X. Dong, J. Minhua and T. Zhongke, *Acta Chim. Sinica*, **41**, 570-573 (1983)

[256] R. Ittyachan, P. Sagayaraj and B. Kothandapani, *Acta Cryst. E*, **59**, o886-o888 (2003)

[257] S. B. Monaco, L. E. Davis, S. P. Velsko, F. T. Wang, D. Eimerl and A. Zalkin, *J. Cryst. Growth*, **85**, 252-255 (1987)

[258] D. Xu, X. Q. Wang, W. T. Yu, S. X. Xu and G. H. Zhang, *J. Cryst. Growth*, **253**, 481-487 (2003)

[259] Z. H. Sun, W. M. Sun, C. T. Chen, G. H. Zhang, X. Q. Wang and D. Xu, *Spectrochim. Acta A*, **83**, 39-45 (2011)

[260] M. R. Silva, J. A. Paixao, A. M. Beja and L. A. da Veiga, *J. Chem. Cryst.*, **30**, 411-414 (2000)

[261] S. Roy, D. D. Singh and M. Vijayan, *Acta Cryst. B*, **61**, 89-95 (2005)

[262] M. Selvaraj, S. T. S. Roy and M. Vijayan, *Acta Cryst. B*, **63**, 459-468 (2007)

[263] S. Ahn, F. Guo, B. M. Kariuki and K. D. M. Harris, *J. Am. Chem. Soc.*, **128**, 8441-8452 (2006)

[264] Z. Pan, M. Xu, E. Y. Cheung, J. A. Platts, K. D. M. Harris, E. C. Constable and C. E. Housecroft, *J. Solid State Chem.*, **179**, 3214-3223 (2006)

[265] Z. G. Pan, M. C. Xu, E. Y. Cheung, K. D. M. Harris, E. C. Constable and C. E. Housecroft, *J. Phys. Chem. B*, **110**, 11620-11623 (2006)

[266] E. Courvoisier, P. A. Williams, G. K. Lim, C. E. Hughes and K. D. M. Harris, *Chem. Comm.*, **48**, 2761-2763 (2012)

[267] P. A. Williams, C. E. Hughes, G. K. Lim, B. M. Kariuki and K. D. M. Harris, *Cryst. Growth Des.*, **12**, 3104-3113 (2012)

[268] D. A. Jove, E. Tedesco, K. D. M. Harris, R. L. Johnston and E. Y. Cheung, *Cryst. Growth Des.*, **1**, 425-428 (2001)

[269] T. Ogoshi, S. Kanai, S. Fujinami, T. Yamagishi and Y. Nakamoto, *J. Am. Chem. Soc.*, **130**, 5022-5023 (2008)

[270] Y. Chen, H. Q. Tao, Y. H. Kou, H. Meier, J. L. Fu and D. R. Cao, *Chin. Chem. Lett.*, **23**, 509-511 (2012)

[271] D. Cao, Y. Kou, J. Liang, Z. Chen, L. Wang and H. Meier, *Angew. Chem. Int. Ed.*, **48**, 9721-9723 (2009)

[272] X. Hu, Z. Chen, L. Chen, L. Zhang, J. Hou and Z. Li, *Chem. Comm.*, **48**, 10999-11001 (2012)

[273] T. Ogoshi and T. Yamagishi, *Eur. J. Org. Chem.*, 2961-2975 (2013)

[274] W. Si, X.-B. Hu, X.-H. Liu, R. Fan, Z. Chen, L. Weng and J.-L. Hou, *Tet. Lett.*, **52**, 2484-2487 (2011)

[275] T. Ogoshi, R. Shiga, M. Hashizume and T. Yamagishi, *Chem. Comm.*, **47**, 6927-6929 (2011)

[276] T. Ogoshi, R. Shiga, T. Yamagishi and Y. Nakamoto, *J. Org. Chem.*, **76**, 618-622 (2011)

[277] M. Pan and M. Xue, *Eur. J. Org. Chem.*, 4787-4793 (2013)

[278] C. Han, Z. Zhang, G. Yu and F. Huang, *Chem. Comm.*, **48**, 9876-9878 (2012)

[279] M. Pan and M. Xue, *Chin. J. Chem.*, **32**, 128-132 (2014)

[280] L. Wu, Y. Fang, Y. Jia, Y. Yang, J. Liao, N. Liu, X. Yang, W. Feng, J. Ming and L. Yuan, *Dalton Trans.*, **43**, 3835-3838 (2014)

[281] M. Pan and M. Xue, *RSC Adv.*, **3**, 20287-20290 (2013)

[282] Y. Fang, L. Wu, J. Liao, L. Chen, Y. Yang, N. Liu, L. He, S. Zou, W. Feng and L. Yuan, *RSC Adv.*, **3**, 12376-12383 (2013)

[283] M. P. Sonawane, J. Jacobs, J. Thomas, L. Van Meervelt and W. Dehaen, *Chem. Comm.*, **49**, 6310-6312 (2013)

[284] K. Lao and C. Yu, *J. Comp. Chem.*, **32**, 2716-2726 (2011)

[285] H. T. Chifotides and K. R. Dunbar, *Acc. Chem. Res.*, **46**, 894-906 (2013)

[286] D. Quinonero, C. Garau, C. Rotger, A. Frontera, P. Ballester, A. Costa and P. M. Deya, *Angew. Chem. Int. Ed.*, **41**, 3389-3392 (2002)

[287] B. L. Schottel, H. T. Chifotides and K. R. Dunbar, *Chem. Soc. Rev.*, **37**, 68-83 (2008)

[288] P. Gamez, *Inorg. Chem. Front.*, **1**, 35-43 (2014)

[289] D.-X. Wang and M.-X. Wang, *J. Am. Chem. Soc.*, **135**, 892-897 (2013)

[290] A. Frontera, P. Gamez, M. Mascal, T. J. Mooibroek and J. Reedijk, *Angew. Chem. Int. Ed.*, **50**, 9564-9583 (2011)

[291] T. Heinis, S. Chowdhury, S. L. Scott and P. Kebarle, *J. Am. Chem. Soc.*, **110**, 400-407 (1988)

[292] J. Schiedt and R. Weinkauf, *J. Chem. Phys.*, **110**, 304-314 (1999)